Exploring palaeoaridity using stable oxygen and carbon isotopes in small mammal teeth: a case study from two Late Pleistocene archaeological cave sites in Morocco, North Africa

Amy Jeffrey
St Cross College

Hilary Term 2016

Submitted in partial fulfilment of the requirements for the Degree of Doctor of Philosophy

Table of Contents

Abstract

Revised chronologies from Moroccan cave sites have raised questions concerning the timing of changes in human cultural behaviour in relation to past climate shifts. However, many of the inferences about past moisture regimes are based on external records. Therefore, this thesis aimed to develop a palaeoclimate record using oxygen and carbon isotope values ($\delta^{18}O$ and $\delta^{13}C$) in Gerbillinae (gerbil) teeth from two Late Pleistocene cave sites, El Harhoura 2 and Taforalt, in Morocco. Since small mammals are not commonly used to construct proxy climate records, a modern isotope study was undertaken in northwestern Africa to understand the influences on the stable isotope composition of small mammal tissues in semi-arid and arid settings.

The results from the modern study show that $\delta^{18}O$ composition of gerbil teeth is strongly correlated with mean annual precipitation (MAP), and therefore in arid settings reflects moisture availability. Predictably, the $\delta^{13}C$ values of the gerbil teeth reflected C_3 and C_4 dietary inputs, but arid and mesic sites could not be distinguished because of the high variability displayed in $\delta^{13}C$. The $\delta^{18}O$ isotope-based MAP reconstructions suggest that the Mediterranean coastal region of North Africa did not experience hyper-arid conditions during the Late Pleistocene. The $\delta^{13}C$ values of the gerbil teeth show that C_3 vegetation dominated in the Late Pleistocene, but there was a small amount C_4 vegetation present at Taforalt. This indicates that small mammals are extremely sensitive to discreet shifts in past vegetation cover. Both the modern and archaeological studies demonstrated that the isotope values of molars and incisors differed. The results indicate that tooth choice is an important consideration for applications as proxy Quaternary records, but also highlights a new potential means to distinguish seasonal contexts. Comparisons of proxy climate records and cultural sequences at Taforalt and El Harhoura 2 show that Middle Stone Age occupations of both sites occurred during relatively humid and arid climate phases. The transition to the Later Stone Age appears to have taken place during a period of increased aridity, hinting that this cultural transition may be related to changing environmental conditions.

Acknowledgements

Firstly, I would like to thank my supervisors Julia Lee-Thorp, Nick Barton and Abdeljalil Bouzouggar for all their help, support and encourage throughout the project. I am extremely grateful to Christiane Denys and Emmanuelle Stoetzel (Muséum national d'Histoire naturelle), for their collaboration with the modern study. I would like to thank them for allowing me to sample their modern owl pellet collection, for identifying the small mammal material and for sharing their extensive knowledge on small mammals in North Africa. The modern owl pellets were collected thanks to Francis Petter (Tata), Stépahne Aulagnier (INRA Toulouse, France) (Sidi Chicker), Watik Hamdine (Beni Abbes), ANR-09-PEXT-004 MOHMIE project (Berrechid, Ouled Boughadi, Merja Zerga and Guenfouda) and the RHOI (NSF) project for Oued Nfifikh (with help of Abdeleslam Rihane, University of Casablanca).

I am thankful to Roland Nespoulet, Emmanuelle Stoetzel and Mohamed Abeljalil El Hajraoui for allowing me to analyse *Meriones* teeth from El Harhoura 2. I am indebted to Emmanuelle for identifying the material and helping me understand the site stratigraphy. I would also like to thank the Moroccan-French team (directed by R. Nespoulet and M.A. Hajraoui) for allowing me to join their excavation of El Mnasra Cave in 2013. I would like to thank N. Barton, A. Bouzouggar and Simon Parfitt for allowing me to analyse *Meriones* teeth from Taforalt. I am appreciative to Simon Parfitt for arranging access to the material and identifying to species.

I am grateful to several of my family, friends and colleagues who have helped me throughout the DPhil. I would especially like to thank Chris Green, Andrew Gledhill and Peter Ditchfield for technical assistant. I would like to thank Tom Frankland for help in producing graphics and coding in R. I would also like to thank all the Jeffrey's who proof read a chapter of this thesis, even though they had no idea what it was about! And finally I would like to thank my archaeology friends for the laughs, moans and drinks- it has been fun.

I am extremely grateful to NERC for funding my DPhil research (NERC training grant NE/K500811/1). I would also like to acknowledge additional research and conference travel funding from The Boise Trust Fund, St Cross College, The Quaternary Research Association and The School of Archaeology.

List of Abbreviations

D/O - Dansgaard/Oeschger

HE - Heinrich Events

AMOC - Atlantic Meridional Overturning Circulation

LGM - Last Glacial Maximum

LSA - Later Stone Age

MSA - Middle Stone Age

C_3 - C3 plants

C_4 - C4 plants

MAP - mean annual precipitation

MAT - mean annual temperature

$\delta^{18}O_{teeth}$ - oxygen isotope value of molars and incisors

$\delta^{18}O_{mt}$ - oxygen isotope value of molars

$\delta^{18}O_{it}$ - oxygen isotope value of incisors

$\delta^{18}O_{mw}$ – oxygen isotope value of meteoric water

$\delta^{13}C_{teeth}$ - carbon isotope value of molars and incisors

$\delta^{13}C_{mt}$ - carbon isotope value of molars

$\delta^{13}C_{it}$ - carbon isotope value of incisors

$\delta^{13}C_{co2}$ - carbon isotope values of atmospheric CO_2

pCO_2 - partial pressure of carbon dioxide

cal ka BP - Calibrated radiocarbon date (thousand years)

ka BP - uncalibrated radiocarbon date (thousand years)

ka years - thousand years (OSL dates)

THI - Taxonomic Habitat Indices

MI - Mystery Interval

List of Figures

List of Tables

1. Introduction

1.1. Project context

The Mediterranean and Atlantic coastal plain of North Africa forms a unique landscape; the relatively narrow coastal plain is bounded by the Atlas Mountains to the south and west, and lies on the margins of the Sahara Desert. It is a climatically sensitive setting positioned between the westerly-dominated, mid-latitude system emanating from the Atlantic and the monsoon driven low-latitude system from the Gulf of Guinea. Presently, this region experiences a mild oceanic Mediterranean climate; however, available evidence indicates millennial-scale shifts between relatively humid and arid conditions throughout the Late Pleistocene, synchronous with climate changes in the North Atlantic region (Bout-Roumazeilles et al., 2007; Moreno et al., 2005). The Sahara Desert region, to the south, also underwent significant hydrological fluctuation during the Late Pleistocene, resulting in strong shifts between hyper-aridity and 'greening events' caused by the northward penetration of the West African monsoon during periods of high summer insolation (deMenocal et al., 2000; Tierney et al., 2011). As the Mediterranean climate region of North Africa did not experience hyper-aridity, similar to the extremes seen in the Sahara, it has been suggested that the North African coastal strip acted as a refugium for human populations during the Late Pleistocene (Prendergast et al., 2015; Reade et al., 2015).

Archaeological evidence from cave sites located on and overlooking the coastal plain of Morocco, such as Contrebandiers, Dar es-Soltan 1, El Harhoura 2, El Mnasra, Taforalt and Ifri n'Ammar, show that this landscape has been occupied and exploited

by humans since at least the beginning of the Last Interglacial (Barton et al., 2009; Bouzouggar et al., 2007b; Jacobs et al., 2012; Richter et al., 2010). Recently revised chronologies from these cave sites have raised questions concerning the timing of human occupation in relation to global climate and regional climate events during the Late Pleistocene. The Middle Stone Age (MSA) (including the Aterian) occupation of archaeological sites on the Atlantic coast of Morocco appears to be associated with humid climate episodes during MIS 5 and MIS 3, while some sites seem to have been abandoned by humans during MIS5b, a period apparently marked by greater aridity in North Africa (Jacobs et al., 2012; Stoetzel et al., 2011). The period spanning ~40-20ka BP is particularly interesting in North Africa as it includes a marked transition from the MSA to the Later Stone Age (LSA). Radiocarbon ages from Taforalt demonstrate that the MSA Aterian persisted until ~29ka cal BP, after which a non-Levallois lithics industry, which as yet has no known analogue in the Maghreb, appears in the archaeological record (Barton et al., 2016). Radiocarbon dates show that the cultural change between the non-Levallois lithics industry and the LSA occurs around a time equivalent to the Last Glacial Maximum (24-22 ka cal BP) in the Northern Hemisphere with a clear ‘gap’ in occupation between the two cultural periods (Barton et al., 2013).

It is widely considered that humidity and aridity played an important role in regulating and modifying human occupation in the region. However, many of the inferences about past moisture regimes are based on secondary and/or external records that do not provide a local representation of terrestrial palaeoclimate. In addition, palaeoclimate and palaeoenvironmental information from archaeological sites is often limited because humans are frequently responsible for the deposition of

botanical and large mammal remains in cave sites. The thesis addresses this gap by developing an independent terrestrial proxy palaeoaridity archive for the Mediterranean and Atlantic coastal plain of northwestern Africa using oxygen and carbon stable isotopes in small mammal teeth excavated from El Harhoura 2 and Taforalt. These cave sites were selected because they contain environmental material, are well-dated and the rich MSA and LSA sequences are representative of the cultural events that are understood to have occurred in the region. This makes El Harhoura 2 and Taforalt crucial sites for examining questions relating to the emergence of modern humans into North Africa and their cultural responses to climate and environmental change. The palaeoclimate and palaeoenvironmental records will be directly compared with the cultural sequences from both sites and will be used to explore some of the recent questions raised regarding human occupations and cultural change in North Africa.

1.2. Research aims and strategy

This thesis aims to develop a palaeoclimate and palaeoenvironmental record for the Mediterranean and Atlantic coastal region of northwestern Africa using oxygen and carbon isotope values ($\delta^{18}O$ and $\delta^{13}C$) in Gerbillinae (gerbil) teeth from the Late Pleistocene sequences at El Harhoura 2 and Taforalt. This record will be used to explore the role that past climate and environmental change had on human occupations and cultural behaviour in North Africa. Since isotopic methods are not commonly applied to small mammal materials for the construction of proxy records, a further aim of the thesis is to undertake a modern isotope study across northwestern

Africa to understand the influences on the stable isotope composition of small mammals in semi-arid and arid settings.

1.3. Stable isotopes in small mammals as proxy climate and environmental records

The $\delta^{18}O$ and $\delta^{13}C$ of fossil mammalian enamel has been widely applied to infer past climate and environmental conditions such as aridity, rain water sources, climate seasonality, relative humidity and vegetation cover (Ayliffe et al., 1992; Cerling et al., 1997; Hoppe, 2006; Levin et al., 2006). Although small mammals are frequently abundant on archaeological and palaeontological sites they have played little part in such endeavours to date. Their role is instead restricted to traditional faunal abundance methods that rely on the association of taxa with their preferred modern habitats (Fernández-Jalvo et al., 1998; Stoetzel et al., 2011). Few isotope studies have been undertaken on small mammals because little is understood about their isotope ecology and their small size has, until recently, limited sampling methodology. The seminal studies that first identified the links between the isotopic composition of precipitation and faunal tissues experimentally, also cautioned against the effect of faster metabolism in mammals with small body sizes (Luz and Kolodny, 1985; Luz et al., 1984), and as a result most studies have targeted larger bodied mammals (Bryant and Froelich, 1995). The advantages to studying small mammals include their high abundance in the archaeological and palaeontological record, which permits statistically sound sample sizes, and their relatively small home ranges, which allow inferences to be made about local environmental conditions. Small mammals also make up an important component of terrestrial

ecosystems and respond rapidly to environmental change. Consequently, as argued by Grimes et al. (2008) the stable isotope composition of small mammal material has the potential to produce high-resolution temporal records of past environmental changes in terrestrial settings.

1.3.1. Modern isotope studies

Few modern isotope ecology studies have been undertaken on wild small mammal populations, but those that have demonstrate the potential of small mammal tissues as indicators of past climate and environment. Smiley et al. (2015) showed the $\delta^{13}C$ composition of rodent hair tracked variations in C_3 and C_4 vegetation across western North America, while Gehler et al. (2012) showed that the intra- and inter-specific variation shown in the $\delta^{18}O$ and $\delta^{13}C$ values of rodent teeth was similar to that displayed in large mammals. Most modern analogue studies have focussed on exploring the relationship between climate and the $\delta^{18}O$ composition of small mammal teeth in studies generally restricted to cool/mesic environments (D'Angela and Longinelli, 1990; Longinelli and Selmo, 2003; Navarro et al., 2004; Royer et al., 2013a). Since many small mammals obtain most of their water from plants, this means that the visible effects of plant water ^{18}O-enrichment are obscured. Specific relationships between $\delta^{18}O$ of the phosphate component ($\delta^{18}O_{PO4}$) of wild Muroidea teeth and $\delta^{18}O$ local meteoric water ($\delta^{18}O_{mw}$) have been obtained for temperate Europe (D'Angela and Longinelli, 1990; Longinelli et al., 2003; Navarro et al., 2004; Royer et al., 2013a). Although these relationships may be applicable in modern temperate Europe where plant water isotope effects are relatively small, it is decidedly problematic in application to the past in areas or episodes in which aridity was more prevalent. Ignoring the isotope effects of evapotranspiration in plant water

on animal phosphate or carbonate oxygen isotope values limits efforts to reconstruct past hydrological regimes and temperatures. This problem has not gone unnoticed. Delgado Huertas et al. (1995) reported that the $\delta^{18}O_{PO4}$ of rabbit and hare bone from Europe, Africa and Canada did *not* reflect that of $\delta^{18}O_{mw}$, probably because these animals obtain the majority of their bodywater from food rather than from environmental water. In a recent study in western North America, Smiley et al. (2015) also showed that the $\delta^{18}O$ and $\delta^{2}H$ of *Dipodomys ordii* hair was enriched relative to local meteoric water, also suggesting a reliance on evaporated water sources.

The modern study in this thesis explores the $\delta^{18}O$ and $\delta^{13}C$ composition of modern gerbil tooth apatite, and the $\delta^{13}C$ and nitrogen isotope ($\delta^{15}N$) composition of gerbil bone collagen across a rainfall gradient in northwestern Africa (100-600mm MAP), specifically to explore the effects of moisture availability and aridity on the isotopic composition of small mammal tissues. As well as determining whether the isotopic composition of precipitation or moisture availability exerts the primary influence on the $\delta^{18}O$ composition of small mammal tooth apatite, the modern study also investigates the sensitivity of $\delta^{13}C$ composition of small mammal tissues to plant responses to moisture availability, and whether the $\delta^{15}N$ composition of arid adapted small mammals reflect aridity. Given the effect of aridity on $\delta^{13}C$ and $\delta^{15}N$ values in C_3 plants (see Chapter 4) it is predicted that increasing aridity would cause $\delta^{13}C$, $\delta^{15}N$ and $\delta^{18}O$ to co-vary and increase in the gerbil tissues.

The effects of small mammals' relatively fast metabolism, rapid tissue turnover times and short life spans on the isotopic signals reflected in their tissues are not well

understood. In a controlled laboratory study on woodrats, Podelsak et al. (2008) showed that body water turn over was rapid, 1.4 – 3.3 days, suggesting that small mammals are highly sensitive to changes in the external environment and that their body tissues will be isotopically variable. The fast tissue turnover and formation times may also result in their body tissues reflecting particular temporal periods. Gehler et al. (2012) showed that the carbonate component ($\delta^{18}O_{CO3}$) of rodent incisor teeth differed by up to ~4‰ compared to that of the bone bioapatite from the same individual, the authors suggested this reflected a temporal bias in the $\delta^{18}O$ composition of the incisor teeth.

Many rodents have both permanently rooted molar teeth with discrete developmental periods, and continuously growing incisor teeth, meaning that different temporal periods are reflected in each tooth type. Palaeoclimate and palaeoenvironmental reconstructions using isotopes in small mammal teeth have so far tended to use molar and/or incisor teeth indiscriminately with little consideration for the developmental period reflected (Hopley et al., 2006; Hynek et al., 2012). Since these animals reproduce seasonally and have relatively short life spans the period represented by each tooth type might very well influence the isotopic composition. Lindars et al. (2001) suggested that post-weaning teeth should be preferred to avoid a nursing (pre-weaning) effect, but this recommendation was based on a study using only three dormice individuals, in which the stable isotope composition of molar but not incisor teeth was measured. There is also little substantive evidence in the literature for a nursing effect in the $\delta^{18}O$ and $\delta^{13}C$ composition of animal and human teeth. Observations for changes in $\delta^{13}C$ of body tissues formed before and after weaning are highly variable (Fogel et al., 1989; Fuller et al., 2006; Williams et al.,

2005; Wright and Schwarcz, 1998), while teeth formed during the nursing period appear to have slightly higher $\delta^{18}O$ relative to those formed post-weaning (Metcalfe et al., 2010; Wright and Schwarcz, 1998). To the author's knowledge there are no studies that have systemically explored the effects of tooth development period on the isotopic composition of rodents that have permanently rooted molar teeth and continuously growing incisor teeth. Therefore, the modern study in this thesis will also explore isotopic variability between the molars and incisors to evaluate which teeth should be used in the construction of proxy climate and environmental records.

1.3.2. Palaeostudies using small mammal tissues

As discussed above isotopic methods are not commonly applied to archaeological/fossil small mammal materials because little is known about their isotope ecology. Yet, some pioneering studies have demonstrated that isotopes in small mammals can be used successfully as proxy climate and environmental indicators. The carbonate component ($\delta^{13}C_{CO3}$) of small mammal tooth enamel has been used effectively to infer palaeodiet, changes in C_3 and C_4 vegetation cover and palaeohumidity (Freudenthal et al., 2014; García-Alix, 2015; Grimes et al., 2004; Hopley et al., 2006; Hynek et al., 2012; Kimura et al., 2013; Yeakel et al., 2007). Studies demonstrate that small mammal teeth are more sensitive to changes in C_3 and C_4 vegetation cover relative to larger bodied mammals (Arppe et al., 2015; Hynek et al., 2012; Kimura et al., 2013). Hynek et al. (2012) recently detected the presence of C_4 vegetation in Argentina 1-2 million years earlier than seen in isotope records from large mammals and soil carbonate. The small mass of dietary intake by small mammals means there is a greater probability of sampling dietary end-members, and their rapid tissue growth and turnover results in less dampening and

homogenisation of the isotope signals reflected in the tissues (Arppe et al., 2015; Passey et al., 2005; Podlesak et al., 2008). The carbonate component ($\delta^{18}O_{Co3}$) of small mammal teeth is not frequently used to infer past water sources and palaeoaridity (García-Alix et al., 2013; Rogers and Wang, 2002; Yeakel et al., 2007). Instead studies have focussed on using $\delta^{18}O_{PO4}$ to infer $\delta^{18}O_{mw}$ and subsequently seasonal and mean annual air temperatures, based on the principle that in mid and high latitudes mean $\delta^{18}O_{mw}$ is correlated with mean annual air temperature (Héran et al., 2010; Navarro et al., 2004; Royer et al., 2014, 2013b; Tütken et al., 2006). The $\delta^{13}C$ and $\delta^{15}N$ of small mammal organic tissue is mainly restricted to use in modern ecological studies (e.g. Baugh et al., 2004; Codron et al., 2015; Dammhahn et al., 2013; Mauffrey and Catzeflis, 2003; Symes et al., 2013), and because of preservation issues is rarely used as proxy Quaternary climate record (Gąsiorowski et al., 2014).

Large concentrations of small mammal skeletal material are found in cave or rock shelter sediments. They are almost always introduced to these sites by predators such as owls, raptors and mammals (Andrews, 1990). Therefore, the behaviours of the predators that deposited the small mammal accumulations in the cave sites may also influence the isotopic signal reflected in the assemblage. Predators have different home ranges/ hunting ranges and habitat preferences so could potentially provide environmental signals on different spatial and temporal scales. The isotope signal reflected in the small mammal teeth (continually growing incisor teeth in gerbils) may also be affected by a seasonal predation bias due to predators preferentially hunting species in particular seasons, or more prey being available at certain times of the year. Royer et al. (2014, 2013b) showed that the isotope signal

of fossil small mammal teeth from Glacial Europe reflects summer climate conditions because prey numbers are higher (after the breeding season) and there is no snow cover in the summer season. Yet, this is less applicable in North Africa where there is less of a seasonal temperature gradient. In addition to this, the temporal period reflected by small mammal accumulations within archaeological cave sites is unknown. Although the age estimates on cave deposits provide information about the sediment accumulation rates, the small mammal accumulations could represent discreet periods (weeks, months, years) within the longer temporal period reflected by the Level when predators were occupying the cave. For example, small mammal teeth selected for isotope analysis could reflect a particularly humid period within a longer arid period or vice versa. It is also suggested that extensive accumulations of small mammal skeletal assemblages are likely associated with periods when humans were not intensively occupying cave/rock shelter sites, therefore the climate information may reflect periods when humans were not using the site.

It is expected that the $\delta^{18}O$ and $\delta^{13}C$ composition of the archaeological gerbil teeth from El Harhoura 2 and Taforalt will provide a record of Late Pleistocene palaeoaridity and vegetation cover. As both molars and incisors will be used to construct the proxy climate record it is suggested that isotopic offsets may occur between the tooth types because they develop over different temporal periods.

1.4. Summary of research

The thesis research consists of two components. The first is a modern validation study using small mammal material collected from owl pellet sites across a rainfall gradient (100-600mm MAP) in northwestern Africa. This study aims to explore the

influences of the stable isotope composition of small mammals in semi-arid and arid environments, as well as the isotopic variation between rodent molar and incisor teeth. The modern study was under taken in collaboration with Emmanuelle Stoetzel and Christiane Denys (Musèum national d'Histoire naturelle, Paris), who provided and identified the modern material for isotope analysis. The $\delta^{18}O$ and $\delta^{13}C$ data from the modern study is published in Jeffrey et al. (2015). The second component of the thesis is the development of a palaeoaridity record for the Mediterranean and Atlantic coastal region of Morocco using the $\delta^{18}O$ and $\delta^{13}C$ values in *Meriones* sp. (gerbil) teeth. In total $\delta^{18}O$ and $\delta^{13}C$ values are determined on 164 molar and incisor teeth and 74 molar and incisor from Late Pleistocene Levels at El Harhoura 2 and Taforalt, respectively.

The results will be used to test the following hypotheses:

1. The oxygen, carbon and nitrogen isotope values of modern gerbil tissues will increase with aridity.
2. The oxygen and carbon isotope values of modern gerbil molars and incisors from the same individual will reflect the season of tooth formation.
3. The MSA occupation at Taforalt and El Harhoura 2 was associated with humid climate episodes.
4. The cultural change from the MSA to the LSA at Taforalt and El Harhoura 2 was associated with a period of increased aridity.
5. The Mediterranean coastal strip of North Africa acted as a refugium for humans during the Late Pleistocene.

1.5. Thesis structure

The thesis is divided into eight chapters. This chapter explains the rationale behind the project and introduces the aims and research strategy. Chapter 2 provides a brief summary of stone age archaeology in North Africa, introduces the thesis study sites (El Harhoura 2 and Taforalt) and finally provides a review of recent work that has drawn connections between cultural and climate records in North Africa. Chapter 3 explains our current understanding of present and past climate systems within the Mediterranean coastal region and Sahara region of North Africa. Chapter 4 provides further background information describing the principles of stable isotope analysis in the environment and the factors that effect the isotopic composition of food and water consumed by small mammals. The results of the modern small mammal isotope study, and the application of the method to archaeological gerbil teeth from El Harhoura 2 and Taforalt are presented in Chapters 5 and 6, respectively. Chapter 5 presents the results of the modern $\delta^{18}O$ and $\delta^{13}C$ values of gerbil tooth apatite and $\delta^{15}N$ and $\delta^{13}C$ values of gerbil bone collagen from eight sites that lie across a rainfall gradient in northwestern Africa. The Chapter explores the influences of aridity on the isotope composition of small mammal tissues, as well as investigating isotopic variability between different tooth types (molars and incisors) to evaluate which teeth should be used in the construction of proxy climate and environment records. The implications of using gerbil $\delta^{18}O$ and $\delta^{13}C$ tooth apatite as a proxy climate record are discussed. Chapter 6 uses the $\delta^{18}O$ and $\delta^{13}C$ values in *Meriones* teeth from El Harhoura 2 and Taforalt to reconstruct mean annual precipitation (MAP) and vegetation cover in the Mediterranean and Atlantic regions of Morocco. Variability between the $\delta^{18}O$ and $\delta^{13}C$ values of incisors and molars from each site are also

explored. Chapter 7 discusses the palaeoaridity records from El Harhoura 2 and Taforalt and compares them to other records of palaeoenvironment and palaeoclimate from both cave sites, as well as to marine and terrestrial proxy records from the wider western Mediterranean region. Comparisons are drawn between the cultural and proxy climate records at the cave sites. The final chapter, Chapter 8, summarises the main findings of the thesis and outlines suggestions for future research. Appendices are found at the end of the thesis.

2. Archaeology in North Africa

2.1. Introduction

This chapter provides a brief introduction to the Stone Age archaeology of North Africa focussing on lithic industries from the MSA onwards. The main component of the chapter describes the sites of interest, El Harhoura 2 and Taforalt, outlining their stratigraphies, archaeology, chronologies and palaeoenvironmental records. The final section reviews recent work that has drawn connections between cultural records in North Africa and regional climate and environmental records. The need for local palaeoclimate and palaeoenvironmental records that can be directly compared with archaeological sequences is demonstrated.

2.2. Introduction to Archaeology in North Africa

2.2.1. Terminology

Firstly, consideration of the terminology used to describe North African Archaeology is required. Several researchers have argued that archaeology in North Africa should reflect its African setting and affiliation (Garcea, 2012a; Mcbrearty and Brooks, 2000). It is argued that terms such as “Mousterian” and “Middle/Upper Palaeolithic”, which refer to the European archaeological record, are not relevant in North Africa as there are no proven cultural affinities between both continents (Garcea, 2012a). In addition, the term “Mousterian” is associated with Neanderthals, a species known not to be responsible for the MSA in North Africa (Garcea, 2012a). Dibble et al. (2013) observes closer similarities between the MSA Aterian and African MSA with the appearance of shell beads, bone tools and ochre use in the North African

archaeological record. Clearly a wider discussion of North African archaeology terminology is beyond the scope of this thesis. The author will therefore use the terms Middle Stone Age (MSA) and Later Stone Age (LSA) to describe archaeology in North Africa (following Barton et al., 2013). The term “Mousterian” is retained because in the absence of an alternative, this term is still widely used across North Africa (Hublin et al., 1987; Wengler, 1993). The lithic industries present in the sequences at El Harhoura 2 and Taforalt are identified as the MSA Aterian and LSA Iberomaurusian. Since the people responsible for these industries appear to differ in physical features and used different tools (see discussion below in Section 2.2.2 and 2.2.3), I also use these terms to denote the people using the lithic industries.

2.2.2. MSA Aterian

The North African Mousterian has never been described in detail, meaning it is not well defined (Bouzouggar and Barton, 2012). It is seen as an industry with a high Levallois component and an abundance of scrapers, with comparisons to the European Middle Palaeolithic industries (Balout, 1965; Hublin et al., 1987; Wengler, 2006). The Aterian technocomplex is a facies of the MSA across North Africa; Aterian sites are recognised over a large geographic area from the Atlantic coast in the west to almost the Nile Valley in the east, and from the Mediterranean coast in the north to the Sahel region in the south (Caton-Thompson, 1946) (Figure 2.1). The origin of the Aterian is ambiguous. Caton-Thompson (1946) suggested that the technology is indigenous to North Africa, conversely it has also been proposed that the toolkit was introduced from further south via the Nile Valley (Van Peer, 1998), or across humid corridors running through the Sahara Desert (Osborne et al., 2008). Within the Maghreb it is believed that the Aterian developed out of the Mousterian

(Balout, 1965; Camps, 1974). Sites such as Ifri-Ammar (Mikdad et al., 2004; Nami and Moser, 2010; Richter et al., 2010), Contrebandiers (Dibble et al., 2012), Dar es-Soltan I (Barton et al., 2009) and Mugharet el ‘Aliya (Wrinn and Rink, 2003) all have a Mousterian stratigraphically below the Aterian. The Aterian is a Levallois-based MSA industry (Caton-Thompson, 1946) sharing common tool types with the Mousterian (e.g. side scrapers) and “Upper Palaeolithic” (e.g. end-scrapers, burins, pedunculates and bifacial foliates) (Clark, 1982) (Figure 2.2). The industry is traditionally associated with the presence of tanged tools within the lithics assemblage. The most widely accepted classification scheme for the Aterian is that of Tixier (1967), which describes an Aterian assemblage being made up of Levallois blades, end scrapers, and containing approximately one quarter tanged pieces. Raw materials are usually locally derived flints and quartzites sourced up to ~20km from sites (Barton et al., 2009; Nespoulet et al., 2008b).

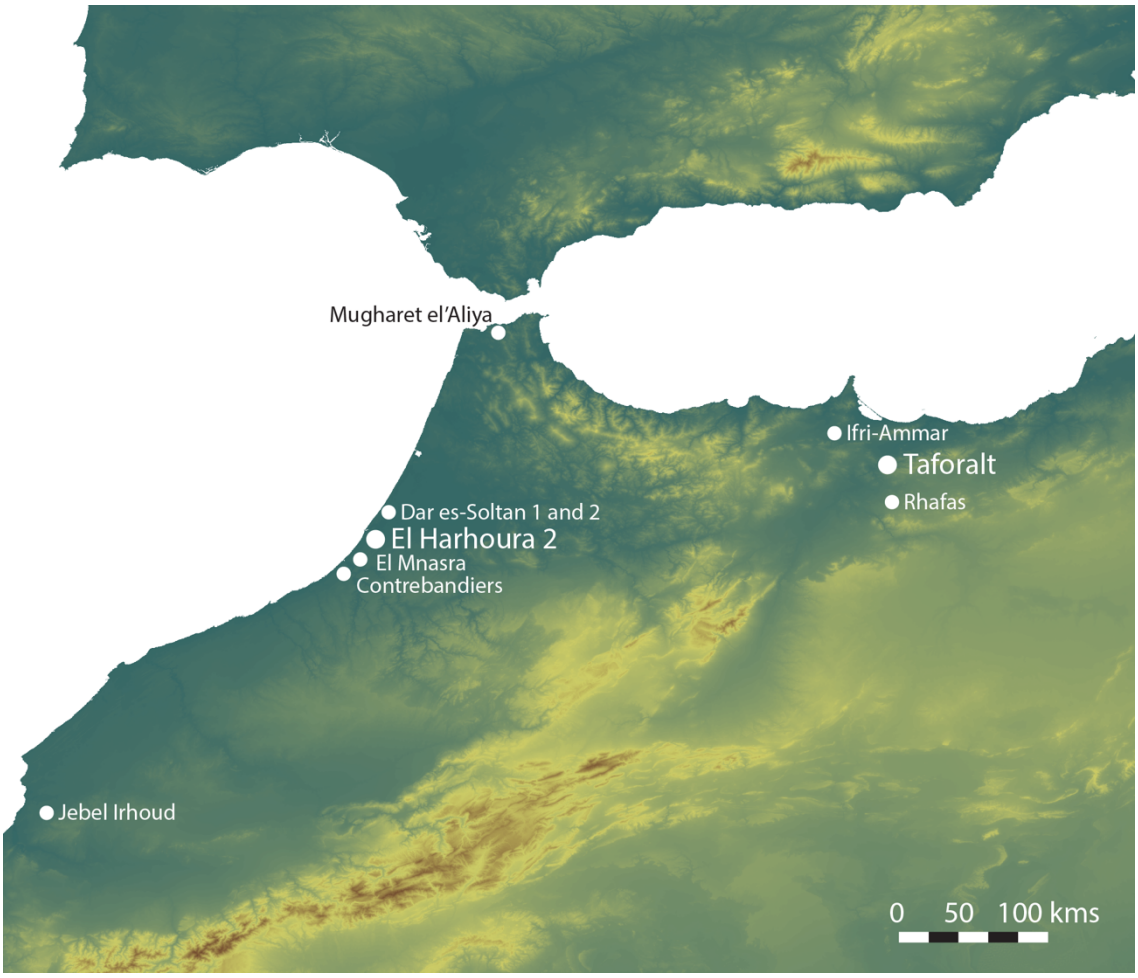

Figure 2.1: Map of the Atlantic and Mediterranean region of Morrocco, showing the location of Taforalt, El Harhoura 2 and other archaeological sites discussed in the text.

Although there are many Aterian sites in North Africa this technology remains relatively poorly researched and defined (Bouzouggar and Barton, 2012). Recently researchers have called for a "review and redefinition" of Aterian technology across North Africa (Bouzouggar and Barton, 2012:93). Several authors suggest that the definition of Aterian should not be merely based on the presence/absence of tanged tools within the assemblage (Dibble et al., 2013; Linstädter et al., 2012; Spinapolice and Garcea, 2014), and even suggest that the Aterian must no longer be treated as a separate entity, but instead should be studied within the wider context of the North

African MSA (Scerri, 2013; Scerri et al., 2014). In a reassessment of Aterian material from sites in Morocco and Algeria, Dibble et al. (2013) showed that apart from the presence or absence of tanged pieces, there are no major distinctions between technology described as Aterian or Mousterian. It must be noted at this point that the intention of this thesis is not to provide an extensive review of MSA lithic technologies in North Africa; therefore, the author will use technological identifications made in the cited literature.

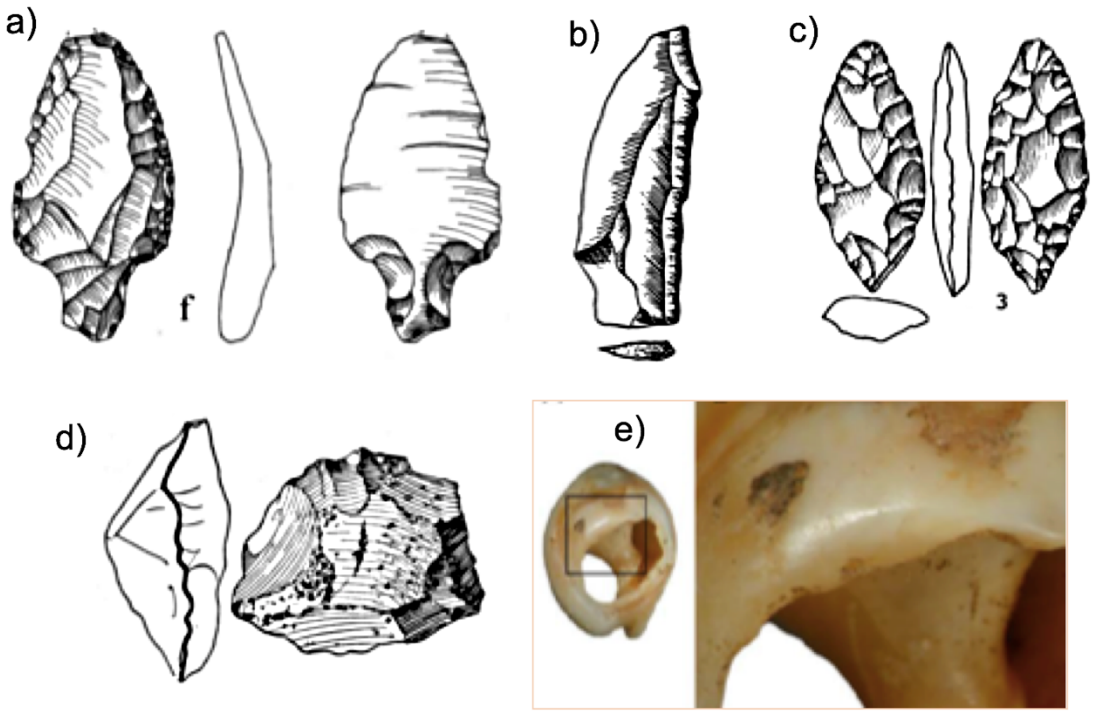

Figure 2.2: Stone and shell artefacts typical of the Aterian, a) Tanged point (from Dibble *et al*. 2013), b) Blade c) Foliate, d) Small Levallois discoidal core, (b-d from Bouzouggar & Barton 2012), e) perforated *Nassarius* shell bead from Grotte Des Pigeons (from Bouzouggar *et al*. 2007).

Until recently it was thought the Aterian had an age of between 40ka BP and 25-20ka BP (Debénath et al., 1982). Although conventional radiocarbon dates produced an infinite age for the Aterian at Taforalt and Dar es-Soltan 1 (Debénath et al., 1986;

Roche, 1976) researchers proposed a relatively recent chronology for the industry. The first major challenge to this model came when Aterian sites in the eastern Sahara were subject to Luminescence dating (Cremaschi et al., 1998; Garcea, 2004). Recently published Optically Stimulated Luminescence (OSL), U-Series and Thermoluminescence (TL) dates now demonstrate that the Aterian dates to >100ka at several sites in Morocco including Contrebandiers (Jacobs et al., 2012; Schwenninger et al., 2010), Dar es-Soltan I (Barton et al., 2009), El Harhoura 2 (Jacobs et al., 2012), El Mnasra (Jacobs et al., 2012; Schwenninger et al., 2010), Taforalt (Bouzouggar et al. 2007; Clark-Balzan, 2012; Clark-Balzan et al., 2012) and Ifri n'Ammar (Richter et al., 2012, 2010). The earliest date for the Aterian in North Africa is currently ~145ka at Ifri n'Ammar (Richter et al., 2010).

Significantly, evidence for human 'symbolic' behaviour is associated with Aterian contexts. *Nassarius* shell beads have now been identified at Taforalt, Ifri n'Ammar, El Mnasra, El Harhoura 2, Rhafas and Contrebandiers (Bouzouggar et al., 2007a; D'Errico et al., 2009; Dibble et al., 2012; Richter et al., 2012; Stoetzel et al., 2014) (Figure 2.2). The shells from Taforalt show evidence of deliberate perforation with use wear indicating they were likely strung as beads (Bouzouggar et al., 2007a). Traces of ochre have been found on *Nassarius* shells from Taforalt, Ifri n'Ammar, Contrebandiers and Rhafas (Bouzouggar et al., 2007a; D'Errico et al., 2009; Dibble et al., 2012; Nami and Moser, 2010; Richter et al., 2012). There is also evidence of pigment use from El Mnasra where small blocks of worked haematite are reported from levels 5 and 7 (El Hajraoui et al., 2012a; Nespoulet et al., 2008a, 2008b). As well as stone artefacts, there is also evidence for worked bone and ivory objects from Aterian contexts. Bone tools have been found at both El Mnasra (Levels 5 and

6) and El Harhoura 2 (Campmas, 2012; El Hajraoui and Debénath, 2012), while two ivory objects were recovered from layer one at Dar es-Soltan I (Ruhlmann, 1951). Another noteworthy find is the evidence for structuring of space with stone lined hearth structures identified in Aterian Levels (5 to 7) at El Mnasra (El Hajraoui et al., 2012b; Stoetzel et al., 2014).

Anatomically modern human fossils have been found at Contrebandiers, Dar es Soltan 2, Mugharet el ‘Aliya, El Harhoura and Jebel Irhoud in Morocco (Hublin, 1992; Mcbrearty and Brooks, 2000), of which the remains from the first four sites are thought to be associated with the Aterian. The mandible and canine from El Harhoura were found *in situ* in association with Aterian points, while the remains from Dar es-Soltan 2 were overlain with Aterian deposits (reviewed in Hublin, 1992). The association of human remains with Aterian levels at Contrebandiers and Mugharet el ‘Aliya remain uncertain (Hublin, 2000; Wrinn and Rink, 2003). During more recent excavations at Contrebandiers (2007-2010) (Dibble et al., 2012) further human remains associated with the earlier Mousterian layers were excavated (Balter, 2011; Dibble et al., 2012). The oldest fossil human remains in North Africa are those from the Mousterian at Jebel Irhoud dating to c. 160ka (Smith et al., 2007). Previously, these remains were considered to have a morphological resemblance to Neanderthals, but they are now categorised as archaic modern human (Hublin, 2000).

2.2.3. LSA Iberomaurusian

The Iberomaurusian is a microlithic bladelet industry considered to be earliest LSA industry in the Maghreb (Bouzouggar et al., 2008; Camps, 1974; Lubell, 2001). Iberomaurusian cave/rockshelter and open-air sites are mainly distributed across the Mediterranean coastal zone of the Maghreb from western Morocco to northern Tunisia (Figure 2.3). The southerly extent is not well defined, but sites have been reported up to 200km inland from the current North African coastline (Camps, 1974; Close and Wendorf, 1990). The term 'Iberomaurusian' was first used by Pallary to show similarities between lithic technologies in Spain and Morocco (Pallary, 1909), but the link was later dismissed by archaeologists recognising stronger affinities with African lithic technologies (Gobert and Vaufrey, 1932; Goetz, 1941). Since being introduced the term Iberomaurusian has persisted in the literature and for consistency is used in this thesis.

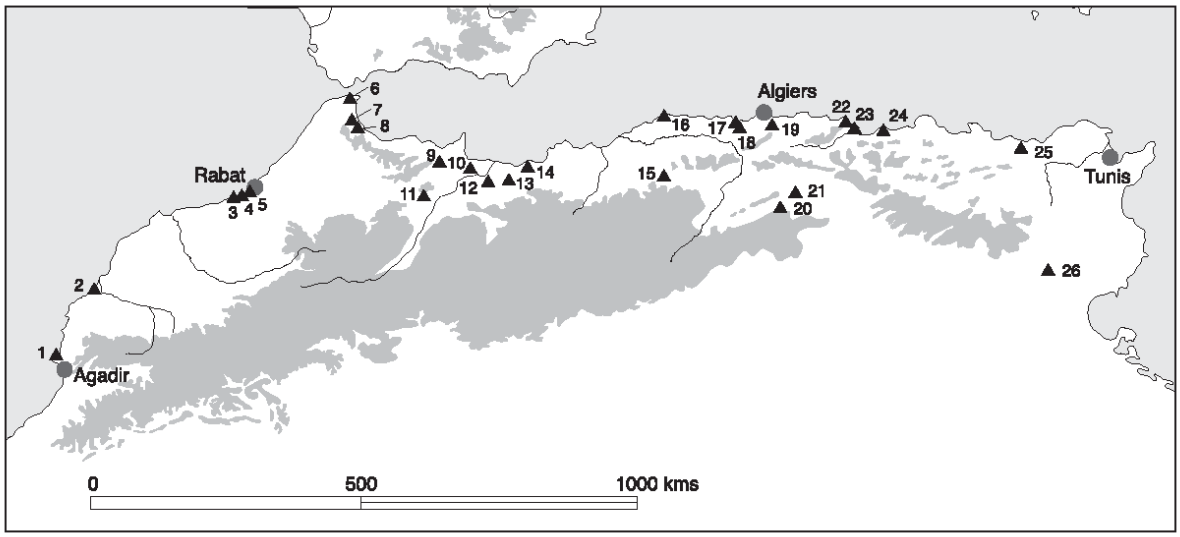

Figure 2.3: Distribution of Iberomaurusian sites in the Maghreb. 1) Cap Rhir, 2) El Khenzia, 3) Contrebandiers, 4) El Harhoura 2, 5) Dar es-Soltan I, 6) Ghar Cahel, 7) Kehf El Hammar, 8) Hattab II, 9) Ifri El Baroud, 10) Ifri n'Ammar, 11) Kifan Bel Ghomari, 12) Taforalt, 13) La Mouillah, 14) Rachgoun, 15) Columnata, 16) Cap Ténès, 17) Rolland, 18) Rassel, 19) Oued Kerma, 20) El Hamel, 21) El-Onçor, 22) Afalou Bou Rhummel, 23) Tamar Hat, 24) Taza, 25) Ouchtata localities, 26) Horizon Collignon (from Barton *et al*. 2013).

The Iberomaurusian marks a clear cultural change from the previous MSA (Barton et al., 2013; Bouzouggar et al., 2008; Lubell, 2001), yet the timing of this cultural transition is poorly understood because few archaeological sequences spanning c. 40-20ka are recorded (Linstädter et al., 2012). At sites such as Contrebandiers, El Harhoura 2 and Ifri n'Ammar (Dibble et al., 2012; Richter et al., 2010; Stoetzel et al., 2014) Iberomaurusian levels are observed to directly overly Aterian levels, yet improved chronological resolution is required to understand the relationship. The oldest dates for the Iberomaurusian in the Morocco were thought to be c. 21.5ka BP at Taforalt (Roche, 1976), yet the validity of these dates has been questioned due to the bulked materials dated (Bouzouggar et al., 2008). Recent radiocarbon dates from Iberomaurusian levels at sites in Morocco, including Gahr Cahal, Kehf el Hammar and Ifri el Baroud (Figure 2.3), show Iberomaurusian occupation began abruptly at c. 18-17ka BP and continued throughout the Late Glacial (Barton et al., 2005; Bouzouggar et al., 2008). Taforalt has been robustly dated using a high-resolution Bayesian radiocarbon age model, allowing the rare opportunity to examine the MSA/LSA transition in the Maghreb (Barton et al., 2013). The age model shows that the Iberomaurusian began at Taforalt between 22,093-21,420 cal BP with a 'gap' of at least 1900 years between the underlying MSA and the LSA Iberomaurusian. The sequence at Taforalt is also unique because the Iberomaurusian is preceded by a non-Levallois flake industry (which as yet has no known analogue in the Maghreb), not the Aterian, like other sites in the Maghreb. The MSA/LSA transition at Taforalt share similarities with this transitional period in other parts of Africa (Barton et al., 2013).

Little is know about the origin of the Iberomaurusian. Previous authors have suggested cultural links between it and the Epigravettian industries of the Italian peninsula (Ferembach, 1985). It has also been proposed that the industry was associated with pan-regional backed bladelet technologies that extended across much of North African and the Near East at c. 20-23ka BP (Close and Wendorf, 1990; Godfrey-Smith et al., 2003; Goring-Morris and Belfer-Cohen, 2003). More recently genetics have shed new light on the origins of the people associated with the Iberomaurusian industry in the Maghreb; two main hypotheses are proposed: 1) the culture originated in populations that spread from Cyrenaica (whose population have older roots in Southwest Asia) west into the Maghreb (Olivieri et al., 2006); 2) the culture developed independently in the Maghreb and moved eastwards with the expansion of the U6a1a lineages (Maca-Meyer et al., 2003). If the first hypothesis were reflected in the archaeological record it would be expected that the oldest Iberomaurusian should be found in eastern North Africa. Early dates have been provided from Egypt, but Barton et al. (2013) suggests that any interpretations from these dates should be tentative. Barton et al. (2013) also note that there is no blade industry, similar to the Dabban, preceding the Iberomaurusian in the Maghreb that might be expected if populations were migrating west across North Africa. Thus far the archaeological evidence appears to suggest that early Upper Palaeolithic blade technologies did not extend very far into the Maghreb, hinting that the Iberomaurusian culture did originate within the Maghreb.

The Iberomaurusian people are the first in the North African archaeological record to bury their dead in numbers hinting that they had a more sedentary lifestyle and/or larger populations. Skeletal remains show that Iberomaurusians were anatomically

modern and are attributed to the biologically distinctive populations of robust Mechta-Afalou human types (Camps, 1974; Ferembach et al., 1962; Humphrey and Bocaege, 2008). They also had complex and varied funerary practices with evidence for the inclusion of grave goods, staining bones with red ochre after decomposition, and possible dismemberment and defleshing practices (Belcastro et al., 2010; Humphrey et al., 2012; Mariotti et al., 2009, 2014). Almost all Iberomaurusian individuals in the archaeological record show evidence of tooth evulsion with removal of the upper central incisors (Humphrey and Bocaege, 2008). Morphometric analysis also reveals no strong similarities between Iberomaurusians and earlier Aterian populations suggesting a possible evolutionary discontinuity between both populations (Harvati and Hublin, 2012).

2.3. Archaeological sites

The archaeology, stratigraphy and chronology of the sites of interest, El Harhoura 2 and Taforalt (Figure 2.1), are described in the following section. Unfortunatley, quantitave methods that can be used as a proxy for occupation intensity or density are not available from Taforalt and El Harhoura 2. Therefore, in the absent of such data, the author uses the archaeologists's interpretation of occupation intensity (based on oberservations and archaeological artefacts and material within each level), which the author recognises to be subjective. The two main methods used to construct chronologies at El Harhoura 2 and Taforalt are OSL and radiocarbon dating. It should be noted that these dating methods differ. OSL dates the last exposure of the cave sediment to light (i.e. when it was buried by sediment), while radiocarbon dates the death of the organism (i.e. animal, plant) selected for dating.

In this thesis OSL dates are referred to in 'ka years' while all radiocarbon ages are reported either as 'cal BP' (calibrated dates) or 'ka BP' (uncalibrated dates). Wherever possible calibrated radiocarbon dates are reported, but uncalibrated radiocarbon dates are stated from archaeological and proxy terrestrial and marine records when used by authors in the original work. It should be noted that 'cal BP' and 'ka BP' are not directly comparable and differ by more than 1000 years.

2.3.1. Grotte des Pigeons (Taforalt)

Grotte de Pigeons, usually referred to as Taforalt, is located in northeastern Morocco ~40km from the Mediterranean Coast (34°48'38" N, 2°24'30" W) (Figure 2.1). The cave is situated 720m asl in the Beni Snassen mountain range within the side of a small hill overlooking the Zegzel Valley (Figure 2.4). It was formed by rekarstification of an earlier karstic deposit that consisted of travertines and fluvial conglomerates. Presently the cave has a large accessible entrance opening to the northeast. It is ~20m wide at the entrance and 25m deep with an interior floor area of ~>400 m^2 (Figure 2.5). The bedrock in the area comprises of steeply folded Permo-Triassic dolomitic limestones (Barton et al., 2013; Bouzouggar et al., 2007a). The cave also has fresh water supply with spring water rising out above the cave. Taforalt currently lies in the semi-arid Mediterranean climate zone receiving ~335mm mean annual precipitation. The mean annual temperature is 15.4°C with a seasonal gradient of ~16°C ranging from 8°C -24°C (Figure 2.6) (data from WorldClim climate model) (Hijmans et al., 2005). The vegetation around the cave consists of open forest/Mediterranean scrub and is dominated by *Tetraclinis articulata* and *Pinus halepensis* alongside *Quercus ilex* (Figure 2.4) (Bouzouggar et al., 2007a).

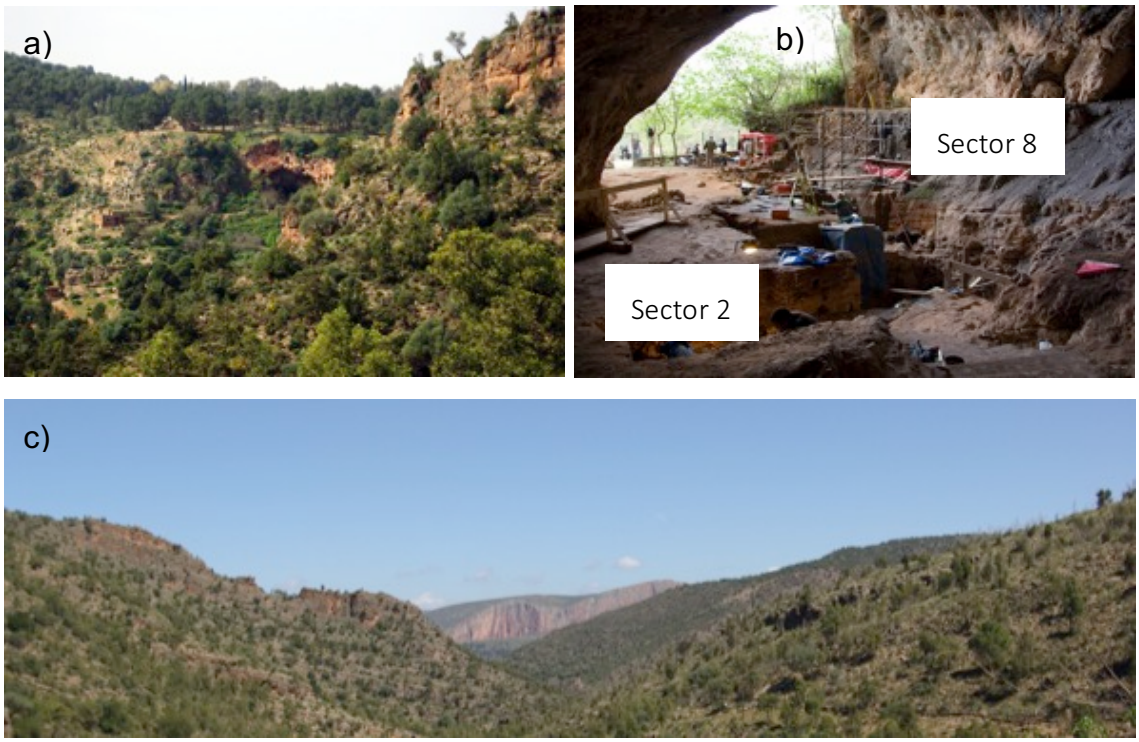

Figure 2.4: a) Taforalt cave, b) View from inside the cave looking out (courtesy of R.N.E Barton) showing sectors 2 and 8 from where gerbil teeth samples were collected, c) View from Taforalt looking down the valley.

2.3.1.1. Excavation history and stratigraphy

The cave was discovered in 1908 and has a long excavation history. The first major excavations took place 1944-1947, 1950-1955 and 1969-1977 (Roche, 1976, 1969, 1967, 1963, 1953), with further investigations carried out in the 1980's (Courty et al., 1989; Raynal, 1980). As a result of previous excavation activity a ~10m thick sediment sequence is exposed in the cave. The sediments have yielded typical MSA Aterian and LSA Iberomaurusian artefacts (Barton et al., 2013; Bouzouggar et al., 2007a; Roche, 1969, 1963), as well as Iberomaurusian human burials in two areas (Belcastro et al., 2010; Ferembach et al., 1962; Humphrey et al., 2012, 2014; Mariotti et al., 2014, 2009; Roche, 1976). The most recent excavations of Taforalt began in 2003 under the co-direction of A. Bouzouggar (Institut National des Sciences de

l'Archéologie et du Patrimoine Morocco) and R.N.E. Barton (University of Oxford). The most recent work in the cave involved excavation of exposed sequences. The project aimed to re-evaluate the site chronology and investigate the archaeological deposits within sediments (Barton et al., 2013).

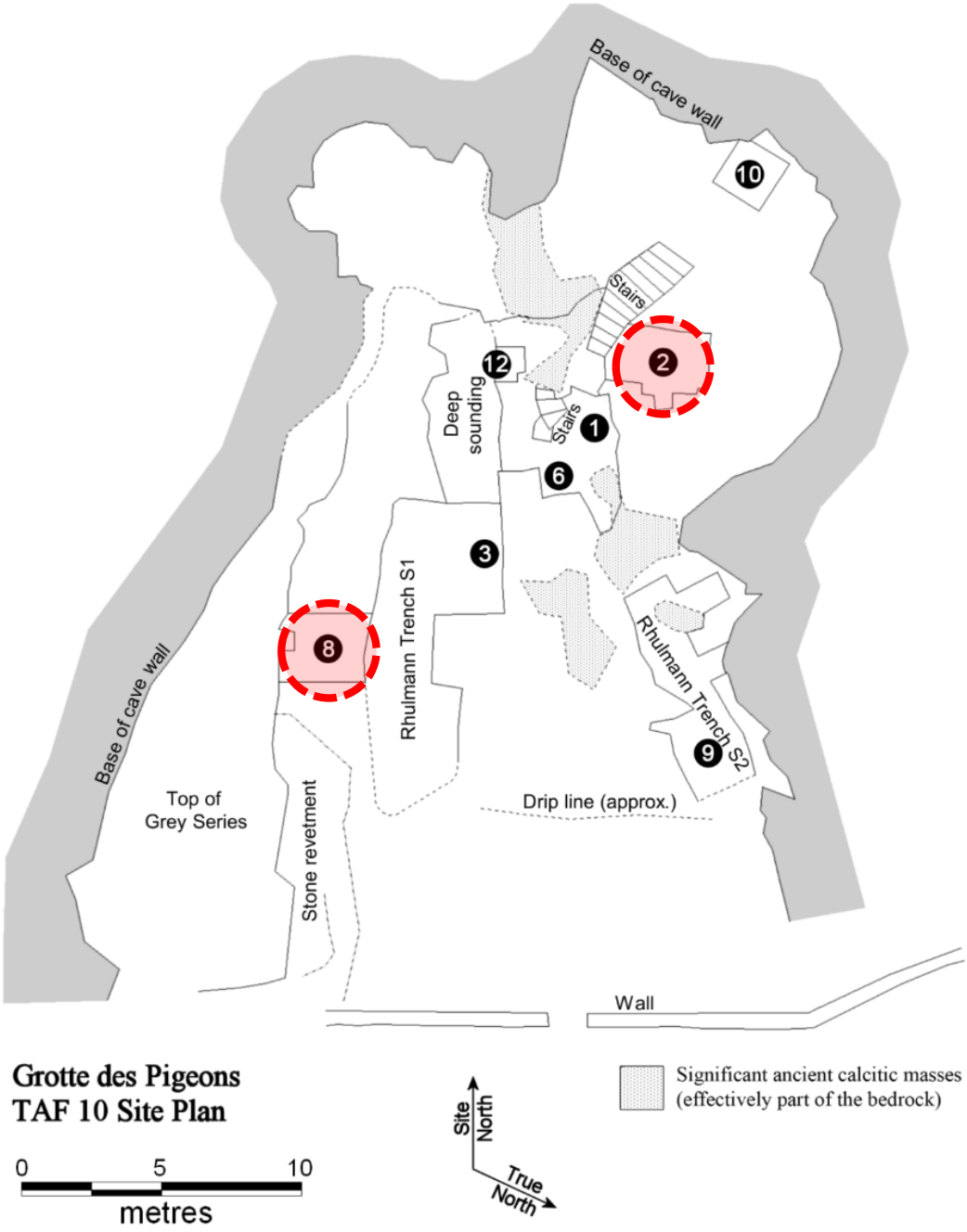

Figure 2.5: Floor plan of Taforalt showing the excavation sectors. The *Meriones* teeth selected for isotope analysis are from Sectors 8 and 2 (adapted from Fig. 2 in Barton et al. 2013).

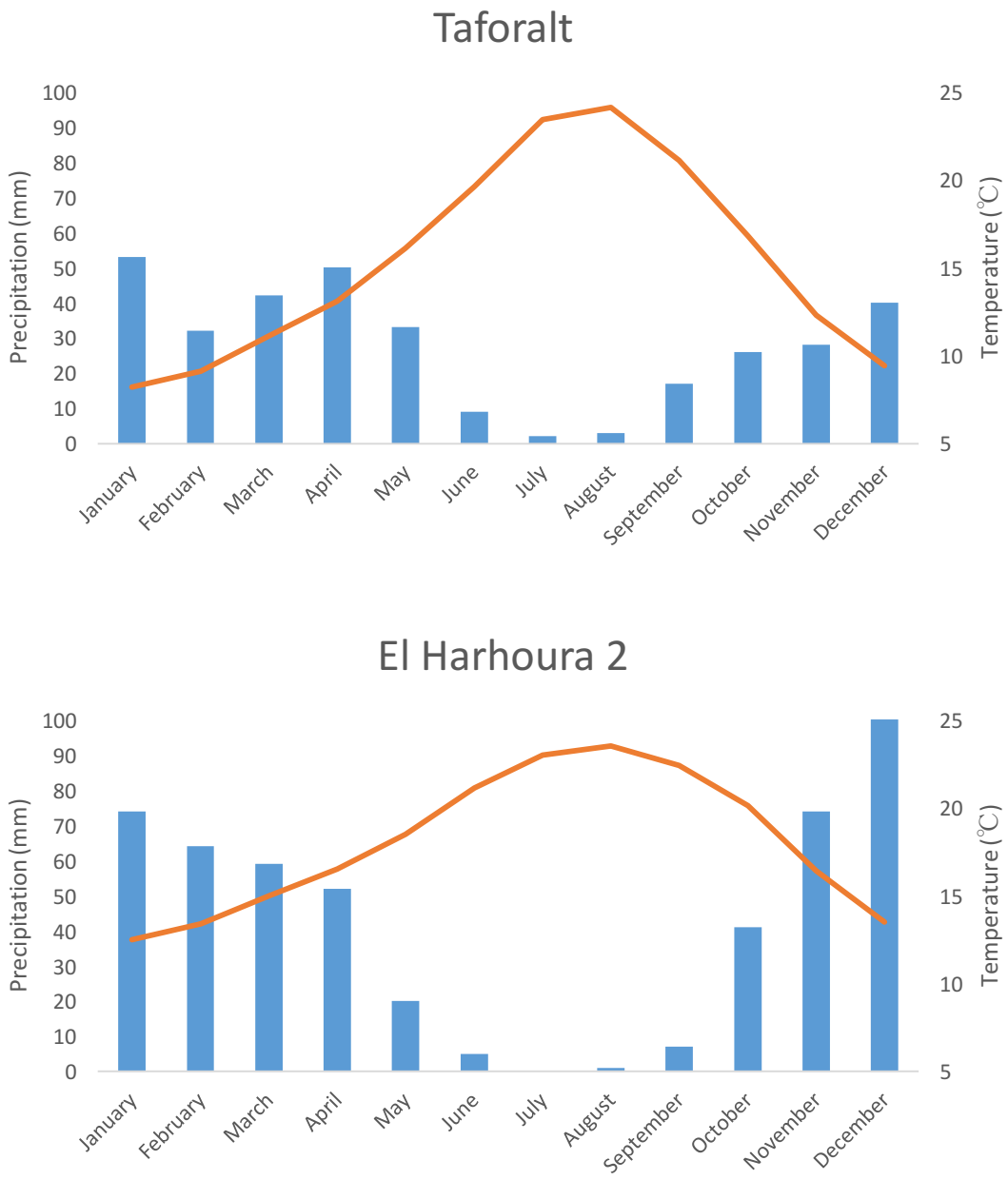

Figure 2.6: Graphs showing modern monthly temperature and precipitation at Taforalt and El Harhoura 2 (data from WorldClim model).

The most recent excavations defined five major sedimentological groups from the upper > 6m of cave infill, described by S. N. Collcutt and correlated with sediments originally described by Raynal (1980) (Figure 2.7). The uppermost group, the Grey Series, accounts for the top ~4m of cave sediments and is primarily composed of

ashy material derived from anthropogenic activity. The lower four groups comprise of ~2.5m of sediment and while there is archaeology present in most levels. The cave sediment in the Calcareous group, Lower Laminated Group, Pink Group and Upper Laminated Group are derived mainly form aeolian transport, with a small amount introduced by water-borne transport (S.N. Collcutt, *pers. comm*). The major groups are listed below in stratigraphic order from oldest to youngest and include summaries of sedimentological descriptions, archaeology, and chronology (Figure 2.7). The prefix 'R' is used if directly correlated with Raynal's layers (Raynal, 1980). The cave has several excavation areas referred to as sectors, which can be located in Figure 2.5.

Calcareous Group (R24-R32)

This is a laterally heterogeneous deposit consisting of interstratified densely cemented carbonate flowstones (approximately 0.5-2cm thick) interbedded with silty/sandy loams (Clark-Balzan et al., 2012). The unit contains MSA Aterian artefacts that include small Levallois cores, pedunculates and bifacial foliates (Bouzouggar and Barton, 2012). The flowstones and sediments from Sectors 1 and 6 of this unit have been dated using OSL and U-series and the results are consistent (Bouzouggar et al., 2007a; Clark-Balzan, 2012; Clark-Balzan et al., 2012). A Bayesian age model that included both the U-series and OSL dates predicted that in Sector 1 the Calcareous Group started to form at 109 ± 2.7ka (duration 12.3 kyr), while the deposition of the Calcareous Group in Sector 6 started later at 100.8 ± 4.0 ka (duration 15.7 kyr). The model infers that the Calcareous Group spanned 25.4 ± 3.7 ka and the boundary to the unit above (Lower Laminated Group) is 82.5 ± 2.8 ka

(Clark-Balzan et al., 2012). This unit was laid down in a time equivalent to MIS 5c to 5a.

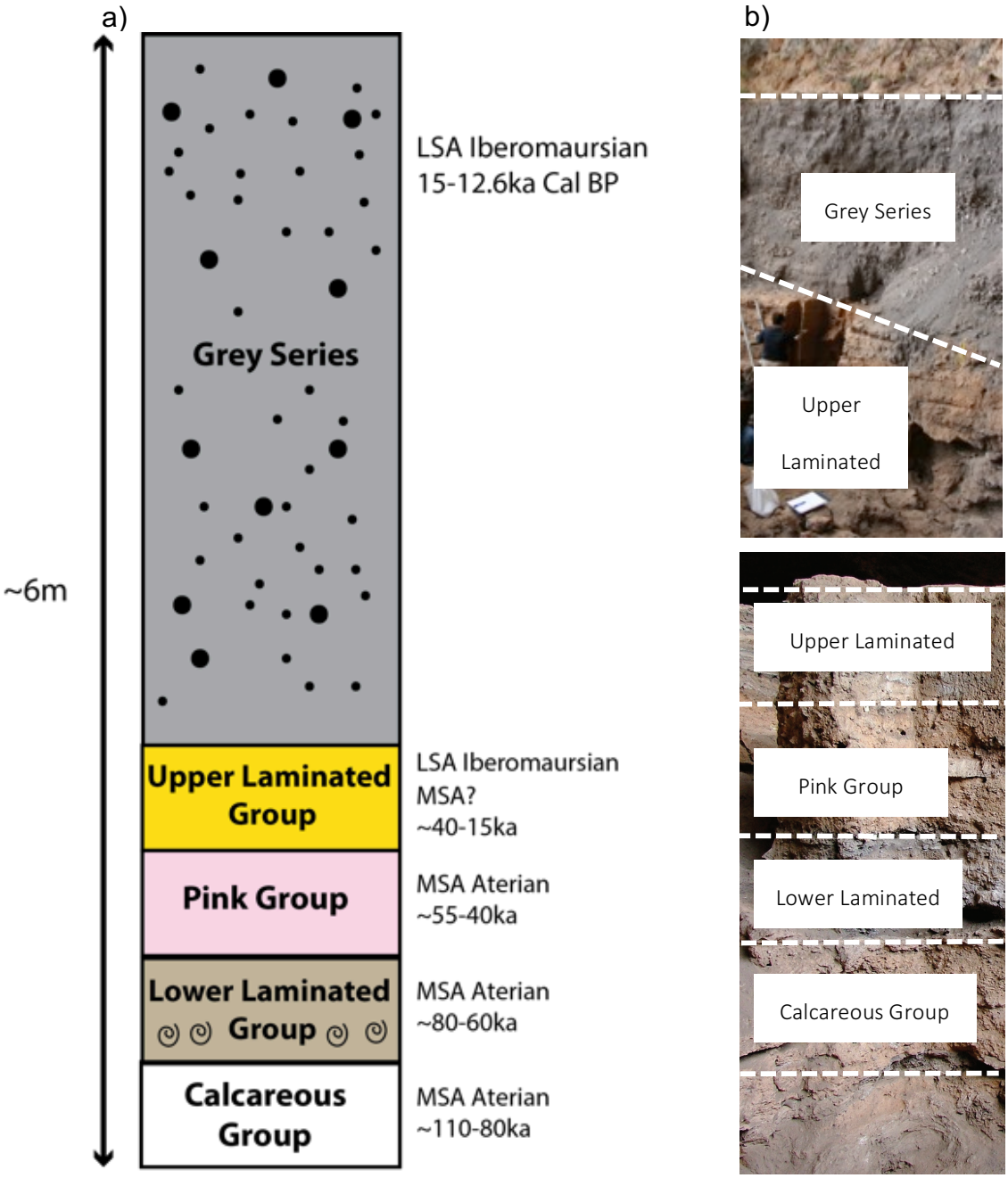

Figure 2.7: a) Schematic diagram of Taforalt stratigraphy compiled from several excavation areas, b) Photograph of Taforalt stratigraphy from Sector 1 and 2 (Sectors 1 and 2 can be directly correlated see Figure 2.5) (bottom) and Sector 8 (top).

Lower Laminated Group (R16-R23)

A dark to pale grey deposit that is coarsely laminated and intercalated with densely cemented beds of microsparitic calcite. The deposit consists of silty to fine sandy loams and is rich in ash (Clark-Balzan et al., 2012). Side scrapers, small radial Levallois cores and bifacial foliates, typical of the MSA Aterian, have been recovered from this unit (Bouzouggar et al., 2007a). *Nassarius gibbosulus* shells, that show evidence of stringing and traces of ochre pigments, (the majority of shells were excavated from R21) along with rich hearth deposits (suggestive of intensive occupation) are present in the lower laminated group (Bouzouggar et al., 2007a) OSL dates on the sediment and TL dates on burnt flints from Sectors 1, 2 and 6 produced a date range for the group of 84.5 ± 4.4- 48.7 ± 3.4 ka. The date range for the unit is reduced to 84.5 ± 4.4ka - 60.1 ± 3.9 ka (Bouzouggar et al., 2007a) if problematic micro OSL dates are not considered (see Clark-Balzan, 2012).

Pink Group (R12-R15)

A massive, clast rich deposit with small traces of lamination. In places this deposit is partly cemented and contains localised scour structures suggestive of running water (Clark-Balzan et al., 2012). This unit contains MSA lithics, similar to those found in the Lower Laminated Group (Bouzouggar et al., 2007a). OSL ages of between 54.9 and 44.3 ka have been obtained from this deposit from Sectors 1, 2 and 6 (Bouzouggar et al., 2007a; Clark-Balzan, 2012). A radiocarbon age of 42.4 ka confirms the younger OSL dates for this unit (Barton et al., 2014).

Upper Laminated Group (R1-R11) (Sector 2)/ Yellow Series (Y1-Y13) (Sector 8)

The Upper Laminated Group in Sector 2 and the Yellow Series in Sector 8 both refer to the same sedimentological group (Figure 2.5), but the group varies temporally across the cave. Sediments coeval with these Groups are also present in Sector 9 at the front of the cave. This is a finely laminated deposit dominated by fine to medium sands with varying amounts of dolomitic limestone debris containing both MSA and LSA archaeology (Barton et al., 2013). MSA lithic technology is present in the lower levels of the Upper Laminated Group. The youngest MSA Aterian occurs in Sector 9 (~29ka cal BP) after which there is a transition to a little understood non-Levallois flake industry that is present in Sectors 8 (Y4-Y6) and 2 (R3-R4) (Barton et al., 2016). The Iberomaurusian lithics at Taforalt has been subdivided into three technologically distinct lithic assemblages (IB1, IB2 and IB3), of which IB1 (units upper Y4-Y2) and IB2 (Unit Y1) are found in the Lower Laminated Group. The IB1 assemblage contains marginally backed ('Ouchtata') blades and bladelets, while IB2 is dominated by microlithic backed bladelets (Barton et al., 2013). Occupation in the Yellow Series was intermittent with sterile levels between occupation levels (Barton et al.2013).

A total of 54 AMS radiocarbon dates from Sector 8 have allowed the construction of a high-resolution Bayesian radiocarbon age model, which provides precise dates for important transitional periods in the cultural sequence (Figure 2.8). The age model shows that the non-Levallois flake industry persisted at Taforalt until c. 24.5 cal BP with Iberomaurusian people occupying the site from 21.1 ka. The age model demonstrates a clear 'gap' in occupation between the LSA people and the people

that made the non-levallois flake industry (Barton et al., 2013). The Bayesian model also predicts a date of 15,190-14,830 cal BP for the Grey/Yellow Series transition (Barton et al., 2013).

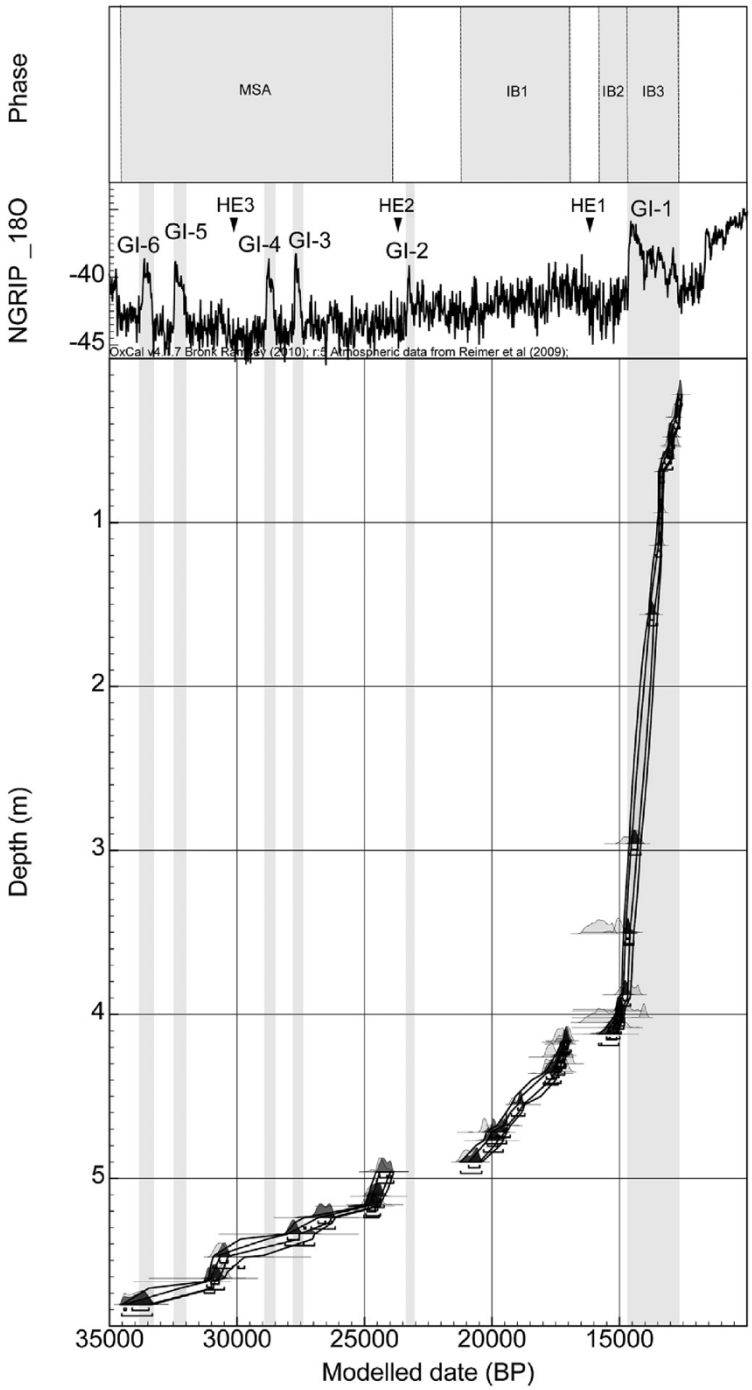

Figure 2.8: Age depth Bayesian model for Taforalt Sector 8 sequence (from Barton *et al*. 2013).

Grey Series

The Grey Series is an anthropological midden deposit consisting of ash, animal bone, terrestrial molluscs, plant remains, charcoal and burnt limestone. Although this group has a homogenous appearance some hearth features and layers of fire-cracked rocks are visible (Taylor et al., 2011). The group contains Iberomaurusian technology belonging to sub-group IB3 that is dominated by backed bladelets (Barton et al., 2013). Unretouched flakes and bladelets are also recorded in the IB3 assemblage, yet in smaller proportions relative to IB1 and IB2 (Yellow Series) (Barton et al., 2013). The Bayesian radiocarbon age model shows that the Grey Series was deposited between 15,000- 12,600 cal BP (Figure 2.8). The rapid deposition (estimated 1.7m/kyr) of the Grey Series is associated with intensification of activity at the cave involving more prolonged occupation periods and/or larger Iberomaurusian populations (Humphrey et al., 2014). Human burials including those of adults, children and infants are found in close proximity towards the rear of the cave (Ferembach et al., 1962; Humphrey et al., 2012; Roche, 1963). Large amounts of terrestrial molluscs with limited species diversity are also found in the Grey Series indicating the exploitation of terrestrial molluscs as a resource (Taylor et al., 2011).

The *Meriones* teeth selected for oxygen and carbon isotope analysis from Taforalt were sampled from Sector 2 and Sector 8 (Figures 2.4 and 2.5). The Sector 2 and 8 stratigraphy, chronology, and levels from which *Meriones* teeth were sampled are outlined in Chapter 6.

2.3.1.2. Palaeoenvironmental information from Taforalt

Several proxy records, such as macrocharcoal, phytoliths and faunal remains, have been used to infer palaeo-climate and environmental conditions at Taforalt. However, due to the nature of this material it is likely heavily influenced by human behaviour. The macrocharcoal record exists for the majority of the Late Pleistocene sequence, and importantly the samples are not associated with hearth deposits (Ward, 2007). The record shows the fluctuating presence of *Cedrus atlantica, Juniperus*/*Tetraclinis articulata*, *Quercus* and *Pinus*, indicating the consistent occurrence of woody taxa in the environment around the cave throughout this period (Ward, 2007). *Cedrus atlantica* and deciduous *Quercus* charcoal dominates in Lower Laminated Unit (Sector 2, Level R21) with the latter declining up the unit, inferring an increasing 'montane' with cooler and/or dryer conditions. Semi-arid conditions are confirmed by the presence of *Ctenodactylus* spp. (gundi), which presently lives in Mediterranean steppe and rocky environments south of Taforalt. Other fauna present in the Lower Laminated Unit includes, *Equus* sp. (equid), *Lepus capensis* (hare), and abundant micromammals such as *Crocidura* spp. (white-toothed shrew), *Elephantulus rozeti* (North African elephant-shrew), bat, *Gerbillus* sp. (gerbil), *Meriones* sp. (jird), *Mus spretus* (Algerian mouse) and *Eliomys quercinus* (garden dormouse), which are indicative of open and sparsely vegetated environments with some locally wooded habitats (Bouzouggar et al., 2007a).

The Bayesian radiocarbon age model for Sector 8 (Barton et al., 2013) allows the direct correlation of the Taforalt sedimentary and cultural stratigraphy with the Greenland Ice Core (NGRIP) $\delta^{18}O$ stratigraphy (proxy for past air temperature in Greenland) (Figure 2.8). Although climate events in Greenland cannot be directly

correlated with those in North Africa, the Greenland record can serve as a proxy for regional climate conditions within the North Atlantic region. The model demonstrates that the Grey Series began to accumulate in a time period equivalent to Greenland Interstadial 1, a period of climate amelioration across the North Atlantic region. An erosive break in the upper Yellow Series (Unit Y2) sediments imply a period of climatic instability, which appears to occur in a time equivalent to Heinrich Event 1 in the Greenland record; coincidently this also marks the time when the IB2 replaces the IB1 lithic assemblage. The age model has also identified a clear lag time between the start of the Iberomaurusian and the non-Levallois flake industry. This 'gap' is noted in the sedimentary record by finer silty sediment and the slowing of the sedimentation rate indicative of a cooler, drier climate (Collcutt in Barton et al., 2013). The 'gap' between the non-Levallois flake industry and LSA includes the time period equivalent to Greenland Stadial 2.

Micromorphological analysis of the cave sediment has also been undertaken on the levels covering the MSA to LSA transition (Courty and Vallverdu, 2001; Courty et al., 1989). Courty and Vallerdu (2001) identified rapid climatic shifts in the sediments and suggested that two discontinuities in the record (one at the Aterian/Iberomaurusian transition and one during Iberomaurusian occupation) correlated with Dansgaard-Oeschger and/or Heinrich events. But it has been difficult to match these observations in the sediments exposed during the most recent excavations (Jones, 2013). In addition the micromorphological work carried out by Courty and Vallerdu (2001) relies on an earlier Taforalt chronology that does not have the precision required to correlate sedimentological changes with millennial-scale climate variation.

The Grey Series and uppermost levels of the Yellow Series yielded large amounts of macro plant remains and phytoliths, although the palaeoenvironmental value of this information is questionable due to the anthropogenic nature of the Grey Series sediments. The phytolith record indicates vegetation variation across the Grey and Yellow Series (Jones, 2013). C_3 grasses dominate at the top of the Yellow Series, where there is a notable absence of woody taxa, indicating relatively arid conditions. There is a large C_4 vegetation component at the base of the Grey Series (c. 15ka cal BP), which along with the presence of *Atlantoxerus getulus* (Barbary ground squirrel) indicates open arid conditions (Bouzouggar et al., 2007a). C_4 vegetation decreases up the Grey Series indicating climate amelioration, with more woody taxa at the top of the Grey Series suggesting higher water availability (Jones, 2013). Plant remins are homogenous throughout the Grey Series probably because the plants were selected by humans for consumption and other uses (Humphrey et al., 2014). Common macro botanical remains found in the Grey Series include *Quercus ilex* (cupule), *Pinus pinaster* (seed, seed scale), *Juniperus phoenicea* (seed), *Pistacia terebinthus* (seed) and *Stipa tenacissima* (rhizome) most of which are present in the environment around Taforalt today (Morales *pers. comm*).

The Taforalt proxy climate and environment records generally show that the Yellow Series was deposited during a relatively cool, arid period, while the Grey Series was deposited during a period of climate amelioration with a relatively warmer, humid climate. The palaeoenvironmental information from the lower levels (Calcareous Group, Lower Laminated Group, Pink Group) is not continuous so only provides snap shots of information.

2.3.2. El Harhoura 2

El Harhoura 2 cave is located on the north Atlantic coast of Morocco in the village of El Harhoura, ~4km south of Rabat (33°57'08.9" N, 6°55'32.5" W) (Figures 2.1 and 2.9). The cave faces west overlooking the Atlantic Ocean and is ~300m from the current coastline, 18m asl (Nespoulet and El Hajraoui, 2012a; Nespoulet et al., 2008a, 2008b). El Harhoura 2 along with other archaeological caves in the Témara region of Morocco (Doukkala 1 and 2, Contrebandiers, El Mnasra, El Harhoura 1 and 2, Dar es Soltane 1 and 2) have similar geological histories forming during the MIS 6-MIS 5 transition, at c. 130ka, by karstic and/or marine erosion of the calcarenites (palaeocliff) (Campmas et al., 2015). El Harhoura 2 has a surface area of >20m^2 with a maximum length and width of 22m and 9m, respectively (Figure 2.9) (Campmas et al., 2015). The cave lies at the boundary between the sub-humid and the semi-arid bioclimate zones (Sauvage, 1963). El Harhoura 2 currently receives ~497mm mean annual precipitation. Mean annual temperature is ~18°C ranging from 12-24°C (data from WorldClim model) (Hijmans et al., 2005) (Figure 2.6); the oceanic influence reduces the daily and seasonal climate gradient. The mosaic landscape around the cave is dominated by *Quercus suber* part of the relict Mamora forest, but recent anthropogenic activity has reduced vegetation cover in the region (Joly, 1962). At periods of lower sea level during the Late Pleistocene El Harhoura 2 would have been further from the sea. As the continental shelf off northwestern Africa is relatively steep, calculations suggest between approximately 5 and 50km's of land would have been exposed at the LGM in this region. This suggests that El Harhoura

2 would have been several kilometres from the coastline throughout the Late Pleistocene (Collina-Girard, 2001; Lambeck and Purcell, 2005).

Figure 2.9: Photograph of El Harhoura 2 Cave (from El Hajraoui *et al*. 2012b).

2.3.2.1. Excavation history and stratigraphy

El Harhoura 2 was discovered by André Debénath in 1977 and two preliminary excavations were undertaken in 1978 and 1996. Since 2001 the site has been excavated by a Moroccan-French team under the direction of R. Nespoulet and M.A. Hajraoui (El Hajraoui et al., 2012b; Nespoulet et al., 2008a, 2008b). The main excavation area is located at the front of the cave (Figure 2.10). The cave sediments are mostly homogenous and dominated by sand derived from the disintergration of the calcarenite bedrock and aeolian wind input (Boudad et al., 2012; Nespoulet et al., 2008b; Niftah et al., 2005). The stratigraphy consists of 11 main archaeological levels determined on sedimentological observations and density of archaeological

material (Table 2.1, Figure 2.11). Preliminary sedimentological analyses by L. Boudad recognises 4 separate lithostratigraphic units that are correlated with the archaeological levels (Boudad et al., 2012). The levels are numbered from most recent Level 1 to the oldest Level 11. Levels 5-11 (the deepest part of the sequence) are recorded in a small excavation area (<2m^2) located at the front of the cave (Figure 2.10). Bedrock has not yet been reached in this area.

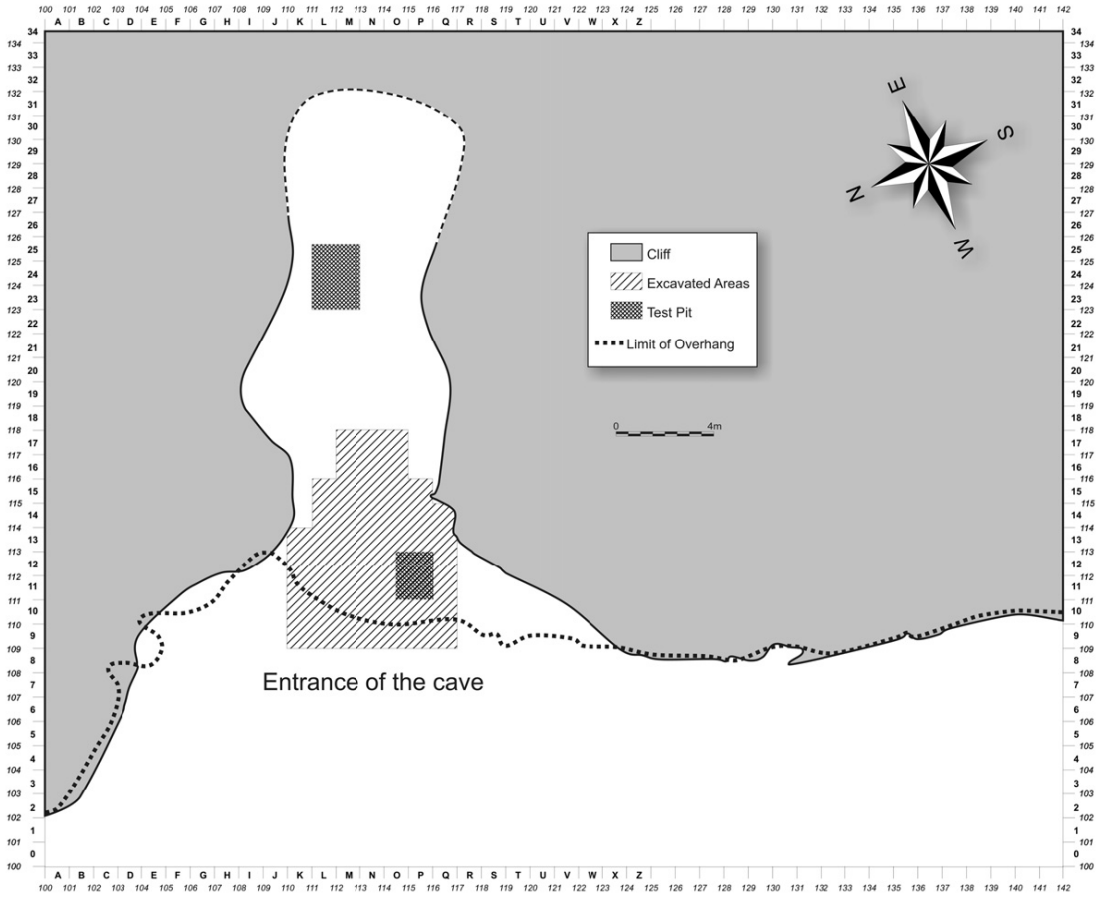

Figure 2.10: Floor plan of El Harhoura 2 showing excavation areas. The 'pit' shows the area in which the deeper levels were excavated (Levels 5-11). Each square represents 1m x 1m (from Stoetzel *et al*. 2011).

Levels 11-3 are attributed to the MSA Aterian with OSL ages from c. 120ka-50ka (Jacobs et al., 2012). Levels 5,7,9,10 and 11 have very low artefact densities and are classed as 'archaeologically sterile'. An Aterian attribution is suggested for the

MSA at El Harhoura 2, even though there is a notable absence of tanged pieces, because the lithic assemblage is similar to other Aterian assemblages in the Témara region. The composition of the lithic technology is homogenous from Levels 8-3. Levels 3 and 4a yielded levallois and micro-levallois technologies, laminar tools, side scrapers and chopping tools (Campmas et al., 2015; Nespoulet and El Hajraoui, 2012b). The composition of the lithic assemblage (low numbers of cores and debitage preparation, relatively high proportions of retouched tools) and low lithic densities in Levels 3 and 4a are indicative of short-term occupations of the site by small mobile groups (Nespoulet and El Hajraoui, 2012b). Whereas, Level 8 appears to have a relatively denser lithic assemblage suggestive of a more intense occupation/use of the cave (Campmas et al., 2015; Nespoulet and El Hajraoui, 2012b). Notably, *Nassarius* sp. shells (4 from Level 8 and 1 from Level 6) have been found in the MSA Levels at El Harhoura 2 (Stoetzel et al., 2014). OSL dates indicate three main periods of sediment deposition during the MSA occupation of El Harhoura 2 (Jacobs et al., 2012). The majority of the MSA sequence was deposited during MIS 5 (Levels 11-4b) from c. 120 to 100ka, while Levels 4a and 3 date to c. 70ka and c. 55ka, respectively. ESR-US ages have also been obtained from Levels 8, 5 and 4a; however these ages are significantly younger than the OSL ages from the respective levels (Janati-Idrissi et al., 2012) (Figure 2.11). Campmas et al. (2015) hypothesises that El Harhoura 2 was intensively occupied during MIS 5, when sea levels were relatively high. This is based on the presence of large numbers of limpet shells, Nassarius sp. shells, hearth features, relatively high lithic densities, and faunal material (brought to the cave by humans) within Level 8. It is suggested that small

mobile groups occupied the site for shorter periods during MIS 4 and 3, when sea levels were lower.

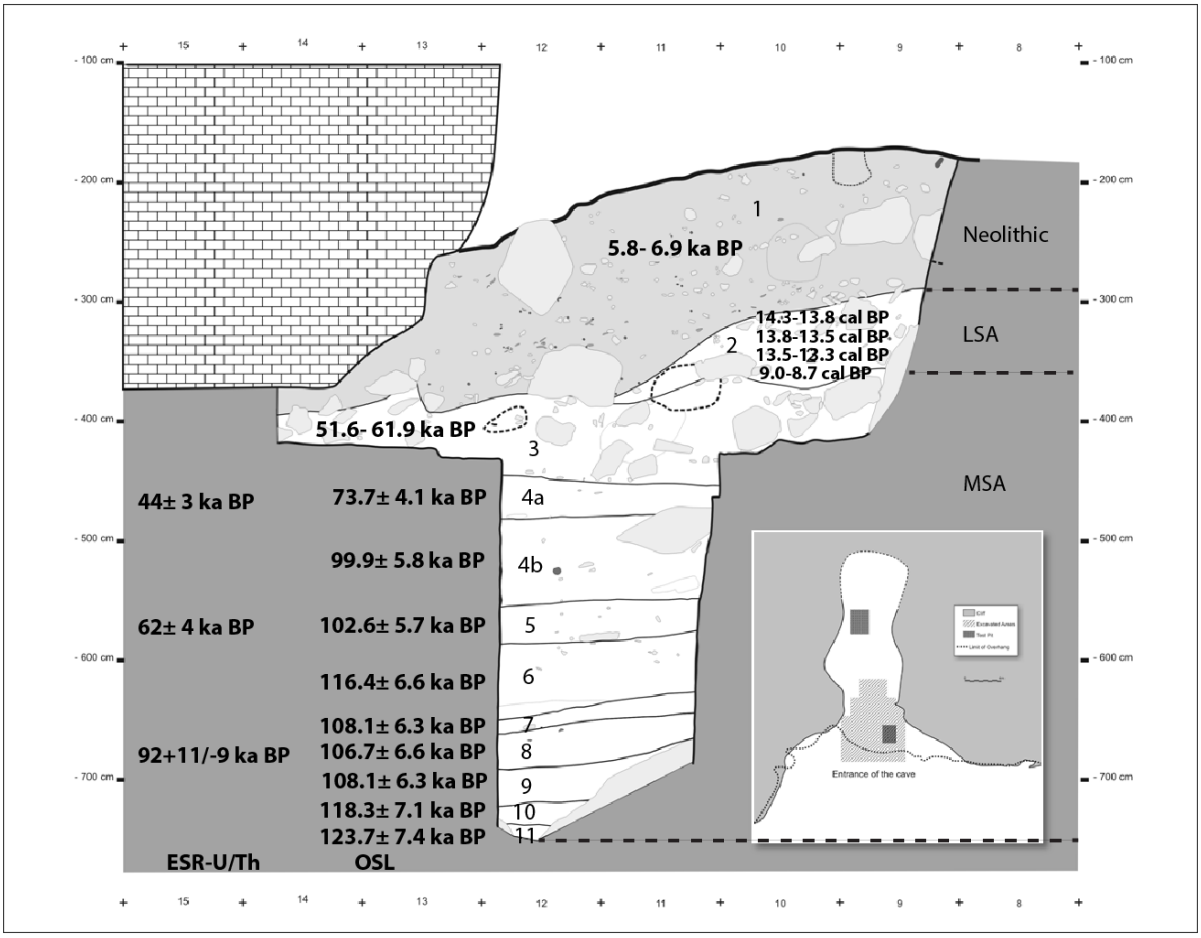

Figure 2.11: Diagram showing 11 stratigraphic levels at El Harhoura 2. The diagram shows the OSL dates from Levels 11-3, calibrated radiocarbon dates from material in Level 2 and ESR-US dates associated with Levels 8, 5 and 4a (adapted from Fig. 2 in Stoetzel et al. 2011).

Table 2.1: Sedimentology of stratigraphic levels at El Harhoura 2 (translated from Boudad et al. 2012)

Level	Thickness (cm)	Sedimentology	Colour	Description	Archaeology
1	110	Fine, ashy	Greyey black	Sediment rich in shells and small stones (<20cm). Contains burnt sandstone.	Neolithic
2	60	Coarse sandy clay	Yellowish	Several small stones and larger rocks (>20cm). Collapsed cave wall resting on top of Level 3	LSA Iberomaurusian
3	49	Very fine sandy clay	Light red brown to reddish orange	Several small stones and larger rocks (>20cm).	MSA Aterian
4a	30	Very fine sandy clay	Light greyish brown. Traces of manganese.	Large boulder resting on the top of Level 4b.	MSA Aterian
4b	69	Fine sandy clay	Reddish brown	Rich in shell fragments.	MSA Aterian
5	33	Coarse sandy clay	Yellowish with brown lenses	Sediment contains few stones.	MSA Aterian
6	46	Fine sandy clay	Red with brown lenses	Sediment contains few stones (maximum size <1 cm)	MSA Aterian
7	12	Very fine sandy clay	Reddish brown	Sediment contains few stones (maximum size <1 cm)	MSA Aterian
8	19	Fine sandy clay	Reddish brown	Rich in Patella (limpets)	MSA Aterian
9	30	Fine sandy clay	Reddish brown	Fragements of snail shells	MSA Aterian
10	34	Fine sandy clay	Reddish brown	Presence of shell and microfauna	MSA Aterian
11	56	Fine sandy clay	Reddish brown		MSA Aterian

Level 2 contains lithic material characteristic of the LSA Iberomaurusian (blades and bladelets) (Nespoulet and El Hajraoui, 2012b). This level has also yielded human remains, including one large robust individual displaying dental evulsion of the first upper incisors (Oujaa and Lacombe, 2012). Although level 2 sediments are not dated directly there are three radiocarbon dates on human bone cut into Level 2, and one radiocarbon date on charcoal from the level (the charcoal date is considered too young) (Nespoulet *pers. comm*) (Table 2.2). It must be noted that the dates on human bone may be younger than the Level 2 sediments, and therefore the microfauna accumulations, as it is unknown how long after the deposit formed that human remains were buried in it. Therefore, the dates from the human bone will act as an age minima for Level 2 and will help constrain the date. OSL and radiocarbon dates demonstrate that this Level dates between c. <50ka and >13.5ka cal BP (Table 2.2). Yet, because Level 2 yields LSA material it can be assumed that it is likely to date to <20ka based on dates from other LSA Iberomaurusian sites in the Maghreb (Barton et al., 2013, 2005; Bouzouggar et al., 2008). Level 1 contains archaeology dating to Neolithic and later periods. The Neolithic assemblage is radiocarbon dated to 5,800 ± 150 BP and has yielded lithics, ceramics and at least 14 individual human burials (Amans, 2012; Daugas, 2002; El Idrissi, 2012; Nespoulet and El Hajraoui, 2003; Nespoulet et al., 2008a, 2008b; Oujaa and Lacombe, 2012). The microfauna assemblage from Level 1 is not considered in the thesis.

The *Meriones* teeth selected for stable isotope analysis from El Harhoura 2 were sampled from Levels 11-2 (Figure 2.11). Detailed sampling methodology is described in Chapter 6.

Table 2.2: Table listing radiocarbon dates from material found in Level 2 at El Harhoura 2. Dates were calibrated in Oxcal v. 4.2 (Bronk Ramsey 2009a) using the IntCal13 calibration curve (Reimer et al., 2013).

Material used for radiocarbon dating	Uncalibrated radiocarbon date (14C years)	Calibrated dates (2σ) (Years cal BP)
Human bone	12,190 ± 60 BP	14,265-13,845 cal BP
Human bone	11, 870 ± 60 BP	13,815- 13,546 cal BP
Human bone	11, 570 ± 60 BP	13,543-13,279 cal BP
Charcoal	8,010 ± 40 BP	9,011-8,725 cal BP

2.3.2.2. Bayesian model of OSL dates

The El Harhoura 2 OSL chronology contains age reversals in the lower part of the sequence (Figure 2.11). In addition to this the Level 3 OSL dates are associated with a large age range probably reflecting the uncertainty from the mixing observed in samples and correction of the beta dose rate (Jacobs et al., 2012). Here, Bayesian modelling is used by the author in an attempt to deal with the chronological uncertainties in the lower part of the sequence and to improve the error range in Level 3.

Bayesian modelling combines prior known stratigraphic/archaeological information about a site with dates (in this case OSL dates) to improve the precision and accuracy of the site chronology. The program OxCal v.4.2 was used to build the Bayesian model (Bronk Ramsey, 2009a). A 'Sequence' deposition model (Ramsey, 2008) was constructed using the OSL dates from El

Harhoura 2 previously published by Jacobs et al. (2012) (Appendix 1.1). The 'Sequence' model suggests the relative order of chronological events and is based on the principles of stratigraphy; no further assumptions are made between samples, for example depth information. A 'Sequence' model is suitable in a cave environment where sediment deposition is non-continuous and there are likely to be hiatuses in the sedimentary record. The six OSL dates from Level 3, which have a date range from 62 ± 4ka to 52 ± 4ka, are included in a 'Phase' within the Bayesian model. A phase is an ordered series of activity, but within the phase the material can be unordered. Formal outlier analysis was used to account for any outliers in the model (Bronk Ramsey, 2009b). If any outliers are identified the overall model is not affected by the extreme value. Each measurement is assigned a prior probability of 5% for being an outlier.

The Bayesian Age model is presented in Figure 2.12, while the model output is presented in Table 2.3. None of the OSL dates used in the model were identified as statistically significant outliers (Appendix 1.2). The model output shows that Levels 11-4b were all deposited during MIS 5 over an 18,000 year period between c. 116 and 100ka. There is a hiatus in the record between Level 4b and 4a with 4a dating to MIS 5/4. The age model provides a date range for Level 3 from 63.3 ± 7.8ka to 51.3 ± 7.4ka. The Bayesian modelled OSL dates from El Harhoura 2 improve the chronology in the lower part of the sequence.

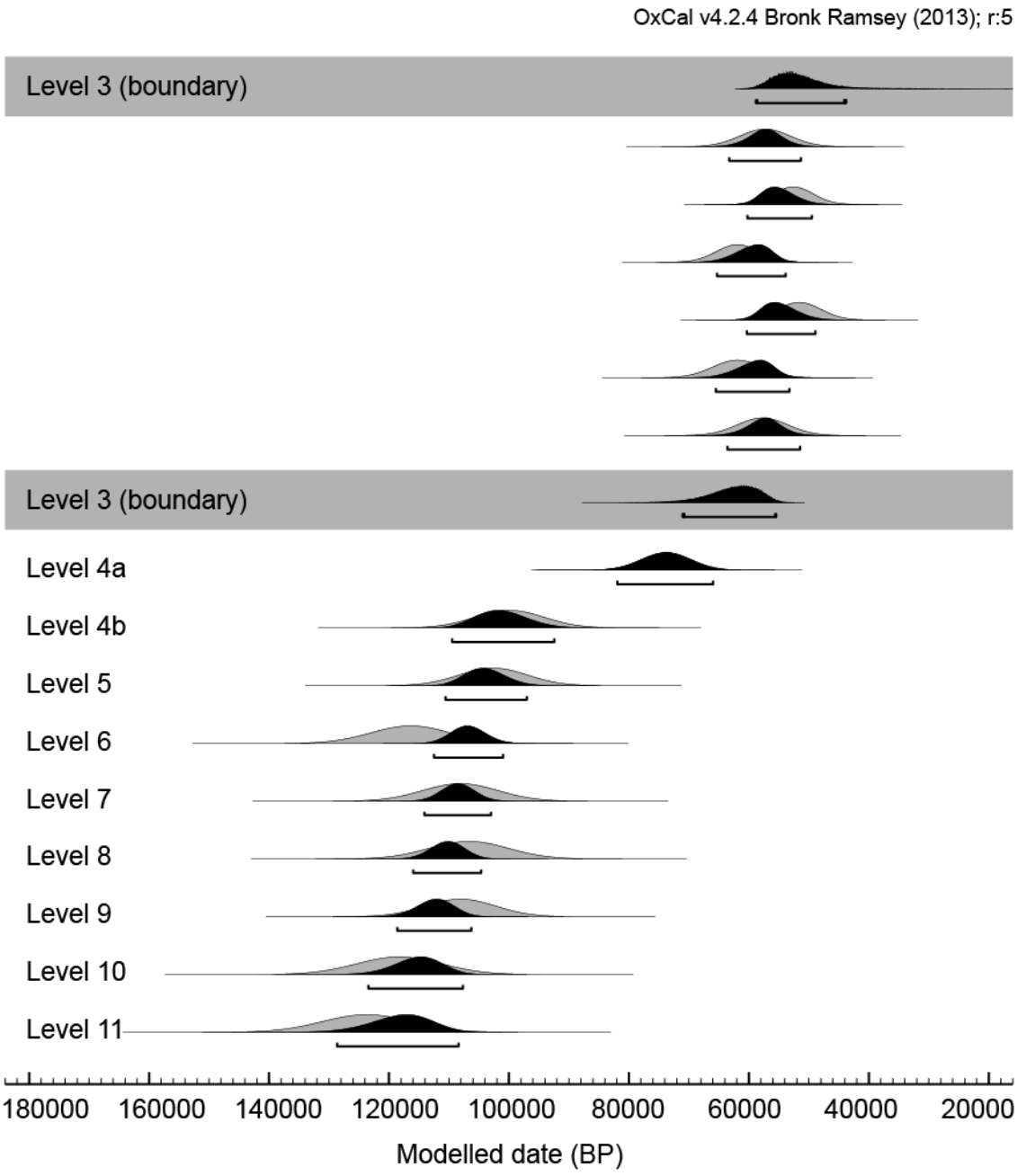

Figure 2.12: Bayesian Age Model of OSL dates (Jacobs et al. 2012) from El Harhoura 2. The grey shaded area shows that OSL date while the black area shows the modelled date (2σ).

Table 2.3: Table presenting the OSL dates and modelled ages (2σ) from El Harhoura 2 (see Figure 2.11 and Appendix 1.1).

Date	Depth (cm)	Level	Unmodelled date (ka) (Jacobs et al. 2012)	Modelled date BP (2σ) (this thesis)
Phase boundary				51.3 ± 7.4
EH09-10	503	Level 3	57.3 ± 4.2	57.3 ± 6.0
EH09-4	462	Level 3	52.6 ± 3.3	54.8 ± 5.4
EH08-10	400	Level 3	61.9 ± 3.5	59.6 ± 5.8
EH09-2	402	Level 3	51.6 ± 3.6	54.6 ± 5.7
EH09-1	406	Level 3	61.9 ± 4.1	59.4 ± 6.2
EH09-3	442	Level 3	57.7 ± 4.2	57.5 ± 6.1
Phase boundary				63.3 ± 7.8
EH08-9	475	Level 4a	73.7 ± 4.1	74.0 ± 8.0
EH08-8	532	Level 4b	99.9 ± 5.8	100.9 ± 8.5
EH08-7	574	Level 5	102.6 ± 5.7	103.8 ± 6.8
EH08-7	613	Level 6	116. 4 ± 6.6	106.7 ± 5.7
EH08-5	648	Level 7	108.1 ± 5.9	108.5 ± 5.5
EH08-4	686	Level 8	106.7 ± 6.6	110.3 ± 5.6
EH08-3	719	Level 9	108.1 ± 5.9	112.4 ± 6.2
EH08-2	755	Level 10	118.3 ± 7.1	115.5 ± 7.8
EH08-1	789	Level 11	123.7 ± 7.4	118.4 ± 10.3

2.3.2.3. Palaeoenvironmental information from El Harhoura 2

The large and small vertebrates remains from El Harhoura 2 have been studied extensively. As well as investigating the taphonomy of the assemblages, the remains have been used to indicate palaeoenvironment in the region based on faunal abundance methods (Michel et al., 2010, 2009; Stoetzel, 2009; Stoetzel et al., 2014, 2012, 2011, 2010). The analysis of faunal remains has focussed on Levels 1-8 (excluding 4b), while the faunal material from Levels 9-11 is yet to be studied. The stable isotope analysis of the *Meriones* teeth will provide the first palaeoclimate information from the lower Levels at El Harhoura 2 (Levels 9-11).

The small mammal assemblage at El Harhoura 2 is extremely large (> 30,000 fragments) (Stoetzel, 2009; Stoetzel et al., 2011, 2010). Notably there is little species turnover in the small mammal populations throughout the Late Pleistocene. The same five taxa (*Mus* cf. *spretus*, *Gerbillus campestris*, *Meriones shawii/grandis, Crocidura* spp and an indeterminable bat species) are present in all of the studied levels, hinting that this region may have provided a relatively stable environment, possibly a refugium, during the Late Pleistocene. The Level 8 fauna suggests a mainly open environment, yet relatively humid conditions are inferred from the presence of *Bufo bufo*, *Pleurodeles* cf. *walti* and *Natrix marura*. The presence of *Jaculus* sp. (not present in the region today), lower numbers of large- and medium-sized mammals and lower proportions of Bovinae relative to gazelles and Alcelaphinae are all indicative of a more arid-open environment in Level 7. The Taxonomic Habitat Index (THI), based on presence/absence of the small mammal taxa, also indicates an increase in

open environments and a decrease of wetland environments in Levels 7 and 5. The fauna infer that Levels 3, 4a and 6 were more open and arid than present conditions, but relatively more humid than Levels 5 and 7. Low numbers of amphibian fauna (no humid indicators species such as *Bufo bufo*, *Discoglossus pictus*) as well as a decrease in Bovinae and increase of gazelles and Alcelaphinae indicate arid conditions in Level 2.

The faunal material suggests that conditions were relatively humid in Level 8, while the environment was more arid and open in Levels 7, 5 and 2. The oxygen and carbon isotope analysis of the *Meriones* teeth will provide a further record of palaeoclimate and palaeoenvironment that will complement the traditional faunal abundance methods.

2.4. North African Archaeology and Palaeoclimate

The previous sections in this chapter show that both the MSA and LSA in the Maghreb existed on timescales extending over glacial/interglacial timescales, when it is known there were major changes to environments in North Africa with the expansion and contraction of the Sahara Desert (Blome et al., 2012; Drake et al., 2013). Palaeoclimate records also infer humid/arid climate fluctuations in the Mediterranean climate zone of North Africa during the occupations of both Taforalt and El Harhoura 2 (Bout-Roumazeilles et al., 2007; Moreno et al., 2005) (see discussion in Chapter 3). This raises questions concerning human occupations on the periphery of the Sahara Desert and human responses to climate and environmental change in this region. These questions remain

largely unexplored in North Africa due to a lack of stratigraphic archaeological deposits associated with palaeoclimate and palaeoenvironmental records.

It has been proposed that the MSA Aterian in North Africa is associated with humid climate episodes (e.g Debénath et al., 1986; Tillet, 1995) or alternatively is an adaptation to arid environments evidenced from the geographic proximity of sites to water sources (Garcea, 2012a, 2012b, 2004). Hypotheses about MSA Aterian adaptations are hard to justify because of the enormous geographic area covered, different bioclimate zones, the long temporal period and often poor chronological control associated with the technocomplex in North Africa (Figure 2.1). Hypothesis testing related to human adaptations to climate and environment are better tackled on small spatial scales, at sites that lie within the same bioclimate zone. For example, recently revised chronologies at several Moroccan Atlantic coast cave sites have allowed direct comparisons between human occupations and palaeoaridity records from two marine cores located off the northwest coast of Africa between 10° and 20°N (Jacobs et al., 2012). OSL dates from El Harhoura 2, El Mnasra, Contrebandiers, Dar es-Soltan 1 and Dar es-Soltan 2 (Figure 2.1) appear to show that Aterian occupation of cave sites on the Atlantic coast of Morocco were associated with humid climate episodes within MIS 5 and 3, while some sites appear to have been abandoned by humans during MIS 5b, a period marked by greater aridity (Jacobs et al., 2012; Stoetzel et al., 2011). However, Jacobs et al. (2012) compared human occupations in the Mediterranean region of North Africa, influenced by the westerly systems, with palaeoclimate records from the Sahara

and Sahel regions, which are controlled by low-latitude monsoon systems (see Chapter 3 for further discussion).

The Sector 8 Bayesian age model at Taforalt (Figure 2.8) has also allowed comparisons between the cultural sequence and palaeoclimate records; however in the absence of a high-resolution North African palaeoclimate record, correlations are made with the Greenland Ice Core record. It indicates that the MSA persisted into MIS 3/2 and that cultural change from the MSA to Iberomaurusian occurred around a time equivalent to the Last Glacial Maximum (24-22 ka cal BP), a period of climatic deterioration across the Northern Hemisphere (Barton et al., 2013). Palaeoenvironmental evidence from Iberomaurusian levels at other sites in the Mediterranean climate zone of Morocco, such as El Harhoura 2 and Contrebandiers, also infer that conditions were more arid relative to the preceding Aterian levels (Aldeias et al., 2014; Stoetzel et al., 2014, 2011).

Revised chronologies at Moroccan archaeological cave sites hint that changes in human cultural behaviour in North Africa may to be associated with major changes in the climate system. They also hint that the MSA Aterian could be associated with humid climate episodes. Yet, as well as further refinement of the chronology at archaeological sites, local palaeoclimate records that can be directly correlated with cultural sequences are required to understand human responses to climate and environmental in the region. In order to address this the thesis will construct terrestrial proxy climate records for Taforalt and El Harhoura 2 (Section 2.3) using oxygen and carbon stable isotopes in *Meriones* teeth at each site. The records from Taforalt and El Harhoura 2 are notable

because they both record periods of cultural stasis during the MSA Aterian for >50ka, while the cultural transition from the MSA to the LSA appears to occur during a period of climatic fluctuation.

2.5. Summary

This chapter has provided a brief introduction to Stone Age Archaeology in North Africa. The archaeology and stratigraphy of cave sites El Harhoura 2 and Taforalt are also described in detail with summaries of previous palaeoenvironmental information from each site. The final section of the chapter highlights the lack of local terrestrial palaeoclimate and palaeoenvironment records in North Africa that can be used to draw connections with cultural sequences. It shows that Taforalt and El Harhoura 2 are crucial for exploring human cultural responses to climate and environmental change because they both have long, well-dated Late Pleistocene sequences with human occupation dating to >100ka. The next chapter describes the climatology of North Africa and summarises Late Pleistocene palaeoclimate and palaeoenvironment in the Western Mediterranean and Sahara regions from marine and terrestrial records.

3. Palaeoclimate in North Africa

3.1. Introduction

Chapter 3 provides an overview of current understanding of present and past climate systems in North Africa. Firstly, the mid- and low-latitude influences on present climate systems in North Africa are summarised. Following this, modern vegetation in northwestern Africa is described. Modern climate and vegetation distributions form the context for the modern isotope ecology study (Chapter 5), but more importantly provide clues as to the climate and environmental shifts that may have occurred in the region during the Late Pleistocene. The second part of the chapter summarises current understanding of Late Pleistocene palaeoclimate and palaeoenvironment using evidence from North African and western Mediterranean marine and terrestrial proxies. The chapter makes a distinction between the Mediterranean coastal and the Sahara Desert region of North Africa, because differing mid- and low-latitude climate systems influence each region.

3.2. Modern climate and vegetation in North Africa

3.2.1. Modern climate systems in North Africa

3.2.1.1. Mediterranean climate system

North Africa has a narrow fringe on the northern and northwestern coasts that experiences a Mediterranean temperate climate, consisting of dry, warm summers, and mild, humid winters (Allen, 2001) (Figure 3.1). Mean annual precipitation, in excess of 250mm, is brought to the region on the predominant

westerly winds during the winter and spring months, as a result of the southward movement of the sub-tropical high-pressure belt (Rohling et al., 2009). In summer sub-tropical high pressure is displaced northwards and the majority of the Mediterranean experiences drought conditions. Along the Moroccan and Algerian coasts of North Africa humid air masses generally originate in the North Atlantic (Ouda et al., 2005; Rohling et al., 2009), and the climate has more of a maritime influence, with higher annual temperatures and rainfall (Harding et al., 2009). Cyclogenesis also occurs in the Mediterranean Basin itself with air masses tracking from west to east, but these are smaller and weaker than North Atlantic storm tracks that enter the Mediterranean region (Allen, 2001). In spring, depressions form at the lee of the Atlas and track north eastward or eastward along the Mediterranean coast of North Africa. As these storm tracks originate from the Sahara they do not carry precipitation, but instead are associated with hot winds and dust storms (Ulbrich et al., 2012). The predominant wind directions are north-westerly during the winter, with southerly and south westerly wind occurring during the summer associated with a weakening of the westerlies (Fletcher et al., 2010a).

Several teleconnections influence climate variability in the Mediterranean region; one of which is North Atlantic Oscillation (NAO). Oscillations in NAO are caused by differences in atmospheric pressure between the Azores high and the Icelandic low-pressure cells located over the North Atlantic. When there is a large pressure gradient between the two atmospheric pressure cells, NAO is in positive phase, this results in drier winters over the Mediterranean region as the westerlies intensify and occupy a more northerly latitude. In negative phase,

when pressure over the Azores and Iceland is similar, the westerlies are weaker and are situated in a more southerly mid-latitude position bringing more precipitation to the Mediterranean and North Africa. NAO varies on a decadal scale and is responsible for present day climatic variability within the Mediterranean region (Rohling et al., 2009). Studies show that NAO has had an influence on winter precipitation in Morocco over the past 500 years (Pauling et al., 2005), demonstrating that climate systems in Morocco are in phase with those in the North Atlantic region.

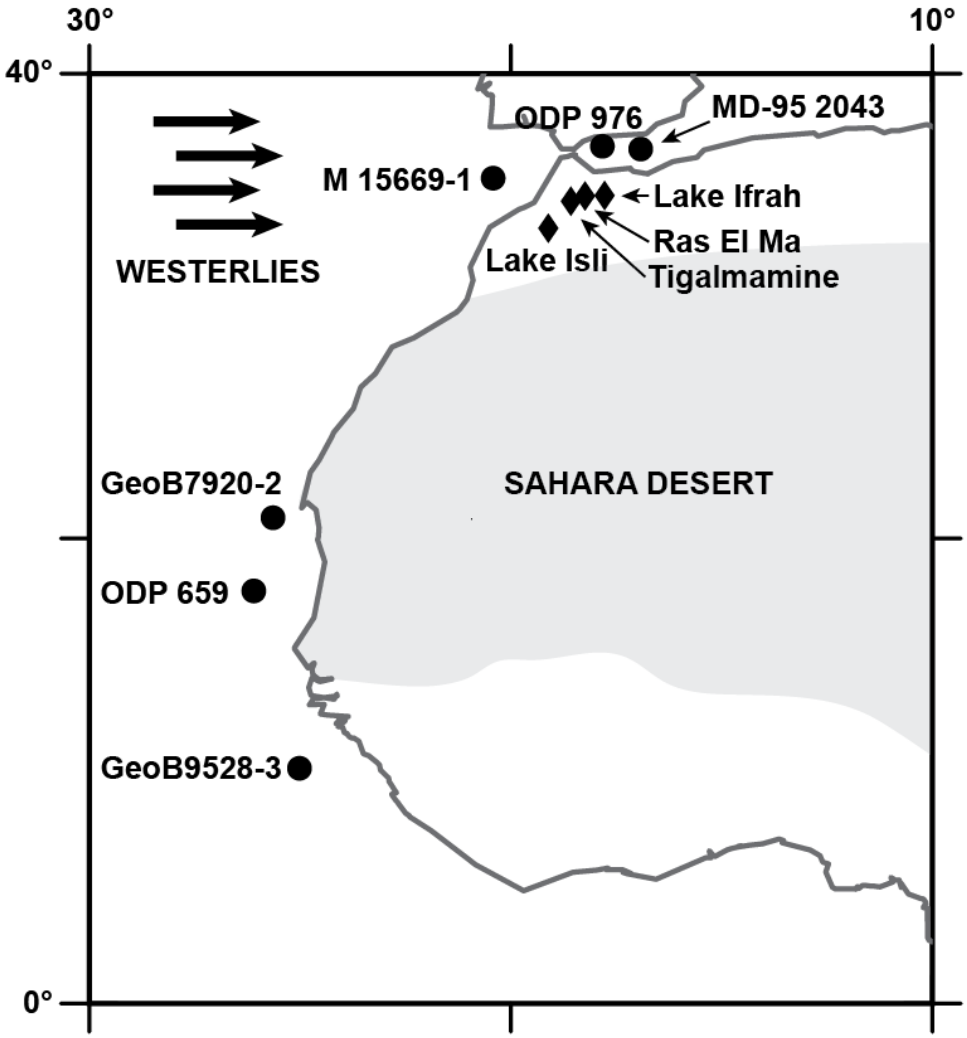

Figure 3.1: Map of Northwestern Africa showing the marine core records (circles) and North African lake records (diamonds) discussed in the text.

3.2.1.2. The West African Monsoon

The Sahara Desert is hyper arid and receives very little precipitation. Climate in the Sahara is influenced by the low-latitude monsoonal system (Figure 3.1). The inter-tropical convergence zone (ITCZ) is responsible for bringing moisture to tropical West Africa, where it is referred to as the monsoon trough. The position and form of the monsoon trough is determined by the difference in density between maritime air from the Atlantic, and tropical continental air from the Sahara Desert. In northern hemisphere summer, a broad low-pressure zone is created that drives the inflow of moist maritime air from the tropical Atlantic, pushing the monsoon trough northwards. Presently, the monsoon reaches its most northerly position of ~20°N in August bringing monsoon rains to the semi-arid Sahel region. During the winter the winds reverse and the monsoon trough shifts southwards towards the equator when North Africa is under the influence of dry Saharan air (see Buckle, 1996; Leroux, 2001; McGregor and Nieuwolt, 1998).

3.2.2. Modern vegetation in North Africa

The vegetation of northwestern Africa is characterised and summarised by White (1983), Hooghiemstra *et al.* (1992) and McGregor *et al.* (2009) with three main vegetation zones identified: 1) Mediterranean vegetation zone, 2) Mediterranean/Sahara transition zone, 3) Sahara Desert vegetation zone (Figure 3.2, Table 3.1). The Mediterranean vegetation zone (Figure 3.2) lies in the winter rainfall region, which receives between 250 and 1000mm of precipitation per year. It has a variable topography and includes the Mediterranean coastal plain of Morocco, as well as mountainous areas such as;

the High Atlas, Middle Atlas and The Rif. Mediterranean sclerophyllous forest can be found in approximately half the total Mediterranean forest area from sea level up to ~2800m asl, with the 400mm precipitation isohyet forming the southern most boundary for these evergreen oak forests (White, 1983). Coniferous forest, consisting of *Abies, Cedrus, Cupressus, Juniperus, Pinus* and *Tetraclinis*, also dominates in the Mediterranean vegetation zone, while deciduous oak forest makes up a smaller percentage of vegetation cover within this zone. Mediterranean bush land and thicket grow in more semi-arid regions and contain 'characteristic' Mediterranean vegetation such as *Pistacia* and *Olea*. Mediterranean shrubland (dwarf shrubs and spiny xerophytic plants) is restricted to mountainous areas in Morocco, such as the Great Atlas and on the summits of the Middle Atlas. Mediterranean mattoral shrubs are considered to be of anthropogenic origin and now cover vast areas of the Mediterranean vegetation zone, consisting of macchia (dense growing evergreen shrubs) and garrique (open communities of smaller shrubs).

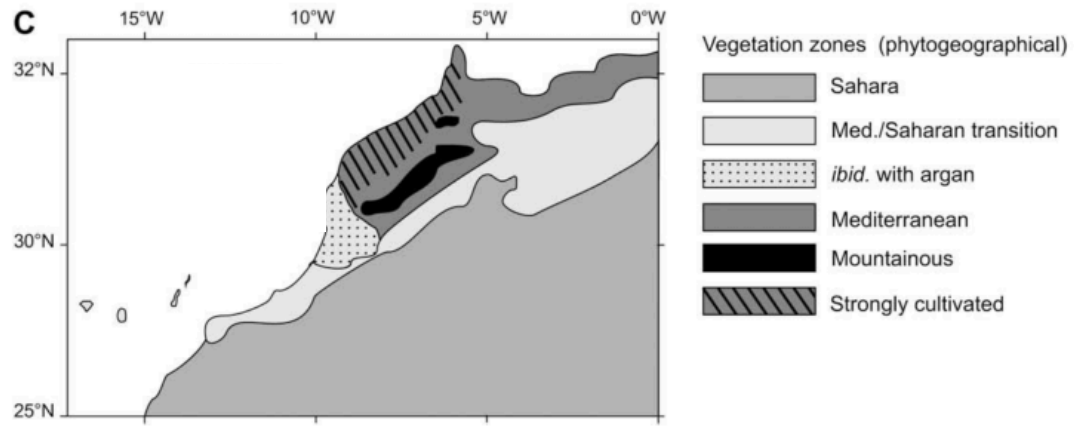

Figure 3.2: Map of Northwestern Africa showing major modern vegetation zones. The vegetation within each zone is described in Table 1 (from McGregor et al. 2009).

The Mediterranean/Sahara transition vegetation zone (Figure 1.1) occupies the semi-arid climate region that receives mean annual precipitation of 100-200mm. In the western Maghreb this vegetation zone is found in the High Plateau (700-1000m asl) most of which occurs in Algeria. Steppe vegetation (*Artemisia, Stipa and Lygeum*) dominates this vegetation zone; however pre-steppe forests dominated by *Argania spinosa* and *Euphorbia* are found in southwestern Morocco. The northern most limit of the Sahara Desert coincides with the 100mm precipitation isohyet, where dominant taxa include chenopodiaceous such as *Agathophora, Anabasis, Haloxylon, Nucularia*.

Table 3.1: Summary of the vegetation that can be found within the major modern vegetation zones in Northwest Africa compiled using data from White (1983), Hooghiemstra *et al.* (1992) and McGregor *et al.* (2009).

North African vegetation zone	Dominant vegetation
Mediterranean vegetation zone	
Mediterranean sclerophyllous forest	*Quercus ilex, Quercus suber, Quercus coccifera*
Mediterranean coniferous forest	*Abies, Cedrus, Cupressus, Juniperus, Pinus, Tetraclinis*
Mediterranean deciduous forest	*Quercus faginea, Quercus pyrenaica, Quercus afares*
Mediterranean bush land and thicket	*Ceratonia, Chamaerops, Jasminum, Juniperus, Olea, Phillyra, Pinus, Pistacia, Quercus, Rhamnum, Rhus, Tetraclinis, Ziziphus*
Mediterranean shrubland	*Alyssum, Amelanchier, Arenaria, Berberis, Cytisus, Erinacea, Juniperus, Lonicera, Ononis, Prunus, Rhamnus, Ribes, Sorbus*
Mediterranean mattoral shrub communities	*Leguminosae, Cistacecae, Ericaceae, Labiatae*

Mediterranean/Sahara transition zone	
Pre-steppe forests (south west Morocco)	*Argania spinosa, Acacia gummifera, Euphorbia, Pinus halepensis, Juniperus phoenicea, Ziziphus lotus, Pistacia atlantica, Tetraclinis*
Steppe	*Stipa tenacissima, Lygeum spartum, Artemisia herba-alba, Artemisia campestris*
Sahara Desert vegetation zone	Widespread vegetation are chenopodiaceous taxa (*Agathophora, Anabasis, Haloxylon, Nucularia*)

3.3. Palaeoclimate in North Africa

When examining palaeoclimate in North Africa it is important to consider the Mediterranean coastal fringe and the Sahara regions separately because they are influenced by different climate systems. Taforalt and El Harhoura 2 are situated in the Mediterranean region, and as yet there is no conclusive evidence to suggest the West African monsoon penetrated above ~30°N during the Late Pleistocene (Abouelmagd et al., 2012; McGee et al., 2013), the majority of the following discussion focuses on records from the western Mediterranean region. Palaeoclimate records from the Sahara are also considered, but there are few well-dated records from this region.

3.3.1. Palaeoclimate in the western Mediterranean

3.3.1.1. Marine cores

Marine cores located off the Atlantic and Mediterranean coasts of Morocco provide high-resolution, well-resolved proxy records for vegetation cover, atmospheric circulation, storm tracks, precipitation, climate seasonality, as well

as records of oceanic conditions. Several marine core records from the western Mediterranean show synchronicity between the North Atlantic and Mediterranean climate systems (Cacho et al., 2000; Colmenero-Hidalgo et al., 2004). Sea surface temperature (SST) records from the Alboran Sea (Cacho et al., 1999; Penaud et al., 2011), Tyrrhenian Sea (Cacho et al., 2001) and Gulf of Lions (Rohling et al., 1998) (Figure 3.1) also appear synchronous with atmospheric climate fluctuations identified in the Greenland Ice-Core record. Cooler SSTs are recorded in the Mediterranean during Dansgaard/Oeschger (D/O) stadials and Heinrich Events (HE) (Bond, 1997; Bond et al., 1993; Dansgaard et al., 1993) (Figure 3.3), when cold polar source surface water from the Atlantic entered the Mediterranean Sea due to changes in thermohaline circulation in the North Atlantic (Cacho et al., 1999; Sierro et al., 2005).

Pollen in marine cores off the Atlantic and Mediterranean coasts of North Africa reflects vegetation on the surrounding continental shelves (Southern Iberia and North Africa) (Hooghiemstra et al., 1992; Sánchez Goñi et al., 2002), and provides a direct proxy for terrestrial vegetation from the western Mediterranean region. One source of uncertainty relying on this proxy may result from pollen sources. Changes in atmospheric circulation over the course of sediment accumulation may vary the pollen source deposited in the core over time. Hoogheimstra (1992) used pollen from four marine cores located across a latitudinal gradient off the Atlantic coast of Morocco and Iberia (~29°-37°N) to explore the expansion and contraction of the Mediterranean, Mediterranean/Sahara transition and Sahara vegetation zones (Section 3.2.2). The records show that during MIS 5 and the beginning of MIS 4 (c. 122-68ka) a

well developed and wide spread Mediterranean vegetation zone expanded from the north coast of Africa to the south of the Atlas (Figure 3.4). Following this throughout MIS 4 and 3 (c. 68-50ka) and MIS 2 (c.24-15ka) Mediterranean vegetation north of the Atlas was almost absent, and instead the region was characterised by the presence of *Pinus* wooded steppe like vegetation that extended to the north slopes of the Atlas, with open steppe existing to the south. In the periods between c. 116ka and 105ka and c. 50ka and 24ka a more transitional vegetation existed between full 'glacial' and 'interglacial' conditions. Pollen from a high-resolution marine record spanning MIS 5 off the Iberian Peninsula shows fluctuations between relatively warm humid events during MIS 5e, 5c and 5a and cool, arid events spanning MIS 5d and 5b (Sánchez Goñi et al., 1999).

High-resolution marine records dating back to c. 50ka from IMAGES MD95-2043 and ODP 976 cores in the Alboran Sea (Figure 3.1) indicate there was cyclic variation between humid and arid periods in the Western Mediterranean during MIS 3 and 2. The vegetation variation on the land surrounding the Alboran Sea looks to have been synchronous with D/O climate variability, with expansions of mixed oak forest (deciduous and evergreen *Quercus*) during interstadials, and spread of semi-desert vegetation (Artemisia, Chenopodiaceae and *Ephedra distachya* type) during stadials and HEs (Bout-Roumazeilles et al., 2007; Combourieu Nebout et al., 2009, 2002; Fletcher and Sánchez Goñi, 2008; Moreno et al., 2005; Sánchez Goñi et al., 2002) (Figure 3.3). During the LGM, heathland dominated with high altitude cedar forest (after c. 20ka) indicating a relatively more humid climate than HE2 (before the LGM) and HE1

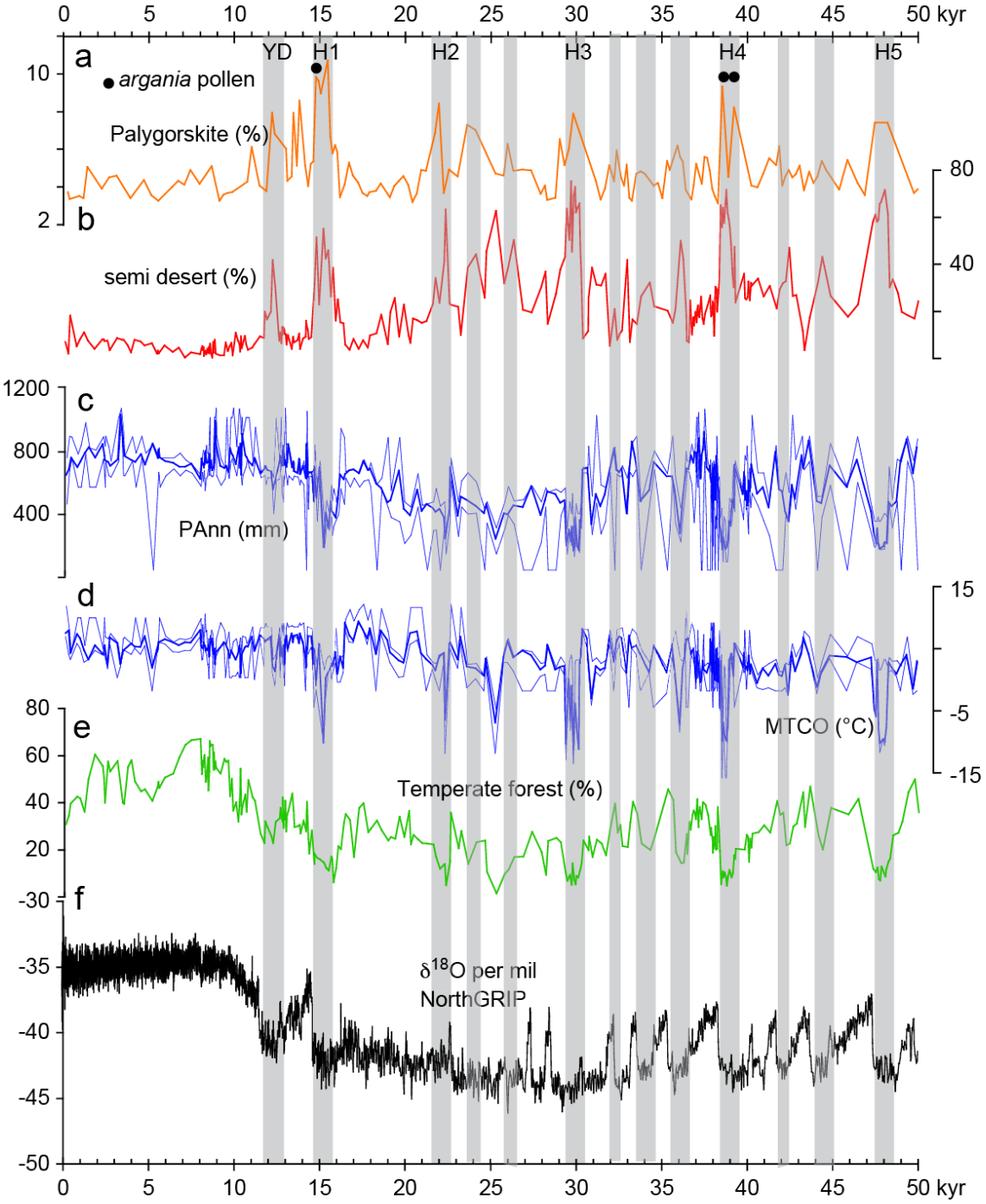

Figure 3.3: 50,000 year proxy climate record from marine core ODP 976 in the Alboran Sea: a) %Palyorskite, b)% semi-desert vegetation, c) annual precipitation (mm), d) mean temperature of coldest month based on modern analogue technique, e) % temperate forest vegetation, f) oxygen isotope ratio at NorthGRIP (‰). The black dot marks the presence of *Argania* pollen, indicative of aridity. HE's and the Younger Dryas are marked by grey lines and coincide with marked colder and arid periods, while during warmer episodes temperate forest expands in the region. The millennial-scale climate variation over the past 50,000 years in the Western Mediterranean is correlated with atmospheric climate fluctuations in the Greenland Ice Core Record (from Bout-Roumazeilles et al. 2007).

(after the LGM) (Combourieu Nebout et al., 2009; Fletcher and Sánchez Goñi, 2008; Fletcher et al., 2010b). Between 14.7 and 12.5ka cal BP there was a period of climate amelioration associated with the expansion of deciduous Mediterranean forest and the presence of *Pistacia*, both of which are indicative of mild winters. Between 12.5ka and 11.7 ka cal BP, semi-desert vegetation expanded rapidly, indicating a period of climatic deterioration in the western Mediterranean. Both events appear synchronous with GI-1 (Greenland Interstadial-1) and GS-1 (Greenland Stadial-1)/Younger Dryas, respectively (Dormoy et al., 2009).

Several authors have hypothesised that the millennial-scale climate variation recorded in the western Mediterranean during the last glacial may have resulted from variations in North Atlantic pressure gradients, similar to present winter NAO, which varies on decadal timescales (see section 3.2.1.1). The model suggests that during D/O stadials and HEs pressure gradients over the North Atlantic were high, as a result of reduced SSTs in the North Atlantic, which caused the westerly winds to increase in intensity and shift northwards bringing drier conditions to the western Mediterranean. In contrast, during D/O interstadials pressure gradients in the North Atlantic were lower, shifting the westerly winds southward over the Mediterranean region, resulting in increased precipitation in the region (Figure 3.5) (Bout-Roumazeilles et al., 2007; Moreno et al., 2005).

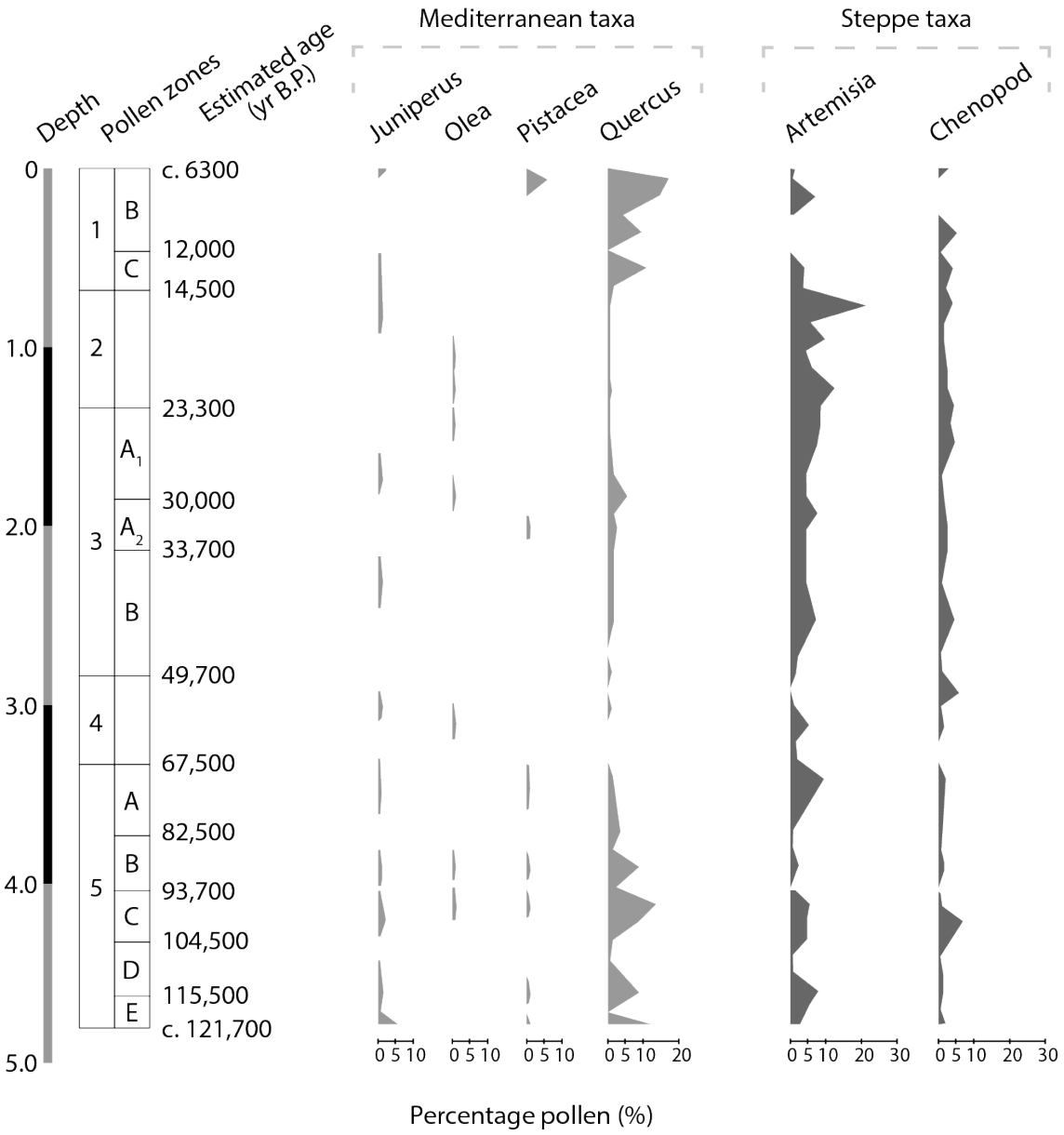

Figure 3.4: Percentage pollen diagram from marine core M 15669-1 located off the Atlantic coast of Morocco, 34°N. Diagram of selected Mediterranean and Steppe pollen taxa indicative of humid, closed and arid, open conditions, respectively (adapted from Fig. 8 in Hooghiemstra et al. 1992).

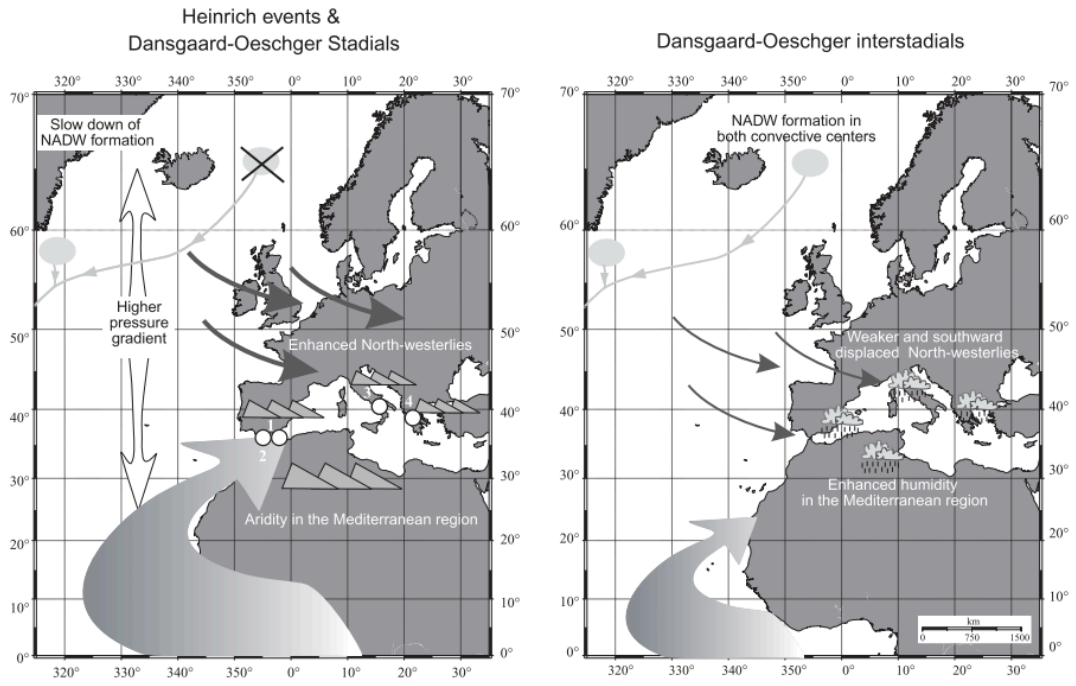

Figure 3.5: Hypothesised position of North Atlantic climate systems during D/O stadials and HEs, and D/O interstadials in the western Mediterranean region during the Last Glacial (from Moreno et al. 2005).

3.3.1.2. Terrestrial records

The patterns of vegetation change recorded in the western Mediterranean marine cores are comparable to terrestrial records from southern Spain (e.g. Carrión et al., 2007;Pons and Reille, 1988) and northern Morocco (Cheddadi et al., 2009, 1998; Lamb et al., 1989), and also with terrestrial pollen records from across the Mediterranean region (Allen et al., 1996; Naughton et al., 2009; Roucoux et al., 2005; Tzedakis et al., 2002). This shows that the marine records are good indicators of terrestrial climate in the western Mediterranean region.

Continuous palaeoclimate records from Morocco itself are rare and tend not to be associated with robust chronologies. Several lacustrine records from the Atlas Mountains dating to the Late Pleistocene exist, yet in most of them only

the Holocene sequences have been studied in detail (Benkaddour et al., 2005; Cheddadi et al., 1998; Lamb et al., 1999; Roberts et al., 1994). Continuous records dating from MIS 3 have been recovered from Tagalmamine (1626m asl) (Lamb et al., 1989), Lake Ifrah (1610m asl) (Rhoujjati et al., 2010) and Ras El Ma (1633m asl) (El Bait et al., 2014) in the Middle Atlas, and Lake Isli (Lamb et al., 1994; Valero-Garcés et al., 1998) in the High Atlas (2270m asl). The Lake Isli and Lake Ifrah sequences are not well dated. The basal sediments at Lake Isli have a radiocarbon age of 34,850 ± 410 cal BP, but the age-depth relationship is inconsistent throughout the sequence (Lamb et al., 1994). The Lake Ifrah chronology is extrapolated from four radiocarbon dates, with no basal age the oldest date in the sequence is 25,145 ± 400 cal BP (Rhoujjati et al., 2010).

Pollen records from all four lakes show that from c. 30ka to 12ka steppe vegetation (Gramineae, Chenopodiaceace and *Artemisia*) was dominant in the Atlas Mountains, showing that moisture availability was too low to support tree growth, or that temperatures were too low to allow sapling recruitment (El Bait et al., 2014; Lamb et al., 1994, 1989; Rhoujjati et al., 2010). Low microcharcoal concentrations in Lake Ifrah during this period suggest a low biomass landscape with little fuel for wild fires (Reddad et al., 2013). At c. 20ka cal BP an increase in the percentage of arboreal pollen within the Lake Ifrah sequence is noted, which mainly results from an increase of *Cedrus atlantica* pollen (Rhoujjati et al., 2010). The presence of *Cedrus* pollen is also noted in the marine cores from the Alboran Sea during the LGM (Section 3.2.1.1). Modern analogue inferences suggest that the expansion of *Cedrus* at this time is

associated with an increase in MAP from ~300-500mm and an increase in the temperature of the coldest month from -12 to +3°C (Cheddadi et al., 2009). The most arid period in the Lake Isli sequence, deduced from the predominance of steppe vegetation and low organic matter, dates from c. 19.5 to 12ka cal BP. The period after the LGM is also recognised as an extremely arid phase in several Iberian records (17.5-14.5 cal BP), termed the 'Mystery Interval' (MI), it is characterised in the North Atlantic by a strong reduction in Atlantic Meridional Overturning Circulation (AMOC) (Denton et al., 2006; Moreno et al., 2012). At both Lake Isla and Tagalmamine there is a period of increased moisture at c. 14-12ka inferred from the presence of scattered evergreen oaks, while after c. 12ka evergreen oaks disappear and steppe vegetation dominates the pollen records once more (Lamb et al., 1989; Valero-Garcés et al., 1998). These events are likely synchronous with GI-1 and GS-1 noted in Greenland and the North Atlantic region, but improved chronology is required to enable correlations.

The $\delta^{18}O$ values of the lake carbonates at Tigalmamine and Lake Isli are higher during the Late Pleistocene relative to Holocene values (Lamb et al., 1989; Valero-Garcés et al., 1998), a pattern noted in several other Mediterranean lakes (see Roberts et al., 2008). Relatively higher $\delta^{18}O$ values, indicative of greater evaporation, are consistent with the lacustrine pollen data and suggest that the Atlas was an arid, treeless landscape during the glacial. Yet, proxy records show that Lake Isli was relatively high during the Late Pleistocene indicative of greater effective moisture (precipitation-evaporation). Indicators of increased moisture availability during the LGM have also been recorded in the

northern edge of the Sahara between 26 and 18ka (Street and Grove, 1979) and on the Iberian Peninsula (see Moreno et al., 2012). Atmospheric GCM simulations indicate increased MAP/positive hydrological balance during the LGM in the Mediterranean (Jolly et al., 1998; Kageyama et al., 2005). Moreno et al. (2012) proposes that positive hydrological balance characterises the LGM in Iberia due to reduced summer insolation, causing reduced evapotranspiration during the summer months, resulting in increased moisture availability without any significant increase in rainfall.

3.3.2. Palaeoclimate in the Sahara Desert

As mentioned above Saharan climate is distinct to that from the Mediterranean regions of North Africa, because it is influenced by low-latitude monsoonal systems. The Sahara Desert forms a large arid barrier in dry phases, which has a major impact on the timings of dispersals on modern humans out of Sub-Saharan Africa (Armitage et al., 2011; Drake et al., 2011; Osborne et al., 2008), the migration of modern humans into the coastal region of North Africa, and whether the coastal fringe acted as a refugium environment for humans during the Late Pleistocene. The Sahara has undergone significant hydrological fluctuations in the past caused by the northward penetration of the summer monsoonal rains into the region during periods of high solar insolation. The most thoroughly documented event is the African Humid Period during the early and mid Holocene (~11-5 ka), when the Sahara was vegetated with grasslands, forests and several permanent lakes existed (deMenocal et al., 2000; Gasse, 2000; Street-Perrott et al., 1989; Tierney et al., 2011).

Marine cores GeoB7920-2, GeoB9528-3 and ODP 659 off the north west coast of Africa, located between ~10° and 20°, suggest that humid events occurred in the Sahara during MIS 5 and MIS 3 (Castañeda et al., 2009; Kuechler et al., 2013; Tjallingii et al., 2008). The phases during MIS 5 generally coincide with increased summer insolation suggesting the humid periods result from intensification of the summer monsoon; however, less pronounced humid phases during MIS 3 generally occur during low amplitude insolation peaks (Castañeda et al., 2009). Drake et al. (2013), Smith (2012) and Larrasoaña et al. (2013) have all assembled terrestrial records/deposits representative of humid conditions from across the Sahara Desert. The terrestrial data appears to agree with that from the marine records indicating humid pulses during MIS 5. Smith (2012) and Drake et al. (2013) also note the occurrence of pluvial phases during MIS 3 that appear to be restricted to the Mediterranean region or the northern periphery of the Sahara Desert, hinting at a southward or intensification of the westerlies. Palaeoclimate records show that both the Sahara and Mediterranean regions of North Africa experienced humid episodes during MIS 5. Climate models also support this and suggest that an intensification and southward shift of the westerlies may have occurred during increased summer insolation (Jennings et al., 2015).

3.4. Summary

North Africa lies in a climatically sensitive region between mid-latitude and low-latitude climate systems. Marine core records from the western Mediterranean show synchronicity with North Atlantic records implying that Late Pleistocene climate was strongly influenced by mid-latitude systems. The Atlas appears to

have provided a natural geographic barrier in the region with no evidence to show that low-latitude monsoon rains penetrated north of the mountains during periods of high summer insolation in the Late Pleistocene. Therefore, because El Harhoura 2 and Taforalt are located in the Mediterranean climate region of North Africa, the thesis will focus discussions on proxy records, and climate systems from the mid-latitude region. Consideration of climate in the Sahara is important when addressing the role of the North African coastal fringe as a refugium environment.

4. Stable isotopes as indicators of palaeoclimate and palaeoenvironment

4.1. Introduction

The research described in the thesis relies heavily on stable isotope proxies in small mammal tissues to investigate palaeoclimate and palaeoenvironment. This chapter explores the parameters that affect the stable isotope composition of food and water consumed by mammals and the fractionation processes that occur in the construction of mammalian tissues. These processes underpin the modern study and explain how stable isotopes in small mammal tissues reflect local climate factors, and can be used to reconstruct past climate and environment.

4.2. Stable isotopes in the biosphere

4.2.1. $\delta^{18}O$ in terrestrial systems

Drinking water and oxygen from food is the main source of oxygen in mammal tissues. Therefore, in order to interpret the $\delta^{18}O$ values of mammal tissues the fractionation processes within the hydrological cycle and plant water are considered below. The $\delta^{18}O$ values of the drinking water and food consumed by the mammal are passed on to the body water, from which body tissues are precipitated (see section 4.3.2).

4.2.1.1. Meteoric water

Meteoric water is sourced from ocean water, which varies spatially in $\delta^{18}O$ and directly influences the $\delta^{18}O$ value of precipitation (Figure 4.1). It forms when

ocean surface waters evaporate, a kinetic fractionation process, which causes atmospheric water vapour to become depleted in ^{18}O relative to that of ocean water. As air masses rise and move from their source they cool and condense resulting in precipitation, from which the heavy isotopologues of water are preferentially condensed out of the air mass, leaving the water vapour depleted in ^{18}O relative to the precipitation: a process known as 'rainout' (Figure 4.2) (Hoefs, 2009; Sharp, 2007). The $\delta^{18}O$ composition of precipitation displays systematic spatial variation across the lithosphere and decreases with increasing latitude, elevation and continentally (Figure 4.3) (Bowen and Wilkinson, 2002; Dansgaard, 1964; Rozanski et al., 1993). At mid and high latitudes there is strong correlation between temperature and the $\delta^{18}O$ value of precipitation, while at low latitudes the $\delta^{18}O$ value of precipitation is negatively correlated with the amount of monthly precipitation, a process known as the 'amount effect' (Dansgaard, 1964; Rozanski et al., 1993). The change from temperature-dominated to amount-dominated control on the $\delta^{18}O$ value of precipitation occurs at approximately 30°N/S (Mediterranean climate latitudes). Meteoric water is stored on earth in groundwater systems, rivers, lakes and glaciers. Surface water and groundwater generally display the same spatial $\delta^{18}O$ patterns as those demonstrated by $\delta^{18}O$ precipitation at continental scales (Gat, 1996, 1971; Kendall and Coplen, 2001), yet, at a local-scale processes such as mixing, transportation, evaporation and condensation can substantially alter the isotopic composition of local environmental water (Figure 4.2) (Bowen, 2010).

Studies on precipitation in Morocco show that the $\delta^{18}O$ value of precipitation is not dominated by either temperature or amount of rainfall but instead source (Atlantic vs. Mediterranean) and the trajectory of the air mass exerts a greater effect on the isotopic composition of precipitation (Ouda et al., 2005). As discussed in Chapter 3 the majority of precipitation in the Mediterranean region of North Africa originates from the Atlantic Ocean. It is expected that a rainout gradient will exist over the region with lower $\delta^{18}O$ values of precipitation in the west compared to the east. It is also predicted that higher altitude regions in the Atlas Mountains will reflect an altitude effect with lower $\delta^{18}O$ values of precipitation.

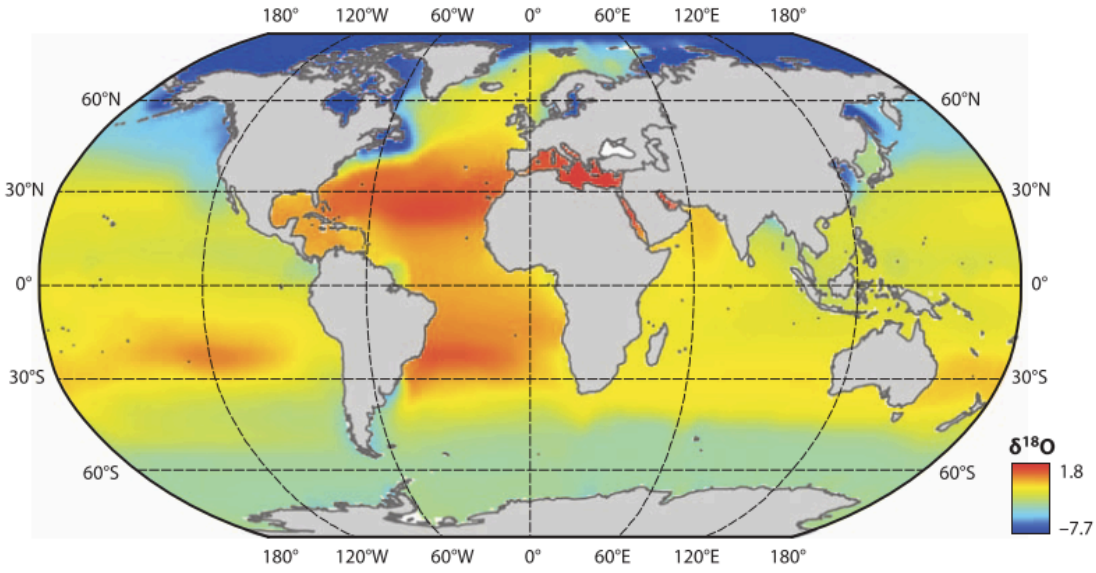

Figure 4.1: Map showing modelled global $\delta^{18}O$ of ocean surface water. The Mediterranean Sea is a closed basin and is therefore ^{18}O-enriched due to evaporative effects (from Bowen et al. 2010).

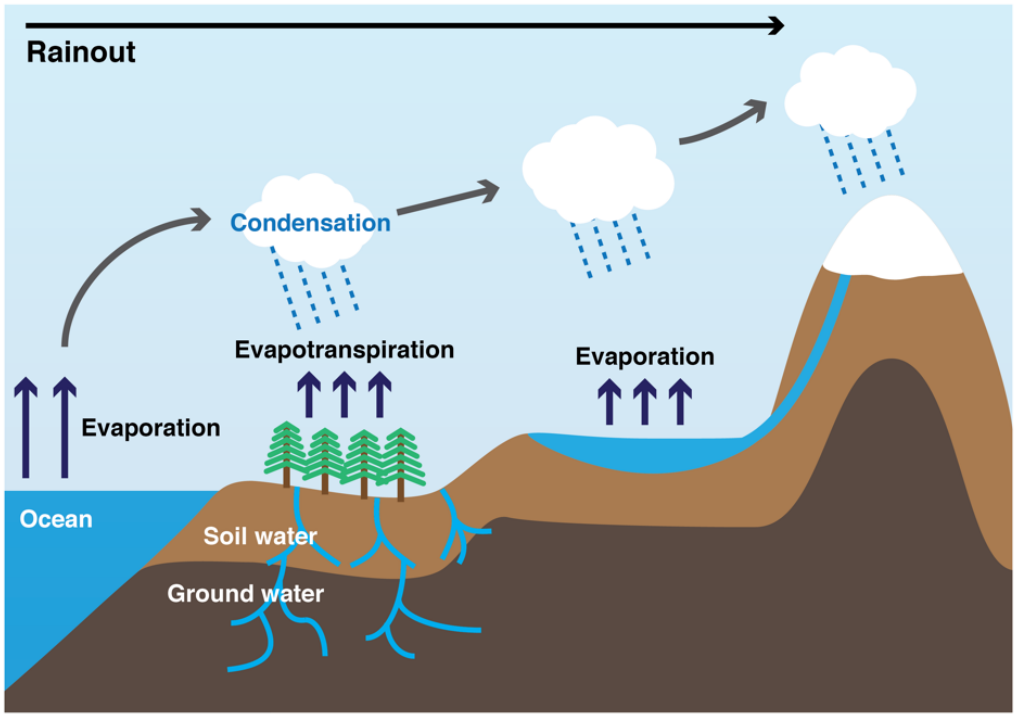

Figure 4.2: Schematic diagram showing 'rainout' and the processes in which oxygen isotope fractionation occurs within the hydrological cycle (adapted from Figure 4.10 in Sharpe 2007).

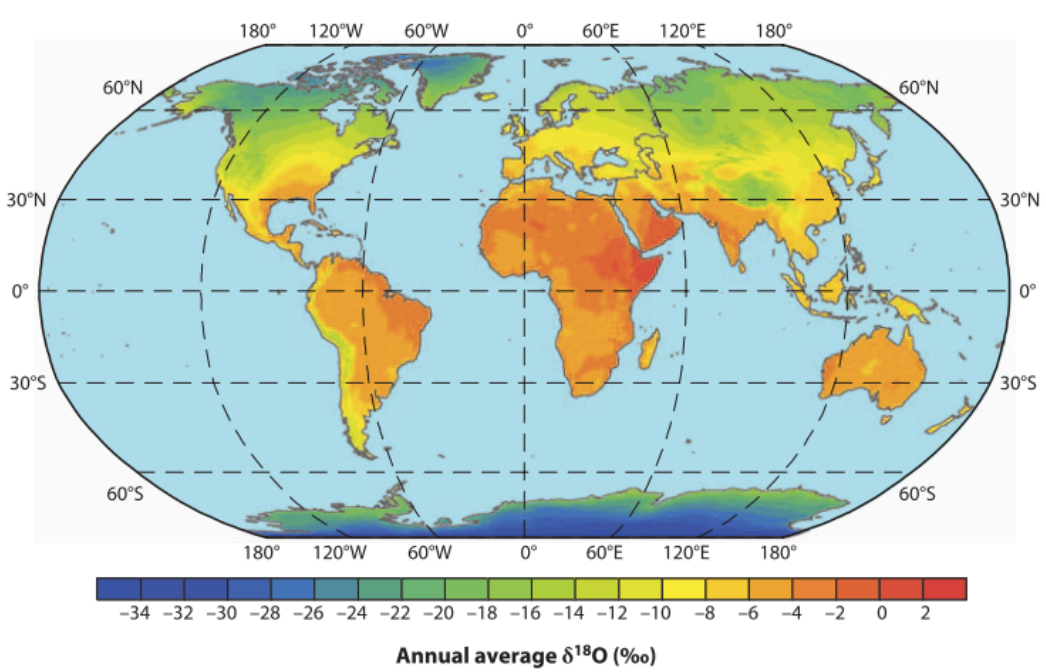

Figure 4.3: Map showing modelled global annual average $\delta^{18}O$ of precipitation from Bowen et al. (2010), modelled using data from the Global Network of Isotopes in Precipitation, using the method of Bowen & Revenaugh (2003).

4.2.1.2. $\delta^{18}O$ in plants

The gerbils used in the modern and archaeological studies obtain most of the water, and therefore oxygen, from the grains and plant parts they consume (Chapter 5). There are no significant observable fractionation effects for plant uptake of soil water (Dawson et al., 2002), meaning that the $\delta^{18}O$ value of soil water strongly influences that of the plant. However, in semi-arid and arid environments the $\delta^{18}O$ value of the soil water may become enriched in ^{18}O relative to that of precipitation, due to evaporative effects from the soil surface (Allison and Hughes, 1983; Gat and Airey, 2006; Yakir, 1998). Plant leaves are enriched in ^{18}O relative to that of the soil, roots and stem water because $H_2{}^{16}O$ is preferentially evaporated from the leaf (Figure 4.4). The degree of isotopic enrichment in the leaf is dependent on relative humidity (dependent on temperature and the pressure of the system of interest), transpiration rate and the isotopic composition of water vapour in the atmosphere (Dongmann et al., 1974; Farquhar et al., 2007, 1989; Flanagan et al., 1991). Controlled experiments on plants show that leaf waters become increasingly enriched in ^{18}O as relative humidity decreases (Barbour and Farquhar, 2000; Flanagan et al., 1991; Helliker and Ehleringer, 2002a; Yakir et al., 1990). The $\delta^{18}O$ value of leaf waters can vary seasonally and diurnally consistent with variations in temperature and relative humidity (Förstel, 1978; Gat et al., 2007). The $\delta^{18}O$ composition of leaf water also influences the isotopic composition of the plants organic matter manufactured in the leaf (Barbour and Farquhar, 2000). As food oxygen, in addition to drinking water, makes up a significant proportion of oxygen in mammalian body water (see section 4.3.2), the $\delta^{18}O$ composition of mammalian tissues reflect these different sources from plants. In the strongly

seasonal Mediterranean climate system (dry summers, wet winters) the $\delta^{18}O$ values of plant, soil and environmental waters will undergo strong seasonal variations.

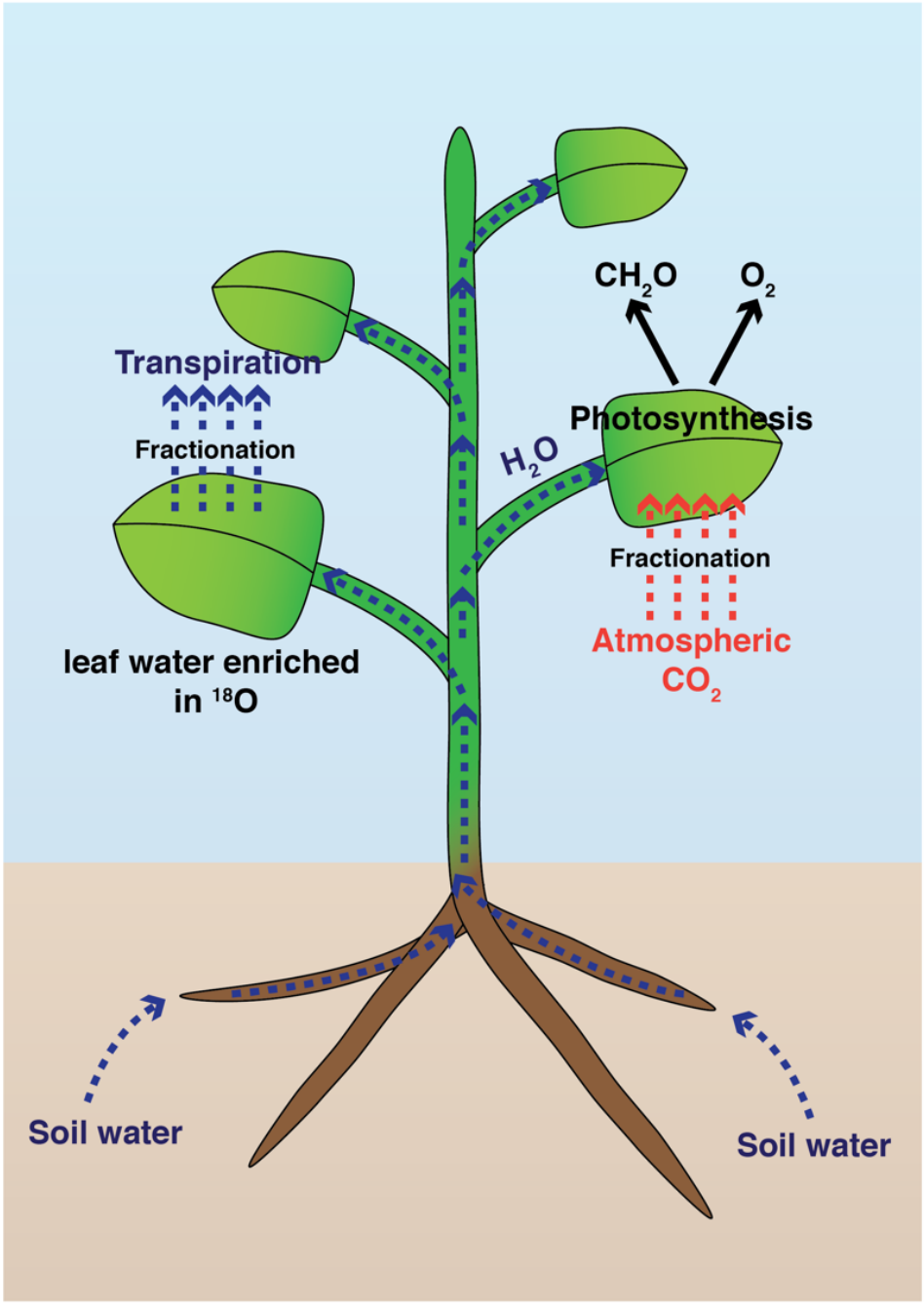

Figure 4.4: Schematic diagram showing the main processes in which oxygen and carbon isotope fractionation occurs in plants (adapted from Fig.1 in Dawson et al. 2002).

4.2.2. Sources of $\delta^{13}C$ variation in terrestrial ecosystems

The majority of variation in $\delta^{13}C$ values of plants is due to their photosynthetic pathways, C_3, C_4 or Crassulacean acid metabolism (CAM). Within C_3 plants, variation in $\delta^{13}C$ occurs due to climate effects (moisture availability, temperature), atmospheric CO_2 and light intensity. Over long-timescales (e.g. Quaternary), as well as changes in atmospheric CO_2, the $\delta^{13}C$ composition of the atmosphere ($\delta^{13}C_{CO2}$) has also varied, meaning that the $\delta^{13}C$ composition of modern plants is ~1.5‰ lower compared to that of archaeological/fossil plants. The $\delta^{13}C$ values of plants are passed on to mammal tissues through a reasonably well-known pathway reflecting mainly the $\delta^{13}C$ composition of diet, but also a small effect related to the body size of the mammal (see Section 4.3.3).

4.2.2.1. Photosynthesis

The $\delta^{13}C$ composition of plants ($\delta^{13}C_{plant}$) is most strongly related to their photosynthetic pathway. The two main pathways, known as C_3 and C_4, are named after the 3-carbon (phosphoglyceric acid) and 4-carbon (carboxylic acid) compounds formed in the first stage of fixation of atmospheric CO_2 within each pathway, respectively. Plants are depleted in ^{13}C relative to the $\delta^{13}C$ composition of the atmosphere as each pathway discriminates against ^{13}C to different extents, meaning that C_3 and C_4 plants have distinct $\delta^{13}C$ distributions (Figures 4.4 and 4.5) (Park and Epstein, 1960; Smith and Epstein, 1971). C_3 plants use the Calvin-Benson Cycle, in which the enzyme ribulose biphosphate carboxylase (RuBisCO) discriminates strongly against ^{13}C. C_4 plants have developed a secondary carbon fixation pathway (Hatch-Slack cycle), which

uses the phophoenolpyruvate (PEP) enzyme that has a smaller fractionation. Farquhar (1982) developed a model to mathematically describe C_3 photosynthesis:

$$\delta^{13}C_{plant} = \delta^{13}C_{co2} - a - (b - a)ci/ca \quad (1)$$

where the $\delta^{13}C_{plant}$ is the isotopic composition of the plant, the $\delta^{13}C_{co2}$ is the isotopic composition of the atmosphere, *a* is the discrimination in ^{13}C during the diffusion of CO_2 in to the internal leaf space, *b* is the net fractionation resulting from carboxylation (mainly by RuBisCO), and C_i and C_a are the partial pressure of CO_2 in the internal air space of the leaf and the external atmosphere, respectively. Equation 1 demonstrates that stomatal conductance is the main factor controlling the expression of fractionation by the RuBisCO enzyme. As a result C_3 plants are sensitive to water availability, pCO_2, light conditions and temperature (Dawson et al., 2002; Ehleringer and Dawson, 1992; Farquhar et al., 1989; Heaton, 1999; Tieszen, 1991).

The global average $\delta^{13}C$ value for C_3 plants (trees, shrubs, herbs and grasses growing under temperate or shaded conditions) is about -27‰, with a large isotopic range from -23 to -36‰. C_4 plants (mainly tropical grasses and sedges) have a narrower $\delta^{13}C$ range (-16 to -9‰). They require high insolation in the growing (wet) season so their distribution is confined largely to environments with warm, summer growing seasons (Sage and Monson, 1998; Teeri and Stowe, 1976) and are therefore very uncommon in winter-rainfall zones where the growing season is cool (Collatz et al., 1998). Physiological considerations of C_4 photosynthesis also shows that C_4 vegetation is better adapted to conditions

of low pCO_2 relative to C_3 vegetation, resulting in an expansion in the ecological range of C_4 plants during glacial conditions (Collatz et al., 1998; Ehleringer et al., 1997, 1991). Currently, the Mediterranean region is dominated by C_3 vegetation, yet C_4 species are found in these environments with seasonal increases in the proporation of C_4 species noted during the summer (Reade et al., 2016). C_4 species are also found in coastal salt marshes, as weeds in arable and in marginal more open steppe habitats in the Mediterranean (Hartman and Danin, 2010; Sage and Monson, 1998; Vogel et al., 1986; Winter and Troughton, 1978).

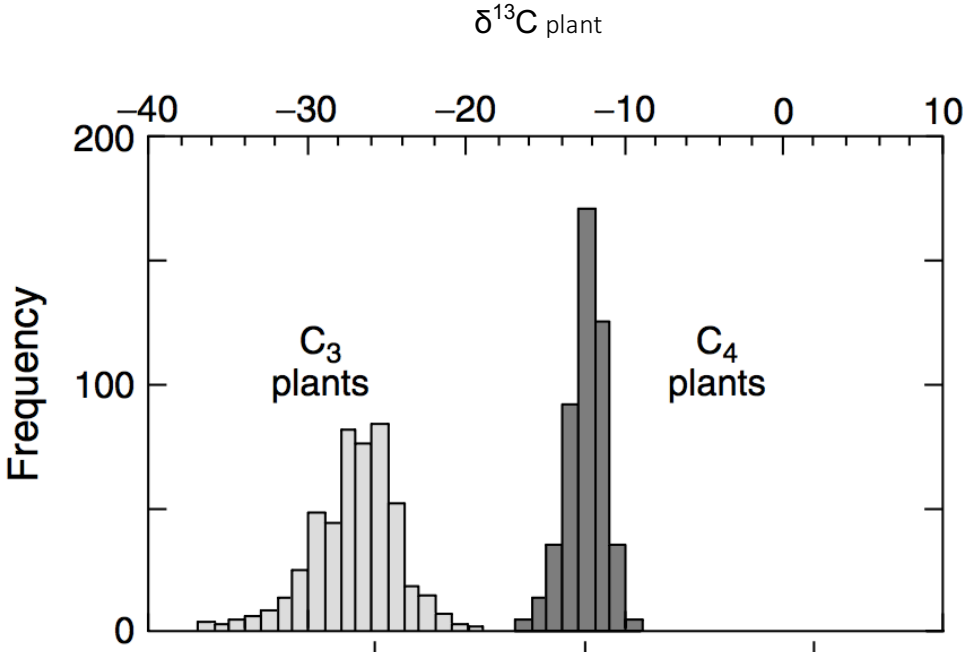

Figure 4.5: Histogram showing the distribution of $\delta^{13}C$ values in C_3 and C_4 plants (from Ehleringer et al., 2002).

4.2.2.2. Environmental influences on $\delta^{13}C$ in plants

Most of the variation in $\delta^{13}C$ displayed by C_3 plants results from response to environmental conditions (Farquhar et al., 1982). Under conditions of low relative humidity and aridity plants close their stomata to limit water loss through transpiration. Equation 1 predicts that this will result in decreased

discrimination against ^{13}C and higher water use efficiency (Farquhar et al., 1982). Observational studies have reported strong negative correlation between the $\delta^{13}C_{plant}$ and MAP on regional and global scales (Hartman and Danin, 2010; Kohn, 2010; Ma et al., 2012; Stewart et al., 1995; Swap et al., 2004; Weiguo et al., 2005). This relationship also stands in Mediterranean ecosystems, where independent correlations between MAP and the $\delta^{13}C$ value of both wet and dry season plants also occurs due to the strong seasonal climate gradient (wet/dry season) in the region (Hartman and Danin, 2010).

4.2.2.3. The canopy effect

In dense forests it is predicted that plant leaves from the upper canopy will have higher $\delta^{13}C$ plant leaf values relative to those within the sub-canopy vegetation. Models suggest that this occurs because respiration processes in plants and the soil are enhanced under the forest canopy, meaning that more CO_2, which is depleted in ^{13}C, is available to these plants. It is also assumed that because light levels are lower under the canopy RuBisCO discrimination is higher, again resulting in lower $\delta^{13}C_{plant}$ (van der Merwe and Medina, 1991; Vogel, 1978). Empirical data from dense tropical rainforests shows that leaves and fruit in the sub-canopy can have $\delta^{13}C$ values as low as -37‰, where the average values of the leaves from the canopy is ~-30‰ (Cerling et al., 2004). Mediterranean Biome forests are unlikely to be very dense so the $\delta^{13}C_{plant}$ canopy gradient will be less. It is expected that in this setting sub-canopy plants will be on average ~2-5‰ lower than standing trees or plants in near-by open areas, similar to values reported across Europe (Heaton, 1999).

4.2.2.4. Spatial and temporal variation in the $\delta^{13}C$ of plants

The main component of gerbil diet is grain supplemented with other plant parts. Several studies have demonstrated variation in $\delta^{13}C$ value of plant tissues and parts (e.g. Badeck et al., 2005; Hobbie and Werner, 2004; Szpak et al., 2013), because different biochemical components that plant tissues are composed of have different $\delta^{13}C$ values. Typically, the $\delta^{13}C$ values of carbohydrates are higher relative to proteins, which are in turn higher relative to lipids (Heaton, 1999; O'Leary, 1981; Tieszen, 1991), resulting in roots, seeds and woody stems being ^{13}C-enriched compared to leaves in C_3 plants (Badeck et al., 2005; Cernusak et al., 2009; Codron et al., 2005; Hobbie and Werner, 2004; Leavitt and Long, 1982).

$\delta^{13}C_{plant}$ vary across the globe mainly due to environmental influences as already discussed, but within environments and ecosystems $\delta^{13}C_{plant}$ can also differ due to species-specific effects. Plants in Mediterranean ecosystems have values that range widely from ~-31 to -22‰ because of the predominantly open and semi-open type vegetation (Hartman and Danin, 2010; Valentini et al., 1992). $\delta^{13}C_{plant}$ varies seasonally with plants observed to have higher $\delta^{13}C$ values during the hotter/drier part of the year (Ehleringer et al., 1991; Hartman and Danin, 2010), especially in environments that have a strong seasonal climate gradient, such as the Mediterranean. It is assumed that animals eating this vegetation will average the majority of the variability; however because small mammal tissues form and turnover rapidly they may reflect plant seasonal effects.

4.2.2.5. Atmospheric $\delta^{13}CO_2$

The Farquhar (1982) model (Equation 1) also shows that $\delta^{13}C_{plant}$ is influenced by pCO_2 and $\delta^{13}C_{CO2}$. This becomes especially relevant when exploring past vegetation change as both these parameters have varied on Quaternary timescales. Ice core records show glacial to interglacial shifts in pCO_2 from ~165ppm to ~270ppm, respectively, (Barnola et al., 1987; Jouzel et al., 1993; Lourantou et al., 2010a), and ~1‰ variation in the $\delta^{13}C_{CO2}$ during the Late Pleistocene before recent industrial times (Leuenberger et al., 1992; Lourantou et al., 2010a, 2010b; Schaefer et al., 2011; Schneider et al., 2013) (Figure 4.6). The effect of lower pCO_2 during glacial conditions is predicted to increase $\delta^{13}C$ values in C_3 plants. However, experiments on C_3 plants under controlled pCO_2 and $\delta^{13}C_{CO2}$ show that $\delta^{13}C_{plant}$ linearly reflects $\delta^{13}C_{CO2}$ when pCO_2 varies from 225ppm to 1300 ppm. Furthermore, when both pCO_2 and $\delta^{13}C_{CO2}$ are allowed to fluctuate it is the changes in $\delta^{13}C_{CO2}$ that exerts the greatest influence on $\delta^{13}C_{plant}$ (Arens et al., 2000; Jahren et al., 2008). Yet, these laboratory experiments fail to replicate conditions of simultaneous lower pCO_2, increased $\delta^{13}C_{CO2}$, lower temperatures and lower insolation that existed during the Late Pleistocene. The recent fossil fuel effect has caused $\delta^{13}C_{CO2}$ to decrease by ~1.8‰ relative to pre-industrial values (Francey et al., 1999; Friedli et al., 1986; Rubino et al., 2013) meaning that modern plant and mammalian tissues are depleted in ^{13}C relative to archaeological/fossil plants and tissues by about 2‰ (Figure 4.6). Most authors deal with this issue when comparing modern and fossil $\delta^{13}C$ values by correcting to $\delta^{13}C_{CO2}$ values from the ice core records (e.g. Cerling 1997), but this method does not account for variation in pCO_2 and climate factors on plants.

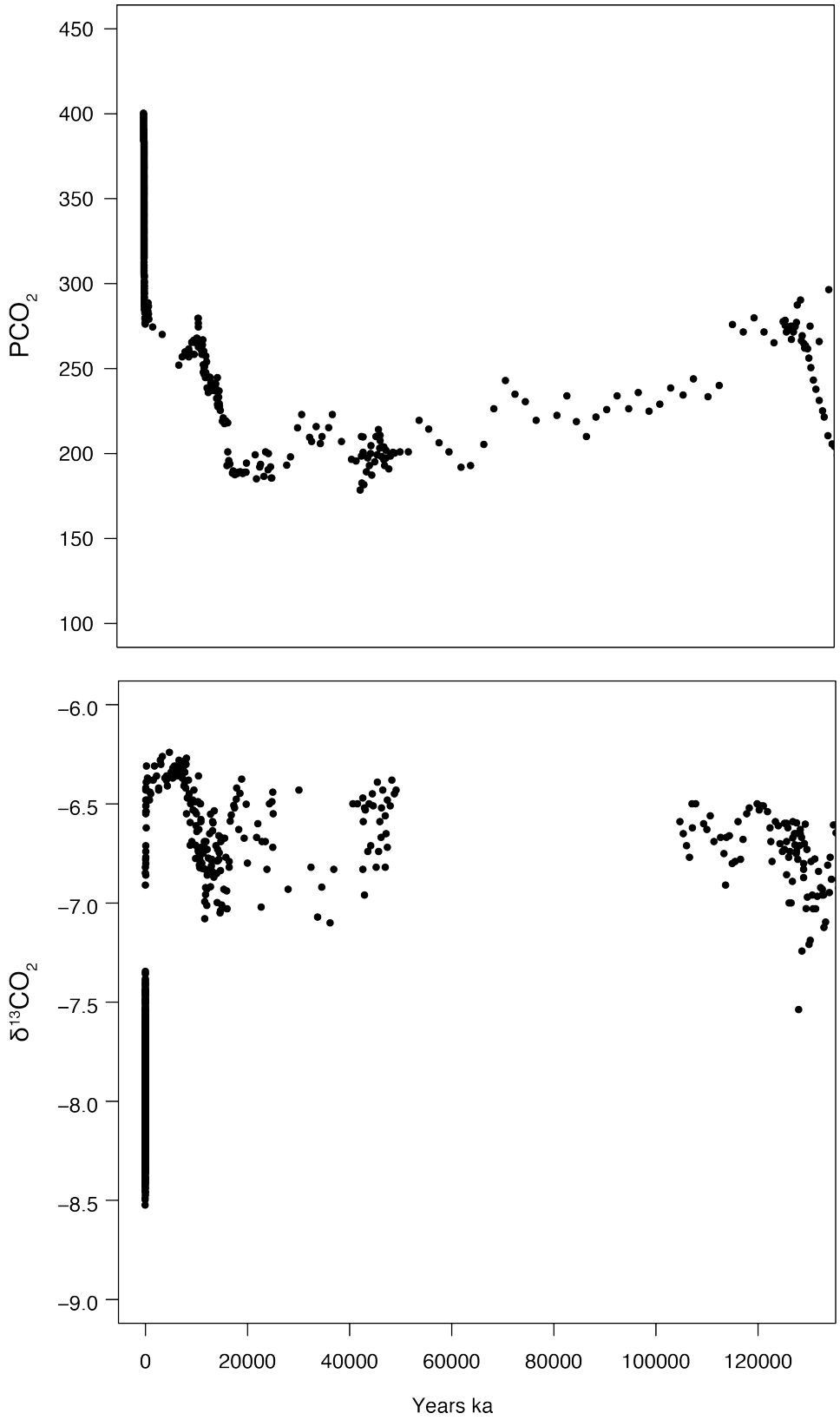

Figure 4.6: a) pCO_2, b) $\delta^{13}C_{CO2}$ over the last 130ka measured from atmospheric air preserved in ice core records (Elsig et al., 2009; Francey et al., 1999; from Leuenberger et al., 1992; Lourantou et al., 2010a, 2010b; Schaefer et al., 2011; Schneider et al., 2013; Smith et al., 1999) and recent observational records (1978-2015) (Keeling et al., 2005).

4.2.3. $\delta^{15}N$ in terrestrial systems

The influence of aridity on $\delta^{15}N$ values of gerbil collagen is explored in the modern study (Chapter 5). The following section outlines the main sources of $\delta^{15}N$ variability in soils and plants. The $\delta^{15}N$ composition of mammal tissues reflects the protein component of the diet, so in granivores, such as gerbils, it reflects plant protein. The $\delta^{15}N$ value of the plant is passed on to the mammal tissue, but the fractionation processes in this pathway are poorly understood (see Sections 4.3.4).

4.2.3.1. $\delta^{15}N$ in soils and plants

The $\delta^{15}N$ values of plants is dependent on several factors, which include the $\delta^{15}N$ composition of the soil, the nitrogen obtained by the plant (e.g. N_2, NH_4^+, NO_3^-) and the process by which nitrogen is assimilated (Sharp, 2007; Szpak, 2014). The $\delta^{15}N$ value of soils also depends on several parameters and are therefore difficult to quantify (see review by Hobbie and Högberg, 2012). Bulk soils have average values of 2-6‰ and $\delta^{15}N$ is shown to increase with depth in the soil profile (Hobbie and Högberg, 2012). Waterlogged, anoxic soils tend to have higher $\delta^{15}N$ values because they undergo more denitrification resulting in the preferential loss of ^{14}N from the soil (Sharp, 2007). The addition of animal fertilisers is also observed to increase the $\delta^{15}N$ value of soil (e.g. Bogaard et al., 2007; Fraser et al., 2011).

The two most common forms of nitrogen obtained by plants from the soil are nitrate (NO_3^-) and ammonium (NH_4^+); therefore the $\delta^{15}N$ values of these plants are also partly determined by the $\delta^{15}N$ value of the soil. On the other hand

nitrogen-fixing plants obtain nitrogen directly from atmospheric nitrogen (N_2), which is fixed by symbiotic bacteria living in the root nodules. As the fractionation between N_2 and labile organic nitrogen is negligible, nitrogen-fixing plants have a $\delta^{15}N$ value close to zero, especially in nitrate poor soils when their only source of nitrogen is that from the atmosphere. The extent to which plants rely on different sources of nitrogen is important in determining the $\delta^{15}N$ value of the plant due to the fractionation processes within the nitrogen cycle (e.g. nitrification, denitrification, ammonification) (see review by Szpak, 2014).

4.2.3.2. Influences on variation in the $\delta^{15}N$ of plants

$\delta^{15}N$ values of plants are influenced by several factors. Strong taxonomic distinctions have been shown to be related to plant functional types or mycorrhizal (fungal) associations (Craine et al., 2009; Hobbie and Högberg, 2012). Globally plants with mycorrhizal associations have lower $\delta^{15}N$ values relative to non-mycorrhizal plants (Craine et al., 2009). The $\delta^{15}N$ values of plants can also vary on a range of temporal and spatial scales. $\delta^{15}N$ values can vary within plants; for example first principles suggest that shoots should have higher $\delta^{15}N$ value relative to the roots (Evans, 2001). The $\delta^{15}N$ values of plants differ across the globe and generally plants in dry, hot environments tend have higher $\delta^{15}N$ values relative to those in cool, wetter environments (Asada et al., 2005; Hartman and Danin, 2010; Szpak et al., 2013); but this is not always the case. Within local areas, environments and ecosystems the $\delta^{15}N$ composition of plants is highly variable (Craine et al., 2009). Szpak et al. (2013) reported intra-site variation of ~6-15‰ in modern wild plants from individual sampling sites across a transect in Northern Peru. Hartman & Danin (2010) also showed

that the $\delta^{15}N$ composition of plants from dry wash and exposed ridge microhabitats within the same desert environment varied by up to ~5‰. Even within one field the $\delta^{15}N$ composition of soils can vary by ~2‰ (Peukert et al., 2012).

Negative correlations between MAP and foliar $\delta^{15}N$ values have been noted on both regional and global scales (Amundson et al., 2003; Austin and Vitousek, 1998; Craine et al., 2009; Handley et al., 1999; Hartman and Danin, 2010; Murphy and Bowman, 2006). Significantly, this relationship occurs in the eastern Mediterranean across a rainfall gradient similar to the climate in northwestern Africa (Hartman and Danin, 2010). The mechanism for the relationship is uncertain and it has been suggested that it relates to the 'openess' of the nitrogen cycle in more water stressed regions, where losses of nitrogen lead to an ^{15}N-enrichment of the remaining nitrogen in the system (as ^{14}N is preferentially lost from the system). Wetter ecosystems tend to have more 'closed' nitrogen cycles so the rate of nitrogen loss is less (Amundson et al., 2003; Austin and Vitousek, 1998; Handley et al., 1999).

4.3. Stable isotopes in mammalian tissues

Thus far the chapter has described fractionation processes that affect the isotope composition of the drinking water and food consumed by animals, which are crucial for understanding and interpreting the isotope composition of mammalian tissues. As shown in Section 4.2 these factors vary on different temporal and geographic scales, yet it is assumed that the isotopic composition of mammalian skeletal tissues reflect a homogenised average of the

environment. The stable isotope composition of mammalian skeletal material (bone and teeth) does not directly equal the isotope composition of an animal's food and water; instead they also reflect physiological fractionation processes that occur in the mammal's body. The relationship between the isotope composition of mammalian tissues and food/water is species-specific and differs between different tissue types. As discussed in Chapter 1 stable isotope techniques are commonly used in large mammals, but these methods are not commonly applied to small mammals because little is understood about their isotope ecology.

4.3.1. Consideration of mammalian tissues

The inorganic and organic phases of mammalian skeletal tissues are considered separately below. Inorganic tissues are more robust and generally survive longer in the archaeological record in comparison to organic tissues, particularly in warm environments such as North Africa. Here, the modern study uses both bone collagen (organic) and tooth apatite (inorganic) to explore environmental influences on the stable isotope composition of small mammal tissues, while the archaeological study solely uses tooth apatite to construct a proxy climate and environmental record. This is because collagen is not preserved in the small mammal bones at El Harhoura 2 and Taforalt. In this thesis *tooth apatite* is defined as bulk enamel and dentine apatite. Differences between modern and archaeological tooth apatite are described in the methodology sections of Chapters 5 and 6.

4.3.1.1. Tooth bioapatite

The minerals (inorganic) in skeletal mammalian tissues are biological apatites or bioapatites. They are highly substituted hexagonal calcium phosphates resembling the structure of hydroxylapatite [$Ca_{10}(PO_4)_6(OH)_2$] (Lee-Thorp, 2002). Bioapatites vary in the kind and degree of substitutions, function and crystallinity. Carbonate ions are either 1) substituted within the bioapatite in the phosphate position (referred to as structural carbonate or 'B' carbonate) and to a lesser extent in the hydroxyl position (referred to as 'A' carbonate), or, 2) adsorbed onto crystal surfaces (referred to as adsorbed carbonates) (LeGeros and LeGeros, 1983; LeGeros, 1981). Enamel apatite differs from dentine and bone apatite with fewer substitutions, less distortion, greater long-range order and larger crystal size (LeGeros, 1991), characteristics that mean enamel is more resistant to digenesis in comparison to bone and dentine because it's more crystalline and stable structure reduce chances of post mortem recrystallization (Koch et al., 1997; Lee-Thorp and van der Merwe, 1991). The organic matrix of phosphoproteins and amelogenins is negligible in enamel (<1%), while the proportion of organics (collagen) in dentine and bone is larger (~20-30%) (Lee-Thorp, 2002). As tooth enamel and dentine are incremental tissues forming at similar times and rates the isotopic composition of the tooth apatite reflects conditions during tooth formation, which in the majority of mammals is in the early stages of the individuals life (Lee-Thorp, 2008). The $\delta^{18}O$ and $\delta^{13}C$ of mammalian enamel bioapatite is widely applied to infer climate and environmental conditions such as aridity, rain water sources, climate seasonality, relative humidity and vegetation cover (Ayliffe et al., 1992;

Cerling et al., 2004, 1997; Fricke and O'Neil, 1996; Hoppe, 2006; Levin et al., 2006; Sponheimer and Lee-Thorp, 2001).

4.3.1.2. Bone and dentine collagen

Collagen, a protein composed of a multiple helical peptide fibrils, is the main constituent of the organic phase of bone from which the $\delta^{13}C$ and $\delta^{15}N$ of the tissue can be determined. Bone is a living tissue that re-models throughout the life of an individual; therefore the isotope composition of the bone collagen reflects a long-term average that depends on the age and/or life-span of the individual (Hedges et al., 2007; Lee-Thorp, 2008). The $\delta^{13}C$ and $\delta^{15}N$ composition of human bone collagen is commonly used to investigate palaeodiet (Richards et al., 2003, 2001; e.g. Vogel and van der Merwe, 1977), while the $\delta^{13}C$ and $\delta^{15}N$ composition of mammal tissues has been used to explore palaeoclimate and palaeoenvironment (Drucker et al., 2011; Stevens et al., 2008).

4.3.2. $\delta^{18}O$ in mammalian bioapatite

Mammalian bioapatite is precipitated in isotopic equilibrium with body water. The isotopic composition of the tissue is influenced by: 1) the $\delta^{18}O$ composition of body water and 2) the temperature at which the reaction takes place; however, because mammals have a constant body temperature the second variable is not a factor (Longinelli, 1984). Body water $\delta^{18}O$ is controlled by the balance of oxygen inputs and outputs; inputs include drinking water, food oxygen, and atmospheric O_2 and outputs comprise of fluids (e.g sweat, urine), respired CO_2 and water vapour (Bryant and Froelich, 1995; Kohn, 1996; Luz

and Kolodny, 1985; Luz et al., 1984) (Figure 4.7). The $\delta^{18}O$ composition of bioapatite is enriched relative to that of ingested water with the fractionation between carbonate and body water measured between ~-26 and -27‰ (Bryant et al., 1996; Podlesak et al., 2008).

The physiology of the mammal influences the $\delta^{18}O$ composition of body water because of mass balance. Thus body water in mammals, deriving the majority of their water from plant water (non-obligate drinkers), tends to be enriched in ^{18}O compared to mammals that drink regularly (obligate drinkers) (Kohn, 1996) because plant leaf water is relatively enriched in $H_2{}^{18}O$ compared to local environmental water due to preferential evapotranspiration of the lighter molecule ($H_2{}^{16}O$) (Section 4.2.1.2) (Gonfiantini et al., 1965; Yakir, 1992). Levin et al. (2006) termed these mammals evaporative sensitive and evaporative insensitive because obligate drinkers reflect the $\delta^{18}O$ composition of local meteoric water (Ayliffe et al., 1992; Fricke et al., 1998; Hoppe, 2006), while non-obligate drinkers reflect water availability and aridity (Ayliffe and Chivas, 1990; Cormie et al., 1994; Delgado Huertas et al., 1995; Iacumin and Longinelli, 2002). As arid-adapted animals, gerbils' water requirements are largely met by plant water and they drink only small amounts of free water (Laughlin et al., 1975; Winkelmann and Getz, 1962) and are therefore indirectly sensitive to relative humidity.

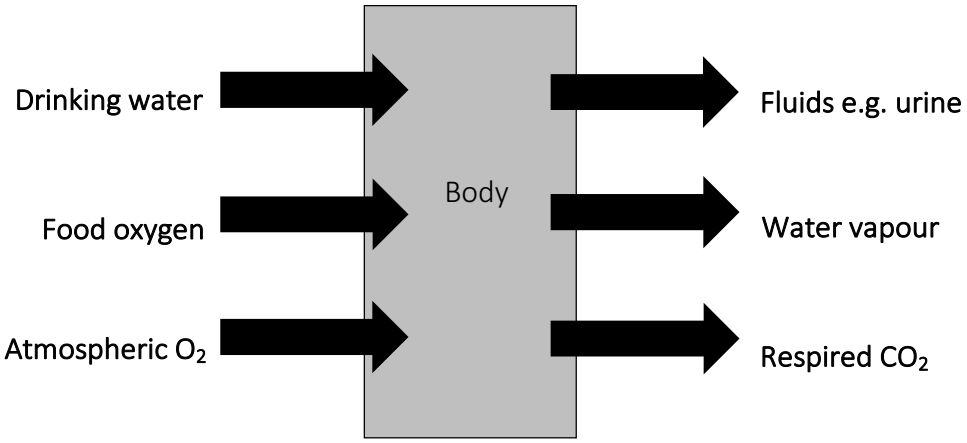

Figure 4.7: Mammalian body water oxygen inputs and outputs (after Luz et al. 1984).

4.3.3. $\delta^{13}C$ in mammalian bioapatite and bone collagen

$\delta^{13}C$ in mammals reflects that of ingested food. The carbon fraction of bioapatite is precipitated from dissolved inorganic carbon (DIC) derived from metabolic CO_2 (Passey et al., 2005). Controlled feeding experiments show that protein carbon in bone tissues is preferentially routed directly to the collagen fraction of the bone (Ambrose and Norr, 1993; Jim et al., 2004; Tieszen and Fagre, 1993). This means that while the $\delta^{13}C$ composition of bioapatite reflects overall diet representing contributions from proteins, carbohydrates and lipids, the $\delta^{13}C$ composition of collagen reflects that of the protein component of the diet. An offset in $\delta^{13}C$ may be expected between the $\delta^{13}C$ composition of modern gerbil bone collagen and tooth apatite because both tissues reflect different dietary components (dietary protein vs. whole diet) as well as distinct temporal periods, although because gerbils get all their dietary protein from plant parts a large offset is not anticipated.

The $\delta^{13}C$ composition of bone collagen and bioapatite are enriched in ^{13}C relative to diet. Several studies on humans and herbivores show that the offset

in $\delta^{13}C$ between diet and collagen is ~5‰ (Kreuger and Sullivan, 1984; Lee-Thorp et al., 1989; Vogel, 1978; Vogel and van der Merwe, 1977), with a smaller spacing noted in small mammals (Ambrose and Norr, 1993). The fractionation between bioapatite and diet is larger and size-specific. Feeding and field experiments show that herbivorous ungulates consistently have an enamel-diet spacing of 12-14‰ (Balasse et al., 2002; Cerling and Harris, 1999; Lee-Thorp and van der Merwe, 1987; Passey et al., 2005; Sullivan and Krueger, 1981). Controlled feeding studies on small mammals report enamel-diet spacing of 11.5 ± 0.3‰ in voles (Passey et al., 2005) and 11.0 ± 0.1‰ in woodrats (Podlesak et al., 2008), which adds to the growing evidence that supports smaller fractionation factors in small mammals (c. 10‰ in bone bioapatite of laboratory rats and mice) (Ambrose and Norr, 1993; DeNiro and Epstein, 1978; Jim et al., 2004; Tieszen and Fagre, 1993). Passey et al. (2005) showed that the fractionation between bioapatite and blood bicarbonate was constant in all animals. This suggests that the fractionation differences between species must occur in the formation of the animal's bicarbonate pool and is related to digestive physiology (Passey et al., 2005).

The $\delta^{13}C$ of mammal tissues is used to infer the amount of C_3 and C_4 vegetation consumed by the animal, which is then used to reconstruct vegetation cover (e.g. Cerling et al., 1997; Hynek et al., 2012). In Mediterranean North Africa one of the environmental effects reflected in the $\delta^{13}C$ of the gerbil tissues will be water deficit/aridity on the on the predominant C_3 vegetation (Section 4.2.2.2). Previous modern studies have shown that the

$\delta^{13}C$ of mammal body tissue is correlated with MAP in C_3 environments (Crowley et al., 2011; Hartman, 2012).

4.3.4. $\delta^{15}N$ in mammalian bone collagen

The $\delta^{15}N$ composition of mammalian tissues reflects the protein component of the diet (DeNiro and Epstein, 1981). The $\delta^{15}N$ value of a mammal is greater than the food it consumes and there is trophic level enrichment in $\delta^{15}N$ of approximately ~3-5‰ up the food chain (Minagawa and Wada, 1984; Schoeninger and DeNiro, 1984), meaning that the $\delta^{15}N$ value of bone collagen can be used to determine trophic level position. As herbivores, the gerbil $\delta^{15}N$ will reflect the same trophic level position so the variation in $\delta^{15}N$ results from other factors.

$\delta^{15}N$ diet-tissue fractionation and the parameters that control this remain poorly understood. Physiological, metabolic, environmental and anthropogenic parameters can all influence the $\delta^{15}N$ composition of herbivore bone collagen, making the interpretation complex (Makarewicz and Sealy, 2015). Diet-tissue fractionation is variable with reported values in different mammal species ranging from ~2-7‰ (Ambrose, 2000; DeNiro and Epstein, 1981; Hare et al., 1991; Robbins et al., 2005; Sponheimer et al., 2003). Sponheimer et al. (2003) showed in controlled feeding experiments that different species have varying $\delta^{15}N$ values even when fed identical diets. Large numbers of $\delta^{15}N$ studies have been undertaken on herbivores from temperate European settings, which has led to the notion that little variation is displayed in the $\delta^{15}N$ of herbivores' bone collagen, and that the $\delta^{15}N$ values of herbivores will be low (~4-6‰) (Makarewicz and Sealy, 2015). In fact, the $\delta^{15}N$ value of herbivores can be

higher than 10‰ and extremely variable, especially in arid environments (Codron et al., 2005; Hartman and Danin, 2010; Hartman, 2011; Heaton et al., 1986; Makarewicz and Tuross, 2006; Murphy and Bowman, 2006).

Several studies have demonstrated a negative correlation between the $\delta^{15}N$ value of herbivore body tissue and rainfall (Crowley et al., 2011; Grocke et al., 1997; Hartman, 2011; Murphy and Bowman, 2006; Pate and Anson, 2008; Sealy et al., 1987). Different hypothesises suggest that animal physiology explains why mammals in arid environments have body tissues enriched in ^{15}N relative to those from more mesic settings (Ambrose and DeNiro, 1986; Balter et al., 2006; Sealy et al., 1987). However, recent modern analogue studies suggest that the $\delta^{15}N$ composition of mammal tissue reflects that of diet (Hartman, 2011; Murphy and Bowman, 2006), and the relationship between herbivore tissue $\delta^{15}N$ and rainfall exists because of the negative correlation noted between $\delta^{15}N$ value of plants and rainfall (Section 4.2.3.2). Considering the variability noted in $\delta^{15}N$ within ecosystems (Section 4.2.3) and that $\delta^{15}N$ varies temporally (Drucker et al., 2011; Stevens et al., 2008), questions have been raised as to how useful the $\delta^{15}N$ composition of bone collagen is as an aridity proxy (Makarewicz and Sealy, 2015).

4.4. Summary

This chapter has summarised the parameters that affect the stable isotope composition of food and water consumed by mammals and how these isotope values are reflected in mammal tissues. Although much of the evidence used was from modern and palaeo studies relating to large mammals, the same

principles can also be applied to small mammal tissues (see Chapter 1). The following chapter describes the modern isotope ecology study undertaken on gerbils in northwestern Africa that aims to understand the influences on the stable isotope composition of their skeletal tissues.

5. Modern Gerbillinae stable isotope ecology in northwestern Africa: implications for reconstructing palaeoenvironment

5.1. Introduction

This chapter describes the modern isotope study that was undertaken on Gerbillinae (gerbil) in northwestern Africa. The $\delta^{18}O$ and $\delta^{13}C$ composition of gerbil tooth apatite and $\delta^{15}N$ and $\delta^{13}C$ composition of gerbil bone collagen was determined to examine the effects of aridity and moisture availability on the isotope composition of small mammal tissues in semi-arid and arid environments. Using modern gerbil material sampled across a rainfall gradient (100-600mm MAP) from the Atlantic coast of North Africa to the to the edge of the Sahara Desert, the study aimed to explore: 1) the sensitivity of $\delta^{13}C$ composition of gerbil tooth apatite and bone collagen to moisture availability; 2) whether the $\delta^{15}N$ composition of gerbil bone collagen reflects aridity; 3) whether the isotopic composition of precipitation or moisture availability exerts the primary influence on the $\delta^{18}O$ composition of gerbil tooth apatite; and 4) the effects of temporal development period on the $\delta^{18}O$ and $\delta^{13}C$ composition of gerbil molar and incisor teeth. Gerbils were chosen because they have known physiological adaptations to aridity, such as reliance on metabolic water, a low metabolic rate and large surface-area-to-volume ratio (Merritt, 2010) and, importantly are also abundant in archaeological and palaeontological sites of northwestern Africa (including Taforalt and El Harhoura 2), where they are considered to be good indicators of open and relatively dry environments (Stoetzel et al., 2011). The implications of using gerbil $\delta^{18}O$ and $\delta^{13}C$ tooth

apatite as a proxy climate record are discussed. The $\delta^{18}O$ and $\delta^{13}C$ results from the modern tooth apatite are published in Jeffrey et al. (2015).

5.2. Material and methods

5.2.1. Gerbil material

Owl pellets (that containing remains of gerbils amongst other prey) were collected from eight sites located in a rainfall gradient in Morocco and Algeria (Figure 5.1, Table 5.1). Figure 5.1 shows that the sites are located across a range of different bioclimatic zones (~30°-35°N), from relatively mesic environments on the Atlantic coast of Morocco, through to semi-arid and arid desert. Merja Zerga is a salt marsh lagoon that lies directly on the Atlantic coast of Morocco and is the most mesic site in the study, receiving ~600mm mean annual precipitation (MAP) (Table 5.1). Guenfouda, Oued Nfifikh, Ouled Boughadi, Berrechid and Sidi Chicker are all located north of the Atlas Mountains in the Atlantic and Mediterranean coastal zones of Morocco. Guenfouda, Sidi Chicker and Ouled Boughadi belong to semi-arid steppic environments. The vegetation at each of these sites is locally variable and includes steppe grasslands, scrub, cultivated fields and open oak forests. Tata and Beni Abbes lie south of the Atlas Mountains in the Moroccan and Algerian Sahara; both are arid sites with <200mm MAP (Table 5.1).

In order to obtain sufficient sample sizes from each site the skulls of *Meriones* sp. and *Gerbillus* sp. (identification to taxa by E. Stoetzel) were removed from individual owls pellets. The hunting range of owls can range between <1km to up to 10km from the nest, but varies according to territory, region, season and

prey availability (Andrews, 1990). The barn owl (*Tyto alba*) is known to have a small territory (<5km from the nest), while the large European eagle owl (*Bubo bubo)* also hunts in a relatively larger territory (<10km from its nest) (Mikkola, 1983). Less is known about the diet and hunting habits of the endemic North African relative of *B. bubo*, *B. ascalaphus* (Stoetzel and Denys, 2011), and it is assumed that it resembles the former (Table 5.1).

Meriones and *Gerbillus* genera belong in the family Muridae and subfamily Gerbilliane so both are classed as gerbils and have similar behaviours and physiologies (Table 5.2). These genera have different distributions across the varied environments of North Africa (Table 5.2). *Meriones shawii* and *Meriones grandis* are found in relatively humid biotopes in the semi-arid Mediterranean climate zone of North Africa and were collected from sites north of the Atlas Mountains. *Meriones crassus* and *Meriones libycus* are distributed across Saharan North Africa and were collected from Beni Abbes. *Gerbillus campestris* is widely distributed across North Africa in Mediterranean and Saharan locations; it is the only *Gerbillus* sp. present at the majority of sites (Oued Nfifikh, Sidi Chicker, Ouled Boughadi, Merja Zerga). Several *Gerbillus* sp. were collected from Tata and Beni Abbes including *G. gerbillus*, *G. henleyi, G. nanus, G. tarabuli, G. pyramidum.*

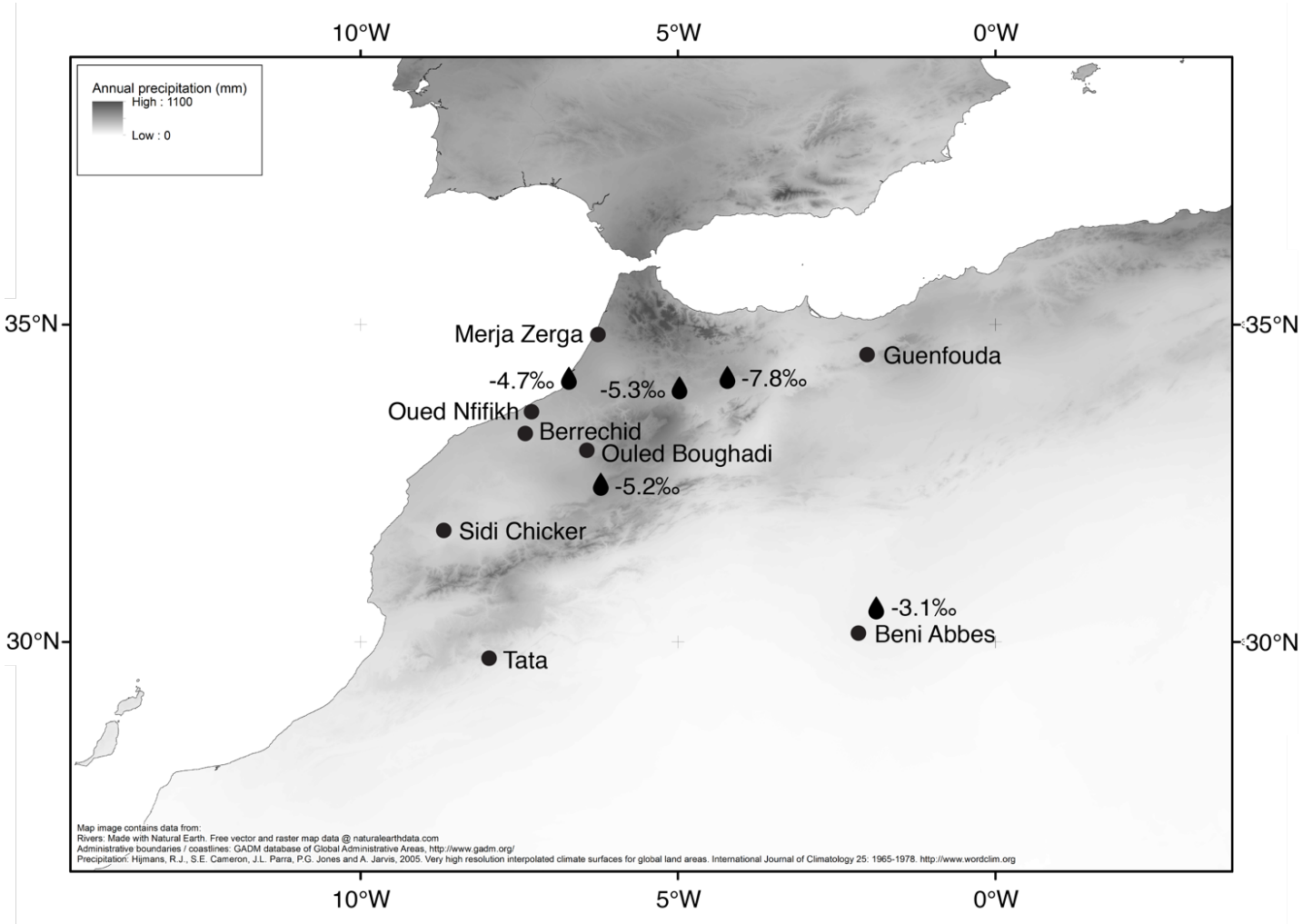

Figure 5.1: Map of northwestern Africa showing modern modelled MAP (downloaded from www.worldclim.org) (Hijmans et al., 2005). Blacks dots show the eight locations from which gerbil teeth were collected. Raindrops show the location of GNIP stations (http://www-naweb.iaea.org/) (Beni Mellal, Rabat-Cnesten, Fes Sais, Bab Bou Idir and Beni Abbes) with the weighted mean annual $\delta^{18}O_{mw}$. Darker shading indicates areas with higher MAP, while lighter shading show areas with low MAP.

Table 5.1: Geographical, environmental, climate and local vegetation data for the gerbil collection sites across northwestern Africa. The modelled mean annual precipitation (MAP) data was downloaded from WorldClim (http://www.worldclim.org/), while the modelled annual $\delta^{18}O_{mw}$ is from the Isotopes in Precipitation calculator (www.waterisotopes.org).

Site Name	GPS coordinates	Altitude (m asl)	Number of Gerbillinae individuals	Owl pellets/nest	Predominant local vegetation	Modelled mean annual precipitation (mm)	Modelled annual $\delta^{18}O$‰mw(VPBD)	Predator
Beni Abbes Algeria	30°07'48 N 02°09'56 W	597	10 (4 *Meriones,* 6 *Gerbillus*)	Pellets	Open desert	106	-5.0	*Tyto alba/Bubo ascalaphus?*
Tata Morocco	29°44'34 N 07°58'21 W	690	8 (8 *Gerbillus*)	Pellets	Cultivated, open	169	-4.7	*Bubo ascalaphus*
Sidi Chicker Morocco	31°45'39 N 08°41'26 W	209	25 (12 *Meriones*, 13 *Gerbillus*)	Nest	Steppe grassland, cultivated, open forest	263	-4.0	*Asio otus*
Guenfouda Morocco	34°31'25 N 02°01'09 W	530	5 (4 *Meriones*, 1 *Gerbillus*)	Pellets	Steppe grassland, scarce olive-trees and pistachio-trees (indigenous), pines (invasive)	326	-5.9	*Bubo ascalaphus*
Berrechid Morocco	33°17'45 N 07°24'30 W	219	2 (2 *Gerbillus*)	Pellets	Wheatfield and diverse cultivation (garden, potato, vegetables)	367	-4.4	*Tyto alba?*
Oued Nfifikh Morocco	33°38'00 N 07°18'00 W	417	6 (6 *Gerbillus*)	Pellets	Wheatfield and potato cultivation , oak forest alternating with open areas	378	-4.3	*Tyto alba*
Ouled Boughadi Morocco	33°00'18 N 06°24'34 W	844	8 (4 *Meriones*, 4 *Gerbillus*)	Pellets	Cultivated (wheat, barley), open areas, locally rocks and scarce trees/scrubs	451	-5.5	Unknown (cf. *Tyto alba?*)
Merja Zerga Morocco	34°51'00 N 06°16'00 W	10	6 (6 *Gerbillus*)	Pellets	Woodland, scrub, grassland, humid meadow	605	-4.2	*Asio capensis?*

Table 5.2: Biogeographical, behavioural and ecological data for Gerbillinae used in this study. Sourced from Aulagnier & Thévenot (1986), Kowalski & Rzebik-Kowalska (1991), Kingdon (1997) and Aulagnier et al. (2009).

Species	Distribution in North Africa	Habitat	Diet	Activity	Collection sites
Meriones shawii and/or *grandis*	Mediterranean semi-arid and arid bioclimate zones in North Africa.	Found in steppes and cultivated areas, sometimes in desert areas but only in gardens and oases.	Granivore that mainly feeds on cereals, but also fruits, stems, leaves and insects.	Nocturnal	Sidi Chicker, Guenfouda, Ouled Boughadi
Meriones cf. *crassus*	Saharan North Africa	Arid areas with compact sandy soils such as wadis and hamadas.	Granivore that mainly feeds on cereal, but also on stems, fruits and insects.	Nocturnal	Beni Abbes
Meriones cf. *libycus*	Saharan North Africa	Arid and semi-arid areas with sparse vegetation cover.	Feeds on fruits of legumes, grasses and chenopods.	Nocturnal or diurnal (depending on region)	Beni Abbes
Gerbillus campestris	Wide spread across North Africa including the Mediterranean and Sahara.	Cultivated areas and Mediterranean steppes. Saharan populations live in oases and rocky areas with sparse vegetation, not in sand dunes.	Granivore that mainly feeds on seeds, but also leaves, stems and fruits, as well as a significant contribution of insects.	Nocturnal	Oued Nfifikh, Sidi Chicker, Ouled Boughadi, Merja Zerga
Gerbillus gerbillus	Widespread across Saharan North Africa.	Adapted to arid habitats, mainly dunes and other large sandy areas with sparse vegetation cover.	Granivore that mainly feeds on cereal, but also on leaves, fruits and buds.	Nocturnal	Tata
Gerbillus henleyi and/or *nanus*	*G. henleyi*: Saharan areas extending east to the Arabian Peninsula. *G. nanus*: Saharan North Africa extending north to the Atlas Mountains.	*G. henleyi*: Extremely arid areas such as sand dunes, salt marshes, wadis, hamadas and stony plains. *G. nanus*: Arid regions with relatively abundant vegetation cover. Favours wadis and other habitats with sandy soil cover.	*G. henleyi*: Granivore. Feeds more on seeds than any other Gerbil species. *G. nanus*: Feeds on gramineous plants, seeds and buds.	Nocturnal	Beni Abbes, Sidi Chicker
Gerbillus tarabuli	Saharan and Sahelian areas of Northwestern Africa	Coastal steppes and inland deserts.	Seeds and fruits.		Beni Abbes

5.2.2. Modern climate data from North Africa

The coastal region of North Africa has a typical Mediterranean climate with the majority of precipitation falling between October and May (Chapter 3). Precipitation mainly originates from the Atlantic Ocean and is transported by the predominant westerly winds, but air masses can occasionally originate from the Mediterranean Sea (Ouda et al., 2005). The northern fringe of the Sahara, where both Tata and Beni Abbes are located, lies on the extreme southern edge of the mid-latitude storm track. Precipitation in this region is infrequent and variable and could be of Atlantic or even monsoon source (Knippertz et al., 2003). Observed precipitation data from Beni Abbes (source: Global Network of Isotopes in Precipitation (GNIP)) shows that precipitation tends to fall during the winter months, suggesting an Atlantic source, because mid-latitudes westerlies predominate during the winter in this region. Although instrumental weather data are available in Morocco and Algeria, the weather stations are distant from the collection sites. Therefore, modelled climate data were used for each site from *WorldClim* (www.worldclim.org) (Hijmans et al., 2005). The Worldclim data are an interpolated climate surface model for global terrestrial areas at a 1-km spatial resolution, developed using observed historical MAP data (1950-2000) from global weather stations. The historical precipitation data coverage from the Mediterranean zone of North Africa are good, and in general suggest that the Worldclim MAP model has a high degree of accuracy for this region. Modelled MAP data were used as a proxy for moisture availability or aridity at each owl pellet location.

Monthly precipitation and directly measured $\delta^{18}O_{mw}$ values are available from five Global Network of Isotopes in Precipitation (GNIP) (http://www.iaea.org/water) stations in the study region (Figure 5.1). The annual weighted $\delta^{18}O_{mw}$ mean from the Atlantic coast towards the Atlas appears to be consistent (~-5‰) according to observations on the coast at Rabat-Cnesten (75m asl) and further inland at slightly higher altitudes at Fes Sais (571m asl) and Beni Mellal (~468m asl). At the higher altitude site of Bab Bou Idir (1500m asl), $\delta^{18}O_{mw}$ is lower (~-7‰), reflecting an altitude effect (Dansgaard, 1964). The annual weighted $\delta^{18}O_{mw}$ mean at Beni Abbes (in the Sahara Desert), based on GNIP observations between 1966-1968, is -3.1‰, suggesting that higher temperatures and evaporation override the Rayleigh distillation (continental) isotope effect on rainfall. The mean monthly $\delta^{18}O_{mw}$ at Beni Abbes is large and ranges from +13.6 to -8.2‰, indicating frequent evaporative enrichment of precipitation in the atmosphere. In addition to greater variability, most precipitation falls within one or two months of the year.

Where there is overlap, modelled $\delta^{18}O_{mw}$ values fit well with that of observed $\delta^{18}O_{mw}$ values for each site from the GNIP stations located across Morocco and Algeria (Table 5.1, Figure 5.1). As Sidi Chicker and Guenfouda have no current nearby GNIP stations, modelled $\delta^{18}O_{mw}$ data were used from the Isotopes in Precipitation Calculator (www.waterisotopes.org) (Bowen and Revenaugh, 2003) for each site. The values used for each site are shown in Table 5.1.

5.2.3. Ecological considerations

Gerbils are classed as granivores, meaning the vast majority of their diet consists of seeds and plant parts (roots, leaves, flowers, stems and fruits); only rarely do they consume insects and other resources (Adamou-Djerbaoui et al., 2013; Adamou-Djerbaouiz et al., 2010; Aulagnier et al., 2009; Petter et al., 1984; Zaime and Gautier, 1989) (Table 5.2). Gerbils have been observed to consume a large number of plant species, and feeding strategies vary between individuals (Belabbas and Butet, 1994; Zaime and Gautier, 1989). Gerbil diets can vary seasonally depending on the availability of food. For example *M. shawii* diet consists almost entirely of leaves and grains during the summer months and flowering plants during the winter months (Adamou-Djerbaoui et al., 2013). In the semi-arid and arid environments of North Africa free water is not readily available, especially during the hot, dry summer season, therefore gerbils obtain water from the grains and the plant parts they consume. This means that they mainly subsist on metabolic water that is made by body cells from the oxidation of food, especially carbohydrates (Merritt, 2010). To avoid the heat and water loss through evaporation gerbils are active and search for food at dusk and during the night. They spend the daytime in their relatively humid and cool burrows, where they store dry seeds to allow the absorption of water vapour (Merritt, 2010).

Reproduction in gerbils is strongly linked to climate factors such as rainfall, which influences the availability and nutritional quality of the plant food available (Zaime and Gautier, 1989, 1988). Consequently their breeding season may vary from year to year. In northern Morocco, *M. shawii* generally breeds in

spring and summer (between March and September), while pregnant *G. campestris* females have been captured up till November (Belabbas and Butet, 1994). In the Moroccan Saharan the gerbil breeding season may occur throughout the winter and spring months, coinciding with the winter rains and vegetation growth (Khammar and Brudieux, 1987; Zaime et al., 1992).

5.2.4. Tissue considerations

Gerbils develop and grow quickly reaching sexual maturity at approximately 40-80 days depending on the species (Koffler, 1972). This is noteworthy for stable isotope studies because, as discussed in Chapter 1, their fast body-tissue turnover times could result in hair, bone and teeth having distinct isotope values (Podlesak et al., 2008). The life-span of gerbils is short, and the average life expectancy of wild gerbils is unknown. It is thought that more are preyed upon during the breeding season when the population increases (Royer et al., 2014), which would result in many being captured young possibly at <6 months of age. Therefore, it is expected that the isotope signal reflected in their bone will reflect average conditions of their lifetime that could range from <6 months up to 2-3 years.

In one half of their mandible and maxilla *Meriones* and *Gerbillus* have one single incisor tooth in the anterior separated from 3 cheek teeth (1st molar, 2nd molar, 3rd, molar) by a wide diastema (Hillson, 2005) (Figure 5.2). The incisors erupt when the animal is approximately 9-18 days old (Daly, 1975; Happold, 1968; Koffler, 1972) and continue to grow (and wear) throughout the individual's life. The enamel layer occurs only on the buccal surface. Studies of incisor growth rates in species of voles, rats and mice all conclude that an incisor is fully replaced within 24-50 days (Addison and Appleton, 1915; Coady et al., 1967; Klevezal et al., 1990; Schour and Massler, 1963). If gerbil incisors grow at similar rates to other rodents, then these teeth reflect the last 4-8 weeks of the animal's life. In contrast, the molars are permanent rooted teeth that begin development *in utero* within days of one another. They are fully mineralised 4-8 days postnatal, except for the M3, which forms just after weaning (around 20 days) (Hiatt et al., 1974).

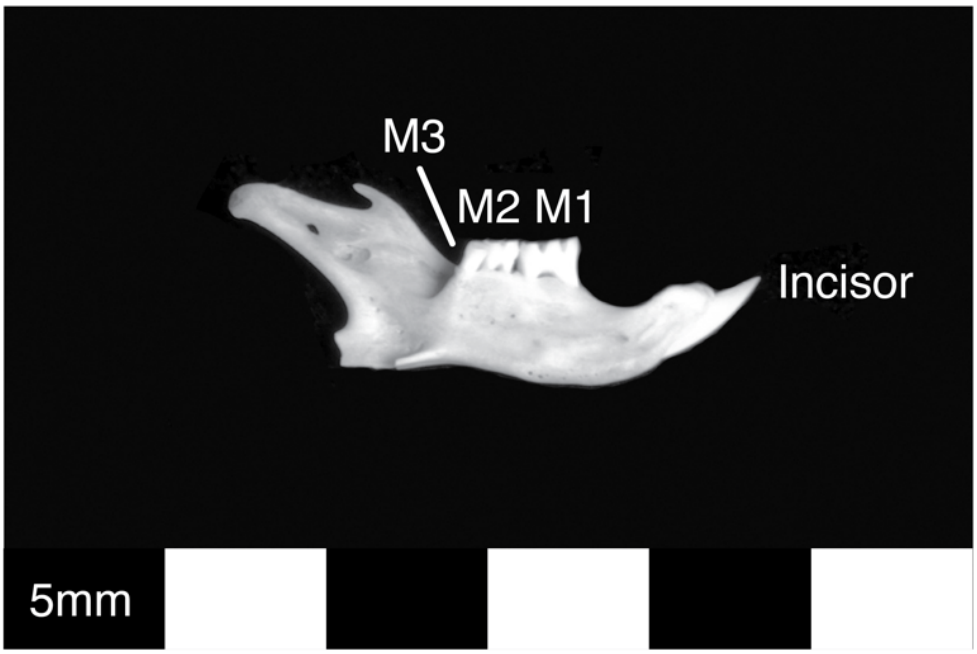

Figure 5.2: Gerbillinae mandible showing position of molar and incisor teeth.

Thus the stable isotope composition of the incisor and molar teeth from the same gerbil individual may differ due to the varying development times of each tooth type. Since most gerbils are born during the spring/summer months, it can be inferred that the isotopic composition of these molar teeth reflects the spring/summer season (breeding season), while the continuously growing incisor teeth are more likely to reflect the season in which the animal died. This will be explored in the inter-tooth analysis (see Section 5.6).

5.2.5. Stable isotope methods

5.2.5.1. Tooth apatite

Teeth selected for analyses were removed from the mandible/maxilla. To examine inter-tooth variation within individual's $\delta^{18}O$ and $\delta^{13}C$, measurements were undertaken on the incisor (I), 1st molar (M1) and 2nd molar (M2) of eleven *Meriones* individuals from the same side (left/right) of either the maxilla or mandible. Inter-tooth variation was more difficult to examine in *Gerbillus* because of the small size of the teeth. Where possible individual I and M1's from larger *Gerbillus* were analysed, but in order to obtain sufficient sample for isotopic measurement, tooth powder from either 2Is, 2 M1s or an M1 and M2 were combined. No attempt was made to analyse M3's for either species as they were small. $\delta^{18}O$ and $\delta^{13}C$ measurements were carried out on seventy gerbil individuals from the eight collection sites (Figure 5.1, Table 5.1), using one M1 from the *Meriones* and larger *Gerbillus* individuals, but either two M1's or an M1+ M2 from the smaller *Gerbillus* species (see Appendix 2). Molar teeth were not present in some of gerbil maxilla/mandible; therefore in a small

number of individuals $\delta^{18}O$ and $\delta^{13}C$ values from incisor teeth were used to increase sample size at three sites (see Table 5.4).

Exterior surfaces of the teeth were cleaned with a sand blaster to remove visible dirt. The roots of the molar teeth were removed and the tooth sectioned to allow removal of dirt from inside the tooth. The tooth was crushed using an agate mortar and pestle following the method of Gehler et al. (2012); no attempt was made to remove the dentine because it was strongly bound to the enamel, the teeth were small, and modern dentine is not considered diagenetic. Given the relatively short formation times for these teeth we assume that dentine apatite and enamel apatite represent the same period and conditions. The tooth samples were not pre-treated other than by mechanical cleaning. This was primarily due to their small size, and because it is extremely difficult to mechanically separate enamel and dentine in small modern teeth. Prior to the analyses of the modern and archaeological teeth, experiments were untaken to understand the influence of standard pre-treatment protocols (1.7% v/v sodium hypochlorite to remove organics, and 0.1M acetic acid to remove secondary carbonates (Sponheimer, 1999)) on bulk tooth material. The experiments on modern bulk molar and incisor material showed no consistent differences between the pre-treated and untreated material (Table 5.3).

Table 5.3: Effect of standard pretreatment methods (1.7% v/v sodium hypochlorite to remove organics, and 0.1M acetic acid to remove secondary carbonates) on bulk molar and incisor gerbil teeth material. Four analyses for $\delta^{18}O$ and $\delta^{13}C$ were carried out on both the incisor and molar material that had undergone different pretreatments; 1) no pretreatment, 2) 1hr NaClO, 10 mins 0.1M acetic acid, 3) 3hr NaClO, 10 mins 0.1M acetic acid, 4) 6hr NaClO, 10 mins 0.1M acetic acid.

	Bulk tooth material	**No Pretreatment**	**1 hr NaClO 10 minutes 0.1M acetic acid**	**3 hr NaClO 10 minutes 0.1M acetic acid**	**6 hr NaClO 10 minutes 0.1M acetic acid**
$\delta^{13}C$ (PDB ‰)	Incisor	-15.1	-15.4	-15.5	-15.6
	Molar	-14.3	-17.0	-14.6	-14.4
$\delta^{18}O$ (PDB ‰)	Incisor	0.4	0.4	0.1	0.4
	Molar	0.8	-1.4	1.1	1.3

Approximately 2mg of tooth powder was reacted with 100% phosphoric acid at 70°C in an automated Thermo Gas Bench II device, coupled with Thermo Delta V Advantage mass spectrometer, in the Stable Light Isotope Facility, University of Bradford. Data are reported in the δ-notation (Equation 2) as per mil (‰) relative to the international reference standard PDB for both $\delta^{18}O$ and $\delta^{13}C$. $\delta^{18}O$ values relative to SMOW were converted to PDB using Equation 3. The analytical precision for all measurements was better than 0.1‰ (1σ) for $\delta^{13}C$ and 0.2‰ (1σ) for $\delta^{18}O$ based on same-run replicates of two in-house standards, BES (tooth bioapatite enamel standard) ($\delta^{13}C$ = -11.1‰ (PDB), $\delta^{18}O$ = 25.0‰ (SMOW)) and Merck $CaCO_3$ ($\delta^{13}C$ = -35.45‰ (PDB), $\delta^{18}O$ = 13.35‰ (SMOW)). In run international standards NBS-19 gave values of 2.02‰ ± 0.01 for $\delta^{13}C$ and 28.76‰ ± 0.13 (n=3 for each run), while CO-1 gave 2.44‰ ± 0.02 for $\delta^{13}C$ and 28.46‰ ± 0.09 (n=4). Any notable outliers (values that fell outside

the data cluster) were re-run. If the value gave a similar value to previous analysis the average of the two analyses was used; however if the value was different to that of the first analysis (and fell into the data cluster) the second value was used.

$$\delta^{18}O = ((R_{sample}-R_{standard})/R_{standard})*1000 \quad (2)$$

$$\delta^{18}O_{VSMOW} = 1.03092\ \delta^{18}O_{VPDB} + 30.92 \quad (3)$$

5.2.5.2. Bone collagen

Gerbil skull and crania fragments (with teeth removed) were cleaned with a sand blaster to remove all visible dirt. Collagen was extracted using the standard protocol (modified Longin 1971)) described by Richards and Hedges (1999). The bone was demineralised in 0.5 M HCL at 5°C for approximately 24 hours and then rinsed three times with distilled water. The residue was then gelatinized in pH3 HCl solution for 48 hours at 75°C and finally freeze-dried. 1mg collagen samples were determined on a SERCON 20/22 continuous flow mass spectrometer coupled with an elemental analyser, at RLAHA, University of Oxford. Data are reported in the δ-notation as per mil (‰) (Equation 2) relative to the international reference standard PDB for $\delta^{13}C$ and AIR for $\delta^{15}N$. The collagen samples were measured over eight separate runs with an internal Alanine standard used to obtain the raw delta values and for drift correction. Runs 1-3 underwent a one-point normalisation because at the time of analysis suitable standards were not available to undertake a two-point normalisation. Two internal standards were included in these runs SEAL1 (Seal collagen, $\delta^{13}C$= -13.40‰ and $\delta^{15}N$ = 17.6‰) and MCC (cow collagen, $\delta^{13}C$= -24.28‰

and $\delta^{15}N$ = 7.76‰) and precision was better than 0.1‰ for $\delta^{13}C$ and 0.3‰ for $\delta^{15}N$. A two-point normalisation was carried out on the remaining runs (4-8) and was calculated on the PBD and AIR scales by interpolating the delta values of the samples against four replicates of two reference materials in each run. Runs 4 to 6 were normalised using USGS40 (-26.39‰ ± 0.04) and IAEA-CH6 (-10.449‰ ± 0.033) for $\delta^{13}C$ and USGS40 (-4.52‰ ± 0.06) and IAEA-N2 (20.3‰ ± 0.2) for $\delta^{15}N$. $\delta^{13}C$ and $\delta^{15}N$ were normalised in Runs 7 and 8 using USGS40 and internal reference material SEAL 2 (Seal collagen, $\delta^{13}C$= -13.33‰ ± 0.11 and $\delta^{15}N$ = 17.32‰ ± 0.29). The analytical precision for all measurements in Runs 4-8 was 0.07‰ (1σ) for $\delta^{13}C$ and 0.11‰ (1σ) for $\delta^{15}N$ based on the reproducibility of the internal Alanine standard that was measured 12 times in each run. All modern collagen samples had a C:N ratio within the accepted range, 2.9-3.6 (DeNiro 1985).

5.2.6. Statistical analyses

Statistical analyses were performed using the freeware statistics package 'R' (http://www.r-project.org/). A Shapiro-Wilk test was used to test for normality in datasets to establish whether parametric or non-parametric tests should be used. A T-test was performed to examine inter-genera variation in $\delta^{18}O$ and $\delta^{13}C$ composition of gerbil molar teeth and $\delta^{15}N$ and $\delta^{13}C$ composition of bone collagen between *Meriones* and *Gerbillus* at the site of Sidi Chicker, where high numbers of each genus were collected from an owl's nest. Low sample numbers limit the statistical exploration of inter-genera variation at the other seven sites. To evaluate whether the differences in the mean $\delta^{13}C$ and $\delta^{18}O$ composition of the gerbil molar teeth and mean $\delta^{15}N$ and $\delta^{13}C$ composition of

the bone collagen between sites was statistically significant an analysis of variance (ANOVA) was performed, followed by post-hoc tests (Tukey) for pairwise comparisons (Berrechid was not considered in the ANOVA due to small sample size). Linear models (least squares regression) were used to explore the relationship between the $\delta^{13}C$ composition of gerbil molar teeth, $\delta^{13}C$ composition of gerbil bone collagen, $\delta^{15}N$ composition of gerbil bone collagen and MAP. A linear model was also used to explore the relationship between the $\delta^{18}O$ composition of gerbil molar teeth, MAP and $\delta^{18}O_{mw.}$

5.3. Summary of modern Gerbillinae dataset

5.3.1. $\delta^{18}O$ and $\delta^{13}C$ in Gerbillinae teeth

Figure 5.3 presents the $\delta^{18}O$ and $\delta^{13}C$ composition of all 109 modern gerbil teeth analysed (1st molars n= 71, 2nd molars n= 11, incisors n=28) from 70 different gerbil individuals (53 *Meriones* and 57 *Gerbillus*) (data listed in Appendix 2). The mean $\delta^{18}O$ and $\delta^{13}C$ composition of the gerbil teeth is -1.8‰ ± 2.1 (1σ) and -13.4‰ ± 2.2(1σ), respectively. The $\delta^{18}O$ variation displayed by the gerbil teeth across northwestern Africa is 10.4‰ ranging from -5.2‰ to 5.2‰. The $\delta^{13}C$ composition of the teeth ranges from -17.7‰ to -4.6‰ with a total variation of 13.1‰. Figure 5.3 shows that the majority of gerbils have a $\delta^{13}C$ value of between ~-17‰ and -11‰, and only 7 teeth have $\delta^{13}C$ values of <-10‰.

5.3.2. $\delta^{15}N$ and $\delta^{13}C$ in Gerbillinae bone collagen

The $\delta^{15}N$ and $\delta^{13}C$ composition of the gerbil bone collagen ($\delta^{15}N_{col}$ and $\delta^{13}C_{col}$) from 79 individual's (26 *Meriones* and 53 *Gerbillus*) is presented in Figure 5.4

(data listed in Appendix 2). The mean $\delta^{15}N_{col}$ and $\delta^{13}C_{col}$ is 6.5‰ ± 2.1 (1σ) and -19.2‰ ± 3.3(1σ), respectively. The $\delta^{15}N_{col}$ variation displayed in the gerbils across northwestern Africa is 8.3‰ ranging from 2.9‰ to 11.2‰, while the $\delta^{13}C_{col}$ variation is 13.4‰, similar to the range recorded in the $\delta^{13}C$ values of the gerbil teeth, ranging from -23.3‰ to -9.9‰. Like the $\delta^{13}C$ values of the Gerbillinae teeth (Figure 5.3), Figure 5.4 also shows that the $\delta^{13}C_{col}$ falls in to two distinct groups; the majority of gerbils have $\delta^{13}C_{col}$ values between ~-23‰ and -17‰, but 8 individuals have higher values (>12.5‰). The 8 individual's with higher $\delta^{13}C_{col}$ also have higher $\delta^{13}C$ values in their teeth (Figures 5.3 and 5.4).

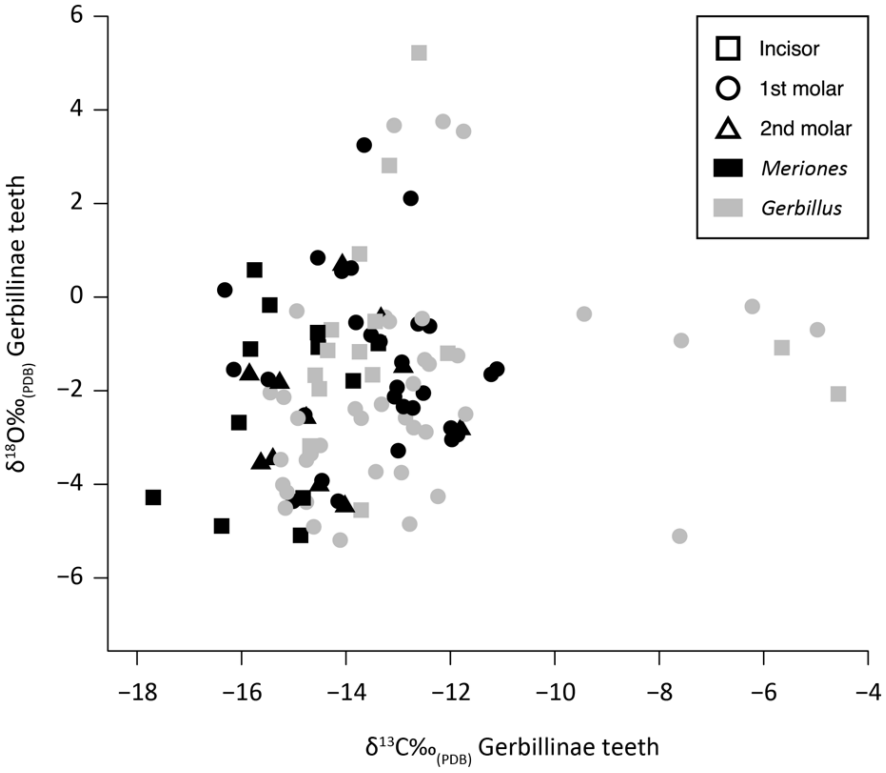

Figure 5.3: $\delta^{18}O$ and $\delta^{13}C$ values of 109 Gerbillinae teeth from sites across northwestern Africa.

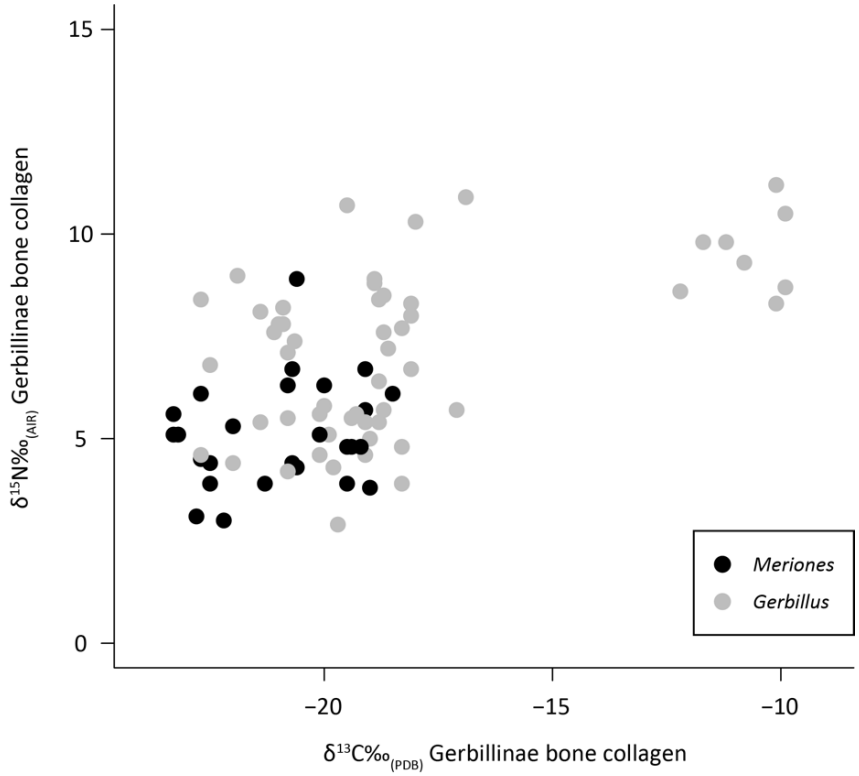

Figure 5.4: The $\delta^{15}N$ and $\delta^{13}C$ values of the bone collagen from the 79 Gerbillinae individuals from sites across northwestern Africa.

5.4. Inter-genus variation between *Meriones* and *Gerbillus* at Sidi Chicker

Inter-genus variation between *Meriones* sp. and *Gerbillus* sp. was examined at the site of Sidi Chicker, where high numbers of each genus were collected from an owl's nest. Variation between *Meriones* sp. and *Gerbillus* sp. was explored to assess whether isotope data from each genera could be combined to examine geographic/climate response. As described in Section 5.2.3 the ecology and behaviours of *Meriones* sp. and *Gerbillus* sp. are similar, and it is therefore hypothesised that there will be no large isotope offsets in either $\delta^{18}O$, $\delta^{13}C$ and $\delta^{15}N$ between the genus.

5.4.1. Inter-genus variation in the $\delta^{18}O$ and $\delta^{13}C$ of Gerbillinae teeth

The $\delta^{18}O$ and $\delta^{13}C$ composition of 12 *Meriones* and 13 *Gerbillus* molar teeth ($\delta^{18}O_{mt}$ and $\delta^{13}C_{mt}$) was analysed from the site of Sidi Chicker (Figure 5.5). Comparison of means for *Meriones* ($\delta^{18}O$ =-1.6‰ ± 1.2, $\delta^{13}C$=-12.9‰ ± 0.9) and *Gerbillus* ($\delta^{18}O$ =-2.0‰ ± 0.8, $\delta^{13}C$=-12.9‰ ± 0.9) molars show that they are similar and statistically indistinguishable (based on T-tests p= <0.05 in both cases). The results demonstrate that there is no inter-genus variation in $\delta^{18}O_{mt}$ and $\delta^{13}C_{mt}$ between *Meriones* sp. and *Gerbillus* sp. at Sidi Chicker (Figure 5.5). This is not entirely unexpected because *Meriones* and *Gerbillus* belong to the same sub-family (Gerbillinae) and have similar behaviours, diets and habitat preferences (Table 5.2). The species at Sidi Chicker (*M. shawii/grandis* and *G. campestris*) are all classed as granivores with very similar diets (Table 5.2). Likewise, they have comparable habitat preferences and can be found in Mediterranean steppes, cultivated areas and oases (Table 5.2). Thus

similarities in $\delta^{18}O$ and $\delta^{13}C$ compositions likely reflect similar moisture conditions and dietary pools, as well as suggesting that both species have a similar physiology and drinking behaviours.

The only other study to examine inter-genus variation in the $\delta^{18}O$ and $\delta^{13}C$ of teeth (CO_3 component) between sub-families of small mammal species was undertaken by Gehler *et al.* (2012). The $\delta^{18}O$ and $\delta^{13}C$ composition of 10 incisor teeth from 7 different species of small mammal, including voles, mice and rats, were measured from one temperate European location. Four species belong in the subfamily Arvicolinae (*Arvciola terrestris, Myodes glareolus, Microtus agretis and Microtus arvalis*), while three species are Murinae (*Apodemus sylvaticus*, *Mus musculus* and *Rattus norvegicus*). The $\delta^{18}O$ and $\delta^{13}C$ data from this study are summarized in Figure 5.6, along with the Gerbillinae data from this study. Gehler *et al.* 2012 reported that the Arvicolinae were statistically indistinguishable in $\delta^{18}O$, yet the $\delta^{18}O$ differed significantly within the Murinae species, between *A. sylvaticus* and *R. norvegicus* (Figure 5.6), probably as a result of different drinking behaviours and physiologies in both species. Gehler *et al.* (2012) showed that there was more inter-species variation in the $\delta^{13}C$ composition of the incisor teeth relative to that of $\delta^{18}O$ between Arvicolinae and Murinae. The $\delta^{13}C$ composition of *M. glareolus* and M. *agretis* incisor teeth were statistically different from one other, as well as differing from the other Arvicolinae species. There were also differences between Murinae species, *A. sylvaticus* and *R. norvegicus* (Figure 5.6). The offsets in tooth $\delta^{13}C$ reflect the species' different dietary behaviours and habitat preferences.

5.4.2. Inter-genus variation in the $\delta^{15}N$ and $\delta^{13}C$ of Gerbillinae teeth

The $\delta^{15}N_{col}$ and $\delta^{13}C_{col}$ from 13 *Meriones* and 19 *Gerbillus* individuals were analysed from Sidi Chicker (Figure 5.7). Comparison of means for *Meriones* ($\delta^{15}N_{col}$ =5.1‰ ± 1.0, $\delta^{13}C_{col}$=-19.9‰ ± 0.8) and *Gerbillus* ($\delta^{15}N_{col}$ =6.2‰ ± 1.7, $\delta^{13}C_{col}$=-19.3‰ ± 0.8) molars show that the $\delta^{13}C_{col}$ between the genus were statistically indistinguishable (T-test p= <0.05): however, the mean $\delta^{15}N_{col}$ between *Meriones* and *Gerbillus* differs by >1‰ showing they are statistically different in $\delta^{15}N$ (T-test p=0.04) (Figure 5.7).

Like in the $\delta^{13}C_{mt}$, there is no statistically significant offset between *Meriones* and *Gerbillus* in $\delta^{13}C_{col}$. As discussed in section 5.4.1 this again reflects the similarities in dietary behaviour and habitat preferences in both genus. Although the results indicate that there is a significant offset in $\delta^{15}N_{col}$ between *Meriones* and *Gerbillus*, Figure 5.7 shows the mean $\delta^{15}N_{col}$ is increased by four *Gerbillus* individuals that have a $\delta^{15}N_{col}$ >7‰, while the remaining *Gerbillus* have lower $\delta^{15}N_{col}$ and cluster with the *Meriones*. If the four *Gerbillus* with $\delta^{15}N_{col}$ >7‰ are removed from mean calculation, the mean $\delta^{15}N_{col}$ for *Gerbillus* at Sidi Chicker decreases to 5.4‰ ± 0.6, similar to that of *Meriones*. The *Gerbillus* with higher $\delta^{15}N_{col}$ may represent a different ecological niche or could have accumulated in a different season/temporal period.

5.4.3. Summary of inter-genera variation between *Meriones* and *Gerbillus* at Sidi Chicker

Comparison of isotope values between *Meriones* and *Gerbillus* show that they were indistinguishable in $\delta^{18}O_{mt}$, $\delta^{13}C_{mt}$ and $\delta^{13}C_{col}$. *Meriones* and *Gerbillus* did significantly differ in $\delta^{15}N_{col}$, but as discussed in section 5.4.2, this offset could

be biased by 4 *Gerbillus* individuals with increased $\delta^{15}N_{col}$. As *Meriones* and *Gerbillus* have similar isotope ecologies it allows the data from both genera, and all species, to be combined for the purposes of examining geographic/climate response variability in $\delta^{13}C$ and $\delta^{18}O$ (Section 5.5). Although $\delta^{15}N_{col}$ data will also be combined from *Meriones* and *Gerbillus* to explore climatic response the results should be treated tentatively due to potential species effects. As demonstrated by Gehler *et al.* (2012) there can be isotopic offsets between species within a sub-family, which is dependent on their physiology and behavioural ecology. Therefore, species effects should be addressed when using multiple species for assessing isotopic response to climate parameters.

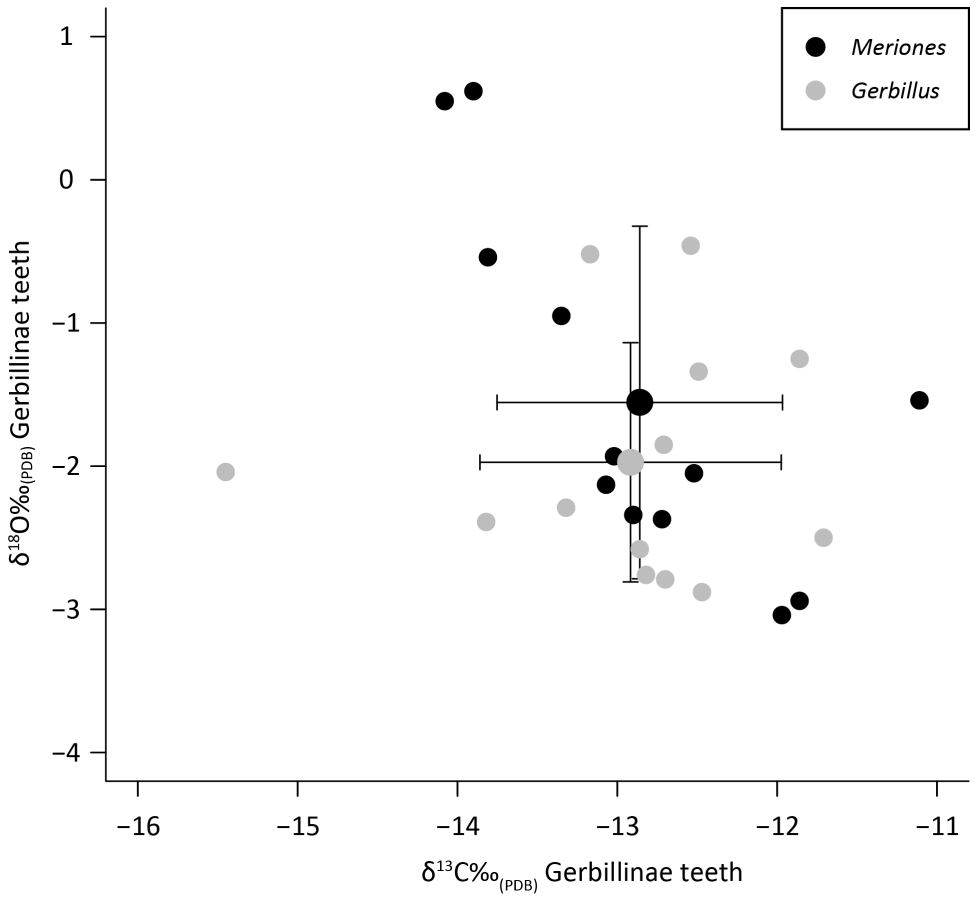

Figure 5.5: The $\delta^{18}O$ and $\delta^{13}C$ composition of *Gerbillus* (n=13) and *Meriones* (n=12) molar teeth at Sidi Chicker (small dots). The large dots show the mean and standard deviation (1σ) of each genus.

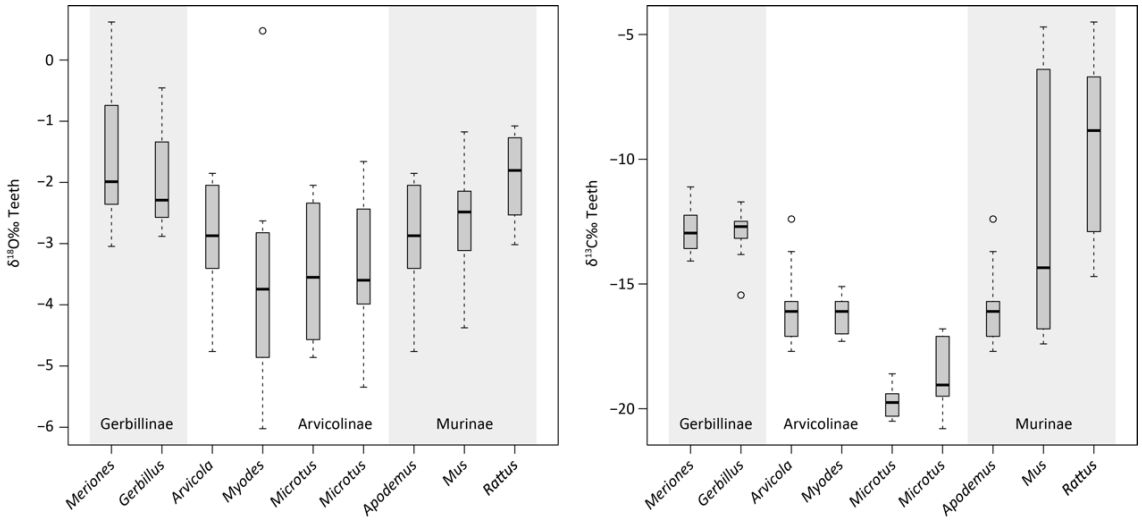

Figure 5.6: Boxplots showing the $\delta^{18}O$ and $\delta^{13}C$ intra-population variation displayed in small mammal teeth from species in the subfamily Gerbillinae (data from this study), Arvicolinae and Murinae (data from Gehler *et al*. 2012).

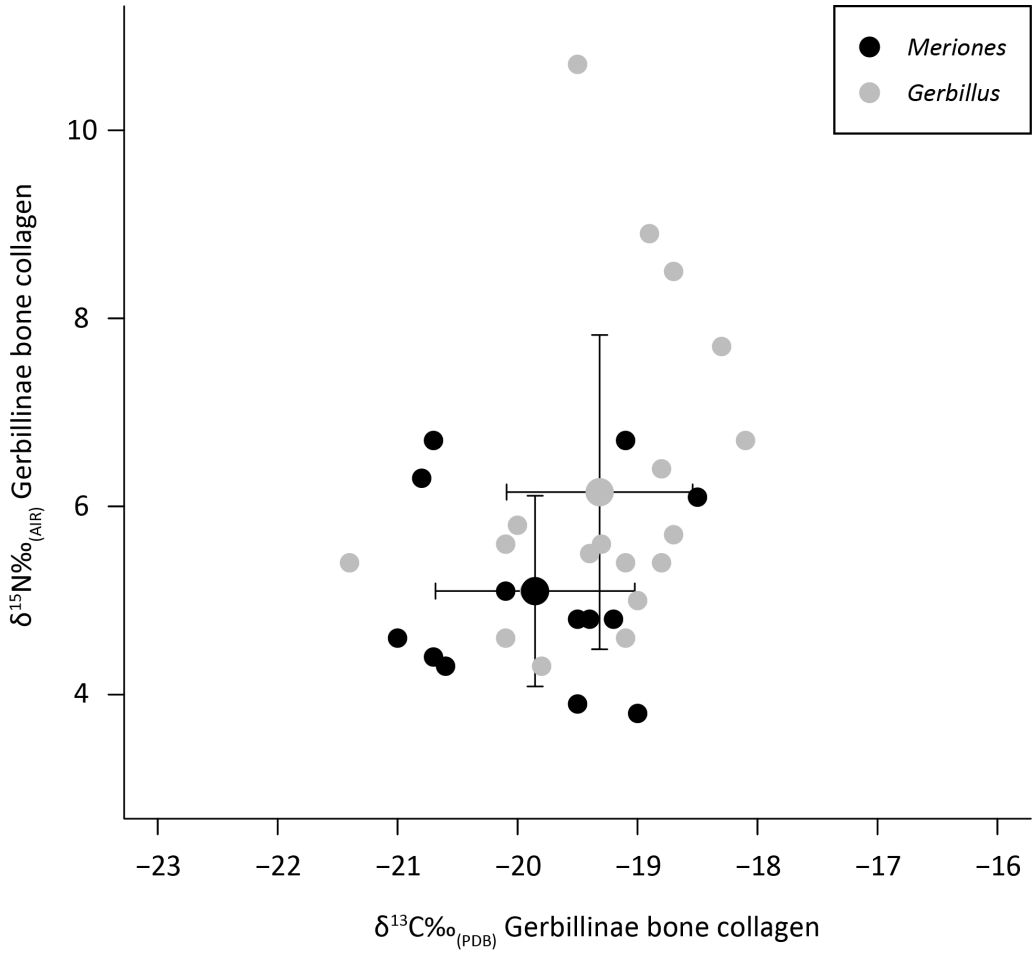

Figure 5.7: The $\delta^{15}N$ and $\delta^{13}C$ composition of *Gerbillus* (n=19) and *Meriones* (n=13) molar teeth at Sidi Chicker (small dots). The large dots show the mean and standard deviation (1σ) of each genus.

5.5. Stable isotope composition of gerbil tissues across northwestern Africa

This section presents the $\delta^{18}O$ and $\delta^{13}C$ values from the gerbil molar teeth and $\delta^{15}N$ and $\delta^{13}C$ values from gerbil bone collagen from the eight sites across northwestern Africa (Figure 5.1, Table 5.1). As discussed in Section 5.4, data from *Meriones* sp. and *Gerbillus* sp. are combined to increase sample size. Intra-population variation is explored and compared with other small mammal and large mammal datasets. The gerbil isotope data and modern climate data from northwestern Africa (Section 5.2.2) are used to test: 1) the sensitivity of $\delta^{13}C_{mt}$ and $\delta^{13}C_{col}$ to moisture availability, 2) whether the $\delta^{15}N_{col}$ reflects aridity, and 3) whether the isotopic composition of precipitation or moisture availability exerts the primary influence on $\delta^{18}O_{mt}$.

5.5.1. $\delta^{18}O$ and $\delta^{13}C$ composition of gerbil molar teeth in northwestern Africa

The gerbil $\delta^{18}O_{mt}$ and $\delta^{13}C_{mt}$ (n=70) data from the eight sites across northwestern Africa are plotted in Figure 5.8 and summary statistics are presented in Table 5.4. Variation in $\delta^{18}O$ for all the gerbil molars ranges from -5.2‰ to 3.8‰. Mean $\delta^{18}O_{mt}$ values at each site are 1.8‰ ± 1.9 (Beni Abbes), -0.9‰ ± 0.6 (Tata), -1.8‰ ± 1.0 (Sidi Chicker), -2.7‰ ± 1.2 (Guenfouda), -3.7‰ ± 0.7(Berrechid), -3.7‰ ± 0.9 (Oued Nfifikh), -3.5‰ ± 0.8 (Ouled Boughadi) and -4.5‰ ± 0.6 (Merja Zerga). Intra-site variation in $\delta^{18}O$ ranges from 1.0‰ at Berrechid to 4.3‰ at Beni Abbes. An analysis of variance (ANOVA) shows significant differences in $\delta^{18}O_{mt}$ between Beni Abbes, Tata, Sidi Chicker, Guenfouda, Oued Nfifikh, Ouled Boughadi and Merja Zerga (F = 30.94, P =

<0.01). A post hoc Tukey test shows significant differences between the $\delta^{18}O_{mt}$ at the arid sites with <300mm MAP (Beni Abbes, Tata and Sidi Chicker) and the mesic sites that have >400mm MAP (Oued Nfifikh, Ouled Boughadi and Merja Zerga) (P= <0.01). Beni Abbes, the site with highest $\delta^{18}O_{mt}$, differs significantly from all six other sites (Tukey test, *P*= <0.01). There are no significant differences between sites with >300mm MAP (Guenfouda, Oued Nfifikh, Ouled Boughadi and Merja Zerga). Overall, these analyses show significant differences in $\delta^{18}O_{mt}$ between arid and mesic sites, but not between sites with similar MAP (Appendix 3.1).

Variation in $\delta^{13}C$ for all gerbil molars ranges from -16.3‰ to -4.6‰. Mean $\delta^{13}C$ values for each site are -13.4‰ ± 1.4 (Beni Abbes), -8.0‰ ± 3.4 (Tata), -12.9‰ ± 0.9 (Sidi Chicker), -14.8‰ ± 1.2 (Guenfouda), -14.8‰ ± 0.5 (Berrechid), -12.9‰ ± 2.7 (Oued Nfifikh), -14.9‰ ± 0.5 (Ouled Boughadi) and -14.0‰ ± 1.3 (Merja Zerga). Beni Abbes, Sidi Chicker, Guenfouda, Berrechid, Ouled Boughadi, Merja Zerga all have relatively low intra-site $\delta^{13}C_{mt}$ variation of 0.6 to 4.6‰, whereas the intra-site variation at Tata and Oued Nififikh is hgiher (8.9‰ and 7.6‰, respectively) (Figure 5.8). An analysis of variance (ANOVA) shows there are significant differences in $\delta^{13}C_{mt}$ between Beni Abbes, Tata, Sidi Chicker, Guenfouda, Oued Nfifikh, Ouled Boughadi and Merja Zerga (*F* = 14.92, *P* = <0.01). A post hoc Tukey test shows that the $\delta^{13}C_{mt}$ at Tata is significantly different to that from all other sites (*P*= <0.01) (Appendix 3.2).

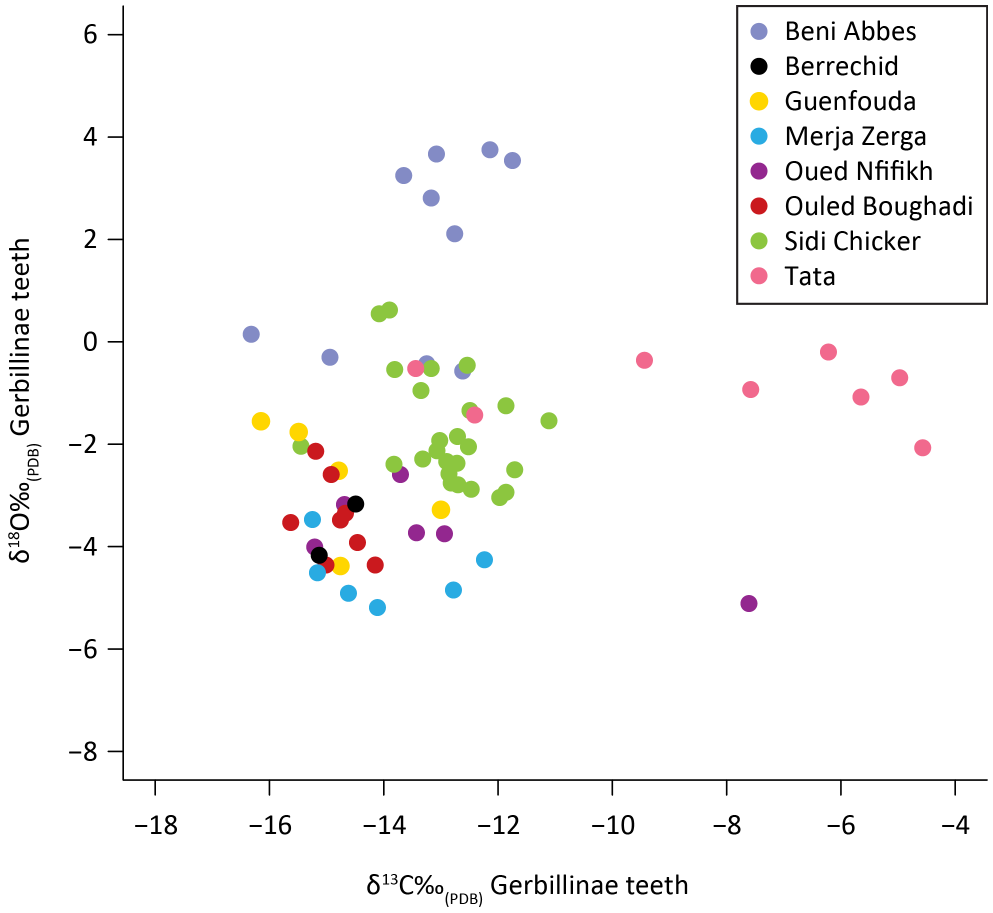

Figure 5.8: Graph showing the $\delta^{18}O$ and $\delta^{13}C$ composition of Gerbillinae teeth from eight locations across northwestern Africa.

5.5.2. $\delta^{15}N$ and $\delta^{13}C$ composition of gerbil bone collagen in NW Africa

The gerbil $\delta^{15}N_{col}$ and $\delta^{13}C_{col}$ (n=79) data from the eight sites across northwestern Africa are plotted in Figure 5.9 and summary statistics are presented in Table 5.5. Mean $\delta^{15}N_{col}$ values at each site are 5.6‰ ± 2.3 (Beni Abbes), 9.6‰ ± 1.0 (Tata), 5.7‰ ± 1.5 (Sidi Chicker), 6.4‰ ± 1.5 (Guenfouda), 8.2‰ ± 1.1 (Berrechid), 8.0‰ ± 0.5 (Oued Nfifikh), 5.9‰ ± 1.9 (Ouled Boughadi) and 5.4‰ ± 1.6 (Merja Zerga). Variation in $\delta^{15}N_{col}$ ranges from 1.3‰ at Oued Nfifikh to 7.4‰ at Beni Abbes. An analysis of variance (ANOVA) shows significant differences in $\delta^{15}N_{col}$ between Beni Abbes, Tata, Sidi Chicker, Guenfouda, Oued Nfifikh, Ouled Boughadi and Merja Zerga (F = 9.21, P =

<0.01). A post hoc Tukey test shows that the $\delta^{15}N_{col}$ at Tata is significantly different to that from Beni Abbes, Guenfouda, Merja Zerga, Ouled Boughadi and Merja Zerga (*P*= <0.05) (Appendix 3.3).

Mean $\delta^{13}C_{col}$ values at each site are -19.7‰ ± 1.4 (Beni Abbes), -12.2‰ ± 3.2 (Tata), -19.5‰ ± 0.8 (Sidi Chicker), -22.2‰ ± 1.0 (Guenfouda), -21.3‰ ± 0.9(Berrechid), -20.1‰ ± 2.0 (Oued Nfifikh), -22.1‰ ± 1.0 (Ouled Boughadi) and -20.0‰ ± 2.2 (Merja Zerga). Similar to the variation displayed in $\delta^{13}C_{mt}$, the sites of Beni Abbes, Sidi Chicker, Guenfouda, Berrechid, Ouled Boughadi, Merja Zerga and Oued Nfifikh have relatively low $\delta^{13}C_{col}$ intra-population variation of 1.2 to 5.6‰, while the $\delta^{13}C_{col}$ intra-population variation at Tata is larger, 9.0‰. An analysis of variance (ANOVA) shows significant differences in $\delta^{13}C_{col}$ between Beni Abbes, Tata, Sidi Chicker, Guenfouda, Oued Nfifikh, Ouled Boughadi and Merja Zerga (*F* = 40.53, *P* = <0.01). A post hoc Tukey test shows that the $\delta^{13}C_{col}$ at Tata is significantly different to that from all other sites (*P*= <0.01). The Sidi Chicker $\delta^{13}C_{col}$ differs to that from Guenfouda and Ouled Boughadi, while the $\delta^{13}C_{col}$ at Beni Abbes differs to that from Ouled Boughadi (Appendix 3.4).

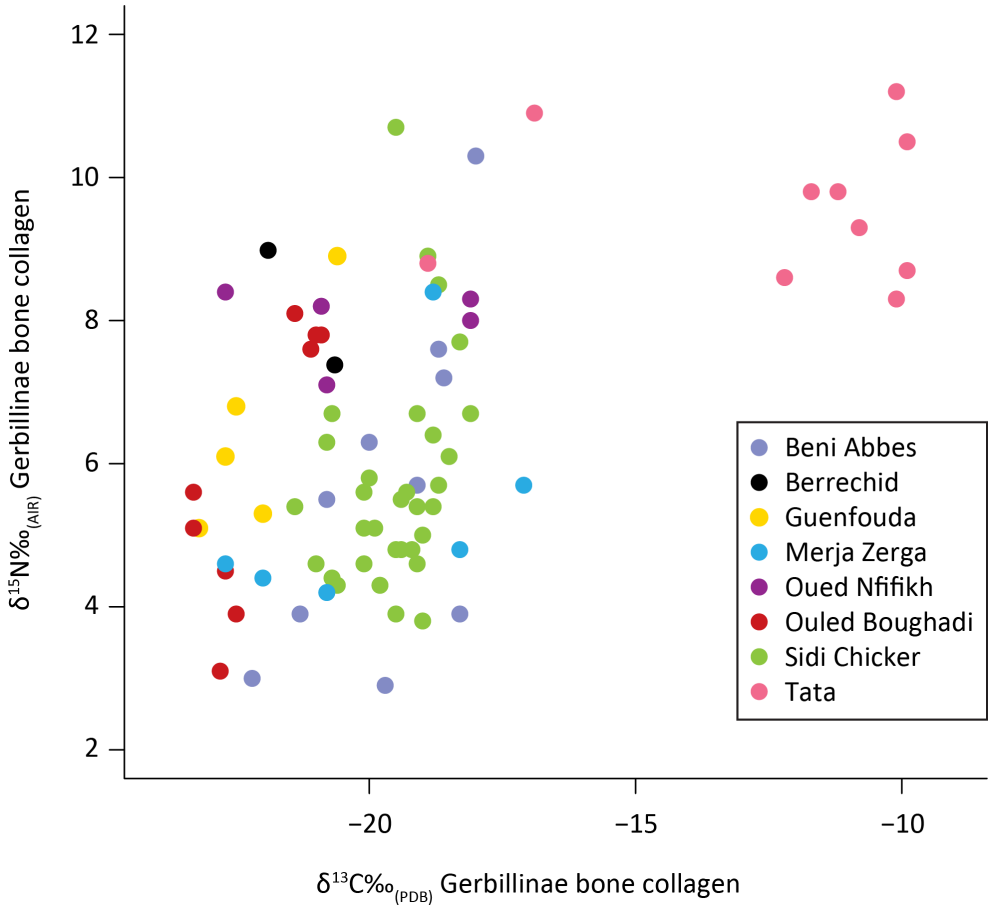

Figure 5.9: Graph showing the $\delta^{15}N$ and $\delta^{13}C$ composition of Gerbillinae bone collagen from eight locations across northwestern Africa.

Table 5.4: Summary statistics for the $\delta^{18}O$ and $\delta^{13}C$ composition of gerbil molar teeth from the eight sites across northwestern Africa. * indicate the number of incisor teeth used at each site.

Site	Number of molar teeth from individuals	$\delta^{18}O_{(PBD)}$					$\delta^{13}C_{(PBD)}$				
		Mean (‰)	Standard deviation (1σ)	Minimum (‰)	Maximum (‰)	Range (‰)	Mean (‰)	Standard deviation (1σ)	Minimum (‰)	Maximum (‰)	Range (‰)
Beni Abbes	*10	1.8	1.9	-0.6	3.8	4.3	-13.4	1.4	-16.3	-11.8	4.6
Tata	***8	-0.9	0.6	-2.1	-0.2	1.9	-8	3.4	-13.4	-4.6	8.9
Sidi Chicker	25	-1.8	1	-3	0.6	3.7	-12.9	0.9	-15.5	-11.1	4.3
Guenfouda	5	-2.7	1.2	-4.4	-1.6	2.8	-14.8	1.2	-16.2	-13	3.2
Berrechid	2	-3.7	0.7	-4.2	-3.2	1	-14.8	0.5	-15.1	-14.5	0.6
Oued Nfifikh	*6	-3.7	-0.9	-5.1	-2.6	2.5	-12.9	2.7	-15.2	-7.6	7.6
Ouled Boughadi	8	-3.5	0.8	-4.4	-2.1	2.2	-14.9	0.5	-15.6	-14.2	1.5
Merja Zerga	6	-4.5	0.6	-5.2	-3.5	1.7	-14	1.3	-15.3	-12.2	3

**indicates number of incisor teeth in sample*

Table 5.5: Summary statistics for the $\delta^{15}N$ and $\delta^{13}C$ composition of gerbil bone collagen from the eight sites across northwestern Africa.

Site	Number of bones from individuals	$\delta^{15}N_{(AIR)}$					$\delta^{13}C_{(PBD)}$				
		Mean (‰)	Standard deviation (1σ)	Minimum (‰)	Maximum (‰)	Range (‰)	Mean (‰)	Standard deviation (1σ)	Minimum (‰)	Maximum (‰)	Range (‰)
Beni Abbes	10	5.6	2.3	2.9	10.3	7.4	-19.7	1.4	-22.2	-18.0	4.2
Tata	10	9.6	1.0	8.3	11.2	2.9	-12.2	3.2	-18.9	-9.9	9.0
Sidi Chicker	32	5.7	1.5	3.8	10.7	6.9	-19.5	0.8	-21.4	-18.1	3.3
Guenfouda	5	6.4	1.5	5.1	8.9	3.8	-22.2	1.0	-23.3	-20.6	2.6
Berrechid	2	8.2	1.1	7.4	9.0	1.6	-21.3	0.9	-21.9	-20.7	1.2
Oued Nfifikh	5	8.0	0.5	7.1	8.4	1.3	-20.1	2.0	-22.7	-18.1	4.6
Ouled Boughadi	9	5.9	1.9	3.1	8.1	5.0	-22.1	1.0	-23.3	-20.9	2.4
Merja Zerga	6	5.4	1.6	4.2	8.4	4.2	-20.0	2.2	-22.7	-17.1	5.6

5.5.3. Isotope intra-population variation in Gerbillinae

The gerbil $\delta^{18}O_{mt}$ intra-population variation ranges from 1.0 to 4.3‰ at the eight sites (Table 5.4, Figure 5.10); however, if Berrechid is not considered (because of low sample numbers) the variation is between 1.7-4.3‰. Higher intra-site variation at Beni Abbes is consistent with the highly variable rainfall at this site. Gehler *et al.* (2012) reports similar intra-population variation in $\delta^{18}O$ between 2.0 to 3.9‰ in teeth of modern Arvicolinae and Murinae populations in temperate Europe. Intra-population variations in $\delta^{18}O$ between ~2 and 4‰ in small mammals are also similar to those recorded in larger mammal bioapatite including *Bison bison* (North American bison) *Capra hircus* (goat), *Bos grunniens* (yak), *Lynx rufus* (bobcat) and *Equus caballus* (horse) (Clementz and Koch, 2001; Hoppe et al., 2004, 2005; Hoppe, 2006; Wang et al., 2008).

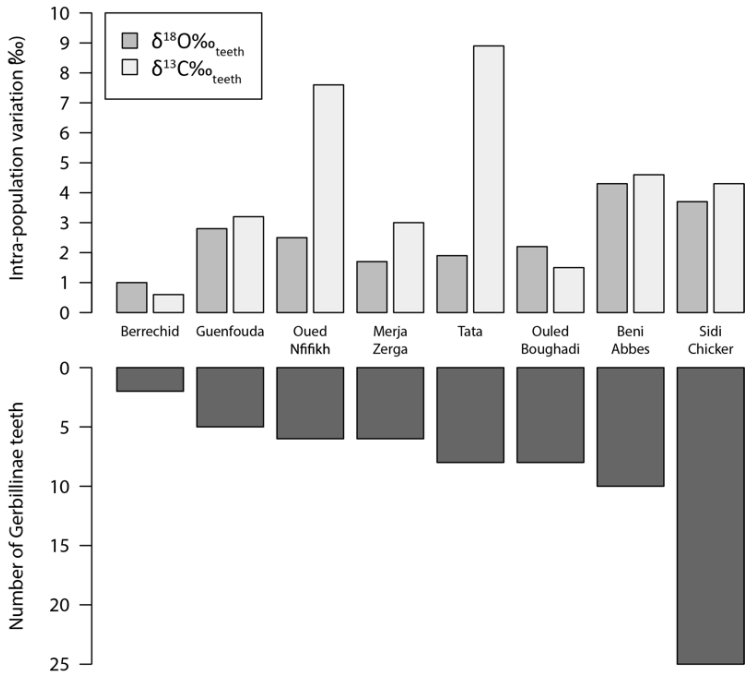

Figure 5.10: Bar chart showing the $\delta^{18}O$ and $\delta^{13}C$ intra-population variation displayed in the gerbil teeth at the eight sites across northwestern Africa and the number of teeth samples at each site.

The $\delta^{13}C_{mt}$ intra-population variation at Beni Abbes, Sidi Chicker, Guenfouda, Berrechid, Ouled Boughadi and Merja Zerga ranges from 0.6 to 4.6‰ (1.5-4.6‰ with Berrechid removed) (Table 5.4, Figure 5.10). $\delta^{13}C_{mt}$ intra-population variation is larger at both Tata and Oued Nfifikh, 8.9‰ and 7.6‰, respectively. Gehler *et al*. reports $\delta^{13}C$ intra-population variation of 1.8- 12.7‰ in modern Arvicolinae and Murinae teeth, while Kimura *et al.* (2013) demonstrates within population variation of 3.4-7.5‰ also in Murinae (*Golunda ellioti*, *Rattus* sp. *Mus booduga* and *Millardia* sp.) teeth (determined using an in-situ infrared laser ablation). Isotopic variation displayed within small mammal populations is similar to that previously reported in large mammal teeth (0.7-8.5‰) (Clementz and Koch, 2001; Hoppe et al., 2004, 2005; Wang et al., 2008). The intra-population variation displayed in $\delta^{13}C_{col}$ at each site is generally larger than that recorded in $\delta^{13}C_{mt}$ (Table 5.5, Figures 5.10 and 5.11). The gerbil intra-population variation at Beni Abbes, Sidi Chicker, Guenfouda, Berrechid, Ouled Boughadi, Oued Nfifikh and Merja Zerga ranges from 1.2 to 5.6‰ (2.4- 5.6‰ with Berrechid removed), while variation at Tata is higher (9.0‰). Reported $\delta^{13}C$ population variation in *Microcebus* sp. (mouse lemur) hair is 1.2-7.3‰ (Crowley et al., 2011). Within population variation in large mammal $\delta^{13}C_{col}$ ranges from 0.8 to 11.3‰ (Ambrose and DeNiro, 1986; Stevens et al., 2006).

The $\delta^{15}N_{col}$ gerbil intra-population ranges from 1.3-7.4‰ across the eight sites (Table 5.5, Figure 5.11). Oued Nfifikh has the lowest intra-population variation, while Beni Abbes displayed the largest within population variation. Gerbil $\delta^{15}N_{col}$ population variation is similar to that reported in large mammal populations (1.6-6.4‰) (Ambrose and DeNiro, 1986; Stevens et al., 2006).

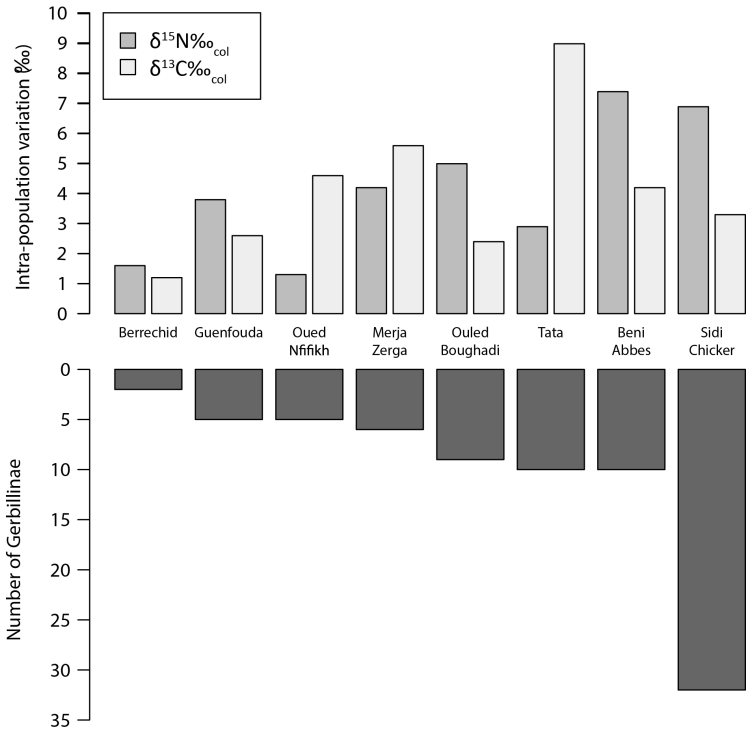

Figure 5.11: Bar chart showing the $\delta^{15}N$ and $\delta^{13}C$ intra-population variation displayed in the gerbil bone collagen at the eight sites across northwestern Africa and the number of bone samples at each site.

The intra-population variation in $\delta^{18}O_{mt}$, $\delta^{13}C_{mt}$, $\delta^{13}C_{col}$ and $\delta^{15}N_{col}$ of gerbil tissues in northwestern Africa is similar to within population variation previously reported in other small mammal analogue studies. Notably, the isotopic variation is not higher than that displayed in large mammal populations. The unique physiology of small mammals such as, fast tissue turnover times and high basal metabolic rate, does not seem to increase the isotopic variation within populations. The variation in gerbil $\delta^{18}O_{mt}$ and $\delta^{13}C_{mt}$ in the semi-arid and arid environments of northwestern Africa is also similar to that in more temperate, humid settings (Gehler et al., 2012). This shows that the proxy climate signal from small mammal tissues will not be masked by high isotopic variability.

5.5.4. The $\delta^{13}C$ composition of Gerbillinae teeth and bone collagen

5.5.4.1. Dietary reconstruction

Using the experimentally observed carbon isotope fractionation between tooth enamel bioapatite and diet in rodents of 11.0‰ (Passey et al., 2005; Podlesak et al., 2008) (see Chapter 4, Section 4.3.3 for discussion), it infers that the gerbils at Beni Abbes, Sidi Chicker, Guenfouda, Berrechid, Ouled Boughadi, Merja Zerga and most individuals at Oued Nfifikh had C_3 diets with average $\delta^{13}C$ compositions from ~-27.5‰ to -21.5‰ (Figure 5.12). At Tata $\delta^{13}C_{mt}$ values range from ~-5 to -13‰, indicating some contribution of C_4 plants to the diet. A single individual at Oued Nfifikh shows a clear C_4 contribution (Figure 5.12). Using a carbon isotope fractionation between bone collagen and diet in mammals of 5‰ (See Chapter 4, Section 4.3.3 for discussion), the $\delta^{13}C_{col}$ values infer that the majority of gerbils had a C_3 diet with an average $\delta^{13}C$ diet composition of between -28.3‰ and -21.9‰ (Figure 5.13), similar to the $\delta^{13}C$ dietary values inferred from the $\delta^{13}C_{mt}$. The $\delta^{13}C_{col}$ at Tata infers that the gerbils had an average $\delta^{13}C$ diet composition of between -17.2‰ and -14.9‰, again showing a clear C_4 plant contribution to diet at this site (Figure 5.13).

The inferred diet $\delta^{13}C$ values show that gerbils at Tata consumed C_4 plants in their diet, while the gerbils at Beni Abbes, Sidi Chicker, Guenfouda, Berrechid, Ouled Boughadi, Merja Zerga and most individuals at Oued Nfifikh had a predominantly/pure C_3 diet. This suggests that either wild C_4 grasses were available to the gerbils at Tata (a small percentage of vegetation within the study region of northwestern Africa does consist of C_4 plants (Sage et al., 1999; Still et al., 2003)) or, alternatively they exploited C_4 crops grown in the region. It

is known that maize (a C_4 crop) is grown presently in the oasis systems around Tata (Jouve and Sourisseau 2003). The inferred average $\delta^{13}C$ composition of gerbil diets from the sites that lie in the coastal Mediterranean and Atlantic coastal zones are ~-26‰, consistent with reported plant $\delta^{13}C$ values from the Mediterranean region (Hartman and Danin, 2010). The average $\delta^{13}C$ value of gerbil diet from the arid sites (Beni Abbes and Sidi Chicker) is higher (~-24.5‰) and is consistent with the $\delta^{13}C$ composition of C_3 *Hordeum vulgare* grains (6-row hulled barley) from rain-fed fields, receiving ~250-300 MAP, in the south of Morocco ($\delta^{13}C$ values = -22.3‰ to -25.4‰) (Styring et al., 2016).

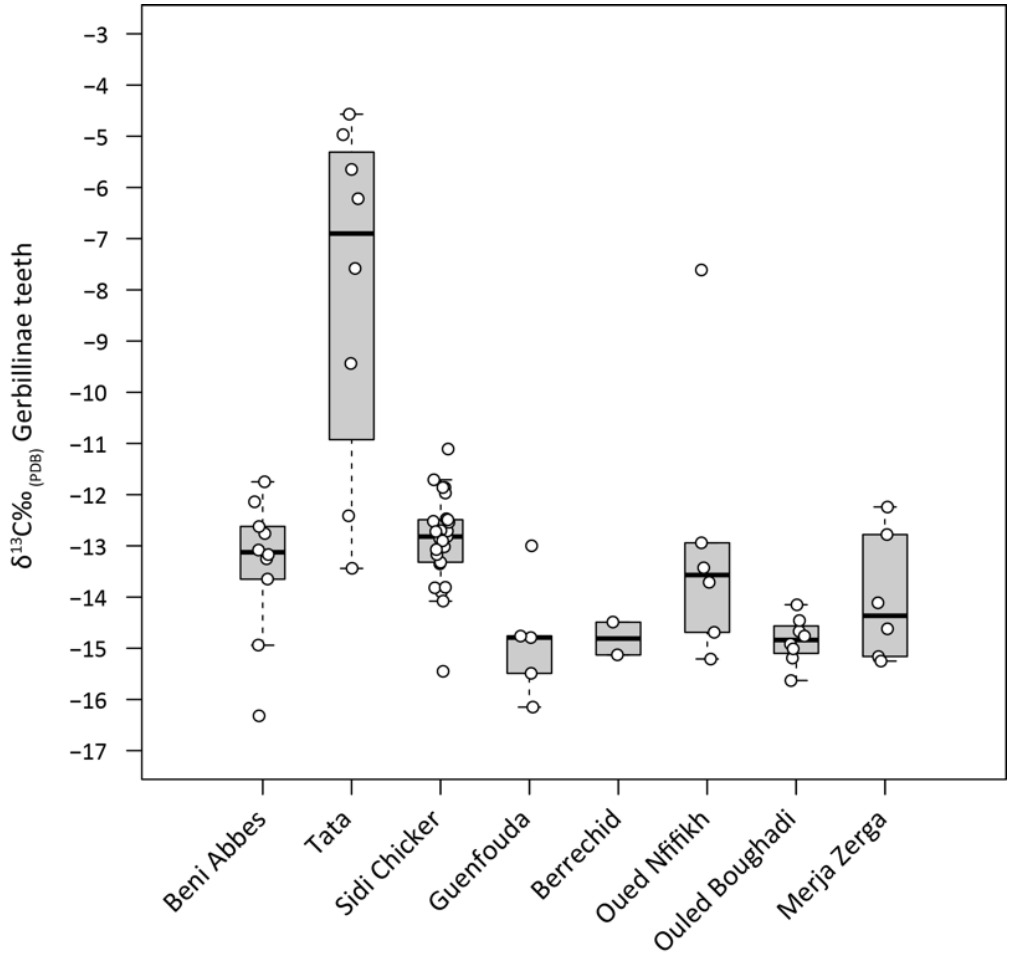

Figure 5.12**: Boxplot showing the $\delta^{13}C$ composition of gerbil molar teeth from the eight sites across northwestern Africa. The $\delta^{13}C$ composition of each individual tooth (white dots) is also marked the graph to demonstrate the intra-site variation at each site.**

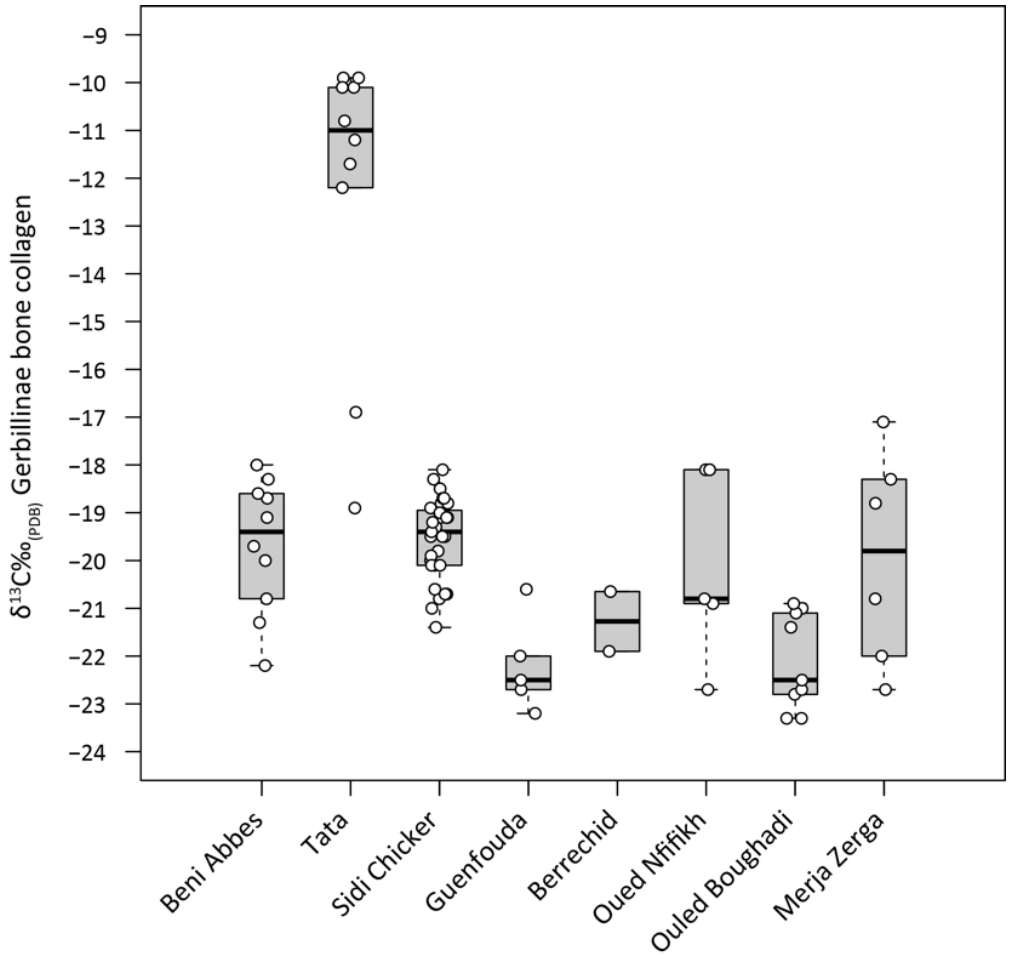

Figure 5.13: Boxplot showing the $\delta^{13}C$ composition of gerbil bone collagen from the eight sites across northwestern Africa. The $\delta^{13}C$ composition of each individual tooth (white dots) is also marked the graph to demonstrate the intra-site variation at each site

5.5.4.2. Relationship between Gerbillinae $\delta^{13}C_{mt}$ and $\delta^{13}C_{col}$

Figure 5.14 shows a strong positive correlation between $\delta^{13}C_{col}$ and $\delta^{13}C_{mt}$ (R^2= 0.81, p= <0.01). The outlier is the gerbil described in section 5.5.4.1 from Oued Nfifikh whose $\delta^{13}C_{mt}$ indicated a C_4 dietary contribution, while $\delta^{13}C_{col}$ indicated a C_3 diet. Positive correlations between the $\delta^{13}C$ composition of bone collagen and bone/enamel bioapatite have also been noted previously in mice, rats, pigs and humans (Kellner and Schoeninger, 2007; Loftus and Sealy, 2012). The strong positive correlation between gerbil $\delta^{13}C_{col}$ and $\delta^{13}C_{teeth}$ suggests that the protein component of the diet generally reflects that of overall diet, but there

is a lot of scatter around the line. It also demonstrates that in the majority of individuals there is no marked temporal bias between teeth and bone tissues.

The spacing between $\delta^{13}C_{mt}$ and $\delta^{13}C_{col}$ ($\delta^{13}C_{mt\text{-}col}$) in the gerbils' ranges from +2.3 to 10.5‰ with an average $\delta^{13}C_{mt\text{-}col}$ of +6.5 ± 1.4‰ (Figure 5.15), similar to that recorded in feeding experiments on mice and rats (Ambrose and Norr, 1993; DeNiro and Epstein, 1978; Jim et al., 2004; Tieszen and Fagre, 1993). Figure 5.15 shows the majority of gerbil individuals have $\delta^{13}C_{mt\text{-}col}$ values of ~+4-9‰, and individuals that fall outside this range are from Tata and Oued Nfifikh (sites where there is evidence of C_4 plant consumption) (Figure 5.15). Two reasons are suggested to explain high and low $\delta^{13}C_{mt\text{-}col}$ noted in some the individuals from Tata and Oued Nfifikh; 1) the $\delta^{13}C$ of the dietary protein does not strongly reflect that of the whole diet; 2) there is a temporal bias reflected in the $\delta^{13}C_{col}$ and $\delta^{13}C_{mt}$. Yet, without observed $\delta^{13}C$ values for gerbil diet these two explanations cannot be teased apart with the data available. The notable outlier from Oued Nfifikh (Figures 5.14 and 5.15) ($\delta^{13}C_{col}$ =-18.1‰ and $\delta^{13}C_{mt}$ = -7.6‰) does demonstrate temporal tissue bias. It is likely that molar tooth of individual reflects a brief period during the spring/summer when C_4 plants were available, while the bone collagen reflects the predominantly C_3 diet of the individual.

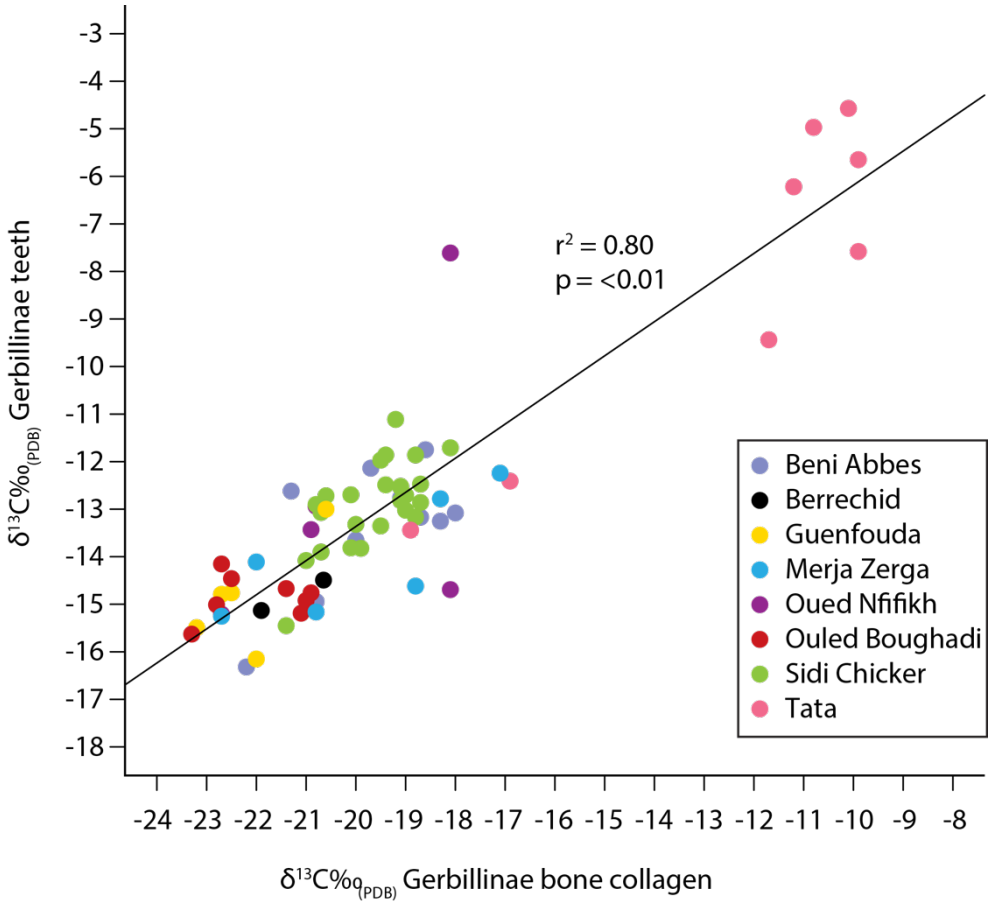

Figure 5.14: Relationship between the $\delta^{13}C$ of gerbil teeth and bone collagen from the same individual. The sites where gerbils consumed a pure/predominately C_3 sit at the bottom of the regression line, while those individuals from Tata that had C_4 plant contribution to their diet sit at the top of the regression line. The outlier from Oued Nfifikh has a C_4 dietary signal inferred from $\delta^{13}C_{teeth}$ and predominantly C_3 dietary signal inferred from $\delta^{13}C_{col}$.

The strong correlation between $\delta^{13}C_{col}$ and $\delta^{13}C_{mt}$ shows that there is no obvious temporal bias reflected in the isotopic signal from both tissues. There is more variability between the $\delta^{13}C_{mt}$ and $\delta^{13}C_{collagen}$ in the gerbils that had a mixed C_3/C_4 diet, probably due to the seasonal availability of C_4 plants. It also hints that although gerbil molar teeth reflect a short temporal period, the dietary signal recorded in their teeth is representative of average diet, especially in those individuals that consumed a pure C_3 diet.

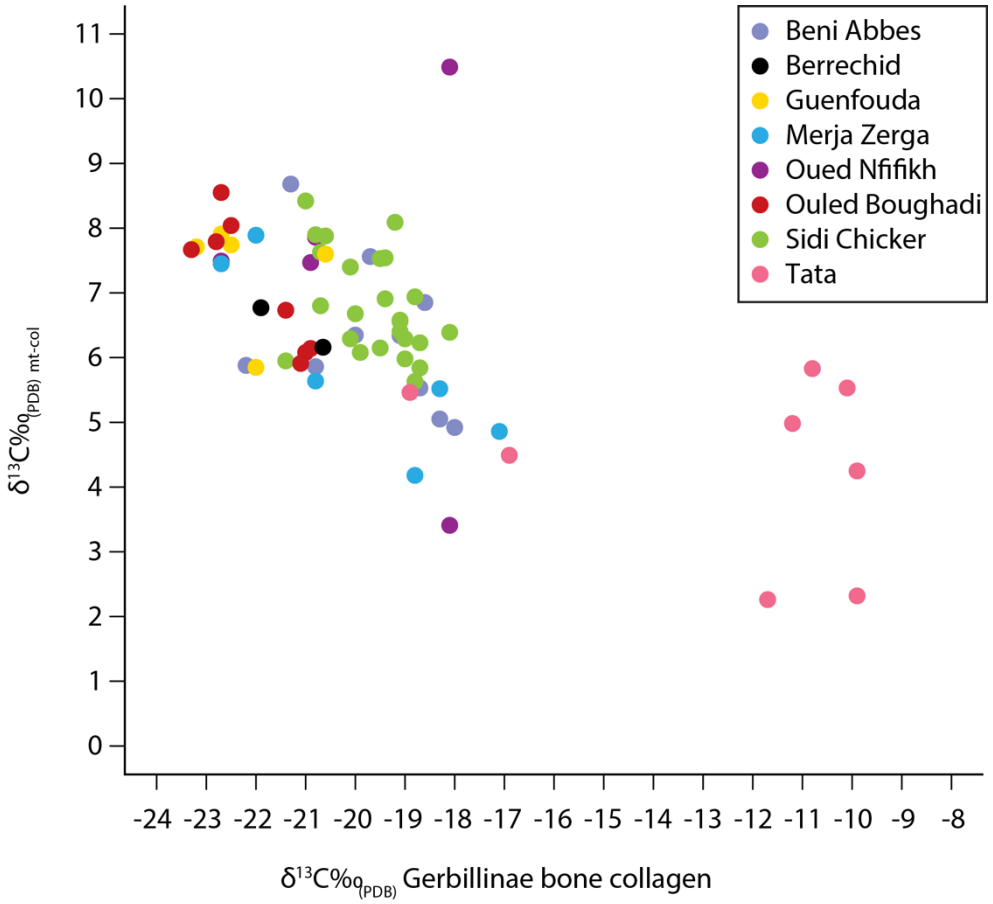

Figure 5.15: Variation in $\delta^{13}C_{mt\text{-}col}$ between gerbil individuals from the eight sites across northwestern Africa. The majority of gerbils have $\delta^{13}C_{mt\text{-}col}$ values of between ~+4 and 9‰, but the $\delta^{13}C_{mt\text{-}col}$ values are more variable in the individuals from Tata and Oued Nfifikh where some individuals had a C_4 plant contribution to their diet.

5.5.4.3. Relationship between MAP and $\delta^{13}C$ Gerbillinae tissue

Similar patterns are reflected in both $\delta^{13}C_{col}$ and $\delta^{13}C_{mt}$ (Figures 5.12 and 5.13). Amongst the gerbils that consumed a pure/predominantly C_3 diet, generally higher $\delta^{13}C$ values ($\delta^{13}C_{mt}$ = ~-12 to - 14‰, $\delta^{13}C_{col}$ = ~-18 to -21‰) are recorded at the arid sites (Beni Abbes, Tata and Sidi Chicker), than at the more mesic sites of Guenfouda, Oued Nfifikh, Ouled Boughadi, Berrechid and Merja Zerga where $\delta^{13}C$ values are tend to be lower ($\delta^{13}C_{mt}$ = ~-14 to -16‰, $\delta^{13}C_{col}$ = ~-21 to -23‰). The gerbils at Oued Nfifikh and Merja Zerga have $\delta^{13}C_{mt}$ and $\delta^{13}C_{col}$ values that span those recorded at both the mesic and arid sites.

Although the arid sites do tend to have higher $\delta^{13}C_{col}$ and $\delta^{13}C_{mt}$ relative to the mesic sites, they do not differ significantly (Section 5.5.1) (with the exception of Tata where the gerbils consumed C_4 plants in their diet).

Linear models were used to explore the relationship between the $\delta^{13}C$ composition of gerbil tissues and aridity. Correlation between MAP and $\delta^{13}C_{plant}$ only occurs in C_3 plants (Hartman and Danin, 2010; Kohn, 2010); therefore the gerbils that had a notable C_4 plant contribution to their diet were removed from statistical analyses (all gerbils from Tata and one gerbil from Oued Nfifikh) (Section 5.5.4.1). There is a significant relationship between both $\delta^{13}C_{mt}$ (p= <0.01) and $\delta^{13}C_{col}$ (p= 0.01), and MAP, but low r^2 values demonstrate high variability (Figures 5.16 and 5.17) (Table 5.6). The slopes of $\delta^{13}C_{col}$ and $\delta^{13}C_{mt}$ are similar and when the $\delta^{13}C_{mt}$ intercept is adjusted to describe the predicted $\delta^{13}C_{col}$ using a $\Delta^{13}C_{mt\text{-}col}$ of 6.5‰ (the average $\Delta^{13}C_{mt\text{-}col}$ in the modern gerbil dataset (see Section 5.5.4.2)) (Figure 5.18). The mean $\delta^{13}C_{col}$ and the $\delta^{13}C_{mt}$ values from each site (Table 5.6) also have no significant relationship with MAP because the values are skewed by the intra-site variation, especially at Merja Zerga, Beni Abbes and Oued Nfifikh (Figures 5.16 and 5.17).

The relationship between MAP and the $\delta^{13}C$ composition of gerbil tissue is compared to that between MAP and the $\delta^{13}C$ composition of gazelle keratin documented by Hartman (2012) in a Mediterranean environment (Equation 4; Figure 5.18). To allow for direct comparison the intercept of the Hartman (2012) line has been adjusted to describe the predicted range of $\delta^{13}C_{col}$ using a standard $\Delta^{13}C_{collagen\text{-}keratin}$ of 1.4‰ (O'Connell et al., 2001)).The gazelle keratin regression line has a steeper slope in comparison to that of the gerbil lines. The

isotopic shift recorded between 100-600mm MAP in gerbil tissue is ~2‰, while in gazelle keratin it is ~5‰.

$$y=-2.67*\mathrm{Ln}(x)-7.11 \quad (4)$$

(Hartman 2012)

The gerbil tissue regression lines can also be compared to those noted between MAP and the $\delta^{13}C$ composition of wet season (Equation 5), dry season (Equation 6) and annual (Equation 7) Mediterranean C_3 plants (Hartman and Danin, 2010) (Figure 5.19). To enable direct comparison, the intercepts of the plant regression lines have been adjusted to describe the predicted range of $\delta^{13}C_{col}$ using a $\Delta^{13}C_{collagen\text{-}diet}$ of 5‰ (Section 5.5.4.1). The regression slopes of the wet season, dry season and annual (combined wet and dry season) C_3 plants are more similar to those noted in the gerbils than that of the gazelle keratin (Figures 5.18 and 5.19). Hartman (2012) suggests that the steep slope of the gazelle keratin regression relative to the plant regressions suggests that the gazelles were consuming more ^{13}C-enriched plants in their diet. The predicted $\delta^{13}C_{col}$ values from the wet season plant regression line are lower than those recorded in the gerbil tissues, whereas the predicted $\delta^{13}C_{col}$ values from dry season and annual plant regression line are similar to those recorded in the gerbil tissues. The correlation with the higher values of the dry season plants could result from gerbils exploiting more open habitats where plants are likely enriched in ^{13}C.

$$y=-1.17*\mathrm{Ln}(x)-20.7 \quad (5)$$

(Hartman & Danin 2010)

$$y=-0.78*\mathrm{Ln}(x)-21.74$$

(6)
(Hartman & Danin 2010)

$y=-0.96*Ln(x)-21.21$

(7)
(Hartman & Danin 2010)

The significant negative correlation between the $\delta^{13}C$ composition of gerbil tissue and MAP shows that $\delta^{13}C$ of gerbil tissues does partly reflect the isotopic effects of water deficit on the predominantly C_3 vegetation consumed by the gerbils, but there is high variability in $\delta^{13}C$ at each site. The variability results from the gerbils' microhabitat and the short period that the tissues (especially the teeth) reflect. The results show that the $\delta^{13}C$ composition of gerbil tissue reflects C_3/C_4 vegetation inputs in arid and semi-arid settings.

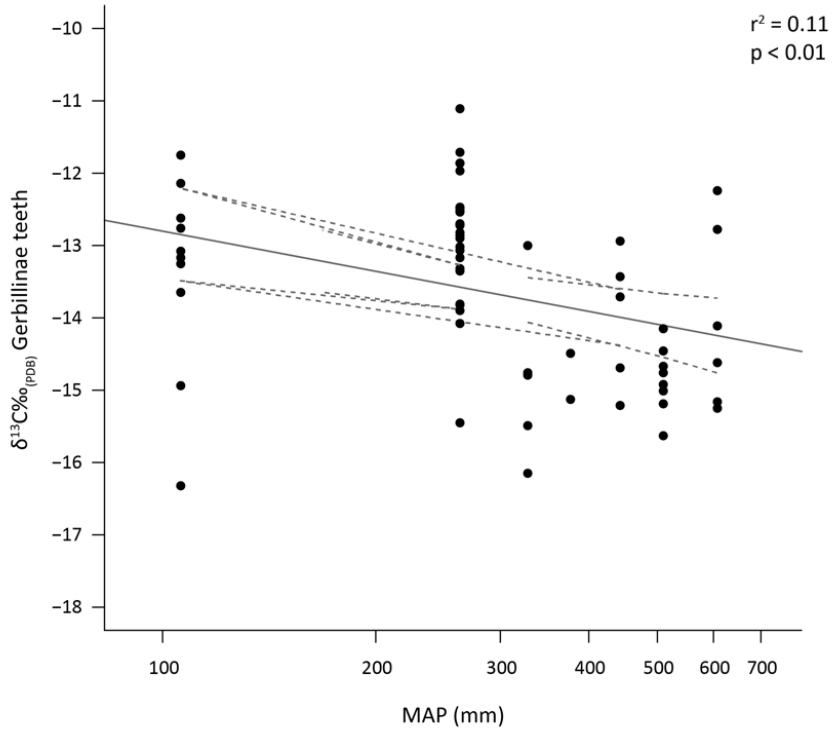

Figure 5.16: The relationship between the $\delta^{13}C_{mt}$ and MAP across northwestern Africa. One individual from Oued Nfifikh and all the individuals from Tata were removed from the regression analysis because they had a significant C_4 plant contribution to their diet.

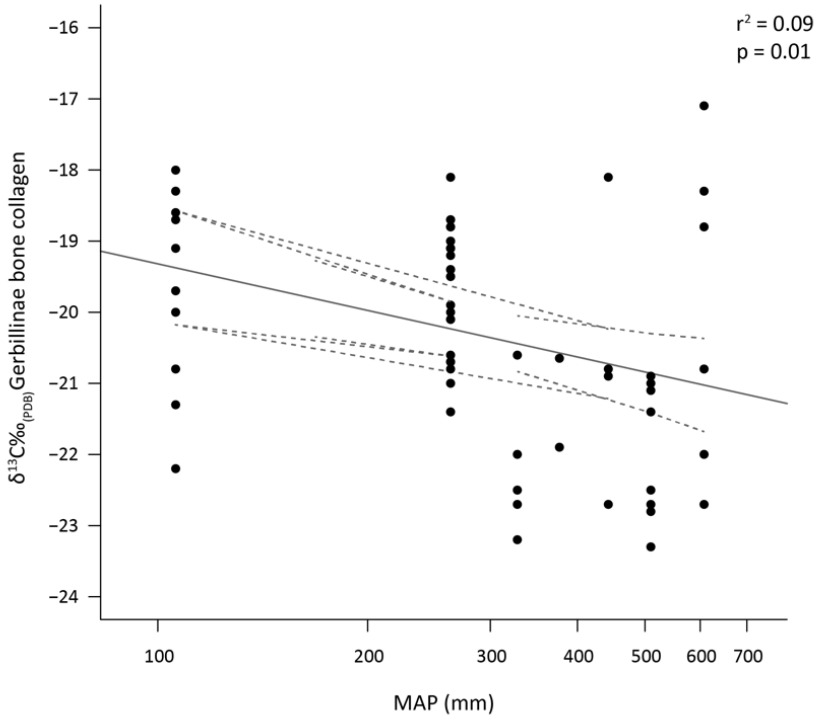

Figure 5.17: The relationship between the $\delta^{13}C_{col}$ and MAP across Northwestern Africa. One individual from Oued Nfifikh and all the individuals from Tata were removed from the regression analysis because they had a significant C_4 plant contribution to their diet.

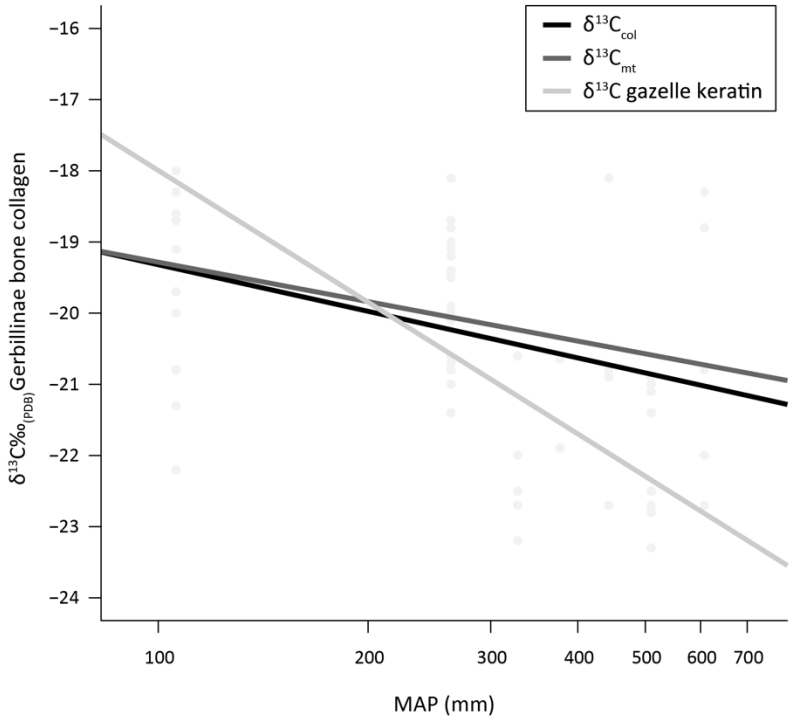

Figure 5.18: Graph comparing the relationship between 1) $\delta^{13}C_{col}$, 2)$\delta^{13}C_{mt}$ (data from this study) and 3) $\delta^{13}C$ gazelle keratin (data from Hartman 2012) and MAP. The intercepts of the $\delta^{13}C_{mt}$ regression and the $\delta^{13}C_{col}$ gazelle keratin regression have been adjusted to describe the predicted $\delta^{13}C_{col}$ to enable comparison of the lines.

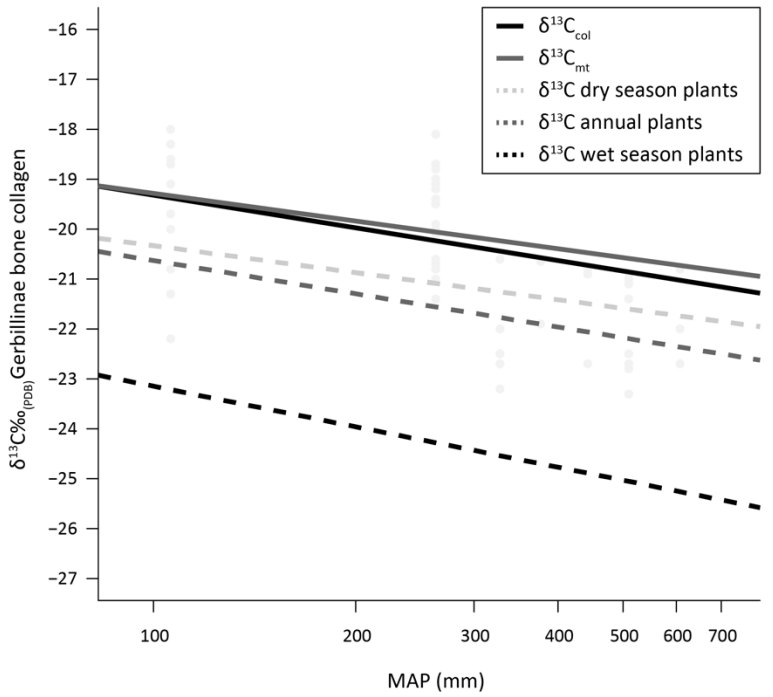

Figure 5.19: Graph comparing the relationship between 1) $\delta^{13}C_{col}$, 2) $\delta^{13}C_{mt}$ (data from this study) and 3) $\delta^{13}C$ dry season Mediterranean plants 4) $\delta^{13}C$ wet season Mediterranean plants 5) $\delta^{13}C$ annual Mediterranean plants (data from Hartman & Danin 2010) and MAP. The intercepts of the $\delta^{13}C_{mt}$ regression and the plant regressions have been adjusted to describe the predicted $\delta^{13}C_{col}$ to enable comparison of the lines.

Table 5.6: Linear relationship between $\delta^{18}O_{mt}$, $\delta^{13}C_{mt}$, $\delta^{13}C_{col}$, $\delta^{15}N_{col}$ and MAP. Bold values are significant (p= <0.05).

Linear Regression Model	$\delta^{18}O_{teeth}$ (intercept)	MAP (Ln mm) (x)	r^2	*P*
$\delta^{13}C_{col}$ v MAP[a]	-14.97	-0.94	0.09	**0.01**
$\delta^{13}C_{teeth}$ v MAP[a]	-9.12	-0.80	0.11	**0.006**
Mean $\delta^{13}C_{col}$ v MAP[a]	-16.07	-0.81	0.01	0.35
Mean $\delta^{13}C_{teeth}$ v MAP[a]	-10.02	-0.70	0.13	0.22
$\delta^{15}N_{col}$ V MAP[b]	8.49	-0.38	0.01	0.42
Mean $\delta^{15}N_{col}$ V MAP	9.11	-0.39	0.14	0.72
$\delta^{15}N_{col}$ V MAP[c]	3.34	0.45	0.01	0.27
$\delta^{18}O_{teeth}$ V MAP	17.16	-3.39	0.72	**<0.001**
Mean $\delta^{18}O_{teeth}$ V MAP	17.05	-3.39	0.94	**>0.001**

'Mean' refers to the mean isotope composition from each location in northwestern Africa

[a] One individual from Oued Nfifikh and all individuals from Tata removed from linear regression model because C_4 plant consumption in diet

[b] All $\delta^{15}N_{col}$ data used in model

[c] Individuals from Tata removed from Linear regression model

5.5.5. $\delta^{15}N$ composition of gerbil bone collagen

5.5.5.1. Relationship between MAP and $\delta^{15}N$ value of gerbil collagen

The inter-site and intra-site $\delta^{15}N_{col}$ values are highly variable across northwestern Africa (Figure 5.20). There is no significant relationship between MAP and $\delta^{15}N_{col}$ (Figure 5.21; Table 5.6), even when the gerbils from Tata (gerbils with C_4 plant contributions to their diets) are removed from the linear model (Figure 5.21; Table 5.6). If $\delta^{15}N_{col}$ were reflecting aridity the arid sites would be expected to have higher $\delta^{15}N_{col}$ relative to the more mesic sites. Yet, the mean $\delta^{15}N_{col}$ at Beni Abbes is similar to that at Sidi Chicker, Guenfouda, Ouled Boughadi and Merja Zerga.

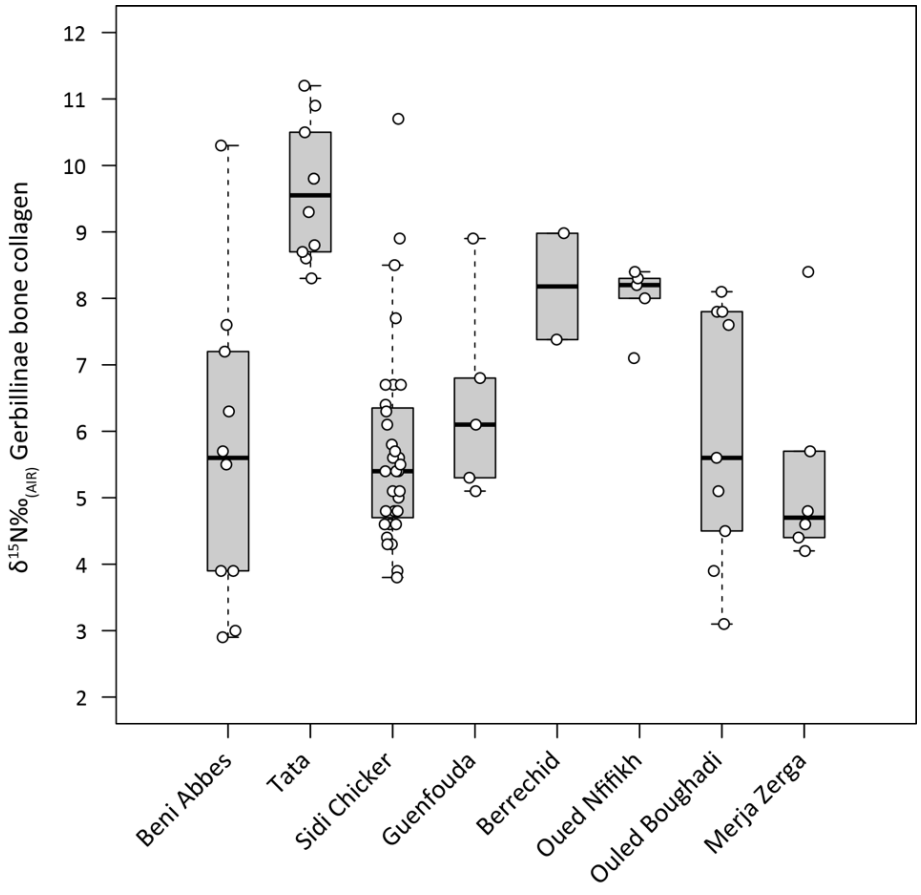

Figure 5.20: Boxplot showing the $\delta^{15}N$ composition of Gerbillinae bone collagen from the eight sites across northwestern Africa. The $\delta^{15}N$ composition of each individual is also marked the graph to show intra-variation.

Instead, the data appears to show that $\delta^{15}N_{col}$ reflects the $\delta^{15}N$ composition of the local vegetation from each site. The $\delta^{15}N_{col}$ variation displayed across northwestern Africa ($\delta^{15}N_{col}$ = ~3-11‰) is similar to $\delta^{15}N$ values reported for plants from a Mediterranean ecosystem (~-3 to 9‰) (Hartman and Danin, 2010). The $\delta^{15}N$ values of agricultural barley grains grown in northern and southern Morocco have a wide range of values ranging from -0.3 to 15.4‰, with lower values from unmanured fields in the north (<1.4‰) and higher values from fields in the south that have been to subjected to different intensities of manuring (fields manured every two years = 4.7-10.6‰, fields manured intensively twice a year = 12.5-15.4‰) (Styring et al., 2016). This hints that the gerbils with higher $\delta^{15}N_{col}$ at Tata and Oued Nfifikh, sites where there is also evidence for the consumption of C_4 plants, may have been consuming plants with higher $\delta^{15}N$ resulting from farming practices (Bogaard et al., 2007; Choi et al., 2006; Fraser et al., 2011). The relatively low intra-site range at Tata (2.9‰) and Oued Nfifikh (1.3‰) suggests a homogenous food source, further indicating the consumption of domestic grains at these sites (see Section 5.5.4.1). Atlernativley, the higher $\delta^{15}N_{col}$ may result from an aridity affect on late summer C_4 plants, as C_4 plants appear to have higher $\delta^{15}N$ values relative to C_3 plants in the Mediterranean (Hartman and Danin 2010).

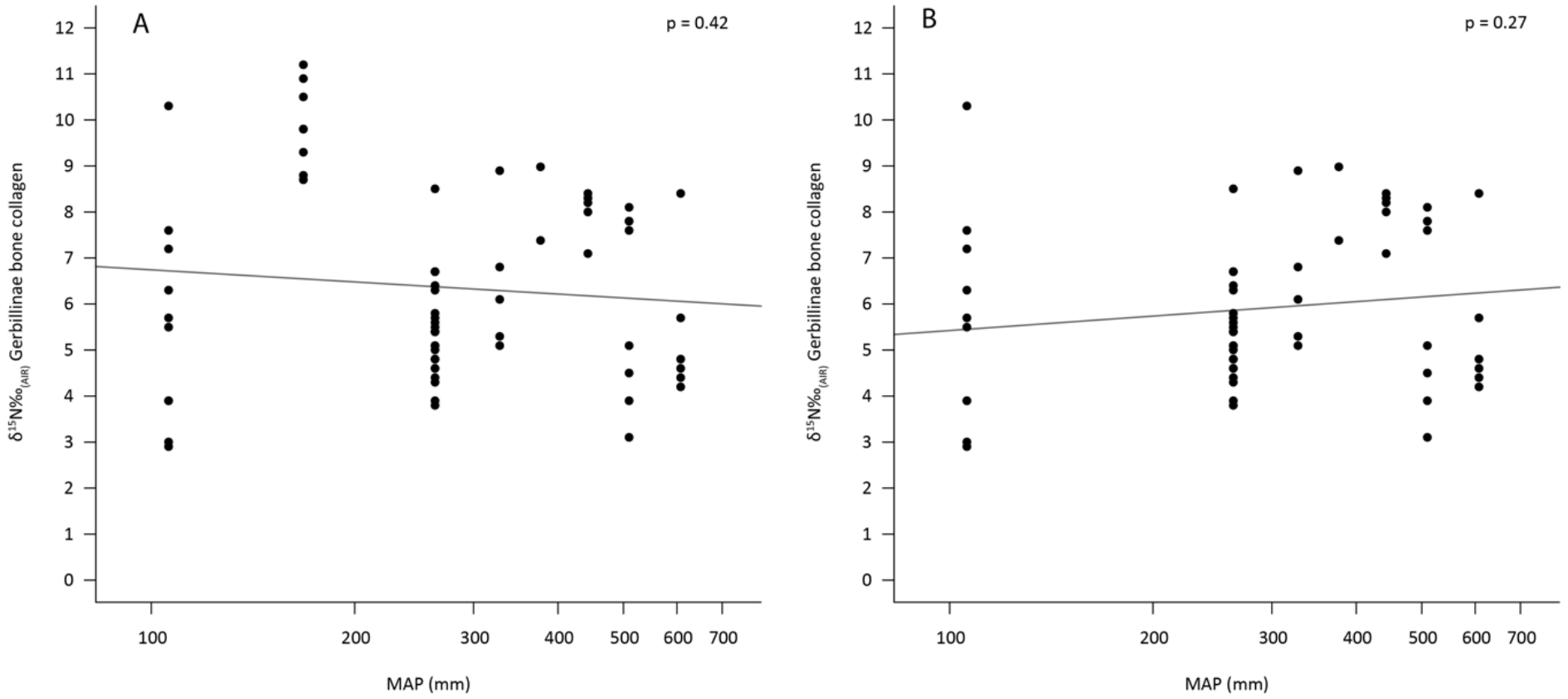

Figure 5.21: Relationship between in $\delta^{15}N_{col}$ and MAP across northwestern Africa: A) all gerbil data; B) gerbils from Tata removed from regression.

The intra-site variation in $\delta^{15}N_{col}$ at Beni Abbes, Sidi Chicker, Guenfouda, Ouled Boughadi and Merja Zerga is ~4-7‰ (excluding Berrechid due to low sample numbers), similar to variation reported in the $\delta^{15}N$ of collagen and hair from other mammal populations (Section 5.5.3). Intra-site variation in gerbil $\delta^{15}N_{col}$ is probably caused by several environmental and physiological factors including spatial variation in plant $\delta^{15}N$ (Sections 4.2.3 and 4.3.4), differing diets, physiological response to aridity, nutritional stress (Fuller et al., 2005; Hobson et al., 1993), and metabolism (Carleton and Martínez del Rio, 2005; Smith et al., 2010; Yi and Yang, 2006). The results demonstrate that $\delta^{15}N_{col}$ does not reflect aridity across a rainfall gradient in northwestern Africa, instead showing that $\delta^{15}N_{col}$ is variable across the region. The aridity signal from the plants may be undetectable in the gerbil $\delta^{15}N_{col}$ because it is highly likely, especially at the sites of Tata and Oued Nfifikh, that these gerbils consumed agricultural grains as part of their diet (they are renowned pests in this region).

5.5.6. $\delta^{18}O$ composition of Gerbillinae teeth

5.5.6.1. Relationship between MAP and $\delta^{18}O$ Gerbillinae teeth

There is a significant inverse correlation between $\delta^{18}O_{mt}$ and MAP (p=<0.01, R^2= -0.72), but no significant relationship between $\delta^{18}O_{mt}$ and the interpolated $\delta^{18}O_{mw}$ (p=0.5) (Figure 5.22). The relationship between $\delta^{18}O_{mt}$ and MAP improves when average $\delta^{18}O$ values from each site are used (p=<0.01, R^2= -0.94) (Figure 5.23, Equation 8, Table 5.6). The linear regression shows that when MAP is <300mm, moisture availability is more closely correlated with $\delta^{18}O_{mt}$ but at the sites where MAP is >400mm, moisture availability has a lesser effect. At the more mesic sites of Berrechid, Oued Nfifikh and Ouled Boughadi

the $\delta^{18}O_{mt}$ are not strongly enriched over local $\delta^{18}O_{mw}$, and at Merja Zerga with ~600mm MAP the $\delta^{18}O_{mt}$ appears to be approximately similar to that of $\delta^{18}O_{mw.}$ Therefore, as moisture availability decreases, $\delta^{18}O_{mt}$ increases, but in more mesic settings aridity has less of an effect on the $\delta^{18}O_{mt}$ and these values more likely reflect that of $\delta^{18}O_{mw}$. Because there is a strong relationship between $\delta^{18}O_{mt}$ and MAP, it suggests that any possible physiological signal (from nursing for example) is overprinted by the climate signal in the gerbil molar teeth.

$$y=-3.39*\mathrm{Ln}\,(x)\ -17.05 \qquad (8)$$

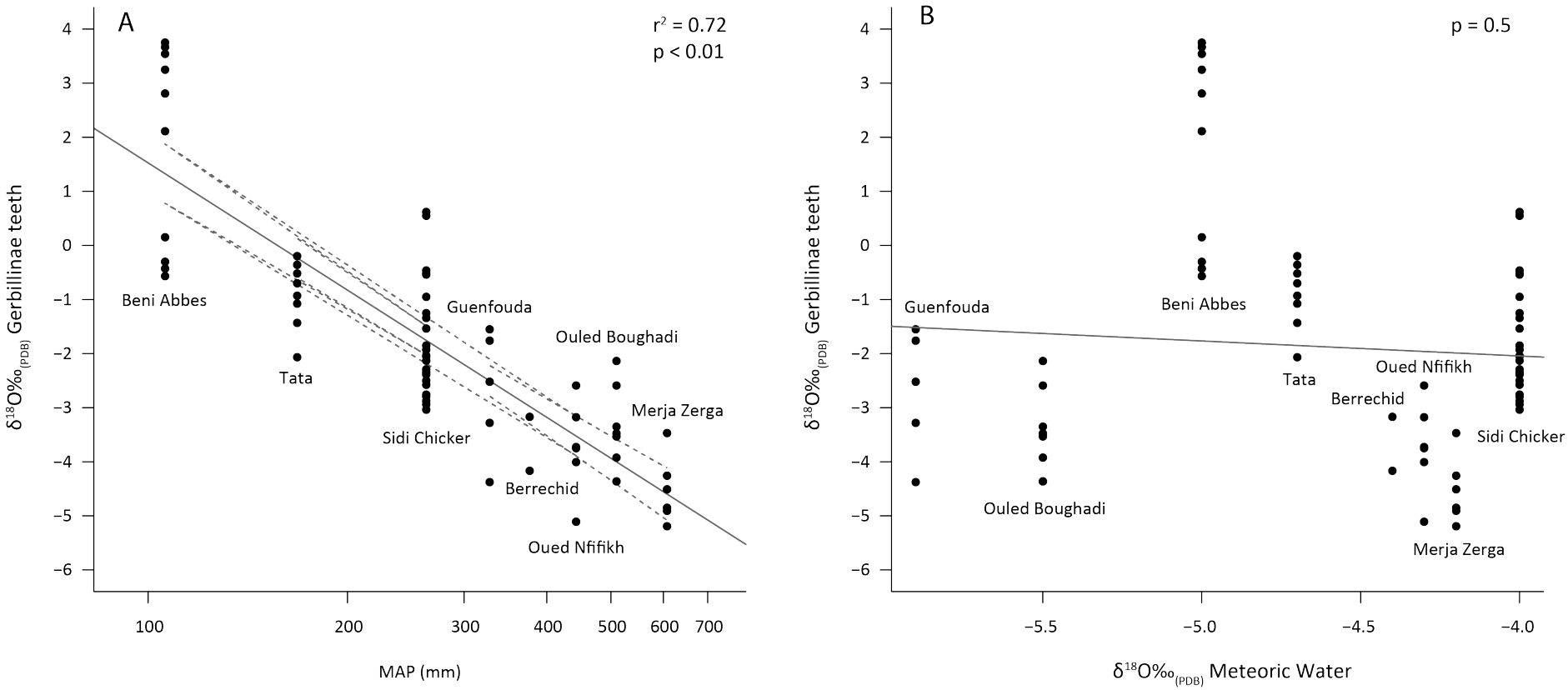

Figure 5.22: Relationship between $\delta^{18}O_{teeth}$ and A) MAP; B) $\delta^{18}O_{mw}$ from the eight sites across northwestern Africa.

The observation that $\delta^{18}O_{mt}$ reflects moisture availability in semi-arid and arid environments such as these rather than $\delta^{18}O_{mw}$, as is commonly assumed, most likely reflects the gerbil's reliance on water from food and the effect of aridity on this water pool. This contribution of water and oxygen from the diet is perhaps greater than anticipated. For instance, an experimental study of woodrats reported that 56% of drinking water and 15% food were responsible for the oxygen in bodywater (Podlesak et al., 2008). These results, however, cannot be interpolated easily to semi-arid and arid settings. Grains make up the largest component of gerbils' diet and in order to conserve water, gerbils store grains in their more humid, cool burrows to absorb soil moisture into the grain (Merritt, 2010). Soil and surface waters are likely to be enriched in ^{18}O compared to meteoric water due to evaporative effects (Gat and Airey, 2006). Gerbils also eat plant leaves, which are known to be highly sensitive to evaporative enrichment in ^{18}O (Barbour and Farquhar, 2000; Flanagan et al., 1991; Helliker and Ehleringer, 2002b; Yakir et al., 1990). Modelled annual $\delta^{18}O$ leaf water values show that values in Mediterranean North Africa are high (~12‰), and on the periphery of the Sahara, where Beni Abbes and Tata are located, modelled leaf water values are extremely high (~22‰) (West et al., 2008). The evaporative effects may not be as strong in nocturnal gerbils as in diurnal animals, because the $\delta^{18}O$ of leaf water is lower at night (Förstel, 1978; Gat et al., 2007), but its effects will still be evident. Relationships between the $\delta^{18}O$ composition of mammal body tissues and aridity/relative humidity in areas with high moisture deficits have been similarly observed in several 'evaporation sensitive' large mammals (Cormie et al., 1994; Iacumin and Longinelli, 2002; Levin et al., 2006).

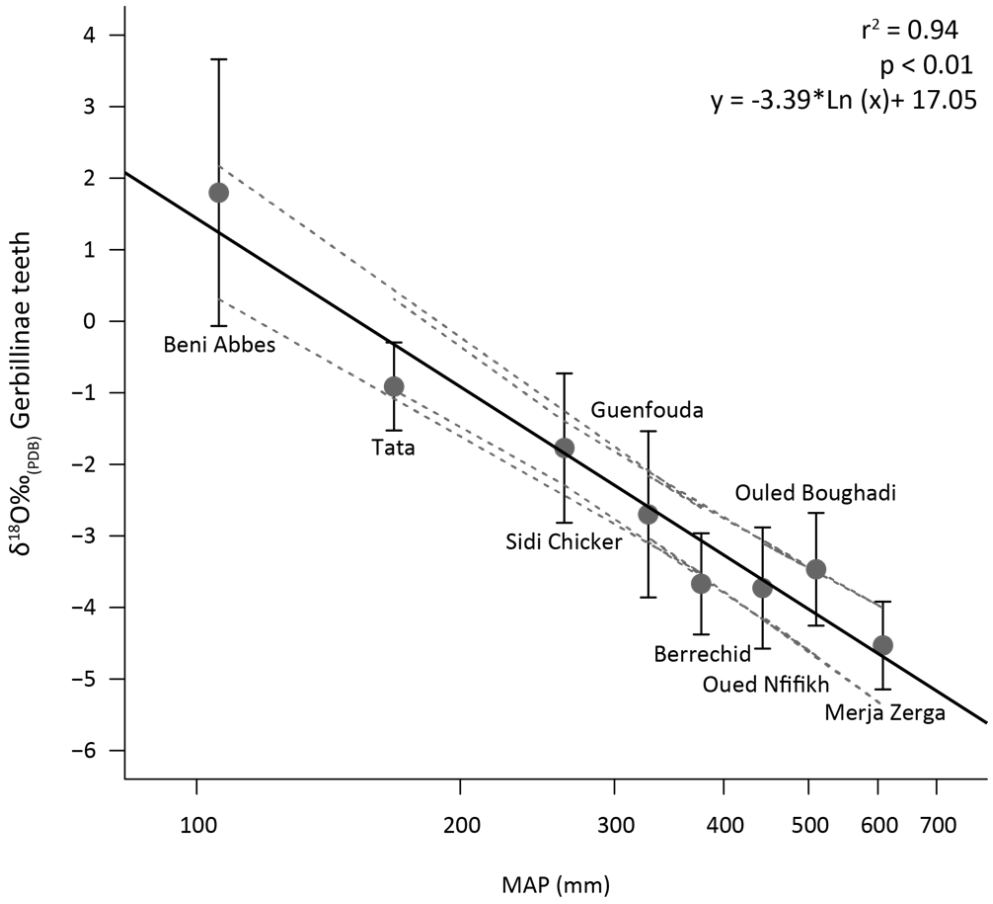

Figure 5.23: Relationship between the mean $\delta^{18}O_{teeth}$ and MAP from each sites across northwestern Africa. The error bars show standard deviation (1σ) It should be noted that only two teeth were analysed from Berrechid.

The low daily water requirements of small mammals compared to larger mammals suggests that small mammal body waters are generally more sensitive to evaporative loss and therefore enrichment in ^{18}O compared to large mammals. Laboratory studies have shown that even when free water is available gerbils drink extremely small amounts (Laughlin et al., 1975; Winkelmann and Getz, 1962) and they can survive for several days without water by relying on metabolic and food water (Edwards et al., 1983). Although gerbils have several adaptive strategies to avoid over-heating and prevent water loss, a controlled laboratory study has shown that evaporative loss increases with temperature in *Meriones unguiculatus* (Buffenstein and Jarvis,

1985). Therefore, in the high temperature arid environments of Beni Abbes and Tata the gerbils' bodywater will undergo a higher level of evaporative enrichment in ^{18}O in comparison to those gerbils in the more mesic environments on the Atlantic coast. All of these factors contribute to the strong effects of reduced moisture availability and increased temperatures on gerbil bodywater $\delta^{18}O$ values.

5.5.7. Summary of stable isotope composition of gerbil tissues across northwestern Africa

The results show that gerbil intra-population variation in $\delta^{13}C_{col}$, $\delta^{13}C_{mt}$, $\delta^{15}N_{col}$ and $\delta^{18}O_{mt}$ at the eight sites is similar to that previously recorded in small and large mammal populations, and it not greater than that noted for small mammals from more temperate settings. The $\delta^{13}C$ composition of gerbil tissues record C_3 and C_4 dietary inputs. There is significant negative correlation between both $\delta^{13}C_{col}$ and $\delta^{13}C_{mt}$ and MAP, demonstrating that $\delta^{13}C$ of gerbil tissues does partly reflect the isotopic effects of water deficit on the predominantly C_3 vegetation consumed by the gerbils, but there is high variability at sites due to the microhabitat represented by the gerbil and the short time periods reflected by the tissue. The $\delta^{15}N_{col}$ does not reflect aridity across northwestern Africa, probably because the gerbils consumed domestic crops as part of their diet. There is a robust relationship between $\delta^{18}O_{mt}$ and MAP showing that $\delta^{18}O_{mt}$ strongly reflects aridity and moisture availability because they get most of their water from food.

5.6. Inter-tooth variation in the $\delta^{18}O$ and $\delta^{13}C$ of Gerbillinae teeth

This section will assess isotopic variability between *Meriones* and *Gerbillus* incisor and molar teeth in order to evaluate which teeth should be used in the construction of proxy palaeo-climate and environmental records. This is the first study that systemically explores how a tooth's development period effects the $\delta^{18}O$ and $\delta^{13}C$ composition of rodents with permanently rooted molar teeth and continuously growing incisor teeth.

5.6.1. $\delta^{18}O$ and $\delta^{13}C$ variation between left-right molar and incisor pairs

The $\delta^{18}O$ and $\delta^{13}C$ composition of gerbil left-right molar teeth should be similar because they occupy the same position in the maxilla/mandible, and therefore would be expected to mineralise at similar times soon after birth. Differing growth rates between the gerbil incisor teeth might cause higher isotopic between the left-right incisor pairs. Figure 5.24 shows the isotopic differences between the left and right maxillary/mandibular incisor and 1st molar pairs in the gerbils expressed as $\Delta^{18}O_{Ml\text{-}Mr}$ ($\delta^{18}O_{M1left}$- $\delta^{18}O_{M1right}$), $\Delta^{13}C_{Ml\text{-}Mr}$ ($\delta^{13}C_{M1left}$- $\delta^{13}C_{M1right}$), $\Delta^{18}O_{Il\text{-}Ir}$ ($\delta^{18}O_{incisorleft}$- $\delta^{18}O_{incisorright}$) and $\Delta^{13}C_{Il\text{-}Ir}$ ($\delta^{13}C_{incisorleft}$- $\delta^{13}C_{incisorright}$) (the $\delta^{18}O$ and $\delta^{13}C$ value of each tooth is listed in Appendix 4.1). The $\Delta^{18}O_{Ml\text{-}Mr}$ and $\Delta^{13}C_{Ml\text{-}Mr}$ varies between individuals from ±0.0 to 1.4‰ (mean $\Delta^{18}O_{Ml\text{-}Mr}$ = 0.5 ± 0.6‰) and ±0.1 to 0.2‰ (mean $\Delta^{13}C_{Ml\text{-}Mr}$ = 0.1 ± 0.0‰), respectively while $\Delta^{18}O_{Il\text{-}Ir}$ and $\Delta^{13}C_{Il\text{-}Ir}$ is ±0.0 to 1.0‰ (mean $\Delta^{18}O_{Il\text{-}Ir}$ = 0.6 ± 0.4‰) and ±0.0 to 0.8‰ (mean $\Delta^{13}C_{Il\text{-}Ir}$ = 0.5 ± 0.3‰). The $\Delta^{13}C_{Ml\text{-}Mr}$ is negligible in the 5 Gerbillinae analysed and falls within analytical error range,

but Figure 5.24 shows that $\Delta^{13}C_{Il\text{-}Ir}$ is more variable. The $\delta^{18}O$ variation between the left and right 1st molar and incisor pairs is similar.

Lindars *et al*. (2001) undertook the only previous study to examine isotope variation between left-right tooth pairs in rodent teeth. This study, using the PO_4 component of the teeth, explored the variation between M1, M2 and M3 left-right tooth pairs in three *Glis glis* (fat dormouse) individuals (a species with permanently rooted molar teeth and permanently growing incisor teeth). Lindars *et al.* (2001) reported that the $\Delta^{18}O_{Ml\text{-}Mr}$ varied between individuals from ±0.0 to 2.4‰, higher than that displayed between the gerbils, but the mean $\Delta^{18}O_{Ml\text{-}Mr}$ in *Glis glis* is 0.6 ± 0.7‰, similar to that of the mean in the gerbil molar pairs (0.5 ± 0.6‰). Studies to examine the left-right tooth pair isotope variation in the CO_3 component of teeth have only been undertaken on large mammal teeth. Gadbury *et al*. (2000) and Brookman & Ambrose (2012) examined the difference between the $\delta^{18}O$ and $\delta^{13}C$ values of left-right tooth pairs (bulk tooth material) in *Bison* and *Macropus* (kangaroo). Both studies yielded similar results with variations between left-right tooth pairs of up to ~1.0‰ in $\delta^{13}C$ and up to ~1.8‰ in $\delta^{18}O$. The mean difference in $\delta^{18}O$ and $\delta^{13}C$ between the left-right molar pairs was 0.5± 0.6‰ and 0.3± 0.2‰ in *Bison*, and 0.8± 0.7‰ and 0.4± 0.4‰ in *Macropus*, similar to those reported in the gerbils and *Glis glis*.

The results show that the left-right isotope tooth variation in gerbils is similar to published data from other small and large mammals. The offsets between the left-right $\delta^{18}O$ and $\delta^{13}C$ values are unlikely to result from analytical inconsistences or sampling bias and instead, as suggested by Brookman & Ambrose (2012), probably result from inherent isotopic variability caused by

asynchronous formation of the teeth/enamel. Both small and large mammals show larger isotope variation in $\delta^{18}O$, relative to $\delta^{13}C$ between left-right molar pairs. Brookman & Ambrose (2012) suggest that this results from a greater inherent variability of $\delta^{18}O$ in enamel. Although there are isotopic offsets between gerbil left and right tooth pairs the mean variation is <1‰ in both $\delta^{18}O$ and $\delta^{13}C$.

5.6.2. Intra-maxilla/mandible tooth variation

Figures 5.25 and 5.26 show the isotopic differences between left or right incisor, and 1st molar teeth, expressed as $\Delta^{18}O_{I\text{-}M1}$ ($\delta^{18}O_{incisor}$- $\delta^{18}O_{M1}$) and $\Delta^{13}C_{I\text{-}M1}$ ($\delta^{13}C_{incisor}$- $\delta^{13}C_{M1}$) in *Meriones*, and the difference between left or right incisor and molar teeth in *Gerbillus* expressed as $\Delta^{18}O_{I\text{-}M}$ ($\delta^{18}O_{incisor}$- $\delta^{18}O_{M}$) and $\Delta^{13}C_{I\text{-}M}$ ($\delta^{13}C_{incisor}$- $\delta^{13}C_{M}$) (specific molars are not attributed in this case) ($\delta^{18}O$ and $\delta^{13}C$ values for inter-tooth analysis are provided in Appendix 4.2). In *Gerbillus* $\Delta^{18}O_{I\text{-}M}$ and $\Delta^{13}C_{I\text{-}M}$ varies between individuals from ±1.1 to 5.4‰ and ±0.4 to 3.7‰, respectively (Figure 5.26), while for *Meriones* $\Delta^{18}O_{I\text{-}M1}$ and $\Delta^{13}C_{I\text{-}M1}$ is ±0.1 to 2.4‰ and ±0.3 to 4.2‰ (Figure 5.25). Figure 5.25 also shows the isotopic difference between the 2nd molar and 1st molar, expressed as $\Delta^{18}O_{M2\text{-}M1}$ and $\Delta^{13}C_{M2\text{-}M1}$ in *Meriones*. In most *Meriones* individuals the $\delta^{18}O$ and $\delta^{13}C$ composition of M2's lies within the error range of the M1. The *Meriones* incisors tend to have lower or similar $\delta^{18}O$ and $\delta^{13}C$ composition to that recorded in the molars. This pattern is also observed in the $\delta^{18}O$ of the *Gerbillus* molar and incisor teeth, but it is not as clear in the $\delta^{13}C$ values of the *Gerbillus* teeth.

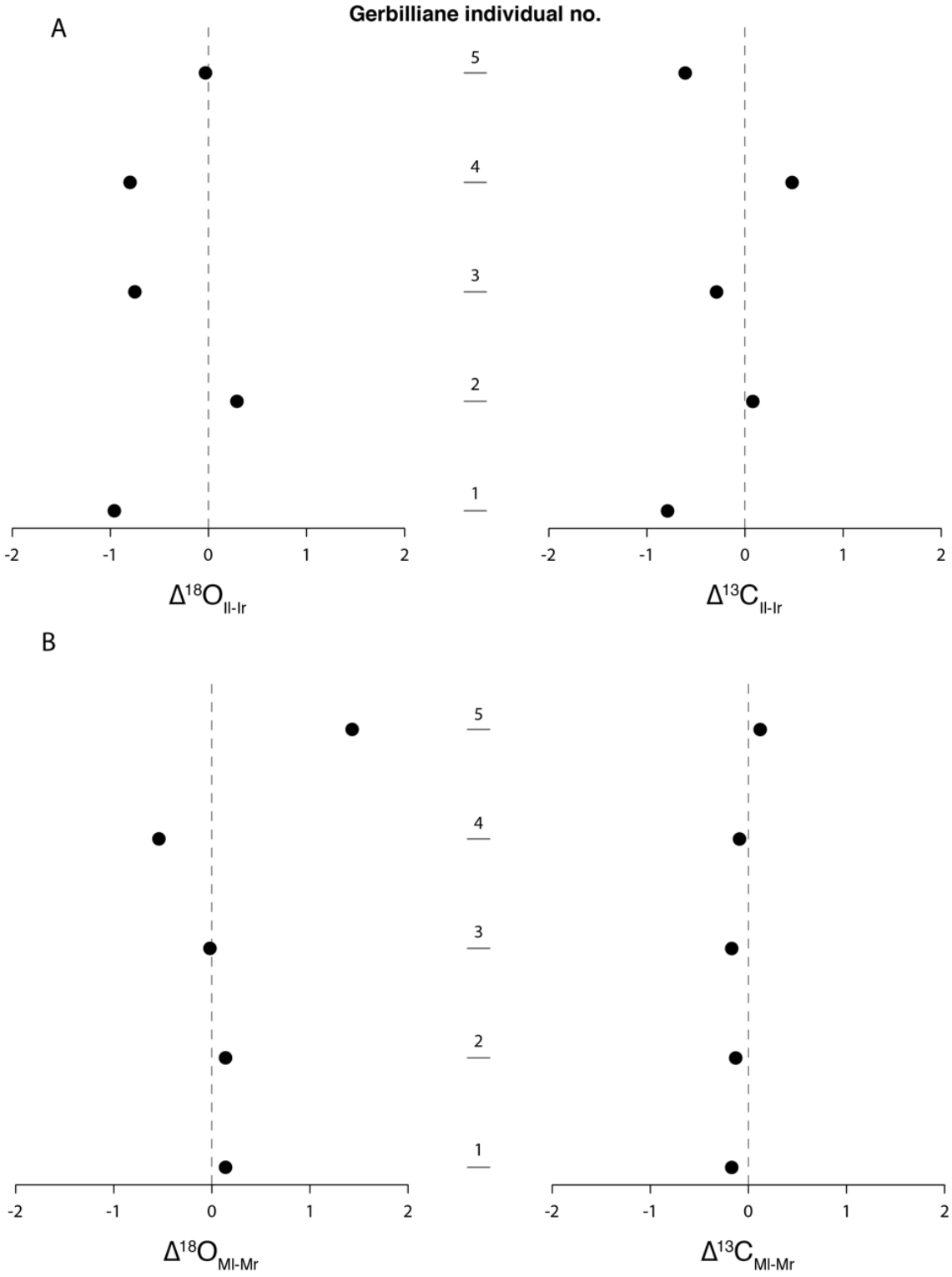

Figure 5.24: Diagram showing A) the $\delta^{18}O_{incisorleft}$- $\delta^{18}O_{incisorright}$ and $\delta^{13}C_{incisorleft}$- $\delta^{13}C_{incisorright}$: B) $\delta^{18}O_{M1left}$- $\delta^{18}O_{M1right}$ and $\delta^{13}C_{M1left}$- $\delta^{13}C_{M1right}$ in 5 Gerbilliane individuals. The dotted 'zero' line shows that there is no difference between the $\delta^{18}O$ and $\delta^{13}C$ composition of the left-right incisor/molar pairs. Negative/positive numbers indicate that the composition of the left side tooth is lower/higher than the right side tooth.

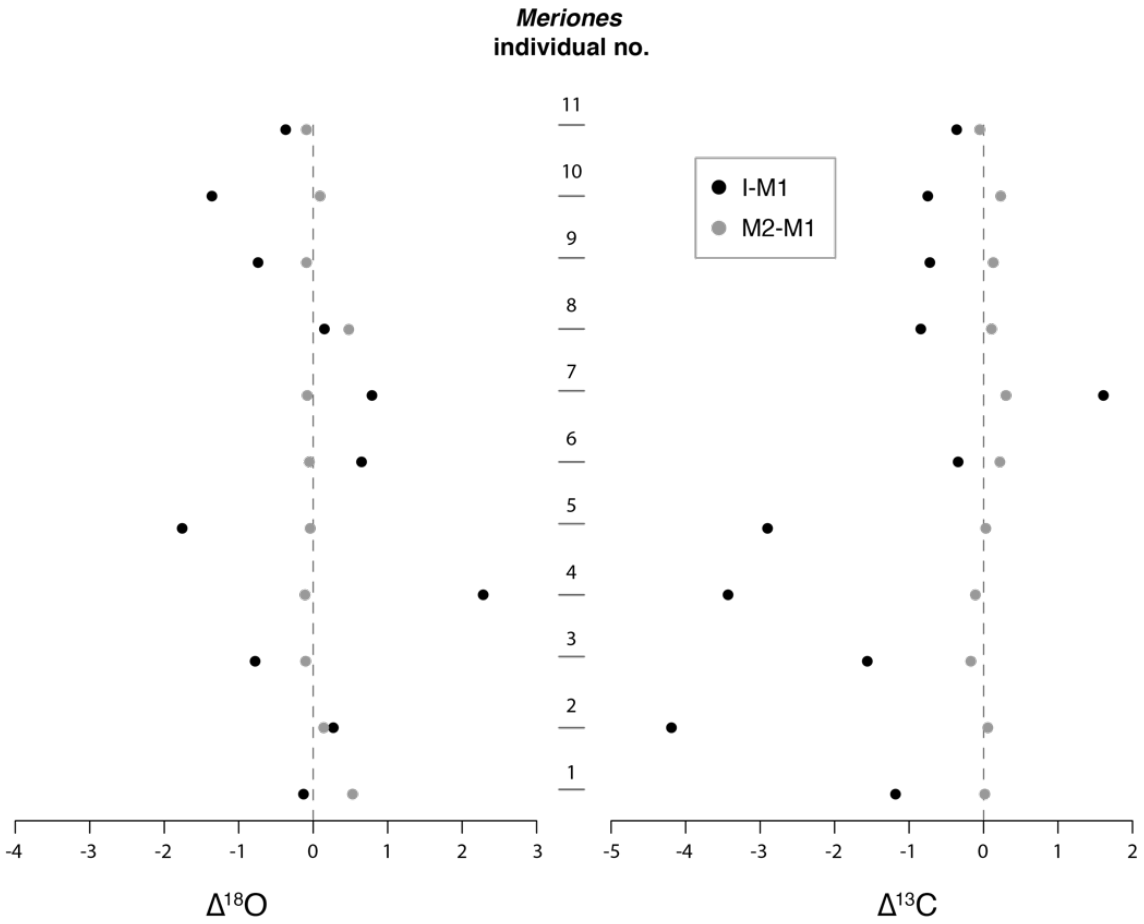

Figure 5.25: Diagram showing the a) $\delta^{18}O_{incisor}$- $\delta^{18}O_{M1}$ (black dots) and $\delta^{18}O_{M2}$- $\delta^{18}O_{M1}$ (grey dotes) b) $\delta^{13}C_{incisor}$- $\delta^{3}C_{M1}$ (black dots) and $\delta^{13}C_{M2}$- $\delta^{13}C_{M1}$ (grey dots) in the eleven *Meriones* individuals in which inter-tooth variation was explored. The dotted 'zero' line indicates there is no isotopic offset between the $\delta^{18}O$ and $\delta^{13}C$ composition of either the I and M1 or M2 and M1. Negative numbers indicate that the I and M2's have a lower isotopic composition in comparison to the M1, while positive numbers show that the I and M2's have a higher isotopic composition compared to the M1.

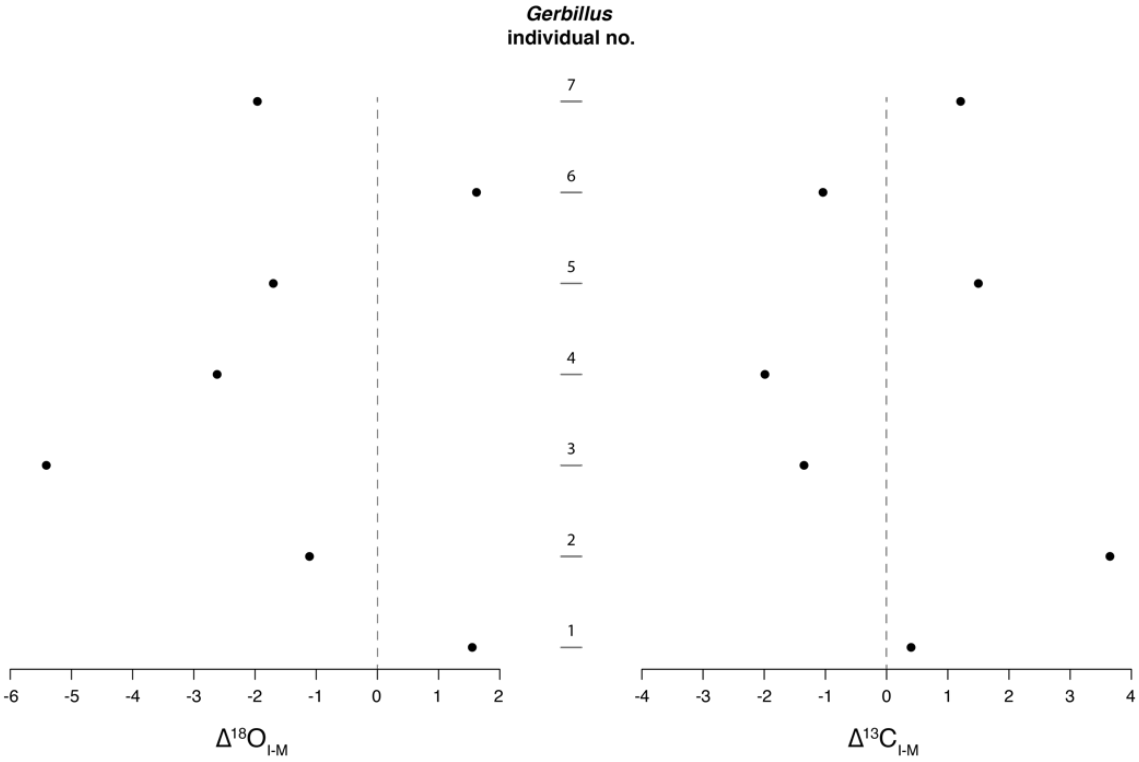

Figure 5.26: Diagram showing the a) $\delta^{18}O_{incisor}$- $\delta^{18}O_M$ and the b) $\delta^{13}C_{incisor}$- $\delta^{13}C_M$ in the seven *Gerbillus* individuals in which inter-tooth variation was explored. The dotted 'zero' line indicates there is no isotopic offset between the $\delta^{18}O$ and $\delta^{13}C$ composition of the molar and incisor teeth. Negative numbers indicate that the incisor teeth have a lower isotopic composition in comparison to the molar teeth, while positive numbers show that the incisor teeth have a higher isotopic composition compared to the molar teeth.

Reasons to explain the isotopic offsets between molar and incisor teeth in gerbils include time of tooth formation, physiological effects (mainly resulting from a nursing effect) and differing amounts of dentine and enamel in each tooth type. Firstly, if the latter was a major effect it would be expected that the offsets would be consistent in both $\delta^{18}O$ and $\delta^{13}C$, and *Meriones* and *Gerbillus*, between the molar and incisor teeth, yet Figures 5.25 and 5.26 show this not the case. As mentioned in Chapter 1 physiological effects from nursing could also reflect differences between the incisor and molar teeth, because there may be a fractionation involved in the production of milk. Isotopic fractionation does

not occur across the placental boundary (Fogel et al., 1989; Metcalfe et al., 2010), so tooth tissue formed in this period directly reflects the isotopic composition of the mother's body water. Gerbil teeth finish forming 4-8 days post-natal so could be influenced by a nursing effect, but as demonstrated in Section 5.5 the climate signal clearly overprints any physiological signal in the molar teeth. It is therefore argued that different temporal times of formation exerts the greatest influence on the isotopic composition of gerbil molar and incisor teeth.

Variation in $\delta^{18}O$ and $\delta^{13}C$ of continuously growing incisors and permanent, rooted molars amongst small mammals has been poorly documented to date. The only existing study to explore this issue documents inter-tooth variation within *Arvicola terrestris,* a species that has both continuously growing molar and incisor teeth (Gehler et al. 2012). Arvicolinae and Gerbillinae teeth share the same uniserial enamel structure and tooth morphology (Korvenkontio, 1934; Koenigswald, 1980). Gehler et al. (2012) reported inter-tooth ranges between M1, M2 and M3 in *Arvicola terrestris* of ±0.2 to 1.0‰ for $\delta^{18}O$, and 0.1 to 0.6‰ for $\delta^{13}C$, slightly higher than the inter-molar range recorded in *Meriones* of ±0.0 to 0.5‰ and ±0.0 to 0.2‰ respectively (see Figure 5.25). The overall inter-tooth range (I, M1, M2 and M3) in *Arvicola terrestris* increased with the inclusion of the incisor tooth to 0.3 to 1.9‰ in $\delta^{18}O$ and 0.3 to 1.5‰ in $\delta^{13}C$, lower than the isotopic differences between incisors and molar teeth in both *Meriones* and *Gerbillus*.

Differences between the inter-molar isotopic ranges in the gerbils and *Arvicola terrestris* are best explained by considering the respective tooth formation times. In *Meriones,* the M1 and M2 mineralise within days of each other after birth (Hiatt et al., 1974) and therefore from the same body water and bicarbonate pools, whereas in *Arvicola terrestris* molars grow continuously, and potentially at different rates. In that case seasonal dietary and environmental differences may be reflected. Overall inter-tooth variation (including the molar and incisor teeth) in the gerbils (up to ~5‰ in $\delta^{18}O$ and ~4‰ in $\delta^{13}C$; Figures 5.25 and 5.26) is higher than that observed in *Arvicola terrestris*. This difference is partly explained by the differences in developmental times of the various teeth. Gerbil molars form only in the spring/summer breeding season whereas incisors grow continuously throughout life (Addison and Appleton, 1915; Schour and Massler, 1963; Coady et al., 1967; Klevezal et al., 1990); in the latter case the isotopic composition may reflect any season. In contrast *Arvicola terrestris* incisors and molars both grow continuously and are thus less likely to show inter-tooth $\delta^{18}O$ and $\delta^{13}C$ disparity.

Isotopic offsets in $\delta^{18}O$ and $\delta^{13}C$ between the gerbil molar and incisor teeth show that as predicted, each tooth type reflects a different temporal period. There are advantages and disadvantages to using permanent molar, or continuously growing incisor teeth, for palaeoclimate reconstructions. Although, molars reflect a short time-span i.e. the breeding season, the $\delta^{18}O$ and $\delta^{13}C$ results are more consistent with less variation. Continuously growing incisor teeth are inherently more variable in that they are not seasonally restricted, although they may provide annually resolved information. The incisor teeth may

also record a seasonal prey bias if owls tend to hunt gerbils preferentially in a particular season (see discussion in Section 6.6). The tendency for higher $\delta^{18}O$ and $\delta^{13}C$ values in molars relative to incisors in gerbils hints at the potential for construction of seasonally resolved palaeorecords (see discussion in section 6.6).

5.6.3. Summary of inter-tooth variation

The $\delta^{18}O$ and $\delta^{13}C$ offsets between the left-right tooth pairs are similar to those found in other small and large mammals, and also as found in other studies there is higher variability recorded in $\delta^{18}O$ between the left-right pairs. The isotopic offset appears to result from asynchronous formation of the teeth in the left-right mandible/maxilla. The incisor and molar teeth (from the same side of the maxilla/mandible) have different $\delta^{18}O$ and $\delta^{13}C$ values reflecting the different temporal periods of formation. The M1 and M2 (from the same side of the maxilla/mandible) have extremely similar $\delta^{18}O$ and $\delta^{13}C$ values because these teeth form only days apart.

5.7. Conclusion: Implications for the use of gerbil tissues as a proxy climate record in North Africa

The results from the modern isotope study demonstrate a robust relationship between $\delta^{18}O_{mt}$ and MAP showing that $\delta^{18}O_{mt}$ responds to moisture availability and aridity in this region, and will therefore provide a record of palaeoaridity in North Africa. Predictably, the $\delta^{13}C_{mt}$ recorded the gerbils diet reflecting both C_3 and C_4 dietary inputs. Although the $\delta^{13}C$ does partly reflect the effects of moisture availability on C_3 plants, there is high variability in $\delta^{13}C_{mt}$. $\delta^{13}C$ data should be used to complement the $\delta^{18}O$ data, but care should be taken during interpretation due to the microhabitat and short temporal period reflected by the gerbil teeth. Habitat preferences of the species should also be considered as this will also be reflected in, and may bias the $\delta^{13}C$. The modern study also shows that the isotopic composition of molars and incisors from the same rodent individual differ, consistent with the different temporal periods reflected by the teeth; molar teeth are permanently rooted and form around the time of birth, whereas incisors grow continuously. Therefore, careful consideration should be given to the signal reflected by each tooth when selecting to build proxy palaeo-climate and environmental records. The data also hints that molars and incisors could potentially be used as a means to distinguish seasonal contexts given the formations times of each tooth type. Although the $\delta^{13}C$ and $\delta^{15}N$ composition of collagen will not be used as a proxy climate record tool in this thesis due to poor collagen preservation, it is noteworthy that $\delta^{13}C_{col}$ and $\delta^{13}C_{mt}$ were strongly correlated showing they reflect similar dietary signals. Significantly, there was no relationship between MAP and $\delta^{15}N_{col}$ showing that gerbil tissue does not reflect aridity in northwestern Africa. The

modern study shows that the isotopic composition of small mammal tissues accurately record local climate and environmental conditions, but close attention to the developmental periods, and behaviour of the animals is required in order to make their climate and environmental interpretation meaningful. The following Chapter will use the $\delta^{18}O$ and $\delta^{13}C$ composition of archaeological *Meriones* sp. teeth from Taforalt and El Harhoura 2 to construct a record of palaeoaridity and past vegetation cover in the Atlantic and Mediterranean region of North Africa.

6. Reconstructing palaeoaridity and past vegetation at El Harhoura 2 and Taforalt using $\delta^{18}O$ and $\delta^{13}C$ values in Gerbillinae teeth

6.1. Introduction

This chapter describes the $\delta^{18}O$ and $\delta^{13}C$ analysis undertaken on archaeological gerbil teeth (*Meriones* sp.) from El Harhoura 2 and Taforalt. Using the relationship established between $\delta^{18}O_{mt}$ and MAP in the modern study, described in Chapter 5, the $\delta^{18}O$ composition of archaeological *Meriones* teeth is used to reconstruct Late Pleistocene MAP in the Atlantic and Mediterranean regions of North Africa. The $\delta^{13}C$ values of *Meriones* are also used to infer the presence of C_3 and C_4 vegetation in the regions surrounding both cave sites. Furthermore, the possibility of extracting seasonal information from isotopic differences between molars and incisors at both sites is explored.

6.2. Material and methods

$\delta^{18}O$ and $\delta^{13}C$ analysis was carried out on *Meriones* sp. teeth from El Harhoura 2 and Taforalt. *Meriones* were selected because they are found throughout the Late Pleistocene sequences at both cave sites, and they are larger than *Gerbillus* sp., therefore providing more sample for isotope analysis. The site stratigraphy and chronology for both El Harhoura 2 and Taforalt is discussed in Chapter 2, while the sampling locations of the teeth is shown in Section 6.2.1 and Section 6.2.2. The behaviours, habitat preferences and physiology of *Meriones* sp. in North Africa are described in Chapter 5 (Section 5.2.3 and Table 5.2).

6.2.1. *Meriones* teeth from El Harhoura 2

The small mammal material from El Harhoura 2 was recovered from the excavation area at the front of the cave (Figure 2.9). All buckets of sediment removed from the cave were given a 3D co-ordinate and unique number. The sediments were then wet sieved on-site through a 3mm and 1mm mesh. The Level 2 sediments were cemented so dilute acetic acid was used to disaggregate them. The residue was dried and sorted to separate environmental and finds materials (Stoetzel et al., 2011). The abundance of small mammal remains at El Harhoura 2 is extremely high with approximately 1,800 identifiable elements per m^3 of sediment in Level 1, increasing to more than 220,000 identifiable elements per m^3 in the lower Levels 7 and 8. Due to the high density of skeletal remains a random sub-sampling strategy was used to select samples for study proportional to the excavated volume of sediment from each level. In total 152 buckets of sediment were sampled for small mammal remains from Levels 1-8 (excluding Level 4b) from which there were 30,896 identifiable elements (29,015 rodents, 47 Erinaceomorpha, 1786 Soricomorpha and 48 bats) (Stoetzel et al., 2011). Taxonomic identification and taphonomic study of the microfauna assemblage was carried out by E. Stoetzel (analysis carried out on Levels 1-8, excluding 4b) (Stoetzel, 2009; Stoetzel et al., 2011, 2010) (results summarised in Table 6.1). The ratio of the skeletal elements, as well as the presence of digestion on much of the material, suggests the assemblage results from the accumulation of pellets/scats from different predators (Table 6.1).

Table 6.1: Summary of palaeoecological and taphonomic information from Levels 1-8 at El Harhoura 2 (From Stoetzel et al. 2011).

	Palaeoecology	**Taphonomy (Predation)**		
Level	**Species present in each level (bold shows the most abundant species in each level)**	**Digestion (based on categories determined by Andrews 1990)**	**Predator pattern (based on skeletal representation ratios (Andrews 1990))**	**Possible predator**
Level 1	*Lemniscomys barbarous* *Apodemus sylvaticus* ***Mus cf. spretus*** *Gerbillus campestris* *Meriones shawii/grandis* *Atelerix algirus* *Crocidura spp.* Chiroptera	Category 2-3	Owl pattern	*Bubo b. ascalaphus*
Level 2	*Mus cf. spretus* *Gerbillus campestris* ***Meriones shawii/grandis*** *Atelerix algirus* *Crocidura spp.* Chiroptera	Category 3-4	Intermediate pattern	*Genetta genetta* *Falco tinnunculus* Several predators?
Level 3	*Mus cf. spretus* *Gerbillus campestris* ***Meriones shawii/grandis*** *Atelerix algirus* *Crocidura spp.* Chiroptera	Category 3-4	Diurnal raptor or carnivore pattern	*Falco tinnunculus* Small mammalian carnivore
Level 4a	*Mus cf. spretus* *Gerbillus campestris* ***Meriones shawii/grandis*** *Atelerix algirus* *Crocidura spp.* Chiroptera	Category 3	Intermediate pattern	Several predators?
Level 5	*Eliomys sp.* *Mus cf. spretus* *Gerbillus campestris* ***Meriones shawii/grandis*** *Jaculus cf. orientalis* *Atelerix algirus* *Crocidura spp.* Chiroptera	Category 3	Intermediate pattern	Several predators?

Level 6	*Mus cf. spretus* *Gerbillus campestris* ***Meriones shawii/grandis*** *Atelerix algirus* *Crocidura spp.* Chiroptera	Category 3-4	Diurnal raptor or carnivore pattern	*Falco tinnunculus* Small mammalian carnivore
Level 7	*Mus cf. spretus* *Gerbillus campestris* ***Meriones shawii/grandis*** *Jaculus cf. orientalis* *Atelerix algirus* *Crocidura spp.* Chiroptera	Category 2-3	Owl pattern	*Bubo b. ascalaphus*
Level 8	*Eliomys sp.* *Mus cf. spretus* *Gerbillus campestris* ***Meriones shawii/grandis*** *Crocidura spp.* Chiroptera	Category 2-3	Owl pattern	*Bubo b. ascalaphus*

Taphonomic analysis shows that the small mammals in Levels 1, 7 and 8 were accumulated by a category 2 to 3 predator (according to Andrew's (1990) classification) such as *Bubo ascalaphus*, the remains in Levels 2, 3 and 6 result from a category 3 to 4 predator like *Falco tinnunculus* or a small carnivore, while the remains in Levels 4 and 5 present an intermediate pattern resulting from an unknown predator or a mix of predators (Table 6.1). All of the predators identified are opportunistic, meaning that there should be minimal predator bias introduced into the small mammal assemblage (Stoetzel et al., 2011). As there is no relationship between type of predator and prey in each level it is assumed that the changes in species abundances between levels reflect environmental changes (Stoetzel, 2009; Stoetzel et al., 2011). The small mammal remains from Levels 11-9 and 4b are yet to undergo detailed palaeoecological and

taxonomic study, but *Meriones* from these levels are included in the isotope analysis.

Meriones is the most abundant taxon at El Harhoura 2 (3903 identifiable elements) and is the most common taxa in the majority of the Late Pleistocene Levels (Table 6.1). Morphometric analysis of the El Harhoura 2 *Meriones* molar teeth shows that they are similar in morphology to *Meriones shawii* and *Meriones grandis*. *M. grandis* was once considered a sub-species of *M. shawii* (Aulagnier and Thevenot, 1986), but now is regarded as a separate species based on external and skull morphometrics (Pavlinov, 2000; Pavlinov et al., 1990). *M. grandis* is, however, poorly studied and little is known about its molar morphology or geographical distribution. In the absence of a precise criterion to distinguish between *M. shawii* and *M. grandis* the attribution of *M. shawii/grandis* was given to all *Meriones* remains at El Harhoura 2 (Stoetzel et al., 2011, 2010). *M. shawii/grandis* are found in relatively humid biotopes, such as steppes and cultivated areas, in the semi-arid Mediterranean climate zone of North Africa (Table 5.2).

All *Meriones* teeth selected for this study were identified by E. Stoetzel. The high abundance of *M. shawii/grandis* at El Harhoura 2 allowed the selection of 10 molar and 5 incisor teeth for $\delta^{18}O$ and $\delta^{13}C$ analysis from Levels 2-11 (with the exception of Level 4b from which 9 molar teeth were analysed) (n= 164 teeth) (Figure 6.1). The majority of *Meriones* teeth come from a small area within the cave. Samples from Levels 11-5 are from accumulations in squares O12 and P12, while teeth from Levels 4b and 4a are from squares O11, Q11 and Q12. The *Meriones* teeth from Levels 3 and 2 are from a wider excavation area (Table 6.2, Figure 2.9). Where possible teeth were selected from different environmental samples to capture isotopic variation across levels. The dates for each level are listed in Table 2.3.

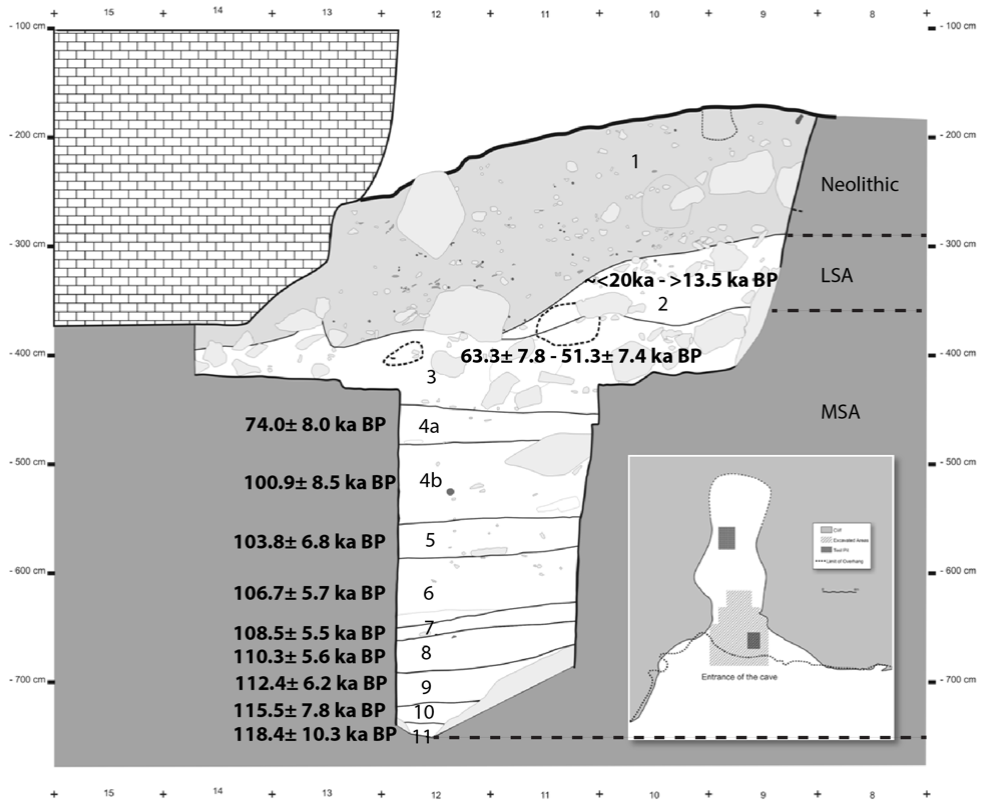

Figure 6.1: Stratigraphic diagram showing Levels 11-1 at El Harhoura 2. The dates shown for Levels 11-3 are the Bayesian modelled OSL ages (2σ) (see discussion in Chapter 2 Section 2.3.1.1.1, Figure 2.11 and Table 2.3). The age range displayed for Level 2 is established from radiocarbon dates and cultural associations (see 2.3.1.1) (adapted from Fig. 2 in Stoetzel at al. 2011).

Table 6.2: Table showing the location and number of incisors and molars sampled for isotope analysis from each level at El Harhoura 2.

Level	Squares	Number of molar teeth	Number of incisor teeth
2	N14	10	5
3	Q11, Q12, O13, P13, D13	10	5
4a	Q11, Q12	10	5
4b	O11	9	5
5	O12, P12	10	5
6	O12, P12	10	5
7	O12, P11	10	5
8	O12, P12	10	5
9	O12, P12	10	5
10	O12, P12	10	5
11	O12	10	5

6.2.2. *Meriones* teeth from Taforalt

The small mammal material at Taforalt was excavated from several sectors in the cave (Figure 2.5). Much of the excavated cave sediment was dry sieved through a 2mm mesh (although this methodology was not systemically applied) to recover finds and environmental material. Sediment containing large quantities of environmental material (including microfauna remains) was sampled (in 2.5-litre sample bags), given a 3D co-ordinate and transported to the U.K, where it was then wet sieved and sorted by C. Price. The small mammal material is currently undergoing taxonomic identification, palaeoecological study and taphonomic study by S.Parfitt. Preliminary investigation indicates that predators were the main accumulation agents (S. Parfitt *pers. comm*).

S. Parfitt taxonomically identified all *Meriones* sp. (as yet no species attribution have been provided) teeth selected for $\delta^{18}O$ and $\delta^{13}C$ analysis from Sector 2 and Sector 8 at Taforalt (Figures 2.4 and 2.5). *Meriones* remains were less abundant throughout the Late Pleistocene sequence at Taforalt relative to El Harhoura 2, limiting the levels from which *Meriones* teeth could be sampled and also the amount of teeth available for analysis. 2-15 *Meriones* teeth were sampled from eight levels (23K, 23I, 23H, 23G, 23F, 23D, R16 and R14) in Sector 2 (Figure 6.2 and 6.3) and four levels (Y6, Y4, Y2 and Y1) in Sector 8 (n= 74) (Figures 6.4 and 6.5) (Table 6.3). Levels R16, 23D, 23F and 23I yielded low numbers of *Meriones* teeth (n= ≤3), therefore teeth from Levels 23D and 23F, and 23I and 23K were combined to improve the statistical power of the data. Dating evidence shows that these levels are of similar age (Figure 6.3).

Levels 23K to 23D located deep in the Sector 2 excavation area (Lower Laminated and Calcareous Group) cannot be directly correlated with Raynal's Levels (Chapter 2, Figure 6.2 and 6.3). Figure 6.3 shows the OSL and U-series ages from Sector 2. The dates suggest that Levels 23K, 23I, 23H, 23G, 23F and 23D form a relatively continuous sequence dating from c.97 to 80 ka. The large errors on the dates do not allow the association of each level with specific ages, but do place the levels within MIS 5c-5a. The lower levels in Sector 2 are associated with apparent intensive use of the cave by humans during the MSA Aterian. Hearth deposits and specific hearth complexes have been found in Levels R22 and R21 (23D), while *Nassarius* shells have been found in Levels R21 (23D) and 23G. R16 dates to the start of MIS 3 and has an OSL age of 60.1 ± 3.9ka in Sector 1/2. R14 is associated with both OSL and radiocarbon

ages from Sector 2, placing this level in the middle of MIS 3 (c.45-40ka) (Figure 6.3). The four Levels from Sector 8 are associated with a Bayesian radiocarbon age model (Section 2.3.1.1, Figure 2.7). The model predicts that Levels Y1 (15.1-15.3ka cal BP), Y2 (17.1-19.0ka cal BP), Y4 (19.9-24.2ka cal BP) and Y6 (24.6-30.8ka cal BP) were deposited during MIS 2 and span the Last Glacial Maximum (LGM) and Last deglaciation.

Table 6.3: Table showing the location and number of incisors and molars sampled for isotope analysis from each level at Taforalt.

Level	Squares	Number of molar teeth	Number of incisor teeth
Y1	B-C22	5	5
Y2	B-C22, B24	8	5
Y4	B-C22, C21, C22	8	1
Y6	D22, D23	3	2
R14	M14, N13	2	5
R16	N14, L13	2	0
23D	O13	2	1
23F	O13, N14/14	1	2
23G	O13, P13	4	1
23H	O13, P13	6	2
23I	O14	2	0
23K	O14	7	0

a)

b)

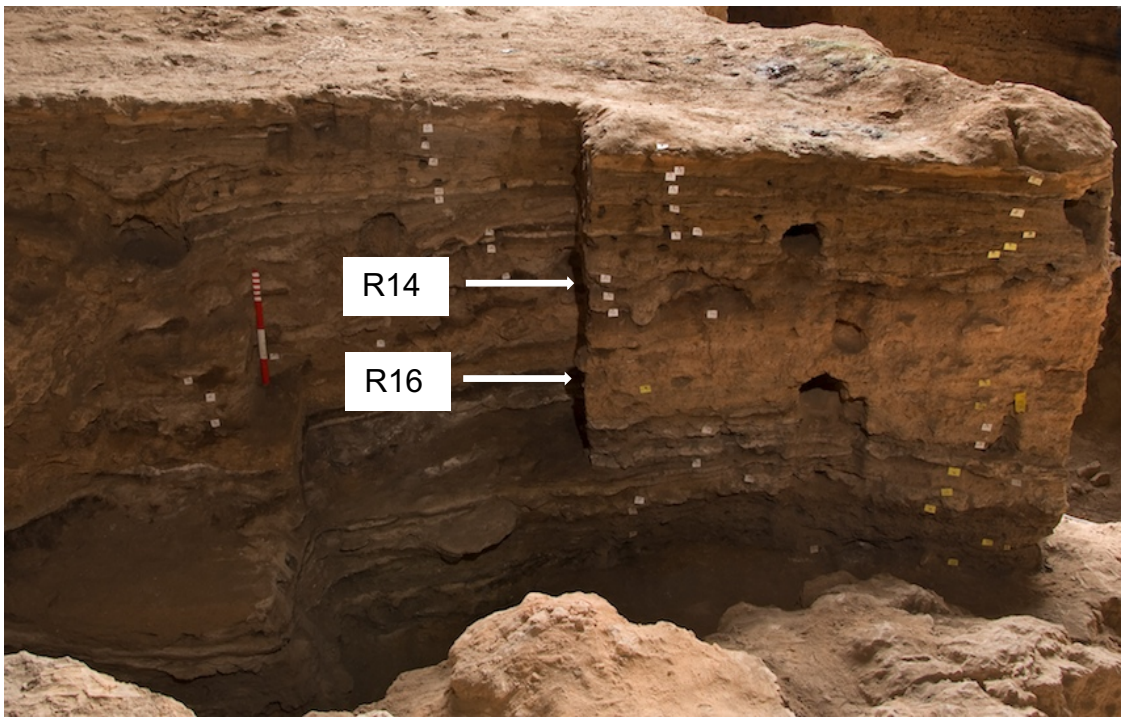

Figure 6.2: Sector 2 excavation at Taforalt a) white boxes show location of levels from which tooth samples were taken, b) Levels R14 and R16 (Photographs Courtesy of Ian Cartwright).

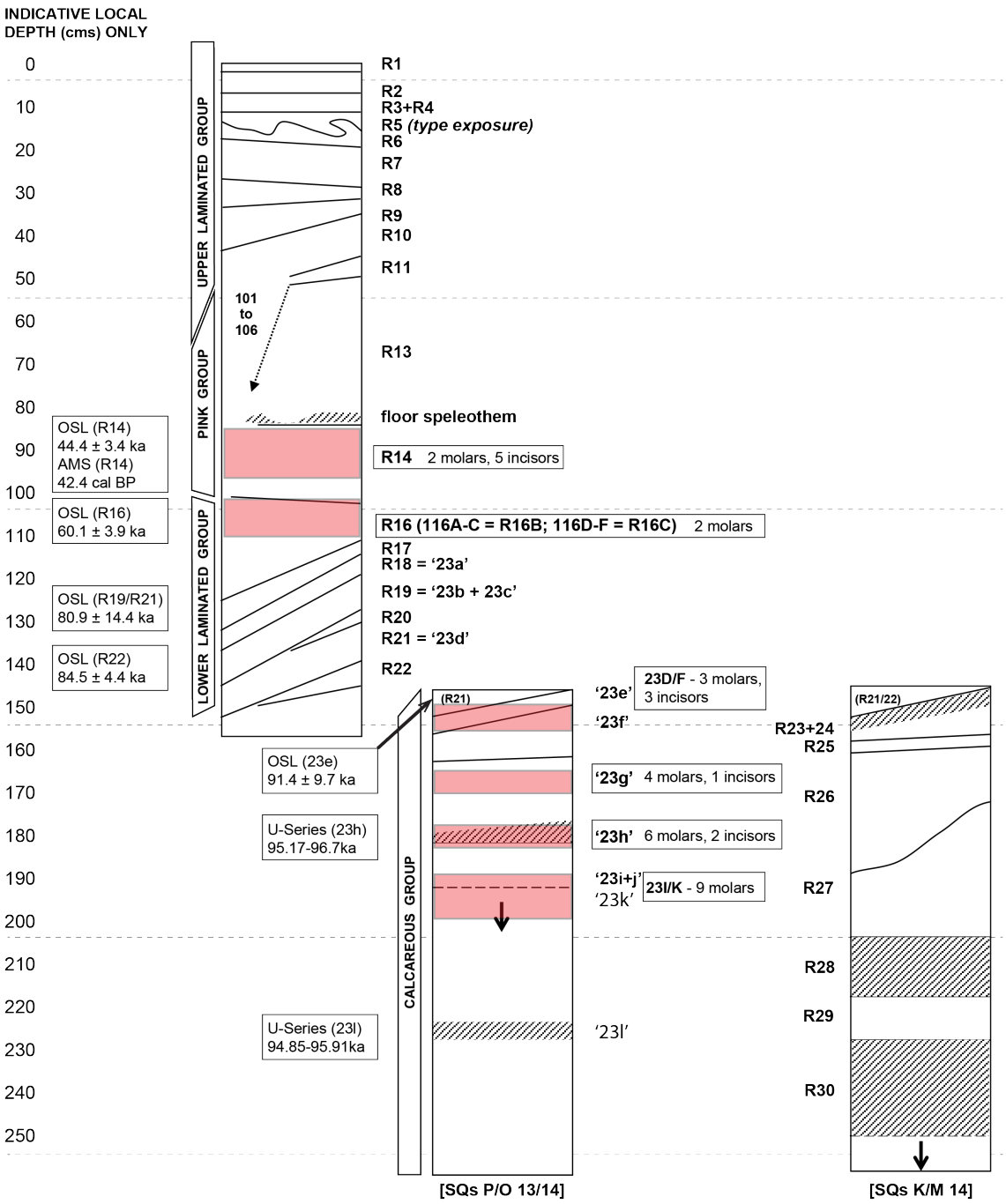

Figure 6.3: Diagram of Taforalt Sector 2 stratigraphy showing Levels from which *Meriones* teeth were sampled for isotope analysis (highlighted by red boxes). OSL and radiocarbon dates from the sequence are shown in boxes (adapted from Fig. 4 in Barton et al. 2013).

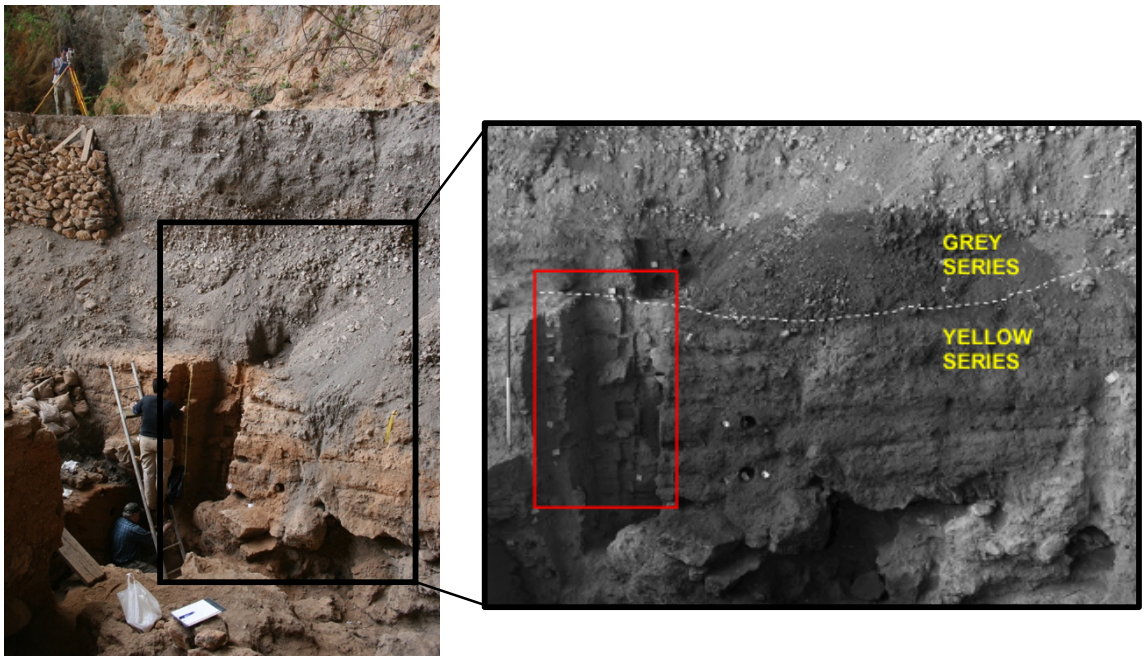

Figure 6.4: Sector 8 excavation at Taforalt (photos courtesy of R.N.E Barton) showing the Grey and Yellow Series. The black box represents the area enlarged in the right hand photo, while the red box shows that excavated in Sector 8. The levels from which *Meriones* teeth were sampled are highlighted on the diagram along with the Bayesian modelled ages (2σ) from Barton et al. (2013). (Photographs Courtesy of Nick Barton).

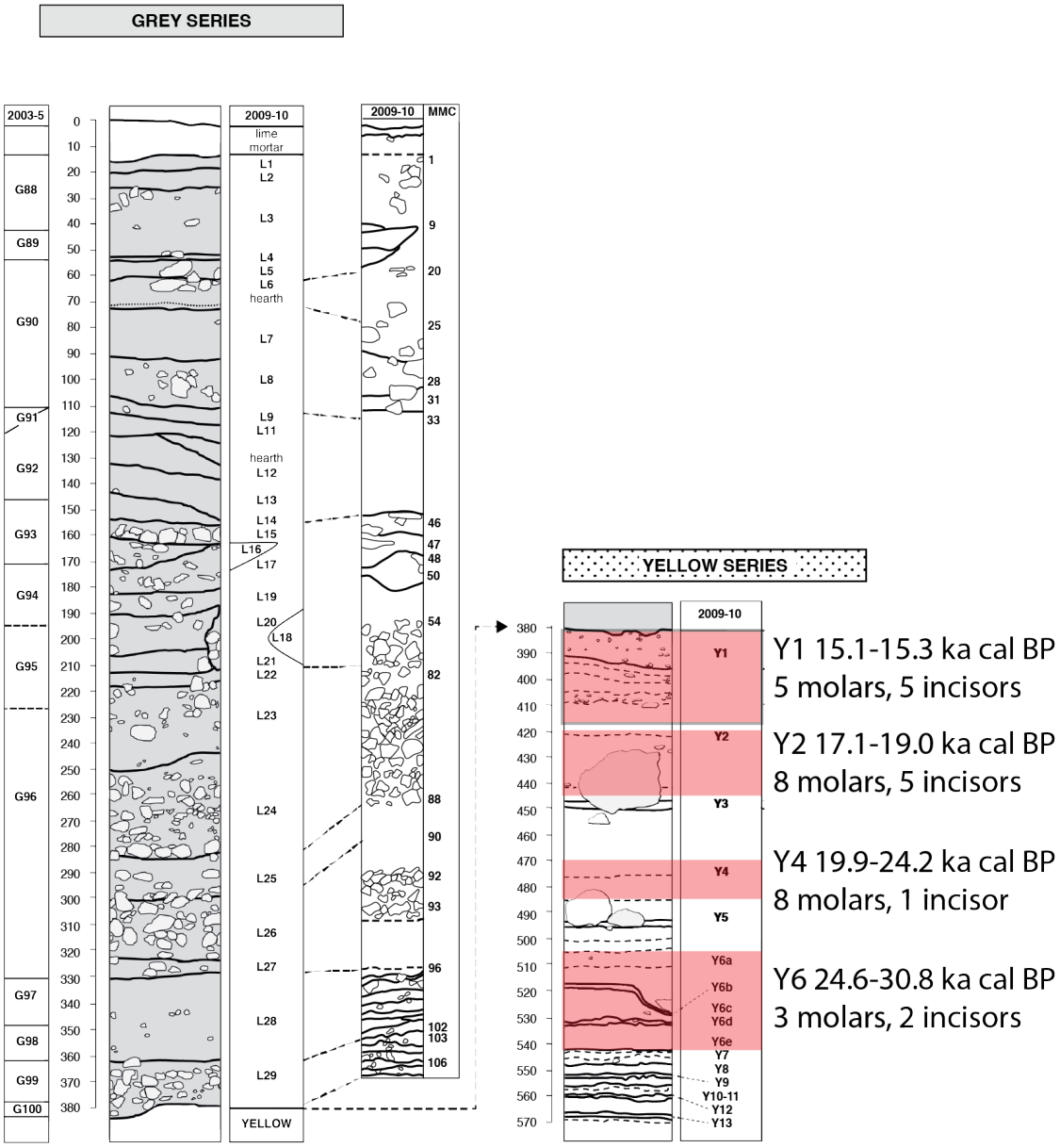

Figure 6.5: Diagram of Taforalt Sector 8 stratigraphy showing Levels from which *Meriones* teeth were sampled for isotope analysis (highlighted by red boxes). Bayesian modelled ages (2σ) (from Barton et al. 2013) are shown for each level.

6.2.3. Stable isotope methodology

Strenuous efforts were made to remove visible dust/sediment and cave matrix from the archaeological teeth using a sand blaster (aluminium oxide). The enamel and dentine of the archaeological incisor teeth was not tightly bound allowing the separation of both tissues by sectioning the buccal surface. As much dentine as possible was removed from the molar teeth through removal of the roots and sectioning of the tooth to clean inside (Figure 6.6). Every effort was made to remove dentine from the molars and incisors, but small amounts may have remained in the sample used for isotope analysis. Tooth samples were crushed using an agate mortar and pestle to produce “tooth apatite” (see discussion in Section 4.3.1.1) powder, so called because of the inclusion of small amounts of dentine. Due to small sample sizes and to maintain consistency with the modern study (Chapter 5) chemical pre-treatment was not undertaken on the tooth powders. Experiments showed a loss of ~25-30% of tooth powder using standard pretreatment methodologies (described in Section 5.2.5.1 and Table 5.3), leaving very little for powder for analysis. Pre-treatment is intended to remove the organic material and secondary carbonates, but in studies on large and small mammal enamel pretreatment does not cause $\delta^{13}C$ or $\delta^{18}O$ to change in a significant or predictable way (Hynek et al., 2012; Passey et al., 2002).

Stable isotope analyses were carried out at the Stable Light Isotope Facility, University of Bradford. Approximately 2mg of tooth powder was reacted with 100% phosphoric acid at 70°C in an automated Thermo Gas Bench II device,

Figure 6.6: The photographs show examples of the archaeological *Meriones* incisor (top) and 1st molar (bottom) teeth. The molars were generally well preserved with the majority of the crown remaining in the majority of the teeth. The incisors from both sites were more fragmentary with only sections of the incisors recovered.

coupled to a Thermo Delta V Advantage mass spectrometer. Data is reported in the δ-notation as per mil (‰) (Equation 2) relative to the international reference standard PDB for both $\delta^{18}O$ and $\delta^{13}C$. The $\delta^{18}O_{VSMOW}$ values were converted to PDB using Equation 3. The fossil teeth were analysed in 4 separate runs on the mass spectrometer. The analytical precision for all measurements was better than 0.2‰ (1σ) for $\delta^{13}C$ and 0.2‰ (1σ) for $\delta^{18}O$ based on replicate analysis of two in-house standards, BES (tooth bioapatite enamel standard) ($\delta^{13}C$ = -11.1 (PDB)), $\delta^{18}O$ = 25.0 (SMOW)) (n=10), and Merck calcium carbonate ($\delta^{13}C$ = -35.45 (PDB)), $\delta^{18}O$ = 13.35 (SMOW)) (n=12), across the 4

runs. In run NBS-19 gave a value of 2.02 ± 0.04 (PDB) for $\delta^{13}C$ and 28.76 ± 0.2 (SMOW) (n=4), while CO-1 gave a value of 2.44 ± 0.2 (PDB) for $\delta^{13}C$ and 28.46 ± 0.2 (SMOW) (n=9). If a $\delta^{18}O$ or $\delta^{13}C$ value fell outside the normal data scatter (based on visual examination of the data) the sample was re-run.

6.2.4. Statistical analysis

Statistical analyses were performed using the freeware statistics package 'R' (http://www.r-project.org/). A Shapiro-Wilk test was used to test for normality in datasets to establish whether parametric or non-parametric statistics should be used. In rare occurrences, where the data did not meet the assumptions of normality, a non-parametric version of a test was used and gave the same result. T-tests were performed to examine differences in $\delta^{18}O$ and $\delta^{13}C$ between Taforalt and El Harhoura 2, differences in $\delta^{18}O$ and $\delta^{13}C$ between molars and incisors at each site, and also within level differences in $\delta^{18}O$ or $\delta^{13}C$ between molars and incisors. Low sample numbers at Taforalt limited the statistical exploration of within-level differences in $\delta^{18}O$ or $\delta^{13}C$ between molars and incisors. Within level t-tests were only performed when $\geq$5 molars and incisors were present in levels. To evaluate whether the differences in the mean $\delta^{13}C$ and $\delta^{18}O$ composition of *Meriones* teeth between levels was statistically significant an analysis of variance (ANOVA) was performed on the data from El Harhoura 2 and Taforalt, followed by post-hoc tests (Tukey) for pairwise comparisons (Taforalt Level 16 was not included in the ANOVA due to small sample size).

6.3. Results: $\delta^{18}O$ and $\delta^{13}C$ composition of *Meriones* teeth from El Harhoura 2 and Taforalt

Figure 6.7 shows the $\delta^{18}O$ and $\delta^{13}C$ composition of 238 *Meriones* molar and incisor teeth ($\delta^{18}O_{teeth}$ and $\delta^{13}C_{teeth}$) from Taforalt (n = 74) and El Harhoura 2 (n= 164). The mean $\delta^{18}O_{teeth}$ and $\delta^{13}C_{teeth}$ is -4.4‰ ± 0.9 and -9.0‰ ± 1.1 (Table 6.4), respectively. The isotopic variation displayed in $\delta^{18}O_{teeth}$ is 5.6‰, ranging from -7.0‰ to -1.4‰. $\delta^{18}O_{mt}$ from the modern sites located north of the Atlas Mountains in the coastal Mediterranean region (Merja Zerga, Ouled Boughadi, Berrechid, Oued Nfifikh, Guenfouda and Sidi Chicker) tend to be higher relative to those of the archaeological teeth (ranging from -5.2‰ to 0.6‰), but the variation in the modern dataset is similar (5.8‰) (Figure 6.7). The variation in $\delta^{13}C_{teeth}$ is -11.1‰ to -5.1‰ with a range of 6‰, lower than that displayed by the modern gerbil teeth from sites north of the Atlas (8.6‰). The archaeological teeth are ^{13}C-enriched relative to the modern teeth, with the exception of $\delta^{13}C_{mt}$ at Tata and Oued Nfifikh where gerbils consumed C_4 plants (Section 5.5.4.1) (Figure 6.7). Comparison of means for El Harhoura 2 and Taforalt show that the $\delta^{18}O_{teeth}$ between sites is statistically indistinguishable (t-test p= >0.05), but, the mean $\delta^{13}C_{teeth}$ between sites is statistically different (t-test p=<0.01).

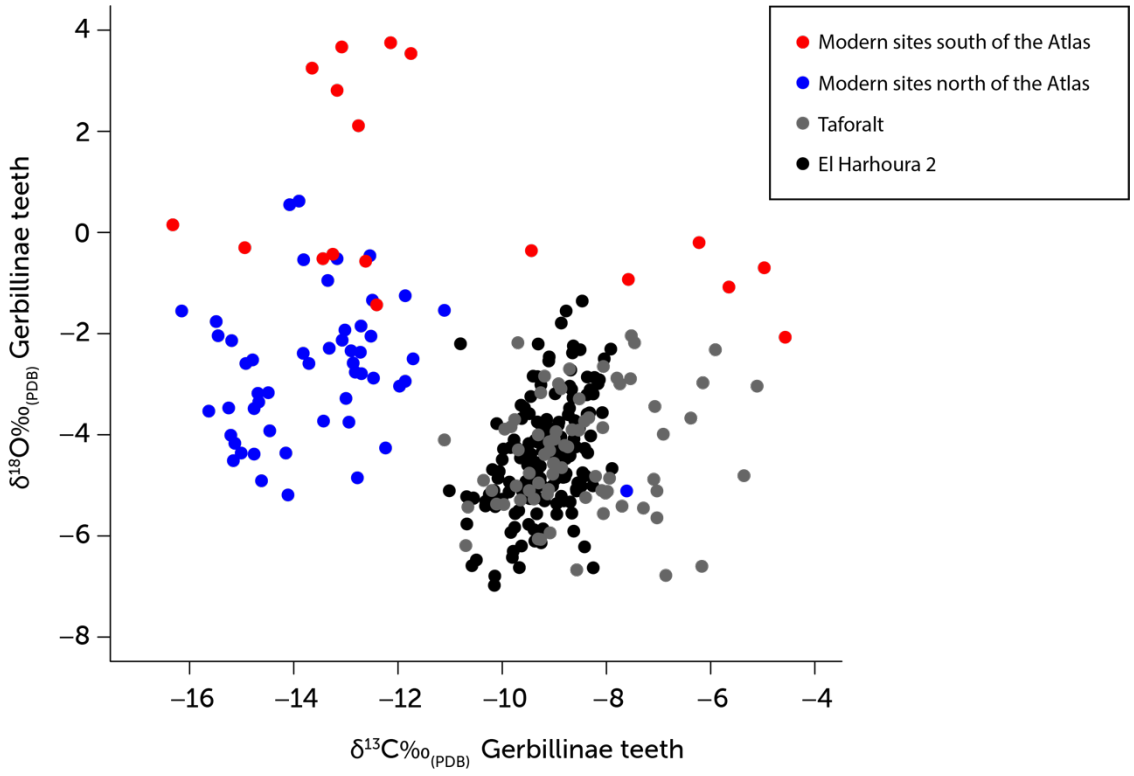

Figure 6.7: Graph showing the $\delta^{18}O$ and $\delta^{13}C$ composition of *Meriones* teeth from El Harhoura 2 and Taforalt plotted with the $\delta^{18}O$ and $\delta^{13}C$ composition of modern gerbil teeth from sites north of the Atlas (Merja Zerga, Ouled Boughadi, Berrechid, Oued Nfifikh, Guenfouda and Sidi Chicker) and South of the Atlas in the hyper-arid climate zone (Tata and Berrechid). NB. The modern $\delta^{13}C$ values of gerbil teeth in this graph have *not* been corrected for the fossil fuel effect and are the values presented in Chapter 5.

Table 6.4: Summary statistics for the $\delta^{18}O$ and $\delta^{13}C$ composition of *Meriones* teeth from Taforalt and El Harhoura 2.

		$\delta^{18}O_{(PBD)}$					$\delta^{13}C_{(PBD)}$				
	Number of individuals	Mean (‰)	Standard deviation (1σ)	Minimum (‰)	Maximum (‰)	Range (‰)	Mean (‰)	Standard deviation (1σ)	Minimum (‰)	Maximum (‰)	Range (‰)
El Harhoura 2- all teeth	164	-4.4	1.1	-7.0	-1.4	5.6	-9.2	0.6	-11.0	-7.9	3.1
El Harhoura 2- molars	109	-4.4	1.2	-7.0	-1.4	5.6	-9.4	0.7	-11.0	-8.0	3.0
El Harhoura 2- incisors	55	-4.5	0.9	-6.6	-2.3	4.3	-8.9	0.5	-10.1	-7.9	2.2
Taforalt- all teeth	74	-4.4	1.1	-6.8	-2.0	4.7	-5.5	1.3	-11.1	-5.1	6.0
Taforalt- molars	50	-4.3	1.0	-6.6	-2.0	4.6	-9.0	1.1	-11.1	-5.4	5.8
Taforalt- incisors	24	-4.7	1.4	-6.8	-2.2	4.6	-7.6	1.0	-9.3	-5.1	4.2

6.3.1. El Harhoura 2

6.3.1.1. Summary of whole dataset

Figure 6.8 shows the $\delta^{18}O_{teeth}$ and $\delta^{13}C_{teeth}$ from El Harhoura 2 (molars n= 109, incisors n= 55) (Table 6.4, data listed in Appendix 5). The mean $\delta^{18}O_{teeth}$ and $\delta^{13}C_{teeth}$ is -4.4‰ ± 1.1 and -9.2‰ ± 0.6, respectively. The variation in $\delta^{18}O_{teeth}$ is 5.6‰, ranging from -7.0‰ to -1.4‰, higher than the intra-population variation in the modern data encompassing multiple rainfall regimes (1.0-4.3‰). The $\delta^{13}C_{teeth}$ ranges from -11.0‰ to -7.9‰ with a total variation of 3.1‰, similar to the intra-population variation displayed at mesic C_3 sites in the modern study. The mean $\delta^{18}O$ composition of molars ($\delta^{18}O_{mt}$) and incisors ($\delta^{18}O_{it}$) is -4.4‰ ± 1.2 and -4.5‰ ± 0.9, with similar variation recorded in each tooth type. A t-test shows that molars and incisors are statistically indistinguishable in $\delta^{18}O$ (p=>0.05). The mean $\delta^{13}C$ composition of molars ($\delta^{13}C_{mt}$) and incisors ($\delta^{13}C_{it}$) is -9.4‰ ± 0.7 (1σ) and -8.9‰ ± 0.5, respectively. Figure 6.8 shows that incisors are ^{13}C-enriched relative to the molars, a trend that is reflected in the $\delta^{13}C_{teeth}$ variation. The maximum value of $\delta^{13}C_{mt}$ and $\delta^{13}C_{it}$ is similar (~-8‰), but the molars have a lower minimum value (–11.0‰) compared to that of the incisors (-10.1‰). Comparison of means for $\delta^{13}C_{mt}$ and $\delta^{13}C_{it}$ show that they are statistically different (t-test p = <0.01).

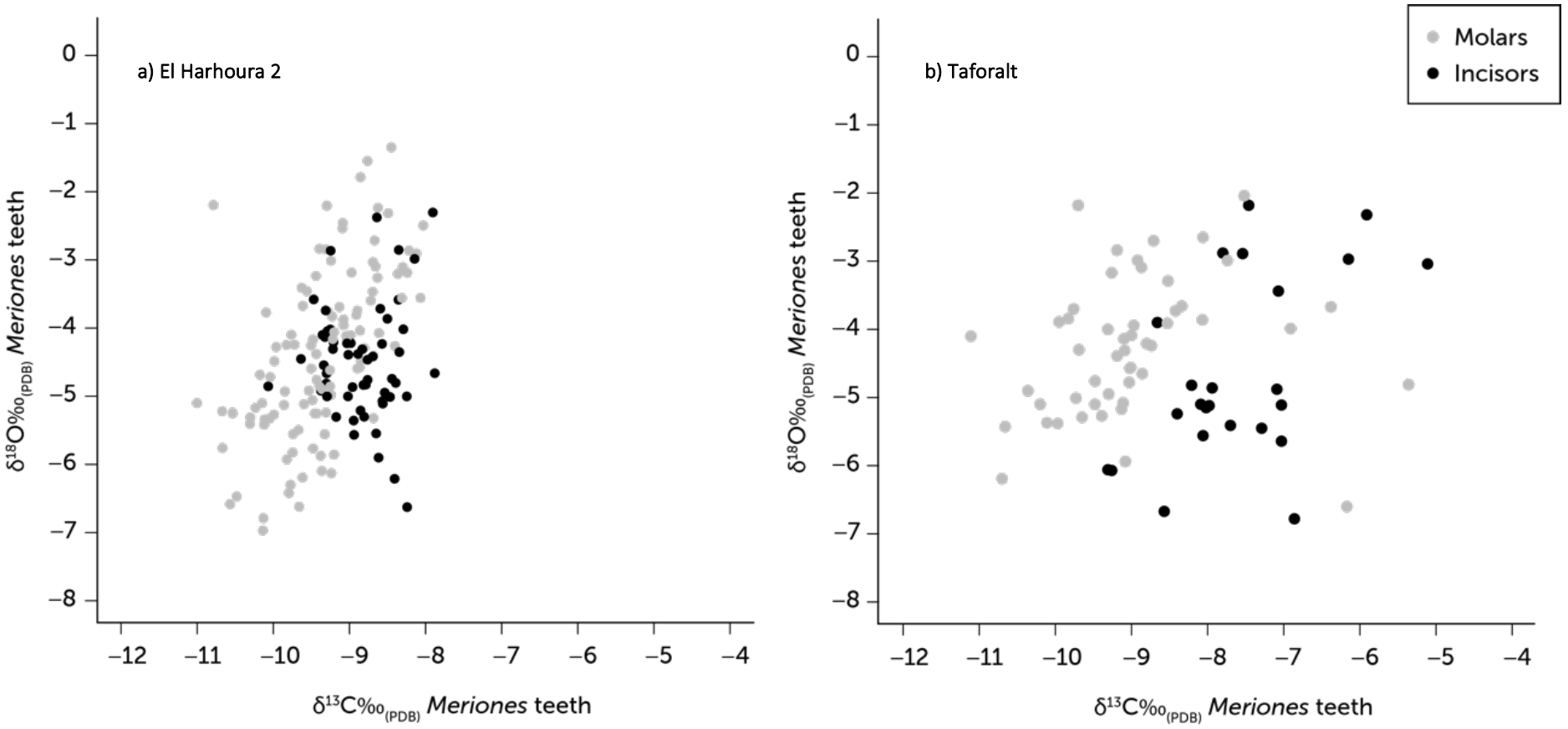

Figure 6.8**: Graphs showing the δ^{18}O and δ^{13}C composition of *Meriones* molars and incisors from a) El Harhoura 2 and b) Taforalt.**

6.3.1.2. Exploring data by Level

The $\delta^{18}O_{teeth}$ and $\delta^{13}C_{teeth}$ from Levels 2-11 at El Harhoura 2 are presented in Table 6.5 and plotted in Figure 6.9. The mean $\delta^{18}O_{teeth}$ in Levels 7-11 is ≤-5‰, while in Levels 6-2 the mean is ≥-4.3‰. Levels 11 and 7 have the lowest $\delta^{18}O_{teeth}$ means (-5.5‰), while the highest mean $\delta^{18}O_{teeth}$ is in Level 2 (-2.6‰). The same trend is not reflected in the $\delta^{13}C_{teeth}$ throughout the Levels. The mean $\delta^{13}C_{teeth}$ varies by only 0.8‰, from -9.5‰ (Levels 7 and 8) to -8.7‰ (Level 3), reflecting consistency in $\delta^{13}C_{teeth}$ throughout the Late Pleistocene. An analysis of variance (ANOVA) shows significant differences in the $\delta^{18}O_{teeth}$ between the 11 Levels at El Harhoura 2 (F = 26.98, P = <0.01). A post hoc Tukey test for pairwise comparisons demonstrates that Level 2 differs significantly in $\delta^{18}O_{teeth}$ from all other levels (P = <0.05), while Levels 3, 4a, 4b and 6 all differ significantly to Levels 7, 8, 9, 10 and 11 (P = <0.05) (Appendix 6.1). Level 5 differs from Levels 7, 8, 10 and 11 (P = <0.05). An ANOVA also shows that there is a significant difference in $\delta^{13}C_{teeth}$ between the Levels at El Harhoura 2 (F = 2.56, P = <0.01). Figure 6.10 shows the $\delta^{18}O$ and $\delta^{13}C$ composition of molars and incisors plotted by Level. Within level t-tests show a significant difference between $\delta^{13}C_{mt}$ and $\delta^{13}C_{it}$ in Levels 7-11 (p=<0.01) with incisors consistently ^{13}C-enriched to molars. There is also a significant difference between $\delta^{18}O_{mt}$ and $\delta^{18}O_{it}$ in Levels 4a and 7 (p=<0.01) (Figure 6.10), but the offset is not consistent between levels. The intra-level variation is relatively low and ranges from 1.1-2.8‰ in $\delta^{18}O_{teeth}$ and 1.3-2.8‰ in $\delta^{13}C_{teeth}$.

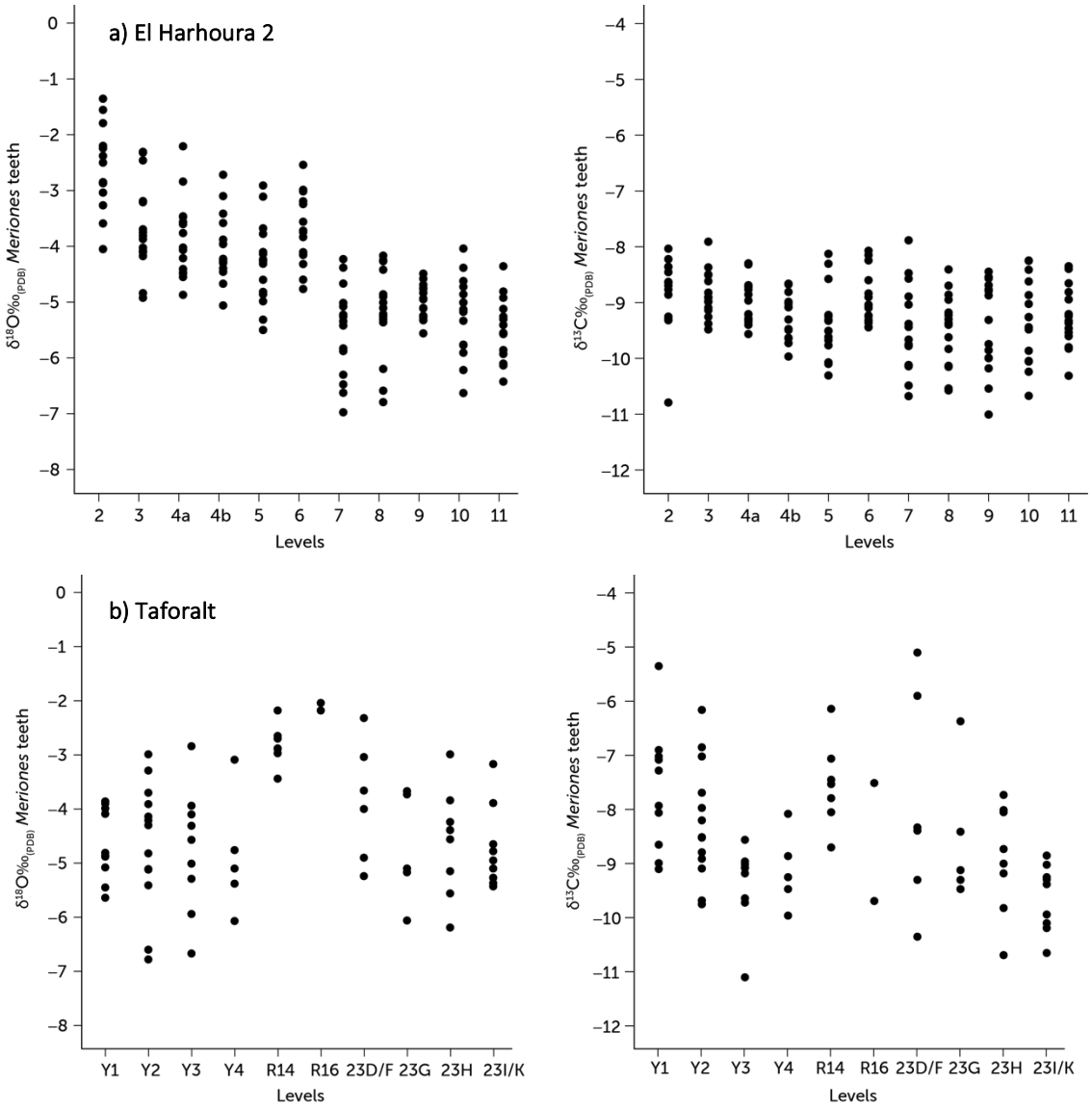

Figure 6.9: Graphs showing the $\delta^{18}O$ and $\delta^{13}C$ values of each individual *Meriones* tooth (molar and incisor) from all Levels at a) El Harhoura 2 and b) Taforalt.

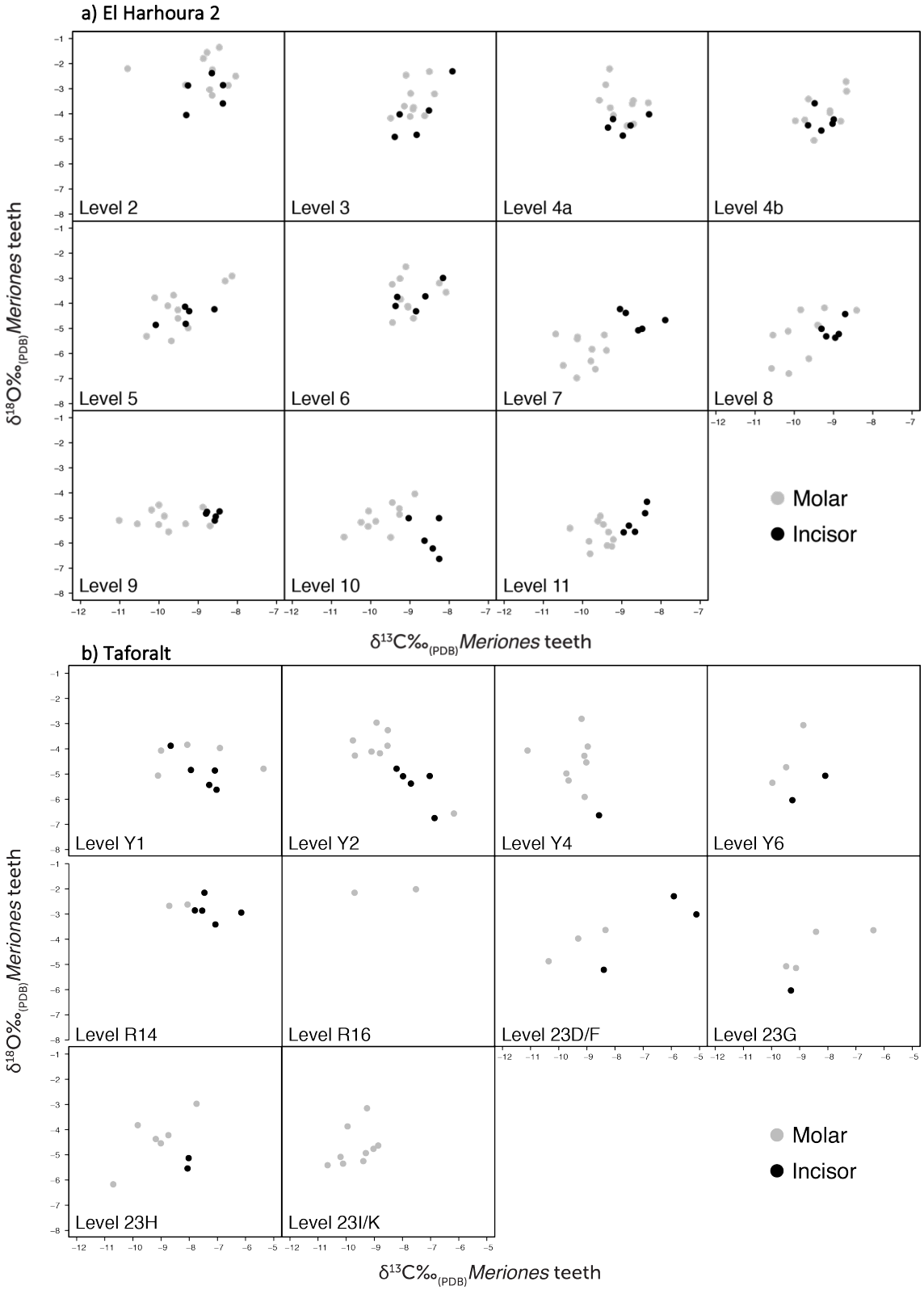

Figure 6.10: Graph showing the $\delta^{18}O$ and $\delta^{13}C$ values of *Meriones* molar and incisor teeth plotted by level at a) El Harhoura 2 and b) Taforalt.

Table 6.5: Summary statistics for the $\delta^{18}O$ and $\delta^{13}C$ values of *Meriones* teeth for each level at El Harhoura 2.

		$\delta^{18}O_{(PBD)}$						$\delta^{13}C_{(PBD)}$					
	Number of *Meriones* teeth	Mean (‰)	Standard deviation (1σ)	Minimum (‰)	Maximum (‰)	Range (‰)	Molars v incisors t-test	Mean (‰)	Standard deviation (1σ)	Minimum (‰)	Maximum (‰)	Range (‰)	Molars vs. incisors t-test
Level 2	15 (10 M, 5 I)	-2.6	0.7	-4.1	-1.4	2.7	*p*=>0.05	-8.8	0.7	-10.8	-8.0	2.8	*p*=>0.05
Level 3	15 (10 M, 5 I)	-3.7	0.8	-4.9	-2.3	2.6	*p*=>0.05	-8.7	0.4	-9.5	-7.9	1.6	*p*=>0.05
Level 4a	15 (10 M, 5 I)	-3.9	0.7	-4.9	-2.2	2.7	*p*=<0.01	-9.0	0.4	-9.6	-8.3	1.3	*p*=>0.05
Level 4b	14 (9 M, 5 I)	-4.0	0.6	-5.1	-2.7	2.3	*p*=>0.05	-9.3	0.4	10.0	-8.7	1.3	*p*=>0.05
Level 5	15 (10 M, 5 I)	-4.3	0.7	-5.5	-2.9	2.6	*p*=>0.05	-9.4	0.6	-10.3	-8.1	2.2	*p*=>0.05
Level 6	15 (10 M, 5 I)	-3.7	0.6	-4.8	-2.5	2.2	*p*=>0.05	-8.9	0.5	-9.5	-8.1	1.4	*p*=>0.05
Level 7	15 (10 M, 5 I)	-5.5	0.8	-7.0	-4.2	2.8	*p*=<0.01	-9.5	0.8	-10.7	-7.9	2.8	*p*=<0.01
Level 8	15 (10 M, 5 I)	-5.2	0.8	-6.8	-4.2	2.6	*p*=>0.05	-9.5	0.7	-10.6	-8.4	2.2	*p*=<0.01
Level 9	15 (10 M, 5 I)	5.0	0.3	-5.6	-4.5	1.1	*p*=>0.05	-9.4	0.8	-11.0	-8.5	2.6	*p*=<0.01
Level 10	15 (10 M, 5 I)	-5.2	0.7	-6.6	-4.0	2.6	*p*=>0.05	-9.3	0.8	-10.7	-8.2	2.4	*p*=<0.01
Level 11	15 (10 M, 5 I)	-5.5	0.6	-6.4	-4.4	2.1	*p*=>0.05	-9.3	0.6	-10.3	-8.4	2.0	*p*=<0.01

6.3.2. Taforalt

6.3.2.1. Summary of whole dataset

Figure 6.8 shows the $\delta^{18}O_{teeth}$ and $\delta^{13}C_{teeth}$ from Taforalt (molars n= 50, incisors n= 24) (Table 6.4, data listed in Appendix 7). The mean $\delta^{18}O_{teeth}$ is -4.4‰ ± 1.1, the same as that at El Harhoura 2. The $\delta^{18}O_{teeth}$ variation is 4.7‰ ranging from -6.8‰ to -2.8‰, lower than that at El Harhoura 2 but still higher than the intra-population variation in modern populations (Chapter 5). The mean $\delta^{13}C_{teeth}$ is -8.5‰ ± 1.3 ranging from -11.1‰ to -5.1‰ (total variation = 6.0‰), higher than those displayed at El Harhoura 2 (Table 6.4). The mean $\delta^{18}O_{mt}$ and $\delta^{18}O_{it}$ is -4.3‰ ± 1.0 and -4.7‰ ± 1.4, with similar variation displayed by both tooth types. Comparison of means for $\delta^{18}O_{mt}$ and $\delta^{18}O_{it}$ show that they are statistically indistinguishable (t-test p=>0.05). The mean $\delta^{13}C_{mt}$ and $\delta^{13}C_{it}$ differ displaying values of -9.0‰ ± 1.1 (1σ) and -7.6‰ ± 1.0, respectively (Table 6.4). Like at El Harhoura 2, incisors are ^{13}C-enriched relative to the molars, a trend that is reflected in the $\delta^{13}C_{teeth}$ variation. The maximum value of $\delta^{13}C_{mt}$ and $\delta^{13}C_{it}$ is similar (~-5‰), but the molars have a lower minimum value (–11.1‰) compared to the incisors (-9.3‰). Comparison of means for $\delta^{13}C_{mt}$ and $\delta^{13}C_{it}$ show that they are statistically different (t-test p = <0.01).

6.3.2.2. Exploring data by Level

The $\delta^{18}O_{teeth}$ and $\delta^{13}C_{teeth}$ from 10 levels at Taforalt are presented in Table 6.6 and Figure 6.9. Where teeth from different levels (23D/F and 23I/K) were combined to increase statistical power there was no obvious offset in $\delta^{18}O$ and $\delta^{13}C$ between individual levels. The mean $\delta^{18}O_{teeth}$ in Levels Y1, Y2, Y4, Y6, 23G, 23H and 23I/K is similar (between -4.9‰ and -4.6‰), while higher means

are displayed in Levels R14, R16 and 23D/F (-2.8‰, -2.1‰ and -3.9‰, respectively) (Table 6.6). The mean $\delta^{13}C_{teeth}$ is variable between levels with values ranging from -7.5‰ (Level 14) to -9.4‰ (Level 23I/K). An analysis of variance (ANOVA) shows significant differences in the $\delta^{18}O_{teeth}$ between the 10 Levels at Taforalt (F = 3.36, P = <0.01) (R16 was not included in the ANOVA due to low sample numbers). A post hoc Tukey test for pairwise comparisons shows that Level R14 is significantly different to Levels Y1, Y2, Y4, Y6, 23G, 23H and 23I/K (P = <0.05) (Appendix 6.2). An ANOVA also shows that there is a significant difference in $\delta^{13}C_{teeth}$ between the Levels at Taforalt (F = 4.16, P = <0.01). A post hoc Tukey test indicates that Levels Y4 and 23I/K differ significantly from Levels Y1 and 14 (P = <0.05) (Appendix 6.3). Figure 6.10 shows the $\delta^{18}O$ and $\delta^{13}C$ composition of the molars and incisors plotted by Level. Low numbers of molars and incisors within the levels at Taforalt prevent statistical exploration of the data in the majority of levels. Y1 and Y2 are the only Levels deemed suitable because ≥5 of each tooth type were analysed. Within level t-tests show that there are significant differences between the $\delta^{18}O$ and $\delta^{13}C$ composition of molars and incisors in Level Y2 (p=<0.05), while the $\delta^{18}O$ and $\delta^{13}C$ composition of the molars and incisors within Level Y1 were statistically indistinguishable. The intra-level variation ranges from 0.2-3.8‰ in $\delta^{18}O$ and 1.8-5.3‰ in $\delta^{13}C$, higher than that displayed at El Harhoura 2. This high variation is unrelated to sample numbers as more teeth were available from each level at El Harhoura 2. Other studies of fossil rodent teeth have reported higher intra-level variation of up to 12.7‰ in $\delta^{18}O_{PO4}$ (Royer et al., 2014, 2013b).The intra-level variation in $\delta^{13}C_{teeth}$ at Taforalt is similar to that

displayed in past environments in which C_3 and C_4 vegetation is present (Hynek et al., 2012; Kimura et al., 2013).

Table 6.6: Summary statistics for the $\delta^{18}O$ and $\delta^{13}C$ values of *Meriones* teeth for each level at Taforalt.

		$\delta^{18}O_{(PBD)}$						$\delta^{13}C_{(PBD)}$					
	Number of *Meriones* teeth	Mean (‰)	Standard deviation (1σ)	Minimum (‰)	Maximum (‰)	Range (‰)	Molars v incisors t-test	Mean (‰)	Standard deviation (1σ)	Minimum (‰)	Maximum (‰)	Range (‰)	Molars vs. incisors t-test
Level Y1	10 (5 M, 5 I)	-4.7	0.7	-5.6	-3.9	1.8	*p*=>0.05	-7.7	1.2	-9.1	-5.4	3.8	*p*=>0.05
Level Y2	13 (8 M, 5 I)	-4.6	1.2	-6.8	-3.0	3.8	*p*=<0.05	-8.3	1.1	-9.8	-6.2	3.6	*p*=<0.05
Level Y4	9 (8 M, 1 I)	-4.7	1.1	-6.7	-2.8	3.8	-	-9.4	0.7	-11.1	-8.6	2.5	-
Level Y6	5 (3 M, 2 I)	-4.9	1.1	-6.1	-3.1	3.0	-	-9.1	0.7	-10.0	-8.1	1.9	-
Level R14	7 (2 M, 5 I)	-2.8	0.4	-3.4	-2.2	1.3	-	-7.5	0.8	-8.7	-6.2	2.6	-
Level R16	2 (2 M)	-2.1	-0.1	-2.2	-2.0	0.2	-	-8.6	1.5	-9.7	-7.5	2.1	-
Level 23D/F	6 (3 M, 3 I)	-3.9	1.1	-5.2	-2.3	2.9	-	-7.9	2.0	-10.4	-5.1	5.3	-
Level 23G	5 (4 M, 1 I)	-4.8	1.0	-6.1	-3.7	2.4	-	-8.5	1.3	-9.5	-6.4	3.1	-
Level 23H	8 (6 M, 2 I)	-4.6	1.0	-6.2	-3.0	3.2	-	-8.9	1.0	-10.7	-7.7	3.0	-
Level 23I/K	9 (9 M)	-4.7	0.8	-5.4	-3.2	2.3	-	-9.6	0.6	-10.7	-8.9	1.8	-

6.3.3. Preservation

There is no standardised methodology to check for diagenetic alteration in the $\delta^{18}O$ and $\delta^{13}C$ values of bioapatites; nevertheless consideration of the data can be used to enhance confidence in the data. The $\delta^{18}O_{teeth}$ and $\delta^{13}C_{teeth}$ values at El Harhoura 2 and Taforalt are similar (Figure 6.6), so for these patterns to be of diagenetic origin diagenesis would have have of had the same effect on the *Meriones* teeth in both cave environments. There is no reason to believe this is the case. The $\delta^{18}O_{teeth}$ values display a similar range and are close to the values shown in the modern teeth from sites north of the Atlas in the Mediterranean region of North Africa. Although the $\delta^{13}C_{teeth}$ values are higher relative to modern values the majority of this offset results from the fossil fuel effect (see Section 6.5). As discussed in Section 4.3.1.1 and Section 6.2.4 the tooth apatite powder, although consisting of mostly enamel apatite, does contain a small amount of dentine apatite. Dentine apatite is more likely to undergo alteration of its original isotopic composition compared to enamel apatite because it is not very crystalline and has an organic matrix, which may be replaced by exogenous carbonates (see discussion in Section 4.3.1.1). Due to sample preparation used on the *Meriones* teeth (Section 6.2.4) it is probable that molar teeth samples contained a higher proportion of dentine compared to the incisor teeth samples (because the enamel and dentine could be separated easily). An isotopic offset between the molars and incisors may therefore be expected if the dentine component had introduced altered bioapatites into the bulk tooth apatite. Yet, the data show that there is no significant isotopic offset in $\delta^{18}O$ between molars and incisors. The incisors are ^{13}C-enriched relative to

molars: however, this pattern is not consistent across all levels, which instead suggests it reflects an environmental signal. Extensive studies undertaken on the preservation of small mammal bones (similar chemical structure to dentine) from El Harhoura 2 show that across all levels in the cave the microstructure of the rodent bone is generally well preserved with few secondary minerals encrusted into the bone surface. In addition, the study showed that the mineralogy of the bone has not undergone visible alteration (Farre et al., 2014).

6.4. A record of palaeoaridity in northwestern Africa using $\delta^{18}O$ in archaeological *Meriones* teeth

The modern study demonstrated a robust linear relationship between $\delta^{18}O_{mt}$ and MAP suggesting that the greatest influence on modern gerbil $\delta^{18}O_{mt}$ is moisture-related, as represented by MAP, and not $\delta^{18}O_{mw}$. The quantitative relationship between $\delta^{18}O_{mt}$ and MAP (Equation 8) is used to reconstruct Late Pleistocene MAP in Atlantic and Mediterranean region of northwestern using the $\delta^{18}O$ values of *Meriones* teeth from both El Harhoura 2 and Taforalt. This section will discuss the application of palaeoaridity reconstructions at El Harhoura 2 and Taforalt, as well as examining some of the assumptions associated with this method.

6.4.1. Exploring the use of molar and/or incisor teeth in MAP reconstruction

Before applying the MAP reconstruction at El Harhoura 2 and Taforalt the *Meriones* tooth type (molars and/or incisors) used to perform the reconstructions are considered, because of the isotopic temporal offsets shown between molars and incisors in the modern study. These isotopic offsets

between tooth types may bias the MAP reconstruction and/or could increase the isotope variation within the proxy record. The $\delta^{18}O_{teeth}$ values show that there is no significant difference in $\delta^{18}O$ between molars and incisors at both sites across the whole dataset, but within two Levels at El Harhoura 2 (Levels 4a and 7) and one Level at Taforalt (Y2) (of the levels that had enough samples to be assessed) $\delta^{18}O_{mt}$ and $\delta^{18}O_{it}$ is significantly different. The use of molar teeth (conditions of the modern study) and combined molars and incisors to perform quantitative MAP reconstructions is explored at El Harhoura 2, where ≥5 molars and incisors were measured from each Level. Table 6.7 presents the reconstructed MAP range ($\pm 1\sigma$) (calculated using Equation 8) from the mean $\delta^{18}O_{mt}$ (molar teeth only) and $\delta^{18}O_{teeth}$ (combined molar and incisor teeth) for each Level at El Harhoura 2. The reconstructed MAPs from both $\delta^{18}O_{mt}$ and $\delta^{18}O_{teeth}$ are similar, even in Levels 4a and 7, which differ statistically between $\delta^{18}O_{mt}$ and $\delta^{18}O_{it}$. Furthermore, combining both molars and incisors from each level to perform the MAP reconstruction does not significantly increase the standard deviation of the $\delta^{18}O$ values in each level (Table 6.7). The data show similar MAP reconstructions are provided when the $\delta^{18}O$ values of molars and incisors are used, and using both tooth types appears a more conservative approach. MAP reconstructions at El Harhoura 2 and Taforalt will therefore be undertaken on $\delta^{18}O$ values from molars and incisors.

Table 6.7: Table showing the reconstructed MAP ranges calculated (equation 8) using the mean and SD of $\delta^{18}O_{mt}$ and $\delta^{18}O_{teeth}$ from all Levels at El Harhoura 2.

El Harhoura 2 levels	Mean and SD (1σ) $\delta^{18}O_{mt}$	Reconstructed MAP (mm) range from mean and SD $\delta^{18}O_{mt}$	Mean and SD (1σ) $\delta^{18}O_{teeth}$	Reconstructed MAP (mm) range from mean and SD $\delta^{18}O_{teeth}$	Δ mean $\delta^{18}O_{teeth}$ - $\delta^{18}O_{mt}$
Level 2	-2.4 ± 0.7	252-381	-2.6 ± 0.7	268-405	-0.2
Level 3	-3.5 ± 0.7	349-528	-3.7 ± 0.8	360-576	-0.2
Level 4a	-3.6 ± 0.7	360-543	-3.9 ± 0.7	393-594	-0.3
Level 4b	-3.9 ± 0.7	393-594	-4.0 ± 0.6	417-594	-0.1
Level 5	-4.2 ± 0.9	405-688	-4.3 ± 0.7	442-668	-0.1
Level 6	-3.7 ± 0.7	370-560	-3.7 ± 0.6	381-543	0.0
Level 7	-5.9 ± 0.6	730-1040	-5.5 ± 0.8	612-980	+0.4
Level 8	-5.2 ± 1.0	528-952	-5.2 ± 0.8	550-897	0.0
Level 9	-5.1 ± 0.6	576-821	-5.0 ± 0.3	612-730	+0.1
Level 10	-5.0 ± 0.6	560-797	-5.2 ± 0.7	576-871	-0.2
Level 11	-5.7 ± 0.5	709-952	-5.5 ± 0.6	649-924	+0.2

6.4.2. Late Pleistocene MAP reconstructions for the Atlantic and Mediterranean regions of North Africa

Figures 6.11 and Tables 6.7 and 6.8 show the mean $\delta^{18}O_{teeth}$ and reconstructed MAP for each level at El Harhoura 2 and Taforalt. The MAP reconstructions appear to show that there were humid and arid shifts throughout the Late Pleistocene in the Atlantic and Mediterranean regions of northwestern Africa. At El Harhoura 2 Levels 11-7 (c.118-108ka) have reconstructed MAPs of ~600-900mm, while Levels 6-4b (c.107-100ka) and Level 4a (c.74ka) have MAP values similar to present. The MIS 5 levels at Taforalt (23D/F, 23G, 23H, 23I/K) also indicate higher MAP than at present with reconstructed MAP of ~450-800mm in Levels 23I/k, 23H and 23G (c.97-90ka), and ~350-700mm in Level 23D/F (c.90-80ka). At El Harhoura 2 and Taforalt during MIS 3/4 the reconstructed MAPs are similar to those of the present, with values ranging between 360-575mm in Level 3 (c.64-50ka) at El Harhoura 2 and 275-575mm in Levels R14 (c.45-40ka) and R16 (c.60ka) at Taforalt. Reconstructed MAP values from Level R16 should be treated with caution as only 2 *Meriones* teeth were analysed from this level. There appears to be an isotopic offset in MIS 2 between Taforalt and El Harhoura 2. The reconstructed MAP (250-405mm) from Level 2 (c.20-13.5ka) is the most arid in the Late Pleistocene sequence at El Harhoura 2, but at Taforalt MAP reconstructions from the Levels spanning the LGM and Last deglaciation (Y1-Y6) indicate higher MAP than present (~400-900mm).

Table 6.8: Table showing the reconstructed MAP ranges calculated (equation 8) using the mean and SD of $\delta^{18}O_{teeth}$ from all Levels at Taforalt.

Taforalt levels	Mean and SD (1σ) $\delta^{18}O_{teeth}$	Reconstructed MAP (mm) range from mean and SD $\delta^{18}O_{teeth}$
Level Y1	-4.7 ± 0.7	497-752
Level Y2	-4.6 ± 1.2	417-846
Level Y3	-4.7 ± 1.1	442-846
Level Y4	-4.9 ± 1.1	467-897
Level R14	-2.8 ± 0.4	310-393
Level R16	-2.1 ± 0.1	276-293
Level 23D/F	-3.9 ± 1.1	349-668
Level 23G	-4.8 ± 1.0	469-846
Level 23H	-4.6 ± 1.0	442-797
Level 23I/K	-4.7 ± 0.8	483-774

With the exception of R14 and R16, the Levels at Taforalt have higher intra-level variation relative to those recorded at El Harhoura 2, most likely reflecting the more inland and higher altitude location of Taforalt. The majority of precipitation at El Harhoura 2 is directly sourced from the Atlantic Ocean, whereas Atlantic source precipitation at Taforalt will have undergone continentality effects crossing the land (from west to east) causing more variation in $\delta^{18}O_{mw}$ value. In addition, the closer proximity of Taforalt to the Mediterranean Sea may result in occasional precipitation sourced from the eastern Mediterranean also causing increased variation in $\delta^{18}O_{mw}$.

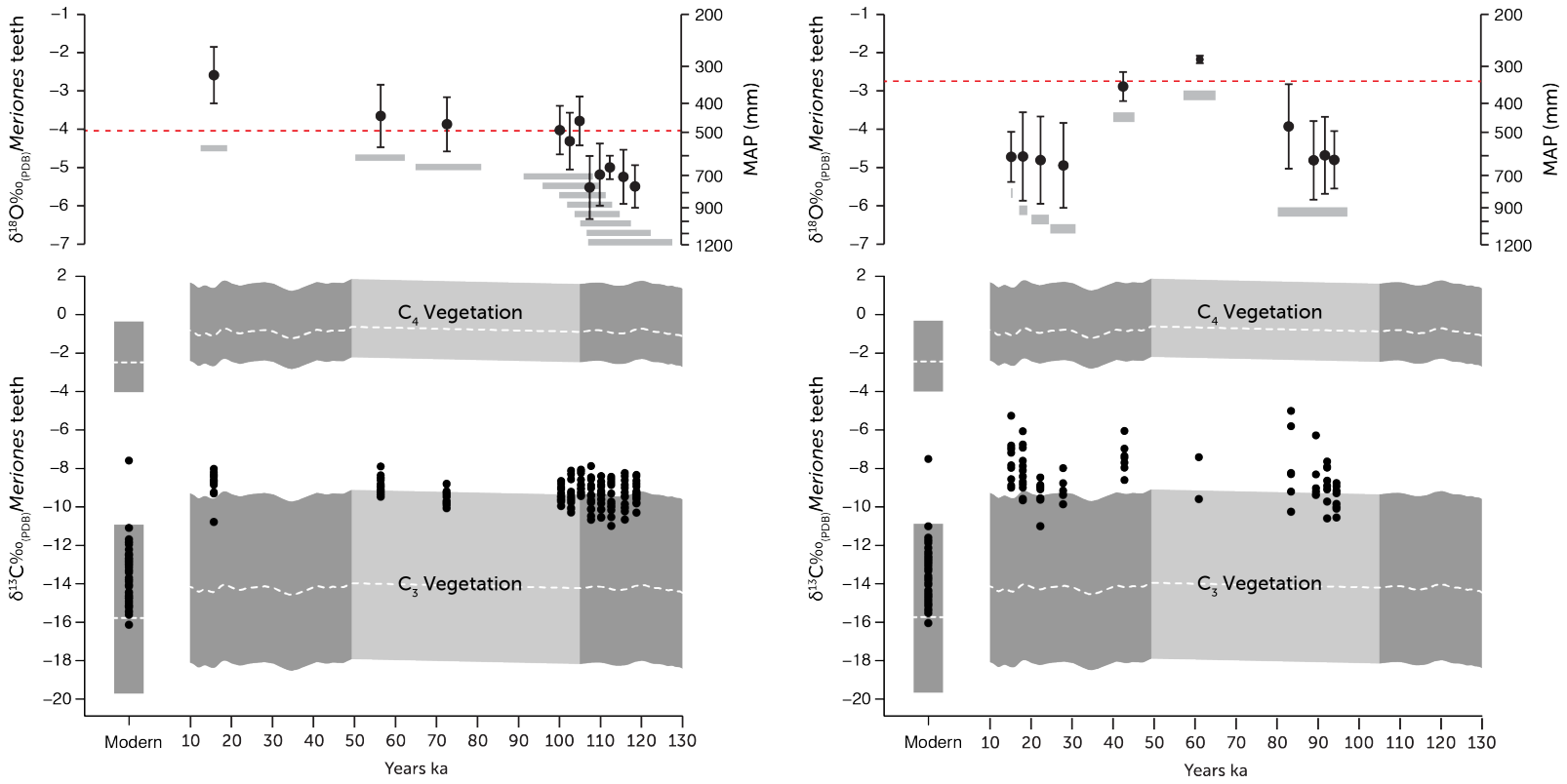

Figure 6.11: The $\delta^{18}O$ (top) and $\delta^{13}C$ (bottom) values of *Meriones* molars and incisors from El Harhoura 2 (left) and Taforalt (right) plotted against age. The top graph shows the reconstructed MAP values calculated using the mean and standard deviation (1σ) from $\delta^{18}O_{teeth}$. The red dotted line shows present MAP values at El Harhoura 2 and Taforalt (values from WorldClim). The bottom graph shows the individual $\delta^{13}C$ values from both molars and incisors. The grey boxes represent the calculated end member values for C_3 and C_4 diet (the white dotted line shows the average diet values) for rodents that corrects for past variations in $\delta^{13}C_{CO2}$ using the method of Passey et al. 2002 (see Section 6.5.1, Appendix 8). The darker grey areas show periods when $\delta^{13}C_{CO2}$ data is available from the ice core records, while the lighter grey areas show where $\delta^{13}C_{CO2}$ is instead interpolated because values are not available from the ice cores. The modern $\delta^{13}C_{mt}$ values are from sites north of the Atlas. The dating errors on the OSL and radiocarbon dates from the Levels are represented by the grey bars in the top graph.

6.4.3. Consideration of MAP reconstruction

The MAP reconstructions from the linear regression (Equation 8) rely on the assumption that modern conditions applied in the past. However, other factors relating to differing conditions during the Late Pleistocene may have influenced the $\delta^{18}O_{teeth}$. Since variation in source water is estimated to be small during the Late Pleistocene it is envisaged that it would have a negligible effect on $\delta^{18}O_{teeth}$ relative to other climatic influences. The $\delta^{18}O$ value of global ocean water has varied throughout the Late Pleistocene by ~≤1‰ (Waelbroeck et al., 2002), yet accounting for this in the Atlantic and Mediterranean region is difficult because of spatial and temporal variability associated with $\delta^{18}O$ of global ocean water (Paul, 2001; Schrag et al., 2002). Furthermore, changes in the $\delta^{18}O$ value of source may be complicated during the Late Pleistocene if the predominant precipitation changed from Atlantic to Mediterranean source, both of which have different isotopic signatures (Abouelmagd et al., 2012; Ouda et al., 2005). For source water change to have significant effect on the $\delta^{18}O_{teeth}$ the shift from Atlantic to Mediterranean storm tracks would have to be consistent and would involve a major change in atmospheric circulation. Palaeoclimate records from the Mediterranean region do not suggest that this occurred. Isotopic values of fossil ground waters across North Africa indicate that precipitation was derived from palaeo-westerlies throughout the Late Pleistocene (Abouelmagd et al., 2012).

Lower atmospheric temperatures during the glacial could cause variation in $\delta^{18}O_{mw}$, as condensation is a temperature dependent fractionation process (Section 4.2.1.1) (Dansgaard, 1964), resulting in precipitation depleted in ^{18}O

relative to that in interglacial conditions. Most importantly, lower atmospheric temperatures reduce rates of evapotranspiration (See section 4.2.1.2). Under such conditions in the past $\delta^{18}O$ values of plants (and therefore *Meriones* teeth) are more likely to reflect the $\delta^{18}O$ value of local meteoric water rather than aridity, particularly if growing season temperatures are reduced. However, it is difficult to account for the effect of temperature on relative humidity and rates of evapotranspiration because these variables are strongly linked to several other climatic factors. If lower atmospheric temperatures did reduce rates of evapotranspiration in northwestern Africa during the glacial, lower $\delta^{18}O_{teeth}$ values during MIS 5 (at El Harhoura 2 and Taforalt) and MIS 2 (at Taforalt) could result from reduced temperatures instead of/or as well as increased MAP. It is suggested that lower temperatures during the glacial would have had a greater influence on $\delta^{18}O_{teeth}$ at the more-continental, higher altitude site of Taforalt compared to that of the low altitude, strongly oceanically- influenced site of El Harhoura 2. Presently, Taforalt has a greater seasonal temperature gradient (8-24°C) compared to El Harhoura 2 (12-24°C) (Figure 2.6). These gradients would likely be amplified during the glacial. Although the effect of temperature variation cannot be quantified, MAP reconstructions and existing palaeoclimate records from North Africa and the western Mediterranean are compared in the following chapter to explore whether the humidity inferences from $\delta^{18}O_{teeth}$ are accurate (see Section 7.2.3).

6.5. Implications for past vegetation cover in northwestern Africa

Presently the Mediterranean region of northwestern Africa consists of predominantly C_3 vegetation: however, proportions on C_3/C_4 vegetation cover in this region may have changed in the Late Pleistocene due to variations in climate, pCO_2 and $\delta^{13}CO_2$. This section will firstly explore if C_4 vegetation was present in the Atlantic and Mediterranean regions of northwestern Africa during the Late Pleistocene, and then go on to discuss whether a climatic signal is reflected in the $\delta^{13}C_{teeth}$ at El Harhoura 2 and Taforalt.

6.5.1. 6.5.1 Was C_4 vegetation present in the Atlantic and Mediterranean region of North African during the Late Pleistocene?

The $\delta^{13}C$ values of end member C_3 and C_4 *Meriones* diet are calculated using an approach adapted from Passey et al. (2002), which accounts for Late Pleistocene variation in $\delta^{13}CO_2$ on the $\delta^{13}C$ values of vegetation by correcting to past records of $\delta^{13}CO_2$ from the Antarctic ice core records (Appendix 8, Figure 6.12). Changes in *p*CO2 are also likely to have influenced the $\delta^{13}C$ value of vegetation during the Late Pleistocene, but presently no model exists that accounts for changes in both pCO_2 and $\delta^{13}CO_2$. Controlled experiments on plants demonstrate that $\delta^{13}CO_2$ exerts the dominant influence on $\delta^{13}C_{plant}$ and during fluctuations in pCO_2 plants can sustain a relatively constant intercellular to atmospheric CO_2 ratio (Arens et al., 2000).

With modern $\delta^{13}CO_2$ = -8.2‰ (the $\delta^{13}CO_2$ value of the atmosphere when the plants were collected in 2006/2007) (Keeling et al., 1995), values for $\varepsilon^*_{plant - CO2}$ that represent average C_3 vegetation ($\varepsilon^*_{averagec3 - CO2}$), maximum C_3 vegetation

($\varepsilon^*_{maxc3 - CO2}$), minimum C_3 vegetation ($\varepsilon^*_{minc3 - CO2}$), average C_4 vegetation ($\varepsilon^*_{averagec4 - CO2}$), maximum C_4 vegetation ($\varepsilon^*_{maxc4 - CO2}$), minimum C_4 vegetation ($\varepsilon^*_{minc4 - CO2}$) are calculated using $\delta^{13}C_{plant}$ leaf values from a Mediterranean ecosystem collected in a wet and dry season throughout 2006/2007 (average C_3= -26.9‰, min C_3= -22.0‰, C_3 max= -31.0‰, average C_4= -13.5‰, min C_4= -15.0‰, C_4 max= -11.0‰ (Hartman and Danin, 2010). The average $\delta^{13}C$ composition of C_3 and C_4 plants are calculated from all plants analysed (trees, shrubs, dwarf shrubs, annuals, forbs and geophytes), while C_3 and C_4 maximum and minimum represent the highest and lowest $\delta^{13}C$ values of each plant type from the Hartman and Danin (2010) dataset, and are selected to show the overall range of C_3 and C_4 plant $\delta^{13}C$ values within a Mediterranean environment. *Meriones* diet is calculated using a $\varepsilon^*_{tooth - diet}$ of 11.0‰ (Passey et al., 2005; Podlesak et al., 2008) (see discussion in Chapter 4) (Figure 6.12).

The results of the calculations show that all the $\delta^{13}C_{teeth}$ at El Harhoura 2 (Figure 6.11) and those from Levels Y4, Y6, 23H and 23I/K at Taforalt (Figure 6.11) suggest a predominantly C_3 diet with a small contribution from C_4 plants. However, the abrupt limit of -8‰ in the Levels at El Harhoura 2 suggests that this value marks the C_3 end member within *Meriones* in the northwestern African setting. Taforalt Levels Y1, Y2, R14, R16, 23D/F and 23G record positive excursions in $\delta^{13}C_{teeth}$ of >-8‰ suggesting a small contribution of C_4 plants to the *Meriones* diet, and that C_4 plants were present in the Mediterranean region of northwestern Africa at periods during the Late Pleistocene. As previously noted in other studies, this shows that small

mammals are extremely sensitive to changes in the proportions of C_3/C_4 vegetation cover (Arppe et al., 2015; Hynek et al., 2012; Kimura et al., 2013).

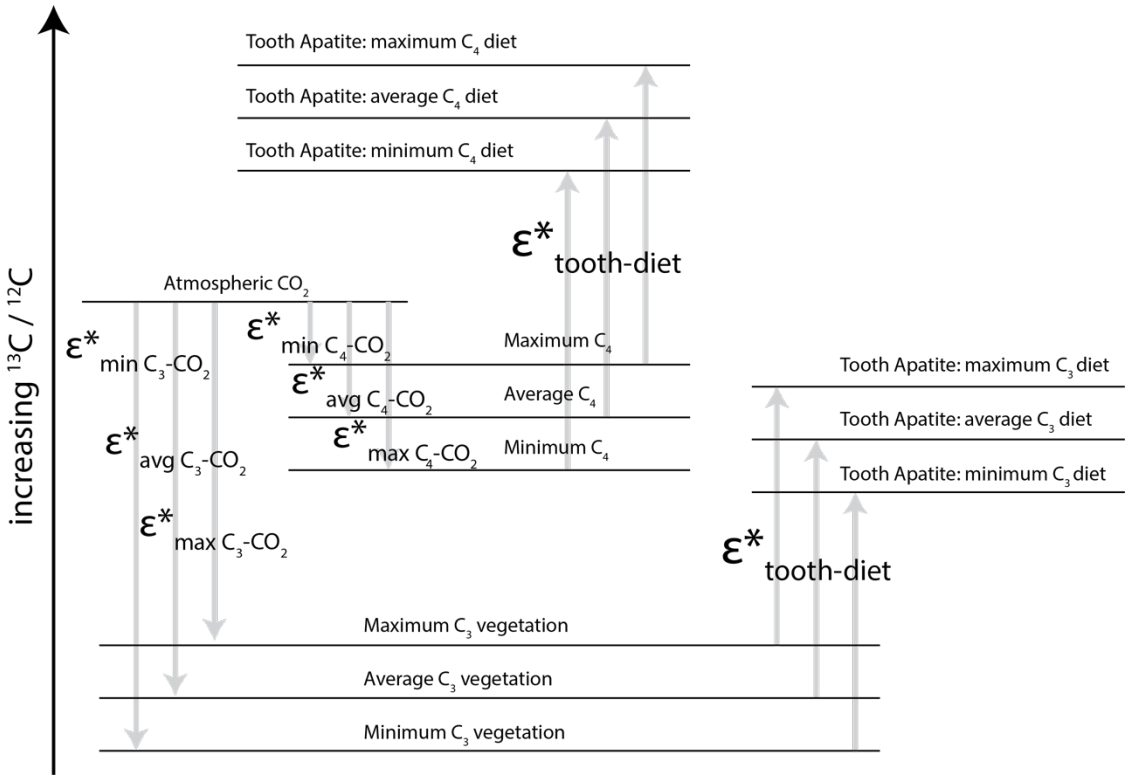

Figure 6.12: Diagram showing method to calculate expected C_3 and C_4 *Meriones* tooth values for C_3 and C_4 diet. ε* is the isotope enrichment between the tooth and diet. See text (Section 6.5.1) for values used in the calculation and Appendix 8 for calculations. (adapted from Fig. 3 in Passey et al. 2002).

Most of the isotopic offset between the $\delta^{13}C$ values of modern and archaeological gerbil teeth (Figure 6.11) is explained by the anthropogenic isotope effect (burning of fossil fuels) that has shifted modern $\delta^{13}CO_2$ ~1.5‰ more negative than pre-industrial levels (Keeling et al., 2005; Leuenberger et al., 1992; Lourantou et al., 2010b). In addition to this, the change from Late Pleistocene to anthropogenic influenced modern vegetation in Morocco may also account for the variation noted between modern and archaeological $\delta^{13}C_{teeth}$. Figure 6.11 shows that modern $\delta^{13}C_{mt}$ values from sites north of the

Atlas lie between the average and maximum calculated C_3 diet values, while the archaeological $\delta^{13}C_{teeth}$ values are close to the maximum calculated C_3 diet values during the Late Pleistocene. It is hypothesised that the modern and archaeological *Meriones* teeth that reflect C_3 vegetation have relatively high $\delta^{13}C$ values (in the maxiumum range of C_3 values) because of the temporal period (spring/summer) reflected in the teeth and because the diet values were calculated using C_3 and C_4 plant values from leaves, not grains, which the *Meriones* are known to mainly consume. As dicussed in Chapter 4, studies have shown that seeds are up to 3‰ ^{13}C-enriched relative to leaves (Cernusak et al. 2002; Cernusak et al., 2009; Codron et al. 2005; Hobbie and Werner, 2004).

6.5.2. Is a climatic signal reflected in the $\delta^{13}C$ values of the Late Pleistocene *Meriones* teeth?

The modern study (Chapter 5) noted a significant relationship between $\delta^{13}C_{mt}$ and MAP in northwestern Africa; although the gradient was small (~2‰ over the rainfall gradient 100-600mm MAP) it is worth examining to see whether aridity has influenced the $\delta^{13}C_{teeth}$ throughout the Late Pleistocene. The $\delta^{13}C_{teeth}$ values at El Harhoura 2 indicate a relatively open C_3 environment during the Late Pleistocene. Values also appear to show a similar environment at Taforalt, but in some levels it appears that C_4 grasses also grew in the surrounding region. The $\delta^{13}C$ values of the *Meriones* teeth imply a relatively open environment throughout the Late Pleistocene in the Atlantic and Mediterranean region of northwestern Africa: this is however unsurprising as the teeth reflect the open, arid and steppic habitats preferred by *Meriones* (Table 5.2). At El Harhoura 2 $\delta^{13}C_{teeth}$ and $\delta^{18}O_{teeth}$ co-vary within levels, although this pattern is

discreet it does suggest that the $\delta^{13}C_{teeth}$ are partly reflecting the effect of water deficit on the C_3 plants. At Taforalt there appears to be no relationship between the $\delta^{13}C_{teeth}$ within the C_3 plant levels, or the occurrence of C_4 plants and $\delta^{18}O_{teeth}$.

The presence of C_4 plants in Levels Y1, Y2, R14, R16, 23D/F and 23G at Taforalt may result from variation in climate, pCO_2 or a combination of both factors. Calculation of crossover temperatures, the day time temperature at which the quantum yields of C_3 and C_4 plants are identical for a given atmospheric CO_2, show the shift between C_3 and C_4 dominance is a function of both temperature and pCO_2 (Figure 6.13). Between 15ka and 100ka, the dates represented at Taforalt, ice core records indicate that pCO_2 varied between 180-230 vppm (Barnola et al., 1987; Jouzel et al., 1993; Lourantou et al., 2010b) (Figure 4.6), and under these conditions models show that C_4 plants are favoured over C_3 plants at lower daytime growing-season temperatures (Collatz et al., 1998; Ehleringer et al., 1997) (Figure 6.13). Reconstructed growing season temperatures from pollen records in the western Mediterranean do not deviate greatly from present values (MIS 2 =~15-20°C) (Combourieu Nebout et al., 2009; Fletcher et al., 2010b), providing suitable growing conditions for the expansion of C_4 in the Mediterranean region of North Africa during the Late Pleistocene. A modelling study aimed at predicting the global distribution of C_4 plants during the LGM calculated that the continental area surrounding the Mediterranean Sea had more C_4 vegetation than present (Collatz et al., 1998). The model prediction is consistent with the $\delta^{13}C_{teeth}$ values from El Harhoura 2 showing C_3 vegetation only (Figure 6.14). Evidence suggests that the most

likely reason for the expansion of C_4 vegetation at Taforalt at periods throughout the Late Pleistocene results from conditions of lower temperature and pCO_2.

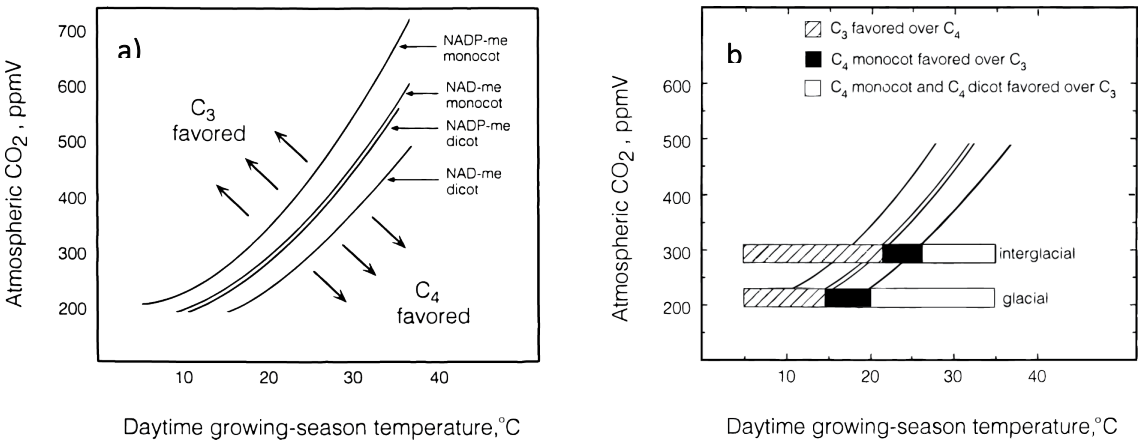

Figure 6.13: a) Modelled cross over temperatures of the quantum yield for CO_2 uptake for monocots and dicots (adapted from Fig. 2 in Ehleringer et al. 1997), b) Modelled cross over temperatures for monocotyledonous and dicotyledonous plants as a function of modern pCO_2 values during interglacial periods (upper bar) and pCO_2 values (~180-230vppm) from the period 100-15ka (lower bar). The cross over temperature is defined from simulation values in diagram (a) (adapted from Fig. 3 in Ehleringer et al. 1997).

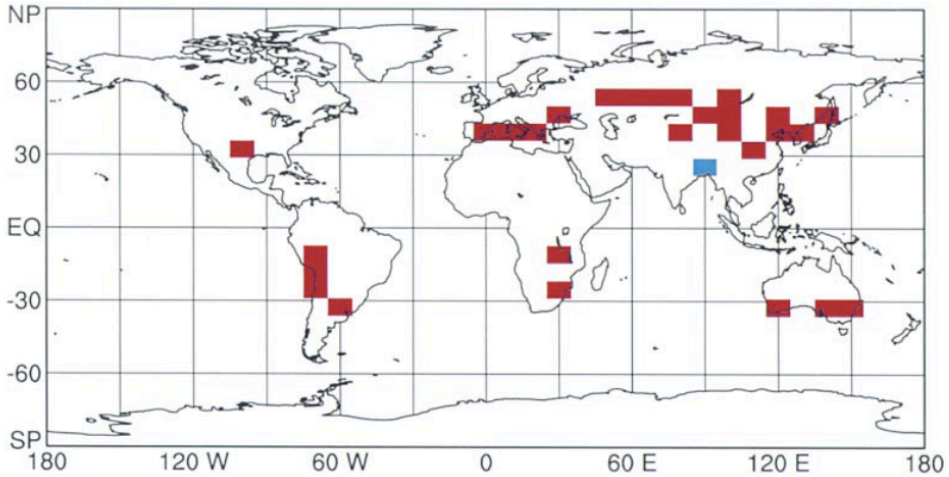

Figure 6.14: Map showing areas that changed from C_4 to C_3 (red) and from C_3 to C_4 (blue) since the last glacial maximum (20ka BP) as a result of combined increases in temperature and pCO_2. Climate conditions were derived from climate model simulations (From Collatz et al 1998).

6.6. Exploring temporal period reflected in molar and incisor teeth

The modern inter-tooth study showed that the $\delta^{13}C$ and $\delta^{18}O$ values of molars and incisors are offset because they form over different temporal periods, hinting at the potential for preservation of seasonal indicators within these teeth. Exploration of the isotope signals in *Meriones* molars and incisors from El Harhoura 2 and Taforalt show that $\delta^{13}C_{mt}$ is significantly lower than $\delta^{13}C_{it}$ at both sites, while there is no significant offset between each tooth type in $\delta^{18}O$. This trend does not occur across all levels at the sites suggesting it is unlikely to result from a physiological or alteration of the isotopes in the tooth apatite, but instead shows that differences in seasonal conditions are being reflected, as related to the periods of tooth formation (Figure 6.10). The general trend for higher $\delta^{13}C$ values in incisor teeth relative to molars at El Harhoura 2 and Taforalt implies that the incisors are more likely to reflect xeric conditions of the dry summer/autumn months when C_3 vegetation is water stressed and C_4 grasses grow (only at Taforalt) (Figure 6.8). This may suggest that a predator bias is reflected in the isotope composition of the incisors, hinting that *Meriones* were more likely to be hunted in the arid summer/autumn months, when there is a peak in small mammal populations after the breeding season. Seasonal predator bias is probably not visible in the $\delta^{18}O$ values of the teeth because $\delta^{18}O$ is inherently more variable in the environment.

In the relatively humid levels (Levels 7-11) at El Harhoura 2 the $\delta^{13}C$ composition of the incisor teeth is significantly higher compared to that of the molars, yet in the more arid levels (Levels 6-2) there is no difference between

$\delta^{13}C_{mt}$ and $\delta^{13}C_{it}$ (Figure 6.10). While smaller sample sizes limit interpretations at Taforalt, the data suggest that $\delta^{13}C_{it}$ values are generally higher than $\delta^{13}C_{mt}$ in Levels Y2, Y6, R14, 23D/F and 23H (Figure 6.10). The change in the $\delta^{13}C$ pattern reflected in molars and incisors within levels at El Harhoura 2 could result from either variation in seasonal climate or predator behaviour throughout the Late Pleistocene. To interpret changes in seasonal climate from the $\delta^{13}C_{mt}$ and $\delta^{13}C_{it}$ values it must be assumed that a summer/autumn seasonal hunting bias is reflected in the incisors across all levels at the site, meaning that the variability noted in the $\delta^{13}C_{teeth}$ results solely from changes to climate. If this assumption is made it suggests greater seasonality in Levels 7-11 (reconstructed MAP= >600mm), with more intense winter rainfall resulting in increased water availability for plants in the growing season, relative to Levels 6-2 in which there is no difference between $\delta^{13}C_{mt}$ and $\delta^{13}C_{it}$. However, the assumption that the same seasonal hunting bias occurs across all levels at the site is dubious given that the accumulation predators vary across the levels (Table 6.1). Although taphonomic study is yet to be undertaken on Levels 9-11, it is noteworthy that a similar predator, e.g. *Bubo ascalaphus*, deposited the small mammal material in Levels 7 and 8 while mixed mammals and raptors accumulated the material in Levels 6-2. This suggests that the change noted in $\delta^{13}C_{mt}$ and $\delta^{13}C_{it}$ between the upper (7-11) and lower levels (6-2) could also result from predator behaviour. Further taphonomic work on the small mammal material from Levels 9-11 will help to determine this.

6.7. Conclusion

This chapter described the application of $\delta^{18}O$ and $\delta^{13}C$ composition of *Meriones* teeth as a proxy for palaeoaridity and vegetation cover during the Late Pleistocene in northwestern Africa. Within site comparisons of tooth type at El Harhoura 2 and Taforalt show that incisors had significantly higher $\delta^{13}C$ values than molars, yet there was no offset in $\delta^{18}O$ between each tooth type. As a result of this, MAP reconstructions were calculated from $\delta^{18}O$ values of the molars and incisors from each level at El Harhoura 2 and Taforalt. The isotope-based MAP reconstructions from both cave sites indicate relatively humid/arid shifts throughout the Late Pleistocene. $\delta^{18}O_{teeth}$ suggets that the MIS 5 levels at both sites were more humid than present, while the MIS 3/4 levels have similar MAP values to present. There appears to be an offset during MIS 2 between the Atlantic and Mediterranean region, with humid conditions implied at Taforalt and a relatively arid episode (with MAP values lower than present) at El Harhoura 2. The accuracy of the isotope-based MAP reconstructions relies on applying the assumptions of the present to the past; however, it is known that several climate variables would have differed during the Late Pleistocene. Therefore, the next chapter compares the palaeoaridity archives from both cave sites to local and regional palaeoclimate and palaeoenvironment records with the aim of assessing whether $\delta^{18}O_{teeth}$ responds to moisture availability and aridity in the Late Pleistocene.

The $\delta^{13}C_{teeth}$ indicate the presence of predominantly C_3 vegetation on the Atlantic coast of northwestern Africa throughout the Late Pleistocene. However, the *Meriones* from Taforalt did have a small C_4 plant contribution to their diet at

periods throughout the Late Pleistocene, indicating the presence of C_4 plants in northeastern Morocco during MIS 2, MIS 3 and MIS 5. The existence of C_4 plants, in what is presently considered a predominant C_3 vegetation Mediterranean zone, most likely results from lower temperatures and pCO_2 in the Late Pleistocene. In addition, the detection of C_4 plants in the $\delta^{13}C_{teeth}$ shows that small mammals are extremely sensitive to changes in environment and vegetation cover. The relatively high $\delta^{13}C_{teeth}$ values for *Meriones* consuming predominantly C_3 diets at El Harhoura 2 and Taforalt, instead of reflecting a climatic signal, probably reflects the *Meriones* habitat preferences for open, steppe environments. At El Harhoura 2 and Taforalt incisors are more ^{13}C-enriched relative to molars, which appears to reflect a predator hunting bias, suggesting *Meriones* were more likely preyed upon during the drier months of the year. It is unclear whether the different patterns reflected in the $\delta^{13}C$ values of molars and incisors between the relatively humid (7-11) and arid (6-2) levels at El Harhoura 2 result from changes to seasonal climate or predator behaviour.

7. Comparison of proxy climate and environmental records in northwestern Africa: implications for human behaviour

7.1. Introduction

This chapter discusses the Late Pleistocene MAP and vegetation reconstructions derived from the $\delta^{18}O_{teeth}$ and $\delta^{13}C_{teeth}$ at El Harhoura 2 and Taforalt (Chapter 6). Firstly, climatic and environmental inferences from the *Meriones* isotope record are compared with other proxy records from both cave sequences. The Late Pleistocene small mammal assemblage from El Harhoura 2 has been extensively studied using palaeoecological, taphonomic and morphometric methods, providing environmental reconstructions that can be directly correlated with the isotope record from the *Meriones*. Taforalt has an extensive macrocharcoal and phytolith record extending throughout the Late Pleistocene providing a proxy vegetation record from the landscape surrounding the cave. The local records of palaeoclimate and palaeoenvironment are then compared with regional marine and terrestrial records from across the western Mediterranean region. It should be noted that proxy records reflect different temporal and spatial scales, are subject to different forms of error, often reflect different climate/environmental factors, and when found in association with archaeological remains can be bias by human activity. Comparisons between proxies should be undertaken with care to ensure the limitations of each method are understood.

The second section of the chapter compares the palaeoclimate, palaeoenvironmental and cultural records from El Harhoura 2 and Taforalt to

explore the influence of climate on human occupations and cultural behaviour. Finally, the possibility that El Harhoura 2 and Taforalt served as refugia for human populations in North Africa during periods of climatic downturn in the Late Pleistocene is considered.

7.2. Comparison of *Meriones* isotope records with local and regional palaeoclimate records from North Africa and the western Mediterranean

7.2.1. Comparison of *Meriones* isotope record with palaeoenvironmental records from El Harhoura 2 and Taforalt.

7.2.1.1. El Harhoura 2

Palaeoenvironmental information at El Harhoura 2 is inferred from faunal material in Levels 1-8 (material from Levels 4b, 9, 10 and 11 remains unstudied). Palaeocological, taphonomic and morphometric studies have all been undertaken on the small mammal assemblage from El Harhoura 2, providing a rare opportunity to compare palaeoenvironmental and palaeoclimate inferences from the *Meriones* isotope record with other proxy records derived from the same small mammal assemblage.

There is no significant species turnover in the small mammal assemblage throughout the Late Pleistocene (Levels 8-2) at El Harhoura 2. Five taxa (*Mus* cf. *spretus*, *Gerbillus campestris*, *Meriones shawii/grandis, Crocidura* spp. and an indeterminate species) are present in Levels 8-2, while *Atelerix algirus* is present in Levels 7-2 (Table 6.1) (Stoetzel et al., 2014, 2011). Notably, *Jaculus orientalis*, which is currently found in continental steppes and arid to semi-arid areas in eastern Morocco (Aulagnier et al., 2009), is also present in Levels 5

and 7. The Taxonomic Habitat Indices (THI), based on the presence/absence of small mammal species within each level, indicates that the environment surrounding the cave did not vary greatly and consisted of open steppes and meadows with bushy/woody areas (Figure 7.1). In Levels 2, 3, 4, 6 and 8 >40% of the landscape consisted of forest and bush (open forest), while open (steppe, meadow) environments increase slightly in Levels 5 and 7 (because *Jaculus orientalis* is present in these levels). The percentage proportion of aquatic species is also relatively consistent throughout the majority of sequence (between ~30 and 40%), with the exception of a small decline in Level 7 (22%) (Figure 7.1).

Geometric morphometric analysis of *Crocidura* spp. mandibles from the El Harhoura 2 small mammal assemblage allowed determination of *Crocidura* species and calculations of the frequency in each Level (1-8) (Cornette et al., 2015). North African *Crocidura* spp. have specific habitat preferences that are used to indicate past environments. *C. russula*, indicative of Mediterranean climates within Morocco, is the most common species in Levels 8-2. *C. lusitania and C. tarfayensis*, that prefer more arid environments, are present but in lower numbers with the largest abundances in Levels 3 and 4a (Figure 7.1). The maximum abundance of *C. russula* occurs in Levels 2 and 7 where the THI indicates more open environments. Cornette et al. (2015) suggested that the disagreement between the THI and presence/absence of *Crocidura* may result from the inter-specific dominance of *C. russula* over the other shrew species. Stoetzel et al. (2013) also analysed the morphology of *Mus spretus* molars from Levels 1-8 at the site. The study showed that there was no significant difference

in molar shape and size during the Late Pleistocene, demonstrating evolutionary stability over c. 100,000 years. This suggests that the preferred habitats of *M. spretus* (grassland, dry shrubland, open woodland) persisted in the landscape around El Harhoura 2 during the Late Pleistocene (Stoetzel et al., 2013).

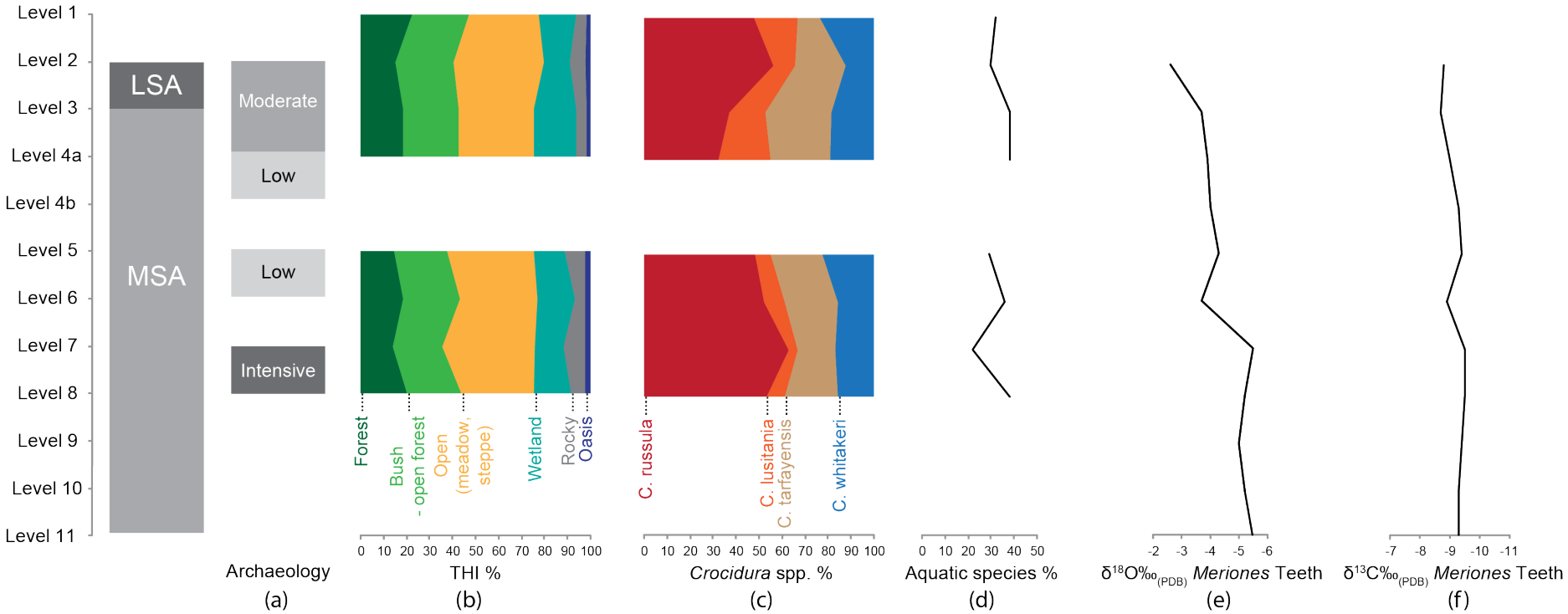

Figure 7.1: Summary diagram displaying palaeoenvironmental proxies and archaeology from Levels 1-11 at El Harhoura 2. (a) shows the cultural stratigraphy and indicates the intensity of occupation (see discussion of archaeological evidence in Chapter 2), (b) relative % of THI values (adapted from Stoetzel et al. 2014), (c) Relative % of shrew species in each level (derived from morphometric analysis) (adapted from Cornette et al. 2015), (d) % of aquatic species (adapted from Stoetzel et al. 2014), (e) mean $\delta^{18}O_{teeth}$ values (from this study), (f) mean $\delta^{13}C_{teeth}$ values (from this study).

The $\delta^{18}O_{teeth}$ values from Levels 7-11 are relatively low, suggesting more humid conditions than present, while the $\delta^{18}O_{teeth}$ values in Levels 6-3 are higher than those in the lower levels and suggest MAP similar to present values (Figure 6.11). Level 2 has the most arid conditions in the sequence with reconstructed MAP of ~250-400mm. The $\delta^{13}C_{teeth}$ values do not vary significantly throughout the sequence ($\delta^{13}C_{teeth}$ range = -11 to -7.9‰), which suggests the presence of arid/open C_3 vegetation around El Harhoura 2 (Figure 6.11), but also shows that the preferred habitats of *Meriones* were also present around the cave site. Within specific levels the *Meriones* isotope record and other proxy records are consistent. The proxy records indicate that although the vegetation in Level 8 was fairly open (evidenced from $\delta^{13}C_{teeth}$ and THI), the climate was relatively humid as inferred from the presence of *Bufo bufo*, *Pleurodeles* cf. *walti* and *Natrix marura* and lower $\delta^{18}O_{teeth}$ values (Figure 7.1). The proxy records also indicate relatively arid conditions in Level 2, from higher $\delta^{18}O_{teeth}$ values, a slight increase in open meadow (steppe), low numbers of amphibian fauna (no humid indicators species such as *Bufo bufo*, *Discoglossus pictus*) (Figure 7.1), as well as a decrease in Bovinae and an increase of gazelles and Alcelaphinae.

The presence of *Jaculus orientalis* in Levels 5 and 7 indicates open and arid conditions (Figure 1.7). Proxy records suggest that Level 5 is relatively arid with high $\delta^{18}O_{teeth}$ (lower than $\delta^{18}O_{teeth}$ values in Level 2), $\delta^{13}C_{teeth}$ indicating open vegetation, a slight reduction in aquatic species, and lower numbers of *C. russula*. Low $\delta^{18}O_{teeth}$ values and maximal percentages of *C. russula* suggest relatively humid/temperate conditions in Level 7; this is converse to the environment inferred from the presence of *J. orientalis* and the reduction in

aquatic species. There are several possible explanations for the apparent difference between the *Meriones* $\delta^{18}O_{teeth}$ record and THI in Levels 5 and 7. Firstly, *J. orientalis* may merely reflect a more continental environment during periods of lower sea level when El Harhoura 2 would have been further from the coastline (Stoetzel et al., 2011) (calculated to be 10's of kms (Collina-Girard, 2001; Lambeck and Purcell, 2005)). It should also be noted that *J. orientalis* is not present in Level 2, which the majority of proxies conclude is an arid level. Secondly, the differences may result from seasonal bias within the $\delta^{18}O$ signal (Level 7 does have a significant offset in $\delta^{18}O$ between molars and incisors), or positive hydrological balance caused by reduced evapotranspiration from cooler summer temperatures (see Section 6.4.4).

In Levels where comparisons can be made, there is generally good agreement between the *Meriones* isotope record and palaeoenvironment from other proxy evidence. The only major disagreement between the proxy records occurs in Level 7; the isotope record indicates this is relatively humid but the species abundance data suggests more arid conditions, mainly indicated by the presence of *J. orientalis*. Unfortunately, comparisons cannot be made between the humid lower levels (9-11) and other proxy records to confirm that the lower $\delta^{18}O_{teeth}$ values reflect increased humidity. All proxy records from El Harhoura 2 suggest that the Atlantic coast of Morocco did not undergo dramatic climatic variation during the Late Pleistocene. The THI, $\delta^{13}C_{teeth}$, *Crocidura* record and evolutionary stasis of *Mus spretus* molars reflect stability in the vegetation and habitats in the surrounding environment around the cave. In addition, the $\delta^{18}O_{teeth}$ record shows that humidity on the Atlantic coast of Africa was higher or

similar to that of today throughout much of the Late Pleistocene. Even in Level 2, the most arid in the sequence (reconstructed MAP= ~250-400mm), the MAP values are consistent with those presently found in steppe environments north of the Atlas showing that the Mediterranean coastal region never experienced hyper-aridity associated with the desert steppe environments found south of the Atlas Mountains.

7.2.1.2. Taforalt

The macrocharcoal and phytolith records from Taforalt are the most continuous palaeoenvironmental records from the site showing the presence/absence of woody taxa and grasses throughout the sequence (Ward, 2007) (Figure 7.2). However, as discussed in Chapter 2 the palaeoenvironemntal information from these records should be interpreted tentatively because plant remains in the cave deposits are likely subject to human bias. The macrocharcoal record shows the fluctuating presence of *Cedrus atlantica, Juniperus*/*Tetraclinis articulata*, *Quercus* and *Pinus* throughout the Late Pleistocene, indicating that woody vegetation was always present in the environment around the cave, and that open steppe conditions never dominated (Ward, 2007). The phytolith record from Sectors 2 and 8 shows clear dominance of C_3 grasses during the Late Pleistocene, but there is also a small contribution of C_4 vegetation. The phytoliths show an increase in C_4 vegetation from Levels Y6 and Y4 to Levels Y2 and Y1, similar to that reflected in the $\delta^{13}C_{teeth}$ (Ward, 2007) (Figure 6.11), but as discussed in the previous chapter expansions in C_4 grasses at Taforalt likely results from changes in pCO_2 and temperature.

The macrocharcoal and phytolith record from lower Sector 2 c. 112-80ka (Levels R27 and R21- see Figure 6.3 for stratigraphic context), equivalent to Levels 23D-23K, is dominated by deciduous *Quercus* and C_3 grasses with presence of *C. atlantic*, *Pinus* lowland and *Juniperus*/*Tetraclinis articulata*. The vegetation during this period is similar to that presently found at Taforalt, except for the presence of *C. atlantica*. Presently, *C. atlantica* is found in the Middle and High Atlas, and the Rif mountains in Morocco between 1300-2600m asl, where MAP ranges from 500-2000mm and the minimum temperature of the coldest month is between -8 and -1C (optimum conditions are in sub-humid conditions (600-800mm MAP)) (Cheddadi et al., 2009). However, its presence at Taforalt during this period may just reflect the species wider and lower altitude distribution during the Late Pleistocene (Ward, 2007). The *Meriones* $\delta^{18}O_{teeth}$ from Levels 23D/F-23I/K are relatively low, suggesting humid conditions c. 97-80ka, while the $\delta^{13}C_{teeth}$ show mainly C_3 vegetation with a small contribution of C_4 in Levels 23D/F and 23G (Figure 6.11). Humid/temperate conditions in lower Sector 2 are inferred from the presence of deciduous *Quercus*, which is often used as an indicator of ameliorated conditions in Mediterranean marine cores (Table 3.1) (Sánchez Goñi et al., 2002)

Level R16 is characterised by a significant expansion of *Juniperus* sp. *Tetraclinis articulata*, persistence of *C. atlantica*, small frequency of *Pinus* lowland and absence of deciduous *Quercus*. Although *C. atlantica* prefers semi-humid conditions (MAP= 600-800mm), the significant increase of *Tetraclinis articulata* that prefers annual precipitation ranges of ~350-630mm, may indicate a shift in environment to more arid conditions (Ward, 2007). In MIS 3 (including

Level R14) the continued decline of *C. atlantica*, coupled with the reappearance of *Quercus* deciduous, *Quercus* evergreen, *Pinus halepensis* and *Pinus* lowland is indicative of slightly temperate, warmer, and possibly dryer conditions relative to MIS 4. The *Meriones* isotope-based MAP reconstructions from Levels R16 and R14 also infer a shift to relatively more arid conditions with MAP values of 300-400mm, similar to those presently found at Taforalt (Figure 6.11).

Juniperus/*Tetraclinis articulata* dominates the macrocharcoal assemblage at the beginning of MIS 2 (c. 30-24 cal BP) with similar woody taxa to that noted in Levels R16. Between c. 20-15ka cal BP (Y3-Y1) there is a significant change in the composition of the vegetation from previous levels. In Levels Y3-Y1 it consists largely of *Juniperus*/*Tetraclinis articulata* with presence of *Pinus halepensis*, *Pinus* lowland, evergreen *Quercus* and *Acer* sp. (Ward, 2007). The appearance and persistence of *Ephedra* sp. during this period in association with the other woody taxa is characteristic of pre-steppic vegetation (Table 3.1) (Ward, 2007). In addition, the notable absence of *C. atlantica* from c. 24-15ka cal BP (upper Y4- Grey Series), as well as sedimentary change in upper Y2 and upper Y4 also indicates an aridification of the environment during the period (Barton et al., 2013). The *Meriones* $\delta^{18}O_{teeth}$ values from c. 30-15ka cal BP (Levels Y6-Y1) are relatively low, and infer that MAP was higher than present (~450-850mm) (Figure 6.11). This is not consistent with palaeoenvironmental inferences from the macrocharcoal and sedimentary record, as well as regional climate records (see Section 7.2.2), which all show this was a cool, arid period.

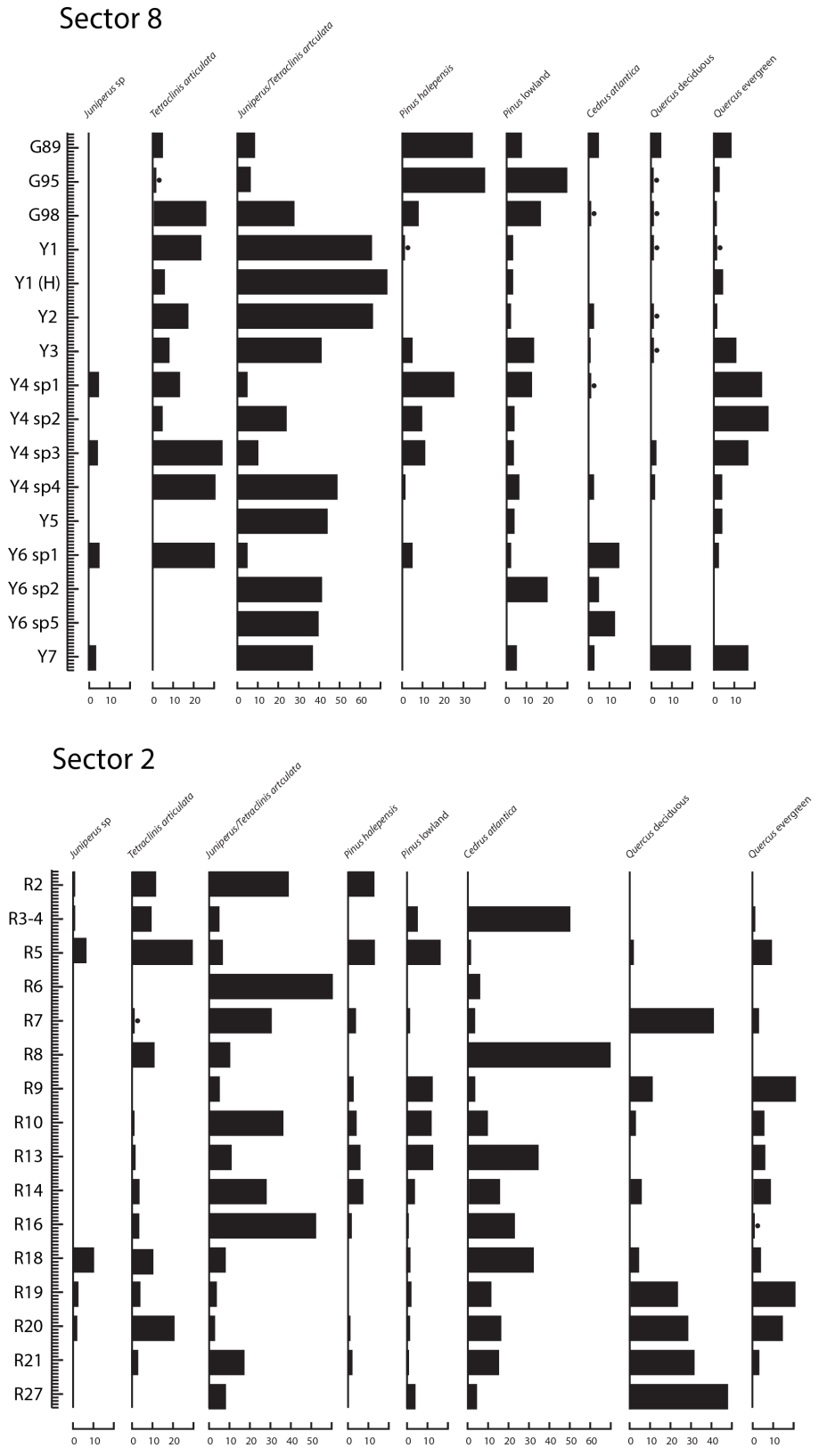

Figure 7.2: Diagram showing the relative percentage of the main macrocharcoal taxa, discussed in the text, from Sector 2 and Sector 8 at Taforalt (redrawn and adapted from Fig.5.7 and Fig. 5.19 in Ward 2007). See Figure 6.3 and 6.5 for stratigraphic information regarding the Levels. 'R' refers to Raynal's layers (see Section 2.3.1.1).

The *Meriones* isotope record and the macrocharcoal record indicates similar palaeoclimate conditions in Levels 23D-23K (lower Sector 2) and Levels R16 and R14; however, the proxy records appear to differ in Sector 8. The *Meriones* isotope-based MAP reconstructions (if interpreted in terms of moisture availability) imply increased MAP/greater moisture availability between 24ka and 15ka cal BP, but sedimentary and macrocharcoal archives show aridification of the environment during this period. This is discussed in more detail in Section 7.2.3.

7.2.2. Correlation of *Meriones* isotope record in marine and terrestrial records from the western Mediterranean

High-resolution records of palaeoclimate in the western Mediterranean region are sparse making detailed inferences from this period complex. However, pollen records from core M 15669-1 (34°N), located off the Atlantic coast of Morocco, (Figure 7.3) provides palaeoclimate information from the region throughout the Late Pleistocene. This record shows that during MIS 5 and the beginning of MIS 4 (c. 122-68ka) a well-developed and widespread Mediterranean vegetation zone extended across the Mediterranean coast of northwestern Africa, revealing that temperate, humid conditions existed throughout this period. The records show specific increases in Mediterranean and humid taxa at c. 115ka and 100ka (Figure 7.3), possibly showing fluctuations equivalent to stadials/interstadials within MIS 5. Macrocharcoal records at Taforalt (Levels R27 and R21), THI and El Harhoura 2 (Level 8) and *Meriones* $\delta^{18}O_{teeth}$ values at El Harhoura 2 (Levels 4a-11) and Taforalt (Levels 23D-23K) also indicate temperate, humid conditions during MIS 5 in northeastern Morocco and the Atlantic coastal region of Morocco. Terrestrial

records/deposits indicative of humidity also increase between c. 120-90ka in the Mediterranean region of North Africa (Smith, 2012). At El Harhoura 2 there is a shift in $\delta^{18}O_{teeth}$ values from the earlier (118-108ka) to the later MIS 5 levels (107ka-80ka) from increased humidity to relatively drier conditions similar to present. This may reflect climatic variability between stadial and inter-stadial conditions within MIS 5 (Sánchez Goñi et al., 2002), and if this is the case, hint that MIS 5 stadials on the Atlantic of Morocco were not very severe with MAP values similar to present.

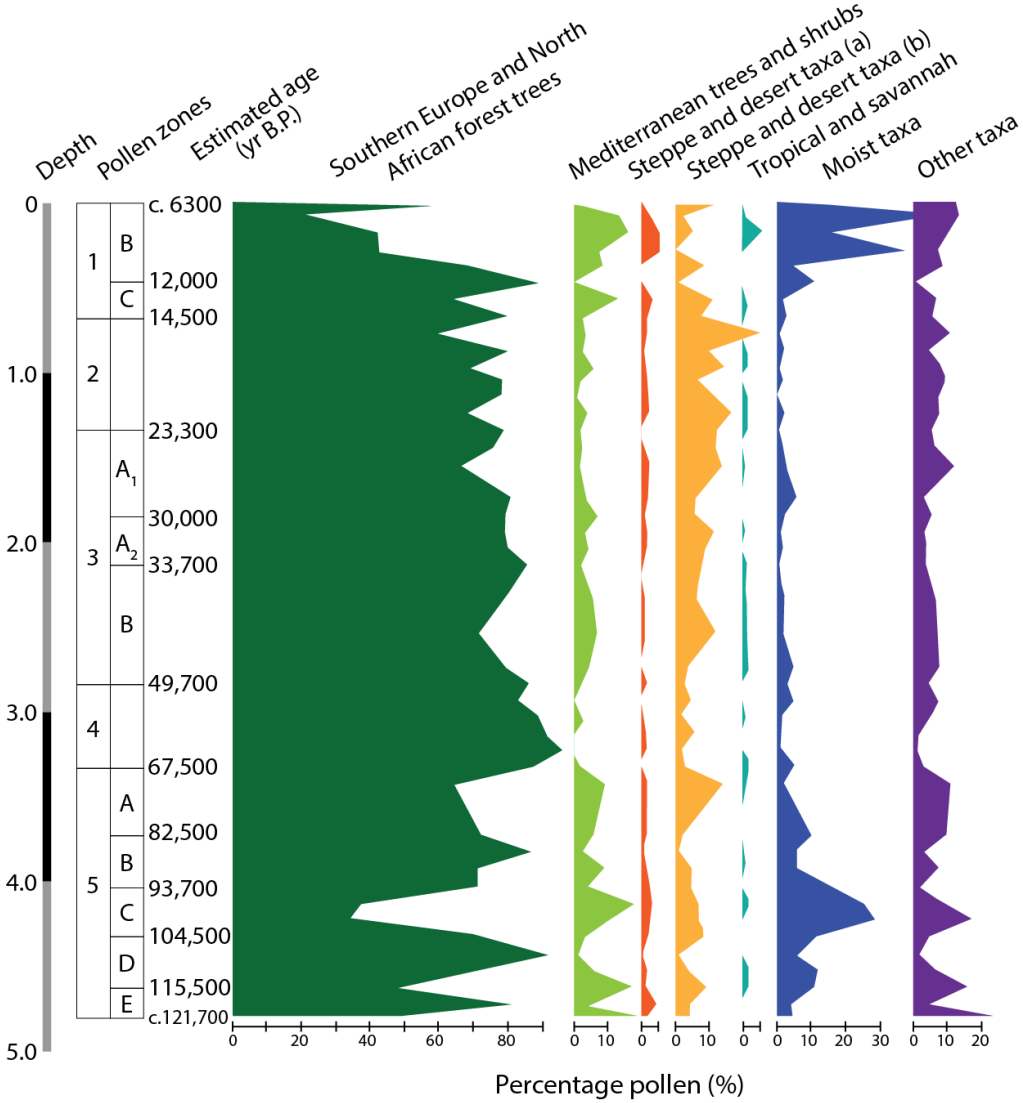

Figure 7.3: Downcore percentage fluctuations of seven groups of pollen based on pollen sum from core M 15669-1 located off the Atlantic coast of Morocco (Figure 3.1) (adapted from Fig. 17b in Hooghiemstra et al., 1992).

Marine core pollen records in the western Mediterranean suggest relatively ameliorated conditions during MIS 3. Pollen evidence from marine cores show small increases in Mediterranean taxa between c. 50-33ka off the Atlantic coast of Morocco (Figure 7.3) (Hooghiemstra et al., 1992), and relatively higher proportions of arboreal pollen in the Alboran Sea (Fletcher and Sánchez Goñi, 2008). Although high-resolution marine core records demonstrate D/O climate variability associated with the expansion and contraction of Mediterranean forest during MIS 3 (Bout-Roumazeilles et al., 2007; Moreno et al., 2005), it is thought that on the North African coast D/O stadials were not accompanied with significant drops in humidity or temperature (Sánchez Goñi et al., 2002). Terrestrial records/deposits indicative of aridity also increase during MIS 3 in the Mediterranean region of North Africa, hinting at an intensification or southward shift in the westerly wind belt (Drake et al., 2013; Smith, 2012). The *Meriones* $\delta^{18}O_{teeth}$ values, THI and macrocharcoal records from levels dating to MIS 3 at Taforalt (Levels R14 and R16) and El Harhoura 2 (Level 3) all suggest relatively temperate conditions with humidity similar to present conditions (at Taforalt conditions in MIS 3 were significantly more arid relative to MIS 5).

Proxy records from El Harhoura 2 suggest that Level 2 (c. 20ka-13ka) is the most arid in the Late Pleistocene sequence with inferred MAP of ~250-400mm, lower than present MAP (~500mm). Sedimentary and macrocharcoal records also indicate arid conditions during MIS 2 at Taforalt, yet the $\delta^{18}O_{teeth}$ values suggested increased MAP (~450-850mm)/greater moisture availability in Levels Y1-Y6 (c. 30-15ka cal BP). Unfortunately the chronological resolution on Level 2 (c. <20ka and >13.5ka cal BP) at El Harhoura 2 does not allow greater

precision on the date of this arid episode and means that direct correlations between levels at Taforalt and El Harhoura 2 cannot be made. Marine records from the Alboran Sea suggest the interval from c. 30-13ka cal BP was relatively cool and arid, and was punctuated by HEs at c.24ka cal BP and 15ka cal BP resulting in rapid further climatic downturn across the western Mediterranean (Bout-Roumazeilles et al., 2007; Combourieu Nebout et al., 2009). Climate models as well as MAP and MAT reconstructions show that the periods preceding and following LGM were relatively colder and drier than the LGM (Fletcher et al., 2010b; Jolly et al., 1998; Kageyama et al., 2005). A particularly arid period dating to between c. 18-15 cal BP, termed the 'Mystery Interval' is recognised in the Alboran Sea marine records (Bout-Roumazeilles et al., 2007; Combourieu Nebout et al., 2009; Fletcher et al., 2010b) (Figure 7.4) and several Iberian lake records (Moreno et al., 2012). Furthermore the Pindal Cave speleothem, located in northern Iberia, ceases growth during this period (18.2-15.4 kyr BP) (Moreno et al., 2010). Climatic reconstructions based on pollen records from core MD95-2043 (Alboran Sea) suggest that between c. 17.5 and 15ka cal BP MAP decreased to ~200mm while the mean temperature of the coldest month ranged between -10 to -15°C across the western Mediterranean region (Figure 7.4) (Fletcher et al., 2010b).

7.2.3. Does $\delta^{18}O$ in *Meriones* teeth reflect aridity at El Harhoura 2 and Taforalt?

The climatic inferences from *Meriones* isotope record show good consistency with those from other local (see Section 7.2.1) and regional proxy climate records from the western Mediterranean region (See section 7.2.2). Complete consistency between local and regional proxy records is not expected because

each record reflects a different climate/environmental variable and is subject to different deposition. As described in Section 7.2.1.2, the *Meriones* isotope-based MAP reconstructions from the Taforalt Sector 8 levels (Y1-Y6), which suggest this was a humid period, differ from all other proxy records in the region. This section discusses whether the $\delta^{18}O_{teeth}$ reflect aridity or whether other factors have influenced the isotope values in the teeth.

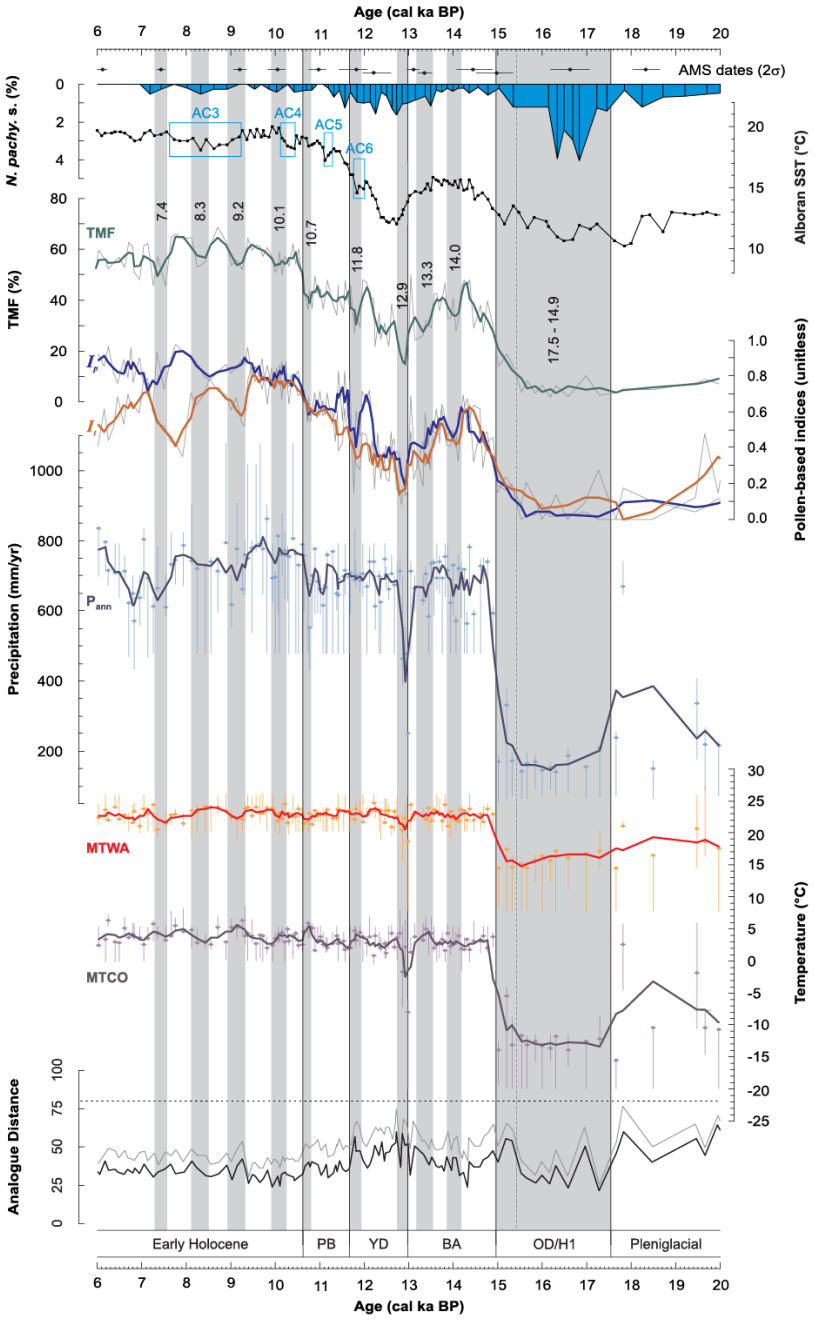

Figure 7.4: Marine and terrestrial proxies and pollen-based MAT and MAP climate reconstructions for the last deglaciation in core MD95-2043 (located off the Mediterranean coast of Morocco), plotted against age (cal ka BP). From top to bottom: % of cold water foraminifer *N. pachyderma* (from Cacho et al. 1999), alkenone SST reconstruction (from Cacho et al. 1999), Pollen percentage of temperate Mediterranean forest taxa (TMF), pollen indices curves reflecting regional temperature and moisture availability, pollen-based MAP reconstruction, pollen-based MAT reconstructions shown as mean temperature of the coldest month (MTCO) and mean temperature of the warmest month (MTWA), the pollen analogue distances from source. The grey vertical box highlights the so-called 'Mystery Interval', a cool, arid period noted across the western Mediterranean region (From Fletcher et al. 2010b).

The $\delta^{18}O_{teeth}$ at El Harhoura 2 appear to reflect palaeoaridity showing a shift from relatively humid conditions during MIS 5, to more arid conditions in MIS 2, a trend that is also recorded in regional palaeoclimate records within the western Mediterranean. The $\delta^{18}O_{teeth}$ at Taforalt also reflect humid conditions during MIS 5 and relatively more arid conditions in MIS 3. However, there is a discrepancy between the increased MAP inferred from lower $\delta^{18}O_{teeth}$ values in MIS 2, and the arid conditions that appear to have dominated the region during this period (especially between c. 18ka and 15ka cal BP). It is hypothesised that low $\delta^{18}O_{teeth}$ values in Levels Y1, Y2, Y4 and Y6 at Taforalt do not reflect moisture availability, due to the effect of lower atmospheric temperatures during MIS 2. As discussed in Chapter 6 (Section 6.4.4), it is assumed that variation in atmospheric temperature would have a greater influence on the $\delta^{18}O_{teeth}$ values at Taforalt because of continental and altitudinal effects. It is suggested that lower temperatures would have reduced rates of evapotranspiration, resulting in a $\delta^{18}O_{teeth}$ signal indicative of greater moisture availability or positive hydrological balance. Therefore, the low $\delta^{18}O_{teeth}$ values in Levels Y1, Y2, Y4 and Y6 are interpreted as reflecting reduced evapotranspiration under cooler conditions. Other proxy records in Morocco and the western Mediterranean region also reflect positive moisture balance during MIS 2. Records from Lake Isli (High Atlas) indicate higher lake levels relative to the present after c. 20ka (Valero-Garcés et al., 1998). Also, lake records in Iberia show increased moisture availability during the LGM, which is suggested to result from reduced evaporation in cooler summer temperatures (Moreno et al., 2012).

7.3. Implications of climate on human occupation and cultural behaviour in North Africa

7.3.1. Human occupation and cultural behaviour at Taforalt and El Harhoura 2

Archaeological evidence suggests that humans were consistently present at Taforalt throughout the majority of the Late Pleistocene (including Levels from which *Meriones* teeth were not sampled), but the intensity of these occupations fluctuated (see Barton et al. 2013) (see Table 7.1). Humans also used and occupied El Harhoura 2 during MIS 5, 3 and 2, but the occupation phases are interspersed with periods when the cave site was not used by humans (Sterile Levels 11, 10, 9, 7 and 5) (Campmas et al., 2015; Stoetzel et al., 2014) (Figure 7.1). At both sites the MSA Aterian technocomplex is present throughout MIS 5-3 (c. 110-50ka at El Harhoura 2, c. >110-30ka at Taforalt), a pattern also reflected at other cave sites in Morocco, suggesting cultural stasis in the Mediterranean coastal strip of North Africa from >110ka- 30ka. The cultural change from the MSA to LSA occurs during MIS 2 at both Taforalt and El Harhoura 2. The MSA/LSA transition is recorded particularly well at Taforalt, where the sediments form an almost continuous sequence from c. 30ka-12ka (Barton et al., 2016, 2013). At Taforalt there is a transition from the MSA Aterian to a non-Levallois flake industry, which as yet is not defined as belonging to the MSA or LSA, at c. 29ka cal BP (Barton et al., 2016). A transition to the LSA Iberomaurusian then occurs at c.21ka cal BP. In contrast, at El Harhoura 2, there is a large hiatus in the record between the MSA and LSA (Level 3 to 2) and the LSA Iberomaurusian has poor chronological control (c. 20ka->13ka cal BP).

Table 7.1: Summary of cultural and palaeoenvironmental evidence from Levels discussed in text at Taforalt.

Level	Culture/lithics	Intensity of occupation (estimates from Barton et al. 2013)	Evidence from $\delta^{18}O$ and $\delta^{13}C$ values in *Meriones* teeth	Evidence from Macrocharcoal/Phytoliths	Other proxy evidence
Grey Series 15,0-12,6 ka Cal BP	LSA Iberomaurusian IB3 lithics dominated by backed bladelets	Intensive	None	C_4 vegetation decreases up the Grey Series indicating climate amelioration, with more woody taxa at the top of the Grey Series.	Correlates with Greenland Interstadial 1
Y1 15.1-15.3 ka cal BP	LSA Iberomaurusian IB2 lithics dominated by microlithic backed bladelets	Present	Reduced evapotranspiration, cool, open C_3-dominated vegetation, small amount of C_4 grasses.	*Juniperus*/*Tetraclinis articulata* with presence of *Pinus halepensis*, *Pinus* lowland, evergreen *Quercus* and *Acer* sp, and Ephedra. Indicative of pre-steppic vegetation	
Y2 17.1-19.0 ka cal BP	LSA Iberomaurusian IB1 lithics containing marginally backed ('Ouchtata') blades and bladelets	Present	Reduced evapotranspiration, cool, open C_3-dominated vegetation, small amount of C_4 grasses.	*Juniperus*/*Tetraclinis articulata* with presence of *Pinus halepensis*, *Pinus* lowland, evergreen *Quercus* and *Acer* sp, and Ephedra. Indicative of pre-steppic vegetation	Probably including Heinrich Event 1. Climatic instability indicated in upper sediments in Y2 (erosive break)
Y4 19.9-24.2 ka cal BP	(Upper) LSA Iberomaurusian IB1 lithics (begins ~21 cal BP) (Lower) non-Levallois flake industry (ends ~24 cal BP)	Present	Reduced evapotranspiration, cool, open C_3-dominated vegetation	(Upper) Negligible amounts of *Cedrus atlantica* indicate arid, cool conditions. (Lower) Dominated by Juniperus/Tetraclinis articulata	Radiocarbon age models shows a clear gap between the LSA and the non-Levallois flake industry. This is represented in the stratigraphy as a 'sterile' body of sediment including significant amounts of non-carbonate silt (probable dust) indicating a markedly arid, cool period.

Y6 24.6-30.8 ka cal BP	non-Levallois flake industry	Present	Reduced evapotranspiration, cool, open C_3-dominated vegetation	Dominated by *Juniperus*/*Tetraclinis articulata*	
(Sector 9) LH units, etc. ~29ka cal BP	MSA Aterian	Intensive - associated with rich hearth deposits	None	None	Charcoal indicates mixed open forest dominated by juniper with the presence of *Quercus*, maple and scrubs.
R14 ~45 to 40 ka BP	MSA Aterian	Present	MAP similar to present (~300-400 mm), open C_3-dominated vegetation, small amount of C_4 grasses.	Decline of *Cedrus atlantica*, coupled with the reappearance of *Quercus* deciduous, *Quercus* evergreen, *Pinus halepensis* and *Pinus* lowland is indicative of slightly temperate, warmer, and possibly dryer conditions	
R16 ~60 ka BP	MSA Aterian	Moderate-some hearth deposits	MAP similar to present (~300 mm), open C_3-dominated vegetation, small amount of C_4 grasses.	Significant expansion of *Juniperus* sp./*Tetraclinis articulata* indicative of shift to relatively arid conditions.	
R23D/F, 23G, 23H, 23I/K ~97-80 ka BP	MSA Aterian	Intensive – associated with rich hearth deposits *Nassarius* shells	MAP higher than present (~400-800 mm), open C_3-dominated vegetation, small amount of C_4 grasses.	(Levels R27 and R21) Dominated by deciduous *Quercus* with presence of *Cedrus atlantic*, *Pinus* lowland and *Juniperus*/*Tetraclinis articulate* (similar to present). Presence of deciduous *Quercus* suggests temperate conditions. C_3 grasses dominant.	

El Harhoura 2 is intensively occupied in Level 8 (110.3 ± 5.6ka BP), as seen by the dense lithics accumulations, large numbers of shell fish (limpets), the presence of *Nassarius* shells, hearths, pigments and bone tools (Stoetzel et al., 2014), with lower intensities of MSA occupation in Levels 6 (106.7 ± 5.7ka BP), 4b (100.9 ± 8.5ka BP), 4a (74.0 ± 8.0ka BP) and 3 (63.3- 51.3ka BP) (Figure 7.1). As discussed in Section 7.2.1.1, the proxy climate records from these levels at El Harhoura 2 indicate general environmental stability and humidity throughout this period (Figure 7.1). The intensive MSA occupation (Level 8) at El Harhoura 2 is associated with humid conditions, yet Levels 9-11 (c. 118-112ka) that were also deposited under climate conditions similar to those in Level 8, do not contain any significant archaeology suggesting that the cave was not used or occupied. The archaeology and palaeoclimate records suggest that the intensive use of El Harhoura 2 (in Level 8) appears to reflect opportunistic intensive use of the site by hunter-gatherers during a period of humid climate, or a period of high sea-level when the cave was used by humans for shell-fish exploitation (Campmas et al., 2015), rather than favourable climate conditions. The intensive use of Taforalt in lower Sector 2 Levels 23D-K during MIS 5 (c. 97-80ka), evidenced from denser finds of lithics, *Nassarius* shell beads and hearth deposits, also occurs during a period a relatively temperate conditions (Table 7.1).

Archaeological evidence from sites in Morocco hints that human populations expanded in North Africa during MIS 5 with an apparent increase of MSA Aterian sites during this period (Jacobs et al., 2012). It is also hypothesised that demographic growth initiated cultural innovation, such as the appearance of

Nassarius shell beads, use of pigments and production of bone tools, in MSA Aterian assemblages (D'Errico et al., 2009). D'Errico et al (2009) suggests that *Nassarius* shells disappear from the North African record after MIS 5 because smaller populations, caused by a climatic downturn, could not maintain the networks needed to transport shells from the coast to inland areas. Interestingly, the occupation of both El Harhoura 2 and Taforalt during MIS 4 and 3 is less intense and occurs during drier conditions, relative to those in MIS 5 (Figure 6.11 and 7.1, Table 7.1). Archaeological and palaeoenvironmental evidence from El Harhoura 2 and Taforalt show that MSA Aterian occupations are not solely associated with humid climate episodes, but more intense use of the sites seems to have occurred during periods of humid climate in MIS 5.

The period spanning c. 40-20ka BP is particularly interesting in North Africa because it includes a major lithic transition recognised as the change from MSA to LSA, as well as being a period of major global climate fluctuation (see Chapter 3). The youngest MSA Aterian at Taforalt dates to c. 29ka cal BP (LH units, Sector 9) and is associated with rich hearth layers containing lithics, bone, ostrich egg shell and charred plant remains suggestive of intensive occupation (Barton et al., 2016). Palaeoenvironmental evidence from these Levels in Sector 9 is sparse, with charcoal from hearth deposits indicating a mixed open forest dominated by juniper with the presence of *Quercus*, maple and scrubs (Barton et al., 2016). After c. 29ka cal BP the industry at Taforalt changes to a lithic assemblage comprised of flakes debitage struck from non-Levallois cores recorded in Sector 8 (Y4-Y6), Sector 2 (R3-R4) and the sediments above the rockfall level in Sector 9 dating to c. 26-24ka cal BP

(Barton et al., 2016). The morphology and stratigraphy of these tools suggest that they do not fall within a typical MSA assemblage or the overlying LSA, and as yet has no known analogue with the Maghreb, so here are termed non-Levallois flake industry. As yet it is unclear whether this industry is a functionally specialised MSA technology or whether it represents cultural change post-dating the MSA Aterian, perhaps resulting from a shift to cooler conditions, inferred from *Meriones* $\delta^{18}O_{teeth}$ Y6 and Y4 (Table 7.1).

The youngest modelled age on the non-Levallois flake in Sector 8 is c. 24 cal BP with a clear 'gap' in the stratigraphy before the LSA begins at c. 21 cal BP. The hiatus in the sequence contains significant quantitates of dust. Sedimentary, macrocharcoal and the *Meriones* isotope record indicate that the Yellow Series LSA at Taforalt (upper Y4 to Y1) was a cool, arid period (Table 7.1). Palaeoenvironmental evidence from LSA Level 2 at El Harhoura 2 also indicates aridity, with MAP that is consistent with that found that presently in open steppe environments in Morocco (Figure 7.1). This evidence hints that the MSA/LSA cultural transition may be related to the changing environmental conditions. The low level occupation of Taforalt in Levels Y4-Y1 indicates small LSA populations, that were adapted to relatively cool arid conditions, were present in northeastern Morocco. The LSA Grey Series midden deposit differs dramatically from the Yellow Series, containing copious quantitates of animal bone, terrestrial molluscs, plant remains, charcoal and artefacts. This dense archaeological deposit indicates intensification in the use of and nature of occupation at Taforalt by LSA populations. Significantly the Grey Series

deposition occurs during a period of humid climate conditions, and appears to correlate with a time equivalent to Greenland Interstadial 1 (Barton et al., 2013).

7.3.2. El Harhoura 2 and Taforalt as refugia during the Late Pleistocene

Archaeological evidence from Taforalt and El Harhoura 2 shows that, as well as being intensively used during MIS 5, both cave sites were occupied by MSA Aterian populations during MIS 5/4, 3 and 2, and LSA Iberomaurusian populations during MIS 2. Occupations of the cave sites during periods of low population density in North Africa may suggest that the regions around the cave sites were refugia for human populations. Proxy climate records from El Harhoura 2 and Taforalt show that climate in MIS 4 and 3 was relatively arid compared to MIS 5, while the LSA Iberomaurusian occupation of both sites occurred during the most cool and dry period of the Late Pleistocene. However, overall conditions were relatively humid in the Mediterranean coastal region of North Africa compared to hyper-arid conditions associated with desert-steppe environments that existed to the south of the Atlas (Blome et al., 2012; Hooghiemstra et al., 1992). It is suggested that the oceanic influenced temperate climate at El Harhoura 2 buffered the Atlantic coastal region of Morocco from extreme humid/arid shifts during the Late Pleistocene making it an excellent refugium for human populations. While the *Meriones* oxygen isotope record from Taforalt indicates greater temperature shifts during the Late Pleistocene, it appears that humans used the site throughout the majority of the Late Pleistocene. It is thought that the landscape around Taforalt would have been particularly appealing to hunter-gatherer populations, and the varied topography around the cave would have acted as micro-refugia for plants and

animal species. The microcharocal record from the site indicates that woody taxa were present around the site throughout the Late Pleistocene. The altitudinal variation in the steep surrounding valleys would also elongate the periods in which hunter-gatherers could exploit seasonal plant resources.

Comparisons can be made with the site of Haua Fteah, northeast Libya, also located in the Mediterranean coastal strip of North Africa. This site has recently been re-excavated and with the aim of refining chronology and placing the site in its palaeoenvironmental context. $\delta^{18}O$ analysis was carried out on *Ammotragus lervia* enamel from the Middle Palaeolithic Levalloiso-Mousterian Levels (c. 73-64ka), and Upper Palaeolithic Dabban (c. 33-31ka) and Oranian (c. 17-13.5ka) Levels to reconstruct palaeoaridity (Reade et al., 2015). The results show little variation in $\delta^{18}O$ across the levels suggesting there were no hyper-arid phases in the Late Pleistocene. The $\delta^{18}O$ of the *A. lervia* enamel indicates that the Dabban Levels, dating to c. 33-31ka, were the most arid in the sequence. Interestingly the Oranian Levels, which are concurrent with LSA Level 2 at El Harhoura 2 and Levels Y1 and Y2 at Taforalt, do not appear to reflect an aridity signal. However, other palaeo-proxies from the site, including land snail shell isotopes and soil micromorphology, do suggest that conditions during the Oranian were some of the coldest and driest of the of the Late Pleistocene in the Gebel Akhdar. Archaeological evidence suggests that Haua Fteah was intensively occupied by humans during this period of climatic downturn (Prendergast et al., 2015). It is proposed that, because conditions in the Gebel Akhdar were not as harsh compared to surrounding regions, and because the cave was occupied more intensively during periods of climatic

deterioration, the region acted as a refugium for human populations in North Africa during the Late Pleistocene (Prendergast et al., 2015; Reade et al., 2015).

7.4. Conclusions

The *Meriones* isotope records from Taforalt and El Harhoura 2 show consistency with other proxies from the cave sites, as well as regional marine and terrestrial records in the western Mediterranean. The proxy records from El Harhoura 2 suggest that the Atlantic coast of Morocco did not undergo marked climatic variation during the Late Pleistocene, and although temperature fluctuations seem greater at Taforalt, it appears that the Mediterranean coastal strip of Morocco did not experience any hyper-arid phases during the Late Pleistocene. Comparisons of the palaeoenvironmental and cultural sequences from both sites show that humans intensively occupied El Harhoura 2 and Taforalt in MIS 5 when the climate was relatively humid. However, MSA occupations of the cave sites are not exclusively associated with humid climate episodes with other occupations occurring at the end of MIS 5, MIS 4 and MIS 3 during which conditions were drier. The cultural transition from the MSA to the LSA occurs during MIS 2, a period of greater aridity across the western Mediterranean region, hinting that this cultural transition may be related to the changing environmental conditions. Because human occupations of El Harhoura 2 and Taforalt occur throughout the Late Pleistocene, during relatively humid and more arid episodes it is suggested that the regions around the cave sites were refugia for human populations. The oceanic influenced climate on the Atlantic coast appears to have buffered the region from large climatic shifts

during the Late Pleistocene. Also, the varied topography in northeastern Morocco would have acted as micro-refugia for plant and animal species.

8. Conclusions

8.1. Small mammal modern isotope study in northwestern Africa

As outlined in Chapter 1, archaeological or fossil small mammal tissues are not commonly used in the construction of palaeoclimate and palaeoenvironmental records because little is understood about their isotope ecology. Recent modern studies have demonstrated that isotopes in small mammal tissues track local climate and environmental factors (Gehler et al., 2012; Smiley et al., 2015). Most modern studies have focussed on exploring the relationship between $\delta^{18}O_{PO4}$ of wild Muroidea teeth and local $\delta^{18}O_{mw}$ in temperate settings, where ^{18}O-enriched water from food has less of an influence on the $\delta^{18}O$ of small mammal body water (D'Angela and Longinelli, 1990; Longinelli et al., 2003; Navarro et al., 2004; Royer et al., 2013a). The specific modern relationships observed between rodent $\delta^{18}O_{PO4}$ and local $\delta^{18}O_{mw}$ are then applied to fossil or archaeological rodent teeth to reconstruct seasonal and mean annual air temperatures, because of the correlation between $\delta^{18}O_{mw}$ and mean annual temperature that occurs at high latitudes (Héran et al., 2010; Navarro et al., 2004; Royer et al., 2014, 2013b; Tütken et al., 2006). In order to explore the influence of moisture availability and aridity on the isotopic composition of small mammal tissue, the $\delta^{18}O$ and $\delta^{13}C$ composition of modern gerbil tooth apatite, and the $\delta^{13}C$ and $\delta^{15}N$ composition of gerbil bone collagen were determined across an aridity transect extending from the Mediterranean coast to the Sahara Desert in northwestern Africa (Chapter 5).

This first hypothesis of the thesis was to test whether the oxygen, carbon and nitrogen isotope values of modern gerbil tissues increased with aridity. The results show a robust relationship between the $\delta^{18}O$ composition of gerbil teeth and MAP, supporting hypothesis 1 (see section 1.4). They show that in semi-arid and arid environments the $\delta^{18}O$ of small mammals strongly reflects moisture availability, rather than local meteoric water. This indicates the significant influence that ^{18}O-enriched water from plants has on the $\delta^{18}O$ composition of small mammal body water and tissues, but also that water from food may significantly influence the $\delta^{18}O$ composition of small mammals during past arid events even in more mesic settings. Predictably, the $\delta^{13}C$ composition of gerbil tissue ($\delta^{13}C_{mt}$ and $\delta^{13}C_{col}$) reflected C_3 and C_4 dietary inputs. A significant negative correlation was also demonstrated between the $\delta^{13}C$ composition of gerbil tissues and MAP, suggesting that $\delta^{13}C$ of gerbil tissues partly reflected the isotopic effects of water deficit on the predominantly C_3 vegetation, also supporting hypothesis 1. However, $\delta^{13}C_{mt}$ was variable at each site, likely reflecting gerbils' individual microhabitats and the short period that the tissues (especially the teeth) reflect. The $\delta^{15}N_{col}$ did not correlate with MAP, and therefore did not reflect aridity, disproving hypothesis 1. It is suggested that gerbils from two of the modern study sites likely consumed agricultural grains as part of their diet, hinting that perhaps the $\delta^{15}N$ aridity signal from plants is undetectable due to farming impacts on soils and crops.

As outlined in Chapter 1, previous studies using isotopes in small mammal tissues to reconstruct past climate have given little consideration to the temporal periods reflected by teeth (Hopley et al., 2006; Hynek et al., 2012).

There is also a suggestion in the literature that post-weaning teeth should be used in the construction of proxy records to avoid a nursing (pre-weaning) effect (Lindars et al., 2001). However, as yet no systematic study determining the isotope values of both molars and incisors have given reason to apply this methodology. Therefore, within the modern study the isotope variation between rodent teeth was also explored to evaluate which tooth type (molars vs. incisors) should be used in the construction of proxy climate records and to test hypothesis 2 (see section 1.4). The inter-tooth variation study showed that M1's and M2's had similar $\delta^{18}O$ and $\delta^{13}C$ values. The similarity is consistent with the observation that the 1st and 2nd molars form and mineralise within days of each other so are formed from the same body water and bicarbonate pools. Larger isotopic offsets were found between the incisor and molar teeth in the gerbils (up to ~5‰ in $\delta^{18}O$ and ~4‰ in $\delta^{13}C$). This offset is explained by the tooth growth and mineralisation periods, supporting hypothesis 2. This is because molars form only in the breeding season, which is in spring and often extending into summer, whereas incisors grow continuously throughout life. The demonstration of these isotopic differences between different tooth types, with distinct growth patterns, leads to a new potential method for the construction of seasonally resolved proxy records from small mammals that have both permanently rooted molar teeth and continuously growing incisor teeth (as explored Chapter 6).

The results from the modern study show that the $\delta^{18}O$ composition of small mammal teeth primarily reflects aridity in semi-arid to arid environments. Thus $\delta^{18}O$ values in non-obligate drinking small mammals should be a good proxy for

terrestrial palaeoaridity. $\delta^{13}C$ data compliment the $\delta^{18}O$ values, but care should be taken with the interpretation of the $\delta^{13}C$ data due to the microhabitat and short time periods reflected in the teeth. The modern study showed that isotopes in small mammal tissues accurately record local climate and environmental conditions, but close attention to the developmental periods, and behaviour of the animals is required in order to make the climate and environmental interpretations from the tissues meaningful.

8.2. Isotope-based proxy climate and environment records from El Harhoura 2 and Taforalt

The second part of the thesis determined the $\delta^{18}O$ and $\delta^{13}C$ values of *Meriones* teeth from Taforalt and El Harhoura 2 to construct a record of Late Pleistocene palaeoaridity and past vegetation cover (Chapter 6). The results showed no significant differences between the $\delta^{18}O$ values of molars and incisors at both cave sites. Therefore, isotope-based MAP reconstructions, using the relationship established in the modern study (Chapter 5), were calculated using $\delta^{18}O$ values from both tooth types. The MAP reconstructions revealed the occurrence of relatively humid and arid shifts during the Late Pleistocene in the Mediterranean coastal strip of North Africa. However, according to these calculations neither the Mediterranean nor the Atlantic coastal regions experienced hyper-arid conditions (e.g. less than 200mm MAP) during the Late Pleistocene. The records show that the MIS 5, 4 and 3 levels at both El Harhoura 2 and Taforalt were wetter, or had similar humidity to present. Level 2 (c.20-13.5ka) at El Harhoura 2 is identified as the driest period in the Late Pleistocene sequence (MAP = 250-400mm), but the MAP reconstructions

indicate that the same period at Taforalt (c.30-15ka cal BP) was wetter than present.

The isotope-based MAP reconstructions from the Late Pleistocene sequences at El Harhoura 2 and Taforalt show good consistency with palaeoclimate evidence from pollen records off the Atlantic and Mediterranean coasts of Morocco (Bout-Roumazeilles et al., 2007; Hooghiemstra et al., 1992; Moreno et al., 2005), macrocharcoal records from Taforalt (Ward, 2007) and faunal proxies from El Harhoura 2 (Cornette et al., 2015; Stoetzel et al., 2014, 2013, 2011) (see Chapter 7). However, the estimations of increased MAP at Taforalt during MIS 2 (Levels Y1-Y6, c.30-15ka cal BP) are not in agreement with other proxies, such as marine records from the Alboran Sea (Bout-Roumazeilles et al., 2007; Combourieu Nebout et al., 2009; Fletcher et al., 2010b) and lake records from the Atlas and Iberia (El Bait et al., 2014; Moreno et al., 2012; Rhoujjati et al., 2010), that all consistently show this was a cool, arid period across the western Mediterranean region. It is notable that the isotope-based MAP reconstructions also show that El Harhoura 2 was arid during this period (Level 2, c.20-13.5ka). In Chapter 6 it was suggested that the low $\delta^{18}O$ values in Levels Y1-Y6 at Taforalt, instead of reflecting increased humidity, may result from the effect of lower atmospheric temperatures on plant water balances. It is widely recognised that global temperatures were lower during MIS 2, and in the western Mediterranean region, it is estimated that growing season temperatures were ~5°C lower than present, while the temperature of the coldest month ranged between -10 to -15°C (Fletcher et al., 2010b). It is known that lower atmospheric temperatures reduce rates of evapotranspiration,

therefore under such conditions in the past, $\delta^{18}O$ values in plants (and thus in gerbils' teeth) are more likely to reflect local meteoric water values rather than humidity. Consequently, relatively low $\delta^{18}O$ values in Levels Y1-Y6 at Taforalt likely reflect reduced evaporation as a result of lower temperatures. It is thought that this effect occurs at Taforalt and not at El Harhoura 2, where $\delta^{18}O$ values indicate aridity during MIS 2, because of the larger annual temperature gradient resulting from the higher altitude, more continental location of Taforalt. This major inconsistency raises a limitation in the use of modern studies to understand the responses of small mammal $\delta^{18}O$ values to rainfall patterns and humidity or aridity. Although modern analogue studies are useful for helping understand and interpret isotope data, it is extremely difficult to have a modern study that covers all potential causes of observed effects, and therefore replicates all conditions in the past.

The $\delta^{13}C$ values of *Meriones* teeth indicate that C_3 vegetation was predominant in the Atlantic coastal region of North Africa throughout the Late Pleistocene, while on the Mediterrenean coast of northeastern Morocco there were small increases in the proportion of C_4 plants relative to C_3 species during MIS 2, 3 and 5. The expansion of C_4 plants during the Late Pleistocene likely results from lower temperatures and pCO_2, conditions in which C_4 plants have an advantage over C_3 plants. This data also shows that small mammals are extremely sensitive to discreet environmental shifts and changes in vegetation cover because of their fast tissue turnover times. The $\delta^{13}C$ values of *Meriones* incisors were found to be significantly higher relative to molar teeth at both El Harhoura 2 and Taforalt. It is assumed that this reflects a predator bias in the

$\delta^{13}C$ composition of the incisors, hinting that the *Meriones* were more likely to be predated upon in the arid summer/autumn months. Furthermore, analysis of inter-tooth variation in $\delta^{13}C$ within levels at El Harhoura 2 showed that the pattern reflected in the $\delta^{13}C$ values of molars and incisors changed throughout the Late Pleistocene levels. In the more humid lower levels (Levels 7-11) incisor teeth $\delta^{13}C$ is significantly higher relative to that of the molars, yet in the more arid levels (Levels 6-2) there is no difference in $\delta^{13}C$ between molars and incisors. This pattern must either result from a change in predator or predator behaviour, or from a change in seasonal climate. These results have significant implications because they suggest that the isotope signals of molars and incisors appear to reflect different seasons, and as suggested in the modern study could provide a method for the construction of seasonally resolved proxy records from small mammal teeth. The analysis of *Meriones* teeth from El Harhoura 2 and Taforalt shows that future studies using small teeth to construct proxy climate records must give consideration the temporal period of tooth formation.

8.3. Past climate in North Africa and implications for human occupations and cultural behaviour

The archaeological evidence suggests that MSA populations occupied El Harhoura 2 and Taforalt intensively in MIS 5, when proxy records from both cave sites show the climate was humid. However, MSA occupations in the region do not only occur during humid climate episodes, and there are further less intense human occupations at both sites occurring when climate was drier at the end of MIS 5 and in MIS 4 and 3, disproving hypothesis 3 which stated

the MSA occupation of Taforalt and El Hahoura 2 was associated with humid climate epsidoes. It is thought that the more intense occupations during MIS 5 at both sites result from greater populations densities in the region during this period. At El Harhoura 2 and Taforalt the cultural transition from MSA to the LSA occurs during MIS 2, which most palaeoclimate records indicate as a marked cool, arid period across the western Mediterranean region (with the exception of the isotope-based MAP reconstruction at Taforalt), supporting hypothesis 4 (see section 1.4). This hints that this significant cultural transition may be related to changing environmental conditions in the region.

The isotope-based MAP reconstructions presented in this thesis, show that the Mediterranean coastal strip of North Africa did not experience hyper-arid conditions during the Late Pleistocene. This implies that the region to the north and north west of the Atlas remained distinct from the arid conditions experienced in the Sahara Desert. It is suggested that the environments around El Harhoura 2 and Taforalt acted as a refugia for human populations. Although the archaeological and palaeoclimate evidence from Taforalt and El Harhoura 2 supports hypothesis 5 by showing that the Mediterranean coastal strip of North Africa acted as a refugium for humans during the Late Pleistocene, more evidence is needed from across the region to explore this further. One plausible explanation for the continuously relatively mild conditions during the Late Pleistocene is the influence of oceanic effects in the Mediterranean region of North Africa. This is particularly the case for El Harhoura 2, which is presently located directly on the coast. Although oceanic influences may have been lower at Taforalt given its distance from the coast (~40km), it is likely that the

topographical variable nature of the landscape around the cave would have been particularly appealing to hunter-gatherers providing shelter and extending seasons for plant and animal exploitation.

8.4. Future Research

The results of the modern study have shown that small mammal tissues accurately record local climate and environmental conditions in semi-arid and arid environments. However, further modern analogue studies on wild small mammal populations, especially in more arid settings, are required to explore the effects of their unique physiologies on the isotope composition of their tissues. It would be useful to carry out further modern studies on different species of small mammal, such as those that live in semi-arid and arid environments but have a greater reliance on drinking water e.g. voles, and also more generalist species to encapsulate a more homogenous dietary signal. Generally, modern and fossil isotope studies need to focus more on understanding how the animals' biology influences the isotope values of the tissues. For example, the modern study in this thesis has highlighted that water from plants can strongly affect the $\delta^{18}O$ values of small mammal tissues.

The modern and archaeological studies also demonstrated that the isotope values of molars and incisors, which form over different temporal periods, differ. A larger systematic study of inter-tooth variation of modern rodent teeth is required to get a better handle on the isotopic variation between tooth types, and to explore whether seasonal climate effects can be detected. Given the strong indications for seasonal differences between tooth types shown in this

study, one more robust way to address the question is to apply high-resolution laser ablation methods to individual teeth (Passey and Cerling, 2006). This method would also allow an understanding of isotopic variation within individual teeth. As molars form over an extremely short period it is hypothesised that the variation within these teeth would be lower in comparison to that of incisors, which are likely to have higher intra-tooth variation because they form over a period of ~3 months.

Meriones is common in cave assemblages in North Africa and across the Mediterranean region as a whole. Now that the isotopic variability within this genus has been established, and that the oxygen isotope values within its teeth are shown to strongly reflect moisture availability, further studies using *Meriones* from other archaeological cave sites could be used to construct records of palaeoaridity from across the region. However, the results from this thesis have outlined the effect that lower temperatures in the past can have on this relationship. Future modern studies could investigate this effect further by exploring the $\delta^{18}O$ values of small mammals across a transect with similar MAPs to those in the modern study, but where MATs are lower.

9. References

Abouelmagd, A., Sultan, M., Milewski, A., Kehew, A.E., Sturchio, N.C., Soliman, F., Krishnamurthy, R.V., Cutrim, E., 2012. Toward a better understanding of palaeoclimatic regimes that recharged the fossil aquifers in North Africa: Inferences from stable isotope and remote sensing data. Palaeogeogr. Palaeoclimatol. Palaeoecol. 329-330, 137–149. doi:10.1016/j.palaeo.2012.02.024

Adamou-Djerbaoui, M., Denys, C., Chaba, H., Seid, M.M., Djelaila, Y., Labdelli, F., Adamou, M.S., 2013. Etude du regime alimentarie d'un rongeur nuisible (*Meriones shawii* Duvernoy, 1842, Mammalia, Rodentia) en Algerie. Leban. Sci. J. 14, 15–32.

Adamou-Djerbaouiz, M., Djelaila, Y., Adamou, M.S., Baziz, B., Nicolas, V., Denys, C., 2010. Préférence édaphique et pullulation chez *Meriones shawii* (Mammalia, Rodentia) dans la region de Tiaret (Algerie). Rev. Écol. (Terre Vie) 65, 63–72.

Addison, W.H.F., Appleton, J.L., 1915. The structure and growth of the incisor teeth of the albino rat. J. Morphol. 26, 43–96.

Aldeias, V., Goldberg, P., Dibble, H.L., El Hajraoui, M.A., 2014. Deciphering site formation processes through soil micromorphology at Contrebandiers Cave, Morocco. J. Hum. Evol. 2013, 1–23. doi:10.1016/j.jhevol.2013.12.016

Allen, H., 2001. Mediterranean Ecogeography. Prentice Hall, Harlow.

Allen, J.R.M., Huntley, B., Watts, W.A., 1996. The vegetation and climate of northwest Iberia over the last 14,000 years. J. Quat. Sci. 11, 125–147.

Allison, G.B., Hughes, M.W., 1983. The use of natural tracers as indicators of soil-water movement in a temperate semi-arid region. J. Hydrol. 60, 157–173.

Amans, A., 2012. L'industrie lithique néolithique (Chapitre XII), in: El Hajraoui, M.A., Nespoulet, R., Debénath, A., Dibble, H. (Eds.), Préhistoire de La Région de Rabat- Témara. Villes et Sites Archéologiques Du Maroc. Partie 2: Grotte d'El Harhoura 2, Vol. III. Royaume du Maroc, Ministere de la culture, Institut National des Sciences de l'Archéologie et du Patrimoine, Rabat, pp. 87–90.

Ambrose, S.H., 2000. Controlled diet and climate experiments on nitrogen isotope ratios of rats, in: Amrose, S.H., Katzenberg, M.A. (Eds.), Biogeochemical Approaches to Palaeodietary Analysis. Kluwer

Academic/Plenum Publishers, New York, pp. 243–259.

Ambrose, S.H., DeNiro, M.J., 1986. The isotopic ecology of East African mammals. Oecologia 69, 395–406.

Ambrose, S.H., Norr, L., 1993. Experimental evidence for the relationship of the carbon isotope ratios of whole diet and dietary protein , in: Lambert, J.B., Grupe, G. (Eds.), Prehistoric Human Bone: Archaeology at a Molecular Level. Springer-Verlag, Heidelberg, pp. 1–37.

Amundson, R., Austin, A. T., Schuur, E. A. G., Yoo, K., Matzek, V., Kendall, C., Uebersax, A., Brenner, D., Baisden, W.T., 2003. Global patterns of the isotopic composition of soil and plant nitrogen. Global Biogeochem. Cycles 17, n/a–n/a. doi:10.1029/2002GB001903

Andrews, P., 1990. Owls, Caves and Fossils. Natural History Museum Publications, London.

Arens, N.C., Jahren, A.H., Amundson, R., 2000. Can C_3 plants faithfully record the carbon isotopic composition of atmospheric carbon dioxide? Paleobiology 26, 137–164.

Armitage, S., Jasim, S., Marks, A., Parker, A., 2011. The Southern Route “Out of Africa”: Evidence for an Early Expansion of Modern Humans into Arabia. Science 331, 453–456. doi:10.1594/PANGAEA.755114

Arppe, L., Kaakinen, A., Passey, B.H., Zhang, Z., Fortelius, M., 2015. Small mammal tooth enamel carbon isotope record of C_4 grasses in late Neogene China. Glob. Planet. Change 133, 288–297. doi:10.1016/j.gloplacha.2015.09.003

Asada, T., Warner, B.G., Aravena, R., 2005. Nitrogen isotope signature variability in plant species from open peatland. Aquat. Bot. 82, 297–307. doi:10.1016/j.aquabot.2005.05.005

Aulagnier, S., Haffner, P., Mitchell-Jones, A.J., Moutou, F., Zima, J., 2009. Mammals of Europe, North Africa and the Middle East. A&C Black, London.

Aulagnier, S., Thevenot, M., 1986. Catalogue des mammifères sauvages du Maroc. Trav. l’Institut Sci. Rabat, Série Zool. 41, 1–164.

Austin, A.., Vitousek, P., 1998. Nutrient dynamics on a precipitation gradient in Hawaii. Oecologia 113, 519–529.

Ayliffe, L.K., Chivas, A.R., 1990. Oxygen isotope composition of the bone

phosphate of Australian kangaroos: Potential as a palaeoenvironmental recorder. Geochim. Cosmochim. Acta 54, 2603–2609. doi:10.1016/0016-7037(90)90246-H

Ayliffe, L.K., Lister, A.M., Chivas, A.R., 1992. The preservation of glacial-interglacial climatic signatures in the oxygen isotopes of elephant skeletal phosphate. Palaeogeogr. Palaeoclimatol. Palaeoecol. 99, 179–191.

Badeck, F.W., Tcherkez, G., Nogués, S., Piel, C., Ghashghaie, J., 2005. Post-photosynthetic fractionation of stable carbon isotopes between plant organs - A widespread phenomenon. Rapid Commun. Mass Spectrom. 19, 1381–1391. doi:10.1002/rcm.1912

Balasse, M., Ambrose, S.H., Smith, A.B., Price, T.D., 2002. The Seasonal Mobility Model for Prehistoric Herders in the South-western Cape of South Africa Assessed by Isotopic Analysis of Sheep Tooth Enamel. J. Archaeol. Sci. 29, 917–932. doi:10.1006/jasc.2001.0787

Balout, L., 1965. Données nouvelles sur le problème du moustérien en Afrique du Nord. Actas del V Congresso Panafricano de Prehistoria y de Estudio del Cuaternario. Publicaciones del Museo Arqueologico Sant Cruz de Tenerife. Tome 1, 137–145.

Balter, M., 2011. Was North Africa the launch pad for modern human migrations? Science 331, 20–23. doi:10.1126/science.331.6013.20

Balter, V., Simon, L., Fouillet, H., Lécuyer, C., 2006. Box-modeling of $^{15}N/^{14}N$ in mammals. Oecologia 147, 212–22. doi:10.1007/s00442-005-0263-5

Barbour, M.M., Farquhar, G.D., 2000. Relative humidity- and ABA-induced variation in carbon and oxygen isotope ratios of cotton leaves. Plant, Cell Environ. 23, 473–485.

Barnola, J.M., Raynaud, Y.S., Korotkevich, Y.S., Lorius, C., 1987. Vostok ice core provides 160,000-year record of atmospheric CO2. Nature 329, 408–414.

Barton, R.N.E., Bouzouggar, a., Collcutt, S.N., Gale, R., Higham, T.F.G., Humphrey, L.T., Parfitt, S., Rhodes, E., Stringer, C.B., Malek, F., 2005. The Late Upper Palaeolithic Occupation of the Moroccan Northwest Maghreb during the Last Glacial Maximum. African Archaeol. Rev. 22, 77–100. doi:10.1007/s10437-005-4190-y

Barton, R.N.E., Bouzouggar, A., Collcutt, S.N., Carrión Marco, Y., Clark-Balzan, L., Debenham, N.C., Morales, J., 2016. Reconsidering the MSA to LSA transition at Taforalt Cave (Morocco) in the light of new multi-proxy dating

evidence. Quat. Int. 1–14. doi:10.1016/j.quaint.2015.11.085

Barton, R.N.E., Bouzouggar, A., Collcutt, S.N., Schwenninger, J., Clark-balzan, L., 2009. OSL dating of the Aterian levels at Dar es-Soltan I (Rabat , Morocco) and implications for the dispersal of modern *Homo sapiens*. Quat. Sci. Rev. 28, 1914–1931. doi:10.1016/j.quascirev.2009.03.010

Barton, R.N.E., Bouzouggar, A., Hogue, J.T., Lee, S., Collcutt, S.N., Ditchfield, P., 2013. Origins of the Iberomaurusian in NW Africa: New AMS radiocarbon dating of the Middle and Later Stone Age deposits at Taforalt Cave, Morocco. J. Hum. Evol. 65, 266–281. doi:10.1016/j.jhevol.2013.06.003

Barton, R.N.E., Lane, C.S., Albert, P.G., White, D., Collcutt, S.N., Bouzouggar, A., Ditchfield, P., Farr, L., Oh, A., Ottolini, L., Smith, V.C., Van Peer, P., Kindermann, K., 2014. The role of cryptotephra in refining the chronology of Late Pleistocene human evolution and cultural change in North Africa. Quat. Sci. Rev. 1–19. doi:10.1016/j.quascirev.2014.09.008

Baugh, A.T., West, A.G., Rickart, E.A., Cerling, T.E., Ehleringer, J.., Dearing, M.D., 2004. Stable Isotope Ratios ($\delta^{15}N$ and $\delta^{13}C$) of Syntopic Shrews (Sorex). Southwest. Nat. 49, 493–500.

Belabbas, S., Butet, A., 1994. The diet of the *Meriones*, *Meriones shawii*, in the nature reserve of Mergueb, Algeria. Pol. Ecol. Stud. 20, 293–303.

Belcastro, M.G., Condemi, S., Mariotti, V., 2010. Funerary practices of the Iberomaurusian population of Taforalt (Tafoughalt, Morocco, 11-12,000 BP): the case of Grave XII. J. Hum. Evol. 58, 522–32. doi:10.1016/j.jhevol.2010.03.011

Benkaddour, A., Lamb, H., Leng, M., Gasse, F., 2005. Stable isotope records of Holocene environmental change from Moroccan lakes: an emerging synthesis, in: PAGES Open Science Meeting, Beijing.

Blome, M.W., Cohen, A.S., Tryon, C. a., Brooks, A.S., Russell, J., 2012. The environmental context for the origins of modern human diversity: A synthesis of regional variability in African climate 150,000–30,000 years ago. J. Hum. Evol. 62, 563–592. doi:10.1016/j.jhevol.2012.01.011

Bogaard, A., Heaton, T.H.E., Poulton, P., Merbach, I., 2007. The impact of manuring on nitrogen isotope ratios in cereals: archaeological implications for reconstruction of diet and crop management practices. J. Archaeol. Sci. 34, 335–343. doi:10.1016/j.jas.2006.04.009

Bond, G., 1997. A Pervasive Millennial-Scale Cycle in North Atlantic Holocene

and Glacial Climates. Science 278, 1257–1266. doi:10.1126/science.278.5341.1257

Bond, G., Broecker, W., Johnsen, S., McManus, J., Labeyrie, L., Jouzel, J., Bonani, G., 1993. Correlations between climate records from North Atlantic sediments and Greenland ice. Nature 365, 143–147.

Boudad, L., Hammouti, K. El, Nespoulet, R., El Hajraoui, M. A., 2012. Chapitire IV. Le remplissage sedimentaire. Etude preliminaire, in: El Hajraoui, M.A., Nespoulet, R., Debénath, A., Dibble, H. (Eds.), Préhistoire de La Région de Rabat- Témara, Villes et Sites Archéologiques Du Maroc, Vol. III. Royaume Du Maroc, Minist? Ere de La Culture. Royaume du Maroc, Ministere de la culture, Institut National des Sciences de l'Archéologie et du Patrimoine, Rabat, pp. 31–34.

Bout-Roumazeilles, V., Combourieu Nebout, N., Peyron, O., Cortijo, E., Landais, a., Masson-Delmotte, V., 2007. Connection between South Mediterranean climate and North African atmospheric circulation during the last 50,000yrBP North Atlantic cold events. Quat. Sci. Rev. 26, 3197–3215. doi:10.1016/j.quascirev.2007.07.015

Bouzouggar, A., Barton, N., Vanhaeren, M., d'Errico, F., Collcutt, S., Higham, T., Hodge, E., Parfitt, S., Rhodes, E., Schwenninger, J.-L., Stringer, C., Turner, E., Ward, S., Moutmir, A., Stambouli, A., 2007. 82,000-year-old shell beads from North Africa and implications for the origins of modern human behavior. Proc. Natl. Acad. Sci. 104, 9964–9. doi:10.1073/pnas.0703877104

Bouzouggar, A., Barton, R.N.E., 2012. The identity and timing of the Aterian in Morocco, in: Hublin, J.-J., McPherron, S.P. (Eds.), Modern Origins: A North African Perspective, Vertebrate Paleobiology and Paleoanthropology. Springer Netherlands, Dordrecht, pp. 93–105. doi:10.1007/978-94-007-2929-2

Bouzouggar, A., Barton, R.N.E., Blockley, S., Bronk-Ramsey, C., Collcutt, S.N., Gale, R., Higham, T.F.G., Humphrey, L.T., Parfitt, S., Turner, E., Ward, S., 2008. Reevaluating the Age of the Iberomaurusian in Morocco. African Archaeol. Rev. 25, 3–19. doi:10.1007/s10437-008-9023-3

Bowen, G.J., 2010. Isoscapes: Spatial Pattern in Isotopic Biogeochemistry. Annu. Rev. Earth Planet. Sci. 38, 161–187. doi:10.1146/annurev-earth-040809-152429

Bowen, G.J., Revenaugh, J., 2003. Interpolating the isotopic composition of modern meteoric precipitation. Water Resour. Res. 39, 1299. doi:10.1029/2003WR002086.

Bowen, G.J., Wilkinson, B., 2002. Spatial distribution of $\delta^{18}O$ in meteoric precipitation. Geology 30, 315–318. doi:10.1130/0091-7613(2002)030<0315

Bronk Ramsey, C., 2009a. Bayesian Analysis of Radiocarbon Dates. Radiocarbon 51, 337–360. doi:10.2458/azu_js_rc.v51i1.3494

Bronk Ramsey, C., 2009b. Dealing with outliers and offsets in radiocarbon dating. Radiocarbon 51, 1023–1045.

Brookman, T.H., Ambrose, S.H., 2012. Seasonal variation in kangaroo tooth enamel oxygen and carbon isotopes in southern Australia. Quat. Res. 78, 256–265. doi:10.1016/j.yqres.2012.05.011

Bryant, D., Froelich, P.N., 1995. A model of oxygen isotope fractionation in body water of large mammals. Geochim. Cosmochim. Acta 59, 4523–4537. doi:10.1016/0016-7037(95)00250-4

Bryant, D., Koch, P., Froelich, P.N., Showers, W.J., Genna, B.J., 1996. Oxygen isotope partitioning between phosphate and carbonate in mammalian apatite. Geochim. Cosmochim. Acta 60, 5145–5148.

Buckle, C., 1996. Weather and Climate in Africa. Longman, Harlow.

Buffenstein, R., Jarvis, J.U., 1985. Thermoregulation and metabolism in the smallest African gerbil, *Gerbillus pusillus*. J. Zool. 205, 107–121.

Cacho, I., Grimalt, J., Canals, M., Sbaffi, L., Shackleton, N., Schonfeld, J., Zahn, R., 2001. Variability of the western Mediterranean Sea surface temperature during the last 25,000 years and its connection with Northern Hemisphere climatic changes. Paleoceanography 16, 40–52.

Cacho, I., Grimalt, J., Pelejero, C., Canals, M., Sierro, J., Flores, J, A., Shackleton, N., 1999. Dansgaard-Oeschger and Heinrich event imprints in Alboran Sea paleotemperatures. Paleoceanography 14, 698–705.

Cacho, I., Grimalt, J.O., Sierro, F.J., Shackleton, N., Canals, M., 2000. Evidence for enhanced Mediterranean thermohaline circulation during rapid climatic coolings. Earth Planet. Sci. Lett. 183, 417–429. doi:10.1016/S0012-821X(00)00296-X

Campmas, E., 2012. Charactérisation de l'occupation des sites de la région de Témara (Maroc) au Pléistocène supérieur et nouvelles données sur la subsistance des Hommes du Paléolithique moyen d'Afrique du Nord. Exemple des approches taphonomiques et archéozoologiques menée. University of Bordeaux. PhD Thesis.

Campmas, E., Michel, P., Costamagno, S., Amani, F., Stoetzel, E., Nespoulet, R., El Hajraoui, M.A., 2015. Were Upper Pleistocene human/non-human predator occupations at the Témara caves (El Harhoura 2 and El Mnasra, Morocco) influenced by climate change? J. Hum. Evol. 78, 122-143. doi:10.1016/j.jhevol.2014.08.008

Camps, G., 1974. Les civilisations préhistoriques de l'Afrique du Nord et du Sahara. Doin, Paris.

Carleton, S. A, Martínez del Rio, C., 2005. The effect of cold-induced increased metabolic rate on the rate of $\delta^{13}C$ and $\delta^{15}N$ incorporation in house sparrows (*Passer domesticus*). Oecologia 144, 226–32. doi:10.1007/s00442-005-0066-8

Carrión, J.S., Fuentes, N., González-Sampériz, P., Sánchez Quirante, L., Finlayson, J.C., Fernández, S., Andrade, A., 2007. Holocene environmental change in a montane region of southern Europe with a long history of human settlement. Quat. Sci. Rev. 26, 1455–1475. doi:10.1016/j.quascirev.2007.03.013

Castañeda, I.S., Mulitza, S., Schefuss, E., Lopes dos Santos, R. A, Sinninghe Damsté, J.S., Schouten, S., 2009. Wet phases in the Sahara/Sahel region and human migration patterns in North Africa. Proc. Natl. Acad. Sci. 106, 20159–63. doi:10.1073/pnas.0905771106

Caton-Thompson, G., 1946. The Aterian Industry: its place and significance in the Palaeolithic world. J. R. Anthropol. Inst. Gt. Britain Irel. 76, 87–130.

Cerling, T.E., Harris, J.M., 1999. Carbon isotope fractionation between diet and bioapatite in ungulate mammals and implications for ecological and paleoecological studies. Oecologia 120, 347–363. doi:10.1007/s004420050868

Cerling, T.E., Harris, J.M., Macfadden, B.J., Leakey, M.G., Quadek, J., Eisenmann, V., Ehleringer, J.R., 1997. Global vegetation change through the Miocene / Pliocene boundary. Nature 389, 153–158.

Cerling, T.E., Hart, J.A., Hart, T.B., 2004. Stable isotope ecology in the Ituri Forest. Oecologia 138, 5–12. doi:10.1007/s00442-003-1375-4

Cernusak, L. A, Pate, J.S., Farquhar, G.D., 2002. Diurnal variation in the stable isotope composition of water and dry matter in fruiting *Lupinus angustifolius* under field conditions. Plant, Cell Environ. 25, 893–907. doi:10.1046/j.1365-3040.2002.00875.x

Cernusak, L. A., Tcherkez, G., Keitel, C., Cornwell, W.K., Santiago, L.S., Knohl,

A., Barbour, M.M., Williams, D.G., Reich, P.B., Ellsworth, D.S., Dawson, T.E., Griffiths, H.G., Farquhar, G.D., Wright, I.J., 2009. Why are non-photosynthetic tissues generally ^{13}C enriched compared with leaves in C_3 plants? Review and synthesis of current hypotheses. Funct. Plant Biol. 36, 199–213. doi:10.1071/FP08216

Cheddadi, R., Fady, B., François, L., Hajar, L., Suc, J.-P., Huang, K., Demarteau, M., Vendramin, G.G., Ortu, E., 2009. Putative glacial refugia of *Cedrus atlantica* deduced from Quaternary pollen records and modern genetic diversity. J. Biogeogr. 36, 1361–1371. doi:10.1111/j.1365-2699.2008.02063.x

Cheddadi, R., Lamb, H.F., Guiot, J., van der Kaars, S., 1998. Holocene climatic change in Morocco: a quantitative reconstruction from pollen data. Clim. Dyn. 14, 883–890. doi:10.1007/s003820050262

Choi, W.J., Arshad, M. a., Chang, S.X., Kim, T.H., 2006. Grain $\delta^{15}N$ of crops applied with organic and chemical fertilizers in a four-year rotation. Plant Soil 284, 165–174. doi:10.1007/s11104-006-0038-8

Clark, J.D., 1982. The Cambridge History of Africa: From the Earliest Times to c. 500 B.C., The Cambridge History of Africa. Cambridge University Press, Cambridge.

Clark-Balzan, L., 2012. Dating the Aterian using techniques of Luminescene dating and implications for mapping the dispersal of modern Homo sapiens. University of Oxford. PhD Thesis.

Clark-Balzan, L.A., Candy, I., Schwenninger, J.-L., Bouzouggar, A., Blockley, S., Nathan, R., Barton, R.N.E., 2012. Coupled U-series and OSL dating of a Late Pleistocene cave sediment sequence, Morocco, North Africa: Significance for constructing Palaeolithic chronologies. Quat. Geochronol. 12, 53–64. doi:10.1016/j.quageo.2012.06.006

Clementz, M.T., Koch, P.L., 2001. Differentiating aquatic mammal habitat and foraging ecology with stable isotopes in tooth enamel. Oecologia 129, 461–472. doi:10.1007/s004420100745

Close, A., Wendorf, F., 1990. North Africa at 18,000 BP, in: Gamble, C., Soffer, O. (Eds.), The World at 18,000 BP. Unwin Hyman, London, pp. 41–57.

Coady, J.M., Toto, P.D., Santangelo, M.V., 1967. Histology of the mouse incisor. J. Dent. Res. 46, 384–388. doi:10.1177/00220345670460021201

Codron, J., Codron, D., Lee-Thorp, J. a., Sponheimer, M., Bond, W.J., de Ruiter, D., Grant, R., 2005. Taxonomic, anatomical, and spatio-temporal

variations in the stable carbon and nitrogen isotopic compositions of plants from an African savanna. J. Archaeol. Sci. 32, 1757–1772. doi:10.1016/j.jas.2005.06.006

Codron, J., Duffy, K.J., Avenant, N.L., Sponheimer, M., Leichliter, J., Paine, O., Sandberg, P., Codron, D., 2015. Stable isotope evidence for trophic niche partitioning in a South African savanna rodent community. Curr. Zool. 61, 397–411.

Collatz, G.J., Berry, A., Clark, J.S., 1998. Effects of climate and atmospheric CO_2 partial pressure on the global distribution of C_4 grasses: present, past, and future. Oecologia 114, 441–454.

Collina-Girard, J., 2001. La Crise Finiglaciaire à Gibraltar et l'Atlantide: tradition et géologie. Prehistoire Anthropol. Mediterr. 53–60.

Colmenero-Hidalgo, E., Flores, J.-A., Sierro, F.J., Bárcena, M.Á., Löwemark, L., Schönfeld, J., Grimalt, J.O., 2004. Ocean surface water response to short-term climate changes revealed by coccolithophores from the Gulf of Cadiz (NE Atlantic) and Alboran Sea (W Mediterranean). Palaeogeogr. Palaeoclimatol. Palaeoecol. 205, 317–336. doi:10.1016/j.palaeo.2003.12.014

Combourieu Nebout, N., Peyron, O., Dormoy, I., Desprat, S., Beaudouin, C., Kotthoff, U., Marret, F., 2009. Rapid climatic variability in the west Mediterranean during the last 25000 years from high resolution pollen data. Clim. Past 5, 503–521.

Combourieu Nebout, N., Turon, J.L., Zahn, R., Capotondi, L., Londeix, L., Pahnke, K., 2002. Enhanced aridity and atmospheric high-pressure stability over the western Mediterranean during the North Atlantic cold events of the past 50 ky. Geology 30, 863–866.

Cormie, A.B., Luz, B., Schwarcz, H.P., 1994. Relationship between the hydrogen and oxygen isotopes of deer bone and their use in the estimation of relative humidity. Geochim. Cosmochim. Acta 58, 3439–3449.

Cornette, R., Stoetzel, E., Baylac, M., Moulin, S., Hutterer, R., Nespoulet, R., El Hajraoui, M.A., Denys, C., Herrel, A., 2015. Shrews of the genus *Crocidura* from El Harhoura 2 (Témara, Morocco): The contribution of broken specimens to the understanding of Late Pleistocene–Holocene palaeoenvironments in North Africa. Palaeogeogr. Palaeoclimatol. Palaeoecol. 436, 1–8. doi:10.1016/j.palaeo.2015.06.020

Courty, M.-A., Goldberg, P., Macphail, R.., 1989. Soils and Micromorphology in Archaeology. Cambridge University Press, Cambridge, Cambridge.

Courty, M.-A., Vallverdu, J., 2001. The Microstratigraphic Record of Abrupt Climate Changes in Cave Sediments of the Western Mediterranean. Geoarchaeology 16, 467– 500.

Craine, J., Craine, J.M., Elmore, A.J., Aidar, M.P.M., Bustamante, M., Dawson, T.E., Hobbie, E. A., Kahmen, A., Mack, M.C., Mclauchlan, K.K., Michelsen, A., Nardoto, G.B., Pardo, L.H., 2009. Global patterns of foliar nitrogen isotopes and their relationships with climate, mycorrhizal fungi, foliar nutrient concentrations, and nitrogen availibility. New Phytologist. 1–13. doi:10.1111/j.1469-8137.2009.02917.x

Cremaschi, M., Lernia, S. Di, Garcea, E.A.A., 1998. Some insights on the Aterian in the Libyan Sahara: chronology, environment, and arcaheology. African Archaeol. Rev. 15, 261–286.

Crowley, B.E., Thorén, S., Rasoazanabary, E., Vogel, E.R., Barrett, M. a., Zohdy, S., Blanco, M.B., McGoogan, K.C., Arrigo-Nelson, S.J., Irwin, M.T., Wright, P.C., Radespiel, U., Godfrey, L.R., Koch, P.L., Dominy, N.J., 2011. Explaining geographical variation in the isotope composition of mouse lemurs (*Microcebus*). J. Biogeogr. 38, 2106–2121. doi:10.1111/j.1365-2699.2011.02551.x

D'Angela, D., Longinelli, A., 1990. Oxygen isotopes in living mammal's bone phosphate: further results. Chem. Geol. Isot. Geosci. Sect. 86, 75–82. doi:10.1016/0168-9622(90)90007-Y

D'Errico, F., Vanhaeren, M., Barton, N., Bouzouggar, A., Mienis, H., Richter, D., Hublin, J.-J., McPherron, S.P., Lozouet, P., 2009. Additional evidence on the use of personal ornaments in the Middle Paleolithic of North Africa. Proc. Natl. Acad. Sci. 106, 16051–16056.

Daly, M., 1975. Early use of solid food by a leaf-eating gerbil (*Psammomys obesus*). J. Mammaology 56, 509–511.

Dammhahn, M., Soarimalala, V., Goodman, S.M., 2013. Trophic Niche Differentiation and Microhabitat Utilization in a Species-rich Montane Forest Small Mammal Community of Eastern Madagascar. Biotropica 45, 111–118. doi:10.1111/j.1744-7429.2012.00893.x

Dansgaard, W., 1964. Stable isotopes in precipitation. Tellus 16, 436–468.

Dansgaard, W., Johnsen, S., Clausen, H.B., Dahl-Jensen, D., Gundestrup, N.S., Hammer, C.U., Hvidberg, C.S., Steffensen, J.P., Sveinbjornsdottir, A.E., Jouzel, J., Bond, G., 1993. Evidence for general instability of past climate from a 250-kyr ice-core record. Nature 364, 218–220.

Daugas, J., 2002. Le Néolithique du Maroc: pour un modèle d'évolution chronologique et culturelle. Bull. d'Archéologie Marocaine 19, 135–175.

Dawson, T.E., Mambelli, S., Plamboeck, A.H., Templer, P.H., Tu, K.P., 2002. Stable Isotopes in Plant Ecology. Annu. Rev. Ecol. Syst. 33, 507–559. doi:10.1146/annurev.ecolsys.33.020602.095451

Debénath, A., Raynal, J.-P., Roche, J., Texier, J.-P., Ferembach, D., 1986. Stratigraphie, habitat, typologie at devenir de l'Atérien Marocain: donneés récentes. L'Anthropologie 90, 233–246.

Debénath, A., Raynal, J.-P., Texier, J.-P., 1982. Position stratigraphique des restes humains paléolithiques marocains sur la base des travaux récents. C.R. Acad. Sci. Paris. 294, 1247–1250.

Delgado Huertas, A., Iacumin, P., Stenni, B., Sánchez Chillón, B., Longinelli, A., 1995. Oxygen isotope variations of phosphate in mammalian bone and tooth enamel. Geochim. Cosmochim. Acta 59, 4299–4305. doi:10.1016/0016-7037(95)00286-9

deMenocal, P., Ortiz, J., Guilderson, T., 2000. Abrupt onset and termination of the African Humid Period: rapid climate responses to gradual insolation forcing. Quat. Sci. Rev. 19, 347–361.

DeNiro, M.J., Epstein, S., 1981. Influence of diet on the distribution of nitrogen isotopes in animals. Geochim. Cosmochim. Acta 45, 341–351.

DeNiro, M.J., Epstein, S., 1978. Influence of diet on the distribution of carbon isotopes in animals pathways. Geochim. Cosmochim. Acta 42, 495–506.

Denton, G.., Broecker, W., Alley, R.B., 2006. The mystery interval 17.5 to 14.5 kyr ago, in: Brigham-Grette, J., Kull, C., Kiefer, T. (Eds.), PAGES News. pp. 14–16.

Dibble, H., Aldeias, V., Alvarez-Fernández, E., Blackwell, B., Hallett-Desguez, E., Jacobs, Z., Goldberg, P., Lin, S., Morala, A., Meyer, M., Olzsewski, D., Reed, K., Reed, D., Rezek, Z., Richter, D., Roberts, R., Sandgathe, D., Schurmans, U., Skinner, A.R., Steele, T.E., El-Hajraoui, M. A., 2012. New Excavations at the Site of Contrebandiers Cave, Morocco. Paleoanthropology 145–201. doi:10.4207/PA.2012.ART74

Dibble, H.L., Aldeias, V., Jacobs, Z., Olszewski, D.I., Rezek, Z., Lin, S.C., Alvarez-Fernández, E., Barshay-Szmidt, C.C., Hallett-Desguez, E., Reed, D., Reed, K., Richter, D., Steele, T.E., Skinner, A., Blackwell, B., Doronicheva, E., El Hajraoui, M. A., 2013. On the industrial attributions of the Aterian and Mousterian of the Maghreb. J. Hum. Evol. 2012.

doi:10.1016/j.jhevol.2012.10.010

Dongmann, G., Nürnberg, H.W., Förstel, H., Wagener, K., 1974. On the enrichment of $H_2{}^{18}O$ in the leaves of transpiring plants. Radiat. Environ. Biophys. 11, 41–52.

Dormoy, I., Peyron, O., Combourieu Nebout, N., Goring, S., Kotthoff, U., Magny, M., Pross, J., 2009. Terrestrial climate variability and seasonality changes in the Mediterranean region between 15 000 and 4000 years BP deduced from marine pollen records. Clim. Past 5, 615–632. doi:10.5194/cp-5-615-2009

Drake, N., Blench, R.M., Armitage, S.J., Bristow, C.S., White, K.H., 2011. Ancient watercourses and biogeography of the Sahara explain the peopling of the desert. Proc. Natl. Acad. Sci. U. S. A. 108, 458–62. doi:10.1073/pnas.1012231108

Drake, N., Breeze, P., Parker, A., 2013. Palaeoclimate in the Saharan and Arabian Deserts during the Middle Palaeolithic and the potential for hominin dispersals. Quat. Int. 300, 48–61. doi:10.1016/j.quaint.2012.12.018

Drucker, D.G., Kind, C.J., Stephan, E., 2011. Chronological and ecological information on Late-glacial and early Holocene reindeer from northwest Europe using radiocarbon (^{14}C) and stable isotope (^{13}C, ^{15}N) analysis of bone collagen: Case study in southwestern Germany. Quat. Int. 245, 218–224. doi:10.1016/j.quaint.2011.05.007

Edwards, B.A., Donaldson, K., Simpson, P., 1983. Water blance and protien intake in the Mongolian gerbil (*Meriones unguiculatus*). Comp. Biochem. Physiol. 76A, 807–815.

Ehleringer, J.., Dawson, T.E., 1992. Water uptake by plants: perspectives from stable isotope composition. Plant, Cell Environ. 15, 1073–1082.

Ehleringer, J.R., Cerling, T.E., Dearing, M.D., 2002. Atmospheric CO_2 as a Global Change Driver Influencing Plant-Animal Interactions. Integr. Comp. Biol. 42, 424–430.

Ehleringer, J.R., Cerling, T.E., Helliker, B.R., 1997. C_4 photosynthesis, atmospheric CO2, and climate. Oecologia 112, 285–299. doi:10.1007/s004420050311

Ehleringer, J.R., Sage, R.F., Flanagan, L.B., Pearcy, R.W., 1991. Climate change and the evolution of C_4 photosynthesis. Trends Ecol. Evol. 6, 95–9. doi:10.1016/0169-5347(91)90183-X

El Bait, M.N., Rhoujjati, a., Eynaud, F., Benkaddour, A., Dezileau, L., Wainer, K., Goslar, T., Khater, C., Tabel, J., Cheddadi, R., 2014. An 18 000-year pollen and sedimentary record from the cedar forests of the Middle Atlas, Morocco. J. Quat. Sci. 29, 423–432. doi:10.1002/jqs.2708

El Hajraoui, M.A., Debénath, A., Nespoulet, R., 2012a. L'hématite (Chapitre XXV), in: El Hajraoui, M. A., Nespoulet, R., Debénath, A., Dibble, H. (Eds.), Préhistoire de La Région de Rabat-Témara. Villes et Sites Archéologiques Du Maroc. Partie 3: Grotte d'El Mnasra, Vol. III. Royaume du Maroc, Ministere de la culture, Institut National des Sciences de l'Archéologie et du Patrimoine, Rabat, pp. 189–190.

El Hajraoui, M.A., Nespoulet, R., Debénath, A., Dibble, H., 2012b. Préhistoire de la région de Rabat-Témara. Villes et Sites Archéologiques du Maroc, vol. III. Royaume du Maroc, Ministere de la culture, Institut National des Sciences de l'Archéologie et du Patrimoine, Rabat.

El Hajraoui, M.A., Debénath, A., 2012. L'industrie osseuse (Chapitre XXIV), in: El Hajraoui, M. A., Nespoulet, R., Debénath, A., Dibble, H. (Eds.), Préhistoire de La Région de Rabat-Témara. Villes et Sites Archéologiques Du Maroc. Partie 3: Grotte d'El Mnasra, Vol. III. Royaume du Maroc, Ministere de la culture, Institut National des Sciences de l'Archéologie et du Patrimoine, Rabat, pp. 179–188.

El Idrissi, A., 2012. La céramique (Chapitre X), in: El Hajraoui, M.A., Nespoulet, R., Debénath, A., Dibble, H. (Eds.), Préhistoire de La Région de Rabat-Témara. Villes et Sites Archéologiques Du Maroc. Partie 2: Grotte d'El Harhoura 2, Vol. III. Royaume du Maroc, Ministere de la culture, Institut National des Sciences de l'Archéologie et du Patrimoine, Rabat, pp. 78–81.

Elsig, J., Schmitt, J., Leuenberger, D., Schneider, R., Eyer, M., Leuenberger, M., Joos, F., Fischer, H., Stocker, T.F., 2009. Stable isotope constraints on Holocene carbon cycle changes from an Antarctic ice core. Nature 461, 507–510. doi:10.1038/nature08393

Evans, R.D., 2001. Physiological mechanisms influencing plant nitrogen isotope composition. Trends Plant Sci. 6, 121–126. doi:10.1016/S1360-1385(01)01889-1

Farquhar, G.D., Cernusak, L. A, Barnes, B., 2007. Heavy water fractionation during transpiration. Plant Physiol. 143, 11–18. doi:10.1104/pp.106.093278

Farquhar, G.D., Ehleringer, J.R., Hubick, K.T., 1989. Carbon isotope discrimination and photosynthesis. Annu. Rev. Plant Physiol. Plant Mol. Biol. 40, 503–537.

Farquhar, G.D., O'Leary, M.H., Berry, J.A., 1982. On the relationship between carbon isotopes discrimination and the intercellular carbon dioxide concentration in leaves. Auntralian J. Plant Physiol. 9, 121–137.

Farre, B., Massard, P., Nouet, J., Dauphin, Y., 2014. Preservation of rodent bones from El Harhoura 2 cave (Morocco, Neolithic – Middle Palaeolithic): Microstructure, mineralogy, crystallinity and composition. J. African Earth Sci. 92, 1–13. doi:10.1016/j.jafrearsci.2013.12.011

Ferembach, D., 1985. On the origin of the Iberomaurusians (Upper palaeolithic: North Africa). A new hypothesis. J. Hum. Evol. 14, 393–397. doi:10.1016/S0047-2484(85)80047-6

Ferembach, D., Dastugue, J., Poitrat-Targowla, M., 1962. La Nécropole Epi-paléolithique de Taforalt (Maroc Oriental): Étude des Squelettes Humains. Edita Casablanca, Rabat.

Fernández-Jalvo, Y., Denys, C., Andrews, P., Williams, T., Dauphin, Y., Humphrey, L., 1998. Taphonomy and palaeoecology of Olduvai Bed-I (Pleistocene, Tanzania). J. Hum. Evol. 34, 137–172. doi:10.1006/jhev.1997.0188

Flanagan, L.B., Comstock, J.P., Ehleringer, J.R., 1991. Comparison of Modeled and Observed Environmental Influences on the Stable Oxygen and Hydrogen Isotope Composition of Leaf Water in *Phaseolus vulgaris* L. Plant Physiol. 96, 588–96.

Fletcher, W.J., Sánchez Goñi, M.F., 2008. Orbital- and sub-orbital-scale climate impacts on vegetation of the western Mediterranean basin over the last 48,000 yr. Quat. Res. 70, 451–464. doi:10.1016/j.yqres.2008.07.002

Fletcher, W.J., Sánchez Goñi, M.F., Allen, J.R.M., Cheddadi, R., Combourieu-Nebout, N., Huntley, B., Lawson, I., Londeix, L., Magri, D., Margari, V., Müller, U.C., Naughton, F., Novenko, E., Roucoux, K., Tzedakis, P.C., 2010a. Millennial-scale variability during the last glacial in vegetation records from Europe. Quat. Sci. Rev. 29, 2839–2864. doi:10.1016/j.quascirev.2009.11.015

Fletcher, W.J., Sanchez Goñi, M.F., Peyron, O., Dormoy, I., 2010b. Abrupt climate changes of the last deglaciation detected in a western Mediterranean forest record. Clim. Past 5, 203–235. doi:10.5194/cpd-5-203-2009

Fogel, M., Tuross, N., Owsley, D., 1989. Nitrogen Isotope Tracers of Human Lactation in Modern and Archaeological Populations. Carnegie Institute, New York.

Förstel, H., 1978. The enrichment of ^{18}O in leaf water under natural conditions. Radiat. Environ. Biophys. 15, 323–344.

Francey, R.J., Allison, C.E., Etheridg, D.M., Trudinger, C.M., Enting, I.G., Leuenberger, M., Langenfelds, R.L., Michel, E., Steele, L.P., 1999. A 1000-year high precision record of ^{13}C in atmospheric CO_2. Tellus B 51, 170–193.

Fraser, R.A., Bogaard, A., Heaton, T., Charles, M., Jones, G., Christensen, B.T., Halstead, P., Merbach, I., Poulton, P.R., Sparkes, D., Styring, A.K., 2011. Manuring and stable nitrogen isotope ratios in cereals and pulses: towards a new archaeobotanical approach to the inference of land use and dietary practices. J. Archaeol. Sci. 38, 2790–2804. doi:10.1016/j.jas.2011.06.024

Freudenthal, M., García-Alix, A., Rios, M., Ruiz-Sánchez, F., Martín-Suárez, E., Delgado Huertas, A., 2014. Review of paleo-humidity parameters in fossil rodents (Mammalia): Isotopic vs. tooth morphology approach. Palaeogeogr. Palaeoclimatol. Palaeoecol. 395, 122–130. doi:10.1016/j.palaeo.2013.12.023

Fricke, H., Clyde, W., O'Neil, J., 1998. Intra-tooth variations in $\delta^{18}O(PO_4)$ of mammalian tooth enamel as a record of seasonal variations in continental climate variables. Geochim. Cosmochim. Acta 62, 1839–1850.

Fricke, H.C., O'Neil, J.R., 1996. Inter- and intra-tooth variation in the oxygen isotope composition of mammalian tooth enamel phosphate: implications for palaeoclimatological and palaeobiological research. Palaeogeogr. Palaeoclimatol. Palaeoecol. 126, 91–99. doi:10.1016/S0031-0182(96)00072-7

Friedli, H., Lotscher, H., Oeschger, H., Siegenthaler, U., Stauffer, B., 1986. Ice core record of the $^{13}C/^{12}C$ ratio of atmospheric CO_2 in the past two centuries. Nature 324, 237–238.

Fuller, B., Fuller, J., Harris, D., Hedges, R.E., 2006. Detection of breastfeeding and weaning in modern human infants with carbon and nitrogen stable isotope ratios. Am. J. Phys. Anthropol. 129, 279–292.

Fuller, B.T., Fuller, J.L., Sage, N.E., Harris, D. A, O'Connell, T.C., Hedges, R.E.M., 2005. Nitrogen balance and $\delta^{15}N$: why you're not what you eat during nutritional stress. Rapid Commun. mass Spectrom. 19, 2497–506. doi:10.1002/rcm.2090

Gadbury, C., Todd, L., Jahren, a. H., Amundson, R., 2000. Spatial and temporal variations in the isotopic composition of bison tooth enamel from the Early Holocene Hudson–Meng Bone Bed, Nebraska. Palaeogeogr.

Palaeoclimatol. Palaeoecol. 157, 79–93. doi:10.1016/S0031-0182(99)00151-0

Garcea, E., 2012a. Modern human desert adaptations: A Libyan perspective on the Aterian complex, in: Hublin, J.-J., McPherron, S.P. (Eds.), Modern Origins: A North African Perspective. Springer, Dordrecht.

Garcea, E., 2012b. Successes and failures of human dispersals from North Africa. Quat. Int. 270, 119–128. doi:10.1016/j.quaint.2011.06.034

Garcea, E., 2004. Crossing deserts and avoiding seas: Aterian North African-European relations. J. Anthropol. Res. 60, 27–53.

García-Alix, A., Delgado Huertas, A., Martín Suárez, E., Freudenthal, M., 2013. Environmental conditions vs. landscape. Assessment of the factors that influence small mammal fauna distribution in Southern Iberia during the latest Messinian by mean of stable isotopes. Palaeogeogr. Palaeoclimatol. Palaeoecol. 386, 492–500. doi:10.1016/j.palaeo.2013.06.017

García-Alix, A., 2015. A multiproxy approach for the reconstruction of ancient continental environments. The case of the mio-pliocene deposits of the granada basin (southern iberian peninsula). Glob. Planet. Change 131, 1–10. doi:10.1016/j.gloplacha.2015.04.005

Gąsiorowski, M., Hercman, H., Socha, P., 2014. Isotopic analysis (C, N) and species composition of rodent assemblage as a tool for reconstruction of climate and environment evolution during Late Quaternary: A case study from Biśnik Cave (Częstochowa Upland, Poland). Quat. Int. 339-340, 139–147. doi:10.1016/j.quaint.2013.09.021

Gasse, F., 2000. Hydrological changes in the African tropics since the Last Glacial Maximum. Quat. Sci. Rev. 19, 189–211. doi:10.1016/S0277-3791(99)00061-X

Gat, J.R., Yakir, D., Goodfriend, G., Fritz, P., Trimborn, P., Lipp, J., Gev, I., Adar, E., Waisel, Y., 2007. Stable isotope composition of water in desert plants. Plant Soil 298, 31–45. doi:10.1007/s11104-007-9321-6

Gat, J.R., 1996. Oxygen and hydrogen isotopes in the hydrologic cycle. Annu. Rev. Earth Planet. Sci. 24, 225–262. doi:10.1146/annurev.earth.24.1.225

Gat, J.R., 1971. Comments on the Stable Isotope Method in Regional Groundwater Investigations. Water Resour. Res. 7, 980–993. doi:10.1029/WR007i004p00980

Gat, J.R., Airey, P.L., 2006. Stable water isotopes in the

atmosphere/biosphere/lithosphere interface: Scaling-up from the local to continental scale, under humid and dry conditions. Glob. Planet. Change 51, 25–33. doi:10.1016/j.gloplacha.2005.12.004

Gehler, A., Tütken, T., Pack, A., 2012. Oxygen and carbon isotope variations in a modern rodent community - implications for palaeoenvironmental reconstructions. PLoS One 7, e49531. doi:10.1371/journal.pone.0049531

Gobert, E., Vaufrey, R., 1932. Deux gisements extrêmes de l'Ibéromaurusian. L'Anthropologie XVII 449–490.

Godfrey-Smith, D., Vaughan, K., Gopher, A., Barkai, R., 2003. Direct luminescence chronology of the Epipalaeolithic Kebaran site of Nahal Hadera V, Israel. Geoarchaeology 18, 461–475.

Goetz, C., 1941. Note d'Archéologie préhistorique Nord-Africaine sur un foyer ora- nien de la sablière d'El-Kçar. Bull. Soc. Préhist. Fr 38, 262–265.

Gonfiantini, R., Gratziu, S., Tongiorgi, E., 1965. Oxygen isotopic composition of water in leaves, in: Isotopes and Radiation in Soil-Plant-Nutrition Studies. International Atomic Energy Commission, Vienna, pp. 405–410.

Goring-Morris, A., Belfer-Cohen, A., 2003. More than Meets the Eye: Studies on Upper Palaeolithic Diversity in the Near East. Oxbow Books, Oxford.

Grimes, S.T., Collinson, M.E., Hooker, J.J., Mattey, D.P., 2008. Is small beautiful? A review of the advantages and limitations of using small mammal teeth and the direct laser fluorination analysis technique in the isotope reconstruction of past continental climate change. Palaeogeogr. Palaeoclimatol. Palaeoecol. 266, 39–50. doi:10.1016/j.palaeo.2008.03.014

Grimes, S.T., Collinson, M.E., Hooker, J.J., Mattey, D.P., Grassineau, N. V., Lowry, D., 2004. Distinguishing the diets of coexisting fossil theridomyid and glirid rodents using carbon isotopes. Palaeogeogr. Palaeoclimatol. Palaeoecol. 208, 103–119. doi:10.1016/j.palaeo.2004.02.031

Grocke, D.R., Bocherens, H., Mariotti, A., 1997. Annual rainfall and nitrogen-isotope correlation in macropod collagen: application as a palaeoprecipitation indicator. Earth Planet. Sci. Lett. 153, 279–285.

Handley, L.L., Austin, A.T., Stewart, G.R., Robinson, D., Scrimgeour, C.M., Raven, J.A., Heaton, T.H.E., Schmidt, S., 1999. The ^{15}N natural abundance ($\delta^{15}N$) of ecosystem samples reflects measures of water availability. Aust. J. Plant Physiol. 26, 185–199.

Happold, D.C.D., 1968. Observations on *Gerbillus pyramidum* (Gerbillinae,

Rodentia) at Khartoum, Sudan. Mammalia 32, 44–53.

Harding, A., Palutikof, J., Holt, T., 2009. The climate system, in: Woodward, J. (Ed.), The Physical Geography of the Mediterranean. Oxford University Press, Oxford, pp. 69–88.

Hare, P.E., Fogel, M.L., Stafford, T.W., Mitchell, A.D., Hoering, T.C., 1991. The Isotopic Composition of carbon and nitrogen in individual amino acids isolated from modern and fossil proteins. J. Archaeol. Sci. 18, 277–292.

Hartman, G., 2012. Impacts of environmental deterioration on the carbon isotope values of modern vegetation and gazelles in the southern Levant: Predicting the severity of the Younger Dryas. Palaeogeogr. Palaeoclimatol. Palaeoecol. 321-322, 55–64. doi:10.1016/j.palaeo.2012.01.015

Hartman, G., 2011. Are elevated $\delta^{15}N$ values in herbivores in hot and arid environments caused by diet or animal physiology? Funct. Ecol. 25, 122–131. doi:10.1111/j.1365-2435.2010.01782.x

Hartman, G., Danin, A., 2010. Isotopic values of plants in relation to water availability in the Eastern Mediterranean region. Oecologia 162, 837–52. doi:10.1007/s00442-009-1514-7

Harvati, K., Hublin, J.-J., 2012. Morphological Continuity of the Face in the Late Middle and Late Pleistocene Hominins from Northwestern Africa: A 3D Geometric Morphometric Analysis, in: Hublin, J.-J., McPherron, S.P. (Eds.), Modern Origins: A North African Perspective, Vertebrate Paleobiology and Paleoanthropology. Springer Netherlands, Dordrecht, pp. 179–188. doi:10.1007/978-94-007-2929-2

Heaton, T.H.E., 1999. Spatial, species, and temporal variations in the $^{13}C/^{12}C$ ratios of C_3 plants: implications for palaeodiet studies. J. Archaeol. Sci. 26, 637–649.

Heaton, T.H.E., Vogel, J.C., Chevallerie, G., Collett, G., 1986. Climatic influence on the isotopic composition of bone nitrogen. Nature 322, 822–823.

Hedges, R.E., Clement, J.G., Thomas, D.L., O'Connell, T., 2007. Collagen turnover in the adult femoral mid-shaft: modeled from anthropogenic radiocarbon tracer measurements. Am. Pournal Phys. Anthropol. 133, 808–816. doi:10.1002/ajpa

Helliker, B., Ehleringer, J., 2002a. Differential ^{18}O enrichment of leaf cellulose in C_3 versus C_4 grasses. Funct. Plant Biol. 29, 435–442.

Helliker, B., Ehleringer, J., 2002b. Grass blades as tree rings: environmentally induced changes in the oxygen isotope ratio of cellulose along the length of grass blades. New Phytol. 155, 417–424. doi:10.1046/j.1469-8137.2002.00480.x

Héran, M.-A., Lécuyer, C., Legendre, S., 2010. Cenozoic long-term terrestrial climatic evolution in Germany tracked by $\delta^{18}O$ of rodent tooth phosphate. Palaeogeogr. Palaeoclimatol. Palaeoecol. 285, 331–342. doi:10.1016/j.palaeo.2009.11.030

Hiatt, J.L., Gartner, L.P., Provenza, D. V, 1974. Molar development in the mongolian gerbil (*Meriones unguiculatus*). Am. J. Anat. 141, 1–22. doi:10.1002/aja.1001410102

Hijmans, R.J., Cameron, S.E., Parra, J.L., Jones, P.G., Jarvis, A., 2005. Very high resolution interpolated climate surfaces for global land areas. Int. J. Climatol. 25, 1965–1978. doi:10.1002/joc.1276

Hillson, S., 2005. Teeth. Cambridge University Press, Cambridge.

Hobbie, E. A, Werner, R. a, 2004. Bulk carbon isotope patterns in C_3 and C_4 plants: a review and synthesis. New Phytol. 161, 371–385. doi:10.1046/j.1469-8137.204.00970.x

Hobbie, E. A., Högberg, P., 2012. Nitrogen isotopes link mycorrhizal fungi and plants to nitrogen dynamics. New Phytol. 196, 367–382. doi:10.1111/j.1469-8137.2012.04300.x

Hobson, K.A., Alisauskas, R.T., Clark, R.G., 1993. Stable-nitrogen isotope enrichment in avian tissues due to fasting and nutritional stress: implications for isotopic analyses of diet. Condor 95, 388–394.

Hoefs, J., 2009. Stable Isotope Geochemistry. Springer, New York.

Hooghiemstra, H., Stalling, H., Agwu, C.O.C., Dupont, L.M., 1992. Vegetational and climatic changes at the northern fringe of the sahara 250,000–5000 years BP: evidence from 4 marine pollen records located between Portugal and the Canary Islands. Rev. Palaeobot. Palynol. 74, 1–53. doi:10.1016/0034-6667(92)90137-6

Hopley, P.J., Latham, A.G., Marshall, J.D., 2006. Palaeoenvironments and palaeodiets of mid-Pliocene micromammals from Makapansgat Limeworks, South Africa: A stable isotope and dental microwear approach. Palaeogeogr. Palaeoclimatol. Palaeoecol. 233, 235–251. doi:10.1016/j.palaeo.2005.09.011

Hoppe, K., 2006. Correlation between the oxygen isotope ratio of North American bison teeth and local waters: Implication for paleoclimatic reconstructions. Earth Planet. Sci. Lett. 244, 408–417. doi:10.1016/j.epsl.2006.01.062

Hoppe, K., Amundson, R., Vavra, M., McClaran, M.P., Anderson, D.L., 2004. Isotopic analysis of tooth enamel carbonate from modern North American feral horses: implications for paleoenvironmental reconstructions. Palaeogeogr. Palaeoclimatol. Palaeoecol. 203, 299–311. doi:10.1016/S0031-0182(03)00688-6

Hoppe, K., Stuska, S., Amundson, R., 2005. The implications for paleodietary and paleoclimatic reconstructions of intrapopulation variability in the oxygen and carbon isotopes of teeth from modern feral horses. Quat. Res. 64, 138–146. doi:10.1016/j.yqres.2005.05.007

Hublin, J.-J., 2000. Modern-nonmodern hominid interactions: a Mediterranean perspective, in: The Geography of Neandertals and Modern Humans in Europe and the Greater Mediterranean. Peabody Museum Bulletin 8, Cambridge, pp. 157–182.

Hublin, J.-J., Tillier, A.-M., Tixier, J., 1987. L'humérus d'enfant moustérien (Homo 4) du Jebel Irhoud (Maroc) dans son contexte archéologique. Bull. Mémoires la Société d'Anthropologie Paris 4, série XIV, 115–142.

Hublin, J.J., 1992. Recent human evolution in northwestern Africa. Philos. Trans. R. Soc. Lond. B. Biol. Sci. 337, 185–91. doi:10.1098/rstb.1992.0096

Humphrey, L., Bello, S.M., Turner, E., Bouzouggar, A., Barton, N., 2012. Iberomaurusian funerary behaviour: evidence from Grotte des Pigeons, Taforalt, Morocco. J. Hum. Evol. 62, 261–73. doi:10.1016/j.jhevol.2011.11.003

Humphrey, L.T., Bocaege, E., 2008. Tooth Evulsion in the Maghreb: Chronological and Geographical Patterns. African Archaeol. Rev. 25, 109–123. doi:10.1007/s10437-008-9022-4

Humphrey, L.T., De Groote, I., Morales, J., Barton, N., Collcutt, S., Bronk Ramsey, C., Bouzouggar, A., 2014. Earliest evidence for caries and exploitation of starchy plant foods in Pleistocene hunter-gatherers from Morocco. Proc. Natl. Acad. Sci. 111, 954–9. doi:10.1073/pnas.1318176111

Hynek, S. A., Passey, B.H., Prado, J.L., Brown, F.H., Cerling, T.E., Quade, J., 2012. Small mammal carbon isotope ecology across the Miocene–Pliocene boundary, northwestern Argentina. Earth Planet. Sci. Lett. 321-322, 177–188. doi:10.1016/j.epsl.2011.12.038

Iacumin, P., Longinelli, A., 2002. Relationship between $\delta^{18}O$ values for skeletal apatite from reindeer and foxes and yearly mean $\delta^{18}O$ values of environmental water. Earth Planet. Sci. Lett. 201, 213–219.

Jacobs, Z., Roberts, R.G., Nespoulet, R., El Hajraoui, M.A., Debénath, A., 2012. Single-grain OSL chronologies for Middle Palaeolithic deposits at El Mnasra and El Harhoura 2, Morocco: implications for Late Pleistocene human-environment interactions along the Atlantic coast of northwest Africa. J. Hum. Evol. 62, 377–94. doi:10.1016/j.jhevol.2011.12.001

Jahren, A.H., Arens, N.C., Harbeson, S.A., 2008. Prediction of atmospheric $\delta^{13}CO_2$ using possil plant tissues. Rev. Geophys. 46, 2-12.

Janati-Idrissi, N., Falgueres, C., Haddad, M., Nespoulet, R., El Hajraoui, M. A., Debénath, A., Bejjit, L., Bahain, J.., Michel, P., Garcia, T., Boudad, L., El Hammouti, K., Oujaa, A., 2012. Datation par ESR-U/Th combinées de dents fossiles de la région de Rabat-Témara: Grottes d'El Mnasra et d'El Harhoura 2. Quaternaire 23, 25–35.

Jeffrey, A., Denys, C., Stoetzel, E., Lee-Thorp, J.A., 2015. Influences on the stable oxygen and carbon isotopes in gerbillid rodent teeth in semi-arid and arid environments: Implications for past climate and environmental reconstruction. Earth Planet. Sci. Lett. 428, 84–96. doi:10.1016/j.epsl.2015.07.012

Jennings, R.P., Singarayer, J., Stone, E.J., Krebs-kanzow, U., Khon, V., Nisancioglu, K.H., Pfeiffer, M., Zhang, X., Parker, A., Parton, A., Groucutt, H.S., White, T.S., Drake, N.A., Petraglia, M.D., 2015. The greening of Arabia: Multiple opportunities for human occupation of the Arabian Peninsula during the Late Pleistocene inferred from an ensemble of climate model simulations. Quat. Int. 382, 1–19. doi:10.1016/j.quaint.2015.01.006

Jim, S., Ambrose, S.H., Evershed, R.P., 2004. Stable carbon isotopic evidence for differences in the dietary origin of bone cholesterol, collagen and apatite: implications for their use in palaeodietary reconstruction. Geochim. Cosmochim. Acta 68, 61–72. doi:10.1016/S0016-7037(03)00216-3

Jolly, D., Harrison, S.P., Damnati, B., Bonnefille, R., 1998. Simulated climate and biomes of Africa during the Late Quaternary: comparison with pollen and lake status data. Quat. Sci. Rev. 17, 629–657.

Joly, F., 1962. Une carte au 1: 1 000 000e del'utilisation du sol au Maroc. Application de la méthode cartographique a la recherché des regions géographiques. Paris University. PhD Thesis.

Jones, S., 2013. Late Pleistocene environmental change and human activity at Taforalt Cave, Morocco: evidence from sediments and phytoliths.

University of Reading. MSc Thesis.

Jouve, P., Sourisseau, B., 2003. Etude de quatre oasis de la région de Tata: contribution au développement rural des zones oasiennes du sud du Maroc. Étude collective des étudiants du CNEARC option DAT-AGIR.

Jouzel, J., Barkov, N.I., Barnola, J.M., Bender, M., Chappellaz, J., Genthon, C., Kotlyakov, V.M., Lipenkov, V., Lorius, C., Petit, J.R., Raynaud, D., Raisbeck, G., Ritz, C., Sowersparallel, T., Stievenard, M., Yiou, F., Yiou, P., 1993. Extending the Vostok ice-core record of palaeoclimate to the penultimate glacial period. Nature 364, 407–412.

Kageyama, M., Nebout, N.C., Sepulchre, P., Peyron, O., Krinner, G., Ramstein, G., Cazet, J.-P., 2005. The Last Glacial Maximum and Heinrich Event 1 in terms of climate and vegetation around the Alboran Sea: a preliminary model-data comparison. C. R. Geosci. 337, 983–992. doi:10.1016/j.crte.2005.04.012

Keeling, C.D., Piper, S.C., Bacastow, R.B., Wahlen, M., Whorf, T.P., Heimann, M., Meijer, H.. A., 2005. Atmospheric CO_2 and $\delta^{13}CO_2$ exchange with the terrestrial biosphere and oceans from 1978 to 2000: observations and carbon cycle implications, pages, in: Ehleringer, J.., Cerling, T.E., Dearing, M.D. (Eds.), A History of Atmospheric CO_2 and Its Effects on Plants, Animals, and Ecosystems. Springer Verlag, New York, pp. 83–113.

Keeling, C.D., Whorf, T.P., Wahlen, M., van der Pilcht, J., 1995. Interannual extremes in the rate of rise of atmospheric carbon dioxide since 1980. Nature 375, 666–669.

Kellner, C.M., Schoeninger, M.J., 2007. A simple carbon isotope model for reconstructing prehistoric human diet. Am. J. Phys. Anthropol. 133, 1112–27. doi:10.1002/ajpa.20618

Kendall, C., Coplen, T.B., 2001. Distribution of oxygen-18 and deuterium in river waters across the United States. Hydrol. Process. 15, 1363–1393. doi:10.1002/hyp.217

Khammar, F., Brudieux, R., 1987. Seasonal changes in testicular contents and plasma concentrations of androgens in the desert gerbil (*Gerbillus gerbillus*). J. Reprod. Fertil. 80, 589–94.

Kimura, Y., Jacobs, L.L., Cerling, T.E., Uno, K.T., Ferguson, K.M., Flynn, L.J., Patnaik, R., 2013. Fossil mice and rats show isotopic evidence of niche partitioning and change in dental ecomorphology related to dietary shift in Late Miocene of Pakistan. PLoS One 8, e69308. doi:10.1371/journal.pone.0069308

Klevezal, G.A., Pucek, M., Sukhovskaja, L., 1990. Incisor growth in voles. Acta Theriol. (Warsz). 35, 331–344.

Knippertz, P., Christoph, M., Speth, P., 2003. Long-term precipitation variability in Morocco and the link to the large-scale circulation in recent and future climates 88, 67–88. doi:10.1007/s00703-002-0561-y

Koch, P.L., Tuross, N., Fogel, M.L., 1997. The Effects of Sample Treatment and Diagenesis on the Isotopic Integrity of Carbonate in Biogenic Hydroxylapatite. J. Archaeol. Sci. 24, 417–429. doi:10.1006/jasc.1996.0126

Koffler, B.R., 1972. *Meriones crassus*. Mamm. Species 9, 1–4. doi:10.1126/science.95.2469.427-b

Kohn, M.J., 2010. Carbon isotope compositions of terrestrial C_3 plants as indicators of (paleo)ecology and (paleo)climate. Proc. Natl. Acad. Sci. 107, 19691–5. doi:10.1073/pnas.1004933107

Kohn, M.J., 1996. Predicting animal $\delta^{18}O$: accounting for diet and physiological adaptation. Geochim. Cosmochim. Acta 60, 4811–4829.

Kreuger, H.W., Sullivan, C.H., 1984. Models for carbon isotope fractionation between diet and bone, in: Turnlund, J., Johnson, P.E. (Eds.), Stable Isotopes in Nutrition. American Chemcial Society, Washington, pp. 205–222.

Kuechler, R.R., Schefuß, E., Beckmann, B., Dupont, L., Wefer, G., 2013. NW African hydrology and vegetation during the Last Glacial cycle reflected in plant-wax-specific hydrogen and carbon isotopes. Quat. Sci. Rev. 82, 56–67. doi:10.1016/j.quascirev.2013.10.013

Lamb, H., Roberts, N., Leng, M., 1999. Lake evolution in a semi-arid montane environment: response to catchment change and hydroclimatic variation. J. Paleolimnol. 21, 325–343.

Lamb, H.F., Duigan, C.A., Gee, J.H.R., Kelts, K., Lister, G., Maxted, R.W., Merzouk, A., Niessen, F., Tahri, M., Whittington, R.J., Zeroual, E., 1994. Lacustrine sedimentation in a high-altitude, semi-arid environment: the palaeolimnological record of Lake Isli, High Atlas, Morocco, in: Millington, A.C., Pye, K. (Eds.), Environmental Change in Drylands: Biogeographical and Geomorphological Perspectives. Wiley, Chicester, pp. 147–162.

Lamb, H.F., Eicher, U., Switsur, V.R., 1989. An 18,000-year record of vegetation, lake-level and climatic change from Tigalmamine, Middle Atlas, Morocco. J. Biogeogr. 16, 65–74.

Lambeck, K., Purcell, A., 2005. Sea-level change in the Mediterranean Sea since the LGM: Model predictions for tectonically stable areas. Quat. Sci. Rev. 24, 1969–1988. doi:10.1016/j.quascirev.2004.06.025

Larrasoaña, J.C., Roberts, A.P., Rohling, E.J., 2013. Dynamics of green sahara periods and their role in hominin evolution. PLoS One 8, e76514. doi:10.1371/journal.pone.0076514

Laughlin, M.E., Donovick, P.J., Burright, R.G., 1975. Consummatory behavior in meadow voles (*Microtus pennsylvanicus*) and mongolian gerbils (*Meriones unguiculatus*). Physiol. Behav. 15, 185–9.

Leavitt, S.W., Long, A., 1982. Evidence for $^{13}C/^{12}C$ fractionation between tree leaves and wood. Nature 298, 742-744. doi:10.1038/298742a0

Lee-Thorp, J.A., 2002. Two decades of progress towards understanding fossilization processes and isotopic signals in calcified tissue minerals. Archaeometry 44, 435–446. doi:10.1111/1475-4754.t01-1-00076

Lee-Thorp, J. A., 2008. On isotopes and old bones. Archaeometry 50, 925–950. doi:10.1111/j.1475-4754.2008.00441.x

Lee-Thorp, J.A., Sealy, J.C., van der Merwe, N.J., 1989. Stable Carbon Isotope Ratio Differences Between Bone Collagen and Bone Apatite and their Relationship to Diet. J. Archaeol. Sci. 16, 585–599.

Lee-Thorp, J.A., van der Merwe, N.J., 1987. Carbon isotope analysis of fossil bone apatite. South African J. Sceince 83, 712–713.

Lee-Thorp, J.A., van der Merwe, N.J. Van Der, 1991. Aspects of the Chemistry of Modern and Fossil Biological Apatites. J. Archaeol. Sci. 18, 343–354.

LeGeros, R.Z., 1991. Calcium phosphates in oral biology and medicine. Karger, Paris.

LeGeros, R.Z., 1981. Apatites in biological systems. Prog. Cryst. Growth Charact. 4, 1–45.

LeGeros, R.Z., LeGeros, J.P., 1983. Carbonate analysis of synthetic, mineral and biological apatites. J. Dent. Res. 82, 259.

Leroux, M., 2001. The Meteorology and Climate of Tropical Africa. Springer in association with Praxis Publishing, Chichester.

Leuenberger, M., Siegenthaler, U., Lanway, C.C., 1992. Carbon isotope

composition of atmopsheric CO_2 during the last ice age from an Antartic ice core. Nature 357, 488–490.

Levin, N.E., Cerling, T.E., Passey, B.H., Harris, J.M., Ehleringer, J.R., 2006. A stable isotope aridity index for terrestrial environments. Proc. Natl. Acad. Sci. 103, 11201–5. doi:10.1073/pnas.0604719103

Linstädter, J., Eiwanger, J., Mikdad, A., Weniger, G.-C., 2012. Human occupation of Northwest Africa: A review of Middle Palaeolithic to Epipalaeolithic sites in Morocco. Quat. Int. 274, 158–174. doi:10.1016/j.quaint.2012.02.017

Loftus, E., Sealy, J., 2012. Technical note: interpreting stable carbon isotopes in human tooth enamel: an examination of tissue spacings from South Africa. Am. J. Phys. Anthropol. 147, 499–507. doi:10.1002/ajpa.22012

Longinelli, A., 1984. Oxygen isotopes in mammal bone phosphate: a new tool for paleohydrological and paleoclimatological research? 48, 385–390.

Longinelli, A., Iacumin, P., Davanzo, S., Nikolaev, V., 2003. Modern reindeer and mice: revised phosphate–water isotope equations. Earth Planet. Sci. Lett. 214, 491–498. doi:10.1016/S0012-821X(03)00395-9

Longinelli, A., Selmo, E., 2003. Isotopic composition of precipitation in Italy: a first overall map. J. Hydrol. 270, 75–88.

Lourantou, A., Chappellaz, J., Barnola, J.-M., Masson-Delmotte, V., Raynaud, D., 2010a. Changes in atmospheric CO2 and its carbon isotopic ratio during the penultimate deglaciation. Quat. Sci. Rev. 29, 1983–1992. doi:10.1016/j.quascirev.2010.05.002

Lourantou, A., Lavrič, J. V, Köhler, P., Barnola, J.-M., Paillard, D., Michel, E., Raynaud, D., Chappellaz, J., 2010b. Constraint of the CO_2 rise by new atmospheric carbon isotopic measurements during the last deglaciation. Global Biogeochem. Cycles 24. doi:10.1029/2009GB003545

Lubell, D., 2001. Late Pleistocene Early Holocene Maghreb, Africa, in: Peregrine, P., Ember, M. (Eds.), Encyclopedia of Prehistory, Vol. 1. Kluwer, New York, pp. 129–149.

Luz, B., Kolodny, Y., 1985. Oxygen isotope variations in phosphate of biogenic apatites, IV. Mammal teeth and bones. Earth Planet. Sci. Lett. 75, 29–36. doi:10.1016/0012-821X(85)90047-0

Luz, B., Kolodny, Y., Horowitz, M., 1984. Fractionation of oxygen isotopes between mammalian bone-phosphate and environmental drinking water.

Geochim. Cosmochim. Acta 48, 1689–1693.

Ma, J.-Y., Sun, W., Liu, X.-N., Chen, F.-H., 2012. Variation in the stable carbon and nitrogen isotope composition of plants and soil along a precipitation gradient in northern China. PLoS One 7, e51894. doi:10.1371/journal.pone.0051894

Maca-Meyer, N., González, A.M., Pestano, J., Flores, C., Larruga, J.M., Cabrera, V.M., 2003. Mitochondrial DNA transit between West Asia and North Africa inferred from U6 phylogeography. BMC Genet. 4, 15. doi:10.1186/1471-2156-4-15

Makarewicz, C., Sealy, J., 2015. Dietary reconstruction, mobility, and the analysis of ancient skeletal tissues: Expanding the prospects of stable isotope research in archaeology. J. Archaeol. Sci. 56, 146–158. doi:10.1016/j.jas.2015.02.035

Makarewicz, C., Tuross, N., 2006. Foddering by Mongolian pastoralists is recorded in the stable carbon ($\delta^{13}C$) and nitrogen ($\delta^{15}N$) isotopes of caprine dentinal collagen. J. Archaeol. Sci. 33, 862–870. doi:10.1016/j.jas.2005.10.016

Mariotti, V., Bonfiglioli, B., Facchini, F., Condemi, S., Belcastro, M.G., 2009. Funerary practices of the Iberomaurusian population of Taforalt (Tafoughalt; Morocco, 11-12,000BP): new hypotheses based on a grave by grave skeletal inventory and evidence of deliberate human modification of the remains. J. Hum. Evol. 56, 340–54. doi:10.1016/j.jhevol.2009.01.001

Mariotti, V., Condemi, S., Belcastro, M.G., 2014. Iberomaurusian funerary customs: new evidence from unpublished records of the 1950s excavations of the Taforalt necropolis (Morocco). J. Archaeol. Sci. 49, 488–499. doi:10.1016/j.jas.2014.05.037

Mauffrey, J.-F., Catzeflis, F., 2003. Ecological and isotopic discrimination of syntopic rodents in a neotropical rain forest of French Guiana. J. Trop. Ecol. 19. doi:10.1017/S0266467403003237

Mcbrearty, S., Brooks, S., 2000. The revolution that wasn't: a new interpretation of the origin of modern human behavior. J. Hum. Evol. 39, 453–563. doi:10.1006/jhev.2000.0435

McGee, D., deMenocal, P.B., Winckler, G., Stuut, J.B.W., Bradtmiller, L.I., 2013. The magnitude, timing and abruptness of changes in North African dust deposition over the last 20,000yr. Earth Planet. Sci. Lett. 371-372, 163–176. doi:10.1016/j.epsl.2013.03.054

McGregor, G.R., Nieuwolt, S., 1998. Tropical Climatology, Second Edi. ed. John Wiley & Sons, Chichester.

McGregor, H. V., Dupont, L., Stuut, J.-B.W., Kuhlmann, H., 2009. Vegetation change, goats, and religion: a 2000-year history of land use in southern Morocco. Quat. Sci. Rev. 28, 1434–1448. doi:10.1016/j.quascirev.2009.02.012

Merritt, J.F., 2010. The Biology of Small Mammals. The John Hopkins University Press, Maryland.

Metcalfe, J.Z., Longstaffe, F.J., Zazula, G.D., 2010. Nursing, weaning, and tooth development in woolly mammoths from Old Crow, Yukon, Canada: Implications for Pleistocene extinctions. Palaeogeogr. Palaeoclimatol. Palaeoecol. 298, 257–270. doi:10.1016/j.palaeo.2010.09.032

Michel, P., Campmas, E., Stoetzel, E., Nespoulet, R., El Hajraoui, M. A., Amani, F., 2010. Upper Palaeolithic (layer 2) and Middle Palaeolithic (layer 3) large faunas from El Harhoura 2 Cave (Témara, Morocco): paleontological, paleoecological and paleoclimatic data. Hist. Biol. 22, 1–3.

Michel, P., Campmas, E., Stoetzel, E., Nespoulet, R., El Hajraoui, M. A., 2009. La Macrofaune du Pléistocène supérieur d'El Harhoura 2 (Témara, Maroc): Données préliminaires. L'Anthropologie 113, 283–312.

Mikdad, A., Moser, J., Nami, M., Eiwanger, J., 2004. La stratigraphie du site d'Ifri n'Ammar (Rif Oriental, Maroc): premiers résultats sur les dépôts du Paléolithique moyen. Beiträge zur Allg. und Vergleichenden Archäologie 24, 125–137.

Mikkola, H., 1983. Owls of Europe. Calton, Poyser.

Minagawa, M., Wada, E., 1984. Stepwise enrichment of ^{15}N along food chains: further evidence and the relation between $\delta^{15}N$ and animal age. Geochim. Cosmochim. Acta 48, 1135–1140.

Moreno, A., Cacho, I., Canals, M., Grimalt, J.O., Sánchez-Goñi, M.F., Shackleton, N., Sierro, F.J., 2005. Links between marine and atmospheric processes oscillating on a millennial time-scale. A multi-proxy study of the last 50,000yr from the Alboran Sea (Western Mediterranean Sea). Quat. Sci. Rev. 24, 1623–1636. doi:10.1016/j.quascirev.2004.06.018

Moreno, A., González-sampériz, P., Morellón, M., Valero-garcés, B.L., Fletcher, W.J., 2012. Northern Iberian abrupt climate change dynamics during the last glacial cycle: A view from lacustrine sediments. Quat. Sci. Rev. 36, 139–153. doi:10.1016/j.quascirev.2010.06.031

Moreno, A., Stoll, H., Jiménez-Sánchez, M., Cacho, I., Valero-Garcés, B., Ito, E., Edwards, R.L., 2010. A speleothem record of glacial (25–11.6kyr BP) rapid climatic changes from northern Iberian Peninsula. Glob. Planet. Change 71, 218–231. doi:10.1016/j.gloplacha.2009.10.002

Murphy, B.P., Bowman, D.M.J.S., 2006. Kangaroo metabolism does not cause the relationship between bone collagen? $\delta^{15}N$ and water availability. Funct. Ecol. 20, 1062–1069. doi:10.1111/j.1365-2435.2006.01186.x

Nami, M., Moser, J., 2010. La Grotte D'Ifri n'Ammar. Reichert Verlag, Deutsches Archaologisches Institut, Wiesbaden.

Naughton, F., Sánchez Goñi, M.F., Kageyama, M., Bard, E., Duprat, J., Cortijo, E., Desprat, S., Malaizé, B., Joly, C., Rostek, F., Turon, J.-L., 2009. Wet to dry climatic trend in north-western Iberia within Heinrich events. Earth Planet. Sci. Lett. 284, 329–342. doi:10.1016/j.epsl.2009.05.001

Navarro, N., Lécuyer, C., Montuire, S., Langlois, C., Martineau, F., 2004. Oxygen isotope compositions of phosphate from arvicoline teeth and Quaternary climatic changes, Gigny, French Jura. Quat. Res. 62, 172–182. doi:10.1016/j.yqres.2004.06.001

Nespoulet, R., Debénath, A., El Hajraoui, M.A., Michel, P., Campmas, E., Oujaa, A., Ben Cer, A., Amani, F., Stoetzel, E., Boudad, L., 2008a. Le contexte archéologique des restes humains Atériens de la région de Témara (Maroc). Apport des fouilles des grottes d'El Mnasra et d'El Harhoura 2, in: Aouraghe, H., Haddoumi, H., El Hammouti, K. (Eds.), Le Quaternaire Marocain Dans Son Contexte Méditerra- Néen. Actes Des Quatri? Emes Rencontres Des Quaternaristes Marocains (RQM4), Oujda (November 2007). Publication de la faculté des Sciences d'Oujda, pp. 356–375.

Nespoulet, R., El Hajraoui, M.A., 2012a. Partie 2. Grotte d'El Harhoura 2: Chapitre III. Présentation du site et archéostratigraphie, in: El Hajraoui, M.A., Nespoulet, R., Debénath, A., Dibble, H. (Eds.), Préhistoire de La Région de Rabat-Témara, Villes et Sites Archéologiques Du Maroc, Vol. III. Royaume du Maroc, Ministere de la culture, Institut National des Sciences de l'Archéologie et du Patrimoine, Rabat, pp. 27–30.

Nespoulet, R., El Hajraoui, M.A., 2012b. L'industrie lithique paléolithique (Chapitre XII), in: El Hajraoui, M.A., Nespoulet, R., Debénath, A., Dibble, H. (Eds.), Préhistoire de La Région de Rabat-Témara. Villes et Sites Archéologiques Du Maroc. Partie 2: Grotte d'El Harhoura 2, Vol. III. Royaume du Maroc, Ministere de la culture, Institut National des Sciences de l'Archéologie et du Patrimoine, Rabat, pp. 91–102.

Nespoulet, R., El Hajraoui, M.A., 2003. Rapport d'activités de la Mission

Archéologique El Harhoura 2. Ministère des Affaires Etrangères et Européennes (France), Ministère de la Culture (Maroc).

Nespoulet, R., Hajraoui, M.A., Amani, F., Ben Ncer, A., Debénath, A., Idrissi, A., Lacombe, J.-P., Michel, P., Oujaa, A., Stoetzel, E., 2008b. Palaeolithic and Neolithic Occupations in the Témara Region (Rabat, Morocco): Recent Data on Hominin Contexts and Behavior. African Archaeol. Rev. 25, 21–39. doi:10.1007/s10437-008-9025-1

Niftah, S., Debénath, A., Miskowsky, J., 2005. Origine du remplissage sédimentaire des grottes de Témara (Maroc) d'après l'étude des minéraux lourds et l'étude exoscopique des grains de quartz. Quaternaire 16, 73–83.

O'Connell, T.C., Hedges, R.E.M., Healey, M. a., Simpson, a. H.R.W., 2001. Isotopic Comparison of Hair, Nail and Bone: Modern Analyses. J. Archaeol. Sci. 28, 1247–1255. doi:10.1006/jasc.2001.0698

O'Leary, M.H., 1981. Carbon isotope fractionation in plants. Phytochemistry 20, 553–567.

Olivieri, A., Achilli, A., Pala, M., Battaglia, V., Fornarino, S., Al-Zahery, N., Scozzari, R., Cruciani, F., Behar, D.M., Dugoujon, J.-M., Coudray, C., Santachiara-Benerecetti, A.S., Semino, O., Bandelt, H.-J., Torroni, A., 2006. The mtDNA legacy of the Levantine early Upper Palaeolithic in Africa. Science 314, 1767–1770. doi:10.1126/science.1135566

Osborne, A.H., Vance, D., Rohling, E.J., Barton, N., Rogerson, M., Fello, N., 2008. A humid corridor across the Sahara for the migration of early modern humans out of Africa 120,000 years ago. Proc. Natl. Acad. Sci. 105, 16444–7. doi:10.1073/pnas.0804472105

Ouda, B., El Hamdaoui, A., Ibn Majah, M., 2005. Isotopic composition of precipitation at three Moroccan stations influenced by Oceanic and Mediterranean air masses, in: Isotopic Composition of Precipitation in the Mediterranean Basin in Relation to Air Circulation Patterns and Climate. International Atomic Energy Commission, Vienna, pp. 125–140.

Oujaa, A., Lacombe, J., 2012. L'occupation humaine néolithique (Chapitre VIII), in: El Hajraoui, M.A., Nespoulet, R., Debénath, A., Dibble, H. (Eds.), Préhistoire de La Région de Rabat-Témara. Villes et Sites Archéologiques Du Maroc. Partie 2: Grotte d'El Harhoura 2, Vol. III. Royaume du Maroc, Ministere de la culture, Institut National des Sciences de l'Archéologie et du Patrimoine, Rabat, pp. 59–69.

Pallary, P., 1909. Instructions pour la Recherche Préhistorique dans le Nord-Ouest de l'Afrique, in: Mémoires de La Société Historique Algérienne, Vol. 3. Jourdan, Algiers.

Park, R., Epstein, S., 1960. Carbon isotope fractionation during photosynthesis. Geochim. Cosmochim. Acta 21, 110–126.

Passey, B.H., Cerling, T.E., 2006. In situ isotope analyses ($\delta^{13}C$, $\delta^{18}C$) of very small teeth using laser ablation GC/IRMS. Chem. Geol. 235, 238–249.

Passey, B.H., Cerling, T.E., Perkins, M.E., Voorhies, M.R., Harris, J.M., Tucker, S.T., The, S., March, N., 2002. Environmental change in the Great Plains: an isotopic record from fossil horses. J. Geol. 110, 123–140.

Passey, B.H., Robinson, T.F., Ayliffe, L.K., Cerling, T.E., Sponheimer, M., Dearing, M.D., Roeder, B.L., Ehleringer, J.R., 2005. Carbon isotope fractionation between diet, breadth CO_2, and bioapatite in different mammals. J. Archaeol. Sci. 32, 1459–1470.

Pate, F.D., Anson, T.J., 2008. Stable Nitrogen Isotope Values in Arid-Land Kangaroos Correlated with Mean Annual Rainfall: Potential as a Palaeoclimatic Indicator 326, 317–326. doi:10.1002/oa

Paul, H., 2001. Oxygen isotopic composition of the Mediterranean Sea since the Last Glacial Maximum: constraints from pore water analyses. Earth Planet. Sci. Lett. 192, 1–14. doi:10.1016/S0012-821X(01)00437-X

Pauling, A., Luterbacher, J., Casty, C., Wanner, H., 2005. Five hundred years of gridded high-resolution precipitation reconstructions over Europe and the connection to large-scale circulation. Clim. Dyn. 26, 387–405. doi:10.1007/s00382-005-0090-8

Pavlinov, I.Y., 2000. Materialy po kraniometricheskoi izmenchivosti i sistematike peschanok gruppy “shawi-grandis” roda *Meriones* (Gerbillidae). Zool Zh 79, 201–209.

Pavlinov, I.Y., Dubrovskly, Y.A., Rossolimo, O.L., Potapova, E.G., 1990. Gerbils of the World. Nauka Publishers, Moscow.

Penaud, A., Eynaud, F., Sánchez-Goñi, M., Malaizé, B., Turon, J.L., Rossignol, L., 2011. Contrasting sea-surface responses between the western Mediterranean Sea and eastern subtropical latitudes of the North Atlantic during abrupt climatic events of MIS 3. Mar. Micropaleontol. 80, 1–17. doi:10.1016/j.marmicro.2011.03.002

Petter, F., Lachiver, F., Chekir, R., 1984. Les adaptations des rongeurs Gerbilidés à la vie dans les régions arides. Bull. la Société Bot. Fr. 131, 365–373. doi:10.1080/01811789.1984.10826676

Peukert, S., Bol, R., Roberts, W., Macleod, C.J. a, Murray, P.J., Dixon, E.R.,

Brazier, R.E., 2012. Understanding spatial variability of soil properties: a key step in establishing field- to farm-scale agro-ecosystem experiments. Rapid Commun. Mass Spectrom. 26, 2413–21. doi:10.1002/rcm.6336

Podlesak, D.W., Torregrossa, A.-M., Ehleringer, J.R., Dearing, M.D., Passey, B.H., Cerling, T.E., 2008. Turnover of oxygen and hydrogen isotopes in the body water, CO2, hair, and enamel of a small mammal. Geochim. Cosmochim. Acta 72, 19–35. doi:10.1016/j.gca.2007.10.003

Pons, A., Reille, M., 1988. The Holocene- and Upper Pleistocene pollen record from Padul (Granada, Spain): A new study. Palaeogeogr. Palaeoclimatol. Palaeoecol. 66, 243–263. doi:10.1016/0031-0182(88)90202-7

Prendergast, A.L., Stevens, R.E., O'Connell, T.C., Fadlalak, A., Touati, M., al-Mzeine, A., Schöne, B.R., Hunt, C.O., Barker, G., 2015. Changing patterns of eastern Mediterranean shellfish exploitation in the Late Glacial and Early Holocene: Oxygen isotope evidence from gastropod in Epipaleolithic to Neolithic human occupation layers at the Haua Fteah cave, Libya. Quat. Int. doi:10.1016/j.quaint.2015.09.035

Ramsey, C.B., 2008. Deposition models for chronological records. Quat. Sci. Rev. 27, 42–60. doi:10.1016/j.quascirev.2007.01.019

Raynal, J.-P., 1980. Taforalt. Mission préhistorique et paléontologique française au Maroc: rapport d'activité pour l'année. Bull. Archéol. Marocaine 12, 69–71.

Reade, H., O'Connell, T.C., Barker, G., Stevens, R.E., 2015. Pleistocene and Holocene palaeoclimates in the Gebel Akhdar (Libya) estimated using herbivore tooth enamel oxygen isotope compositions. Quat. Int. doi:10.1016/j.quaint.2015.10.009

Reade, H., Stevens, R.E., O'Connell, T.C., Barker, G., 2016.Pliestocene and Holocene herbivore diets and palaeoenvironments in the Gebel Akhdar (Libya): implications for past human populations. Palaeogeogr. Palaeoclimatol. Palaeoecol. 449, 62-78. doi:10.1016/j.palaeo.2016.02.003

Reddad, H., Etabaai, I., Rhoujjati, A., Taieb, M., Thevenon, F., Damnati, B., 2013. Fire activity in North West Africa during the last 30,000 cal years BP inferred from a charcoal record from Lake Ifrah (Middle atlas–Morocco): Climatic implications. J. African Earth Sci. 84, 47–53. doi:10.1016/j.jafrearsci.2013.03.007

Reimer, P., Bard, E., Bayliss, A., Beck, J.W., Blackwell, P.G., Bronk Ramsey, C., Buck, C.E., Cheng, H., Edwars, R.L., Friedrich, M., Grootes, P.M., Guilderson, T.P., Haflidason, H., Hajdas, I., Hatte, C., Heaton, T.J., Hoffman, D.L., Hogg, A.G., Hughen, K.A., Kaiser, K.F., Kromer, B.,

Manning, S.W., Niu, M., Reimer, R.W., Richards, D.A., Scott, E.M., Southon, J.R., Staff, R.A., Turney, C.S.M., van der Plicht, J., 2013. IntCal13 and Marine13 Radiocarbon Age Calibration Curves 0–50,000 Years cal BP. Radiocarbon 55, 1869–1887. doi:10.2458/azu_js_rc.55.16947

Rhoujjati, A., Cheddadi, R., Taïeb, M., Baali, A., Ortu, E., 2010. Environmental changes over the past c. 29,000 years in the Middle Atlas (Morocco): A record from Lake Ifrah. J. Arid Environ. 74, 737–745. doi:10.1016/j.jaridenv.2009.09.006

Richards, M.P., Pettitt, P.B., Stiner, M.C., Trinkaus, E., 2001. Stable isotope evidence for increasing dietary breadth in the European mid-Upper Paleolithic. Proc. Natl. Acad. Sci. 98, 6528–6532. doi:10.1073/pnas.111155298

Richards, M.P., Schulting, Rick, J., Hedges, R.E.M., 2003. Sharp shift in diet at onset of Neolithic. Nature 425, 366.

Richter, D., Moser, J., Nami, M., 2012. New Data from the Site of Ifri n'Ammar (Morocco) and Some Remarks on the Chronometric Status of the Middle Paleolithic in the Maghreb. doi:10.1007/978-94-007-2929-2

Richter, D., Moser, J., Nami, M., Eiwanger, J., Mikdad, A., 2010. New chronometric data from Ifri n'Ammar (Morocco) and the chronostratigraphy of the Middle Palaeolithic in the Western Maghreb. J. Hum. Evol. 59, 672–9. doi:10.1016/j.jhevol.2010.07.024

Robbins, C.T., Felicetti, L.A., Sponheimer, M., 2005. The effect of dietary protein quality on nitrogen isotope discrimination in mammals and birds. Oecologia 144, 534–40. doi:10.1007/s00442-005-0021-8

Roberts, N., Jones, M.D., Benkaddour, A., Eastwood, W.J., Filippi, M.L., Frogley, M.R., Lamb, H.F., Leng, M.J., Reed, J.M., Stein, M., Stevens, L., Valero-Garcés, B., Zanchetta, G., 2008. Stable isotope records of Late Quaternary climate and hydrology from Mediterranean lakes: the ISOMED synthesis. Quat. Sci. Rev. 27, 2426–2441. doi:10.1016/j.quascirev.2008.09.005

Roberts, N., Lamb, H.F., El Hamouti, N., Barker, P., 1994. Abrupt Holocene hydro-climatic events: palaeolimnological evidence from North-West Africa, in: Millington, A.C., Pye, P. (Eds.), Environmental Change in Drylands: Biogeographical and Geomorphological Perspectives. Wiley, Chichester, pp. 163–175.

Roche, J., 1976. Cadre chronologique de l'Epipaléolithique marocain, in: Actes Du IXè Congrès de l'UISPP: Chronologie et Synchronisme Dans La

Préhistoire Circum- Méditerranéenne. pp. 153–167.

Roche, J., 1969. Les industries paléolithiques de la grotte de Taforalt (Maroc orien- tal). Quaternaria 11, 89–100.

Roche, J., 1967. L'Aterian de la grotte de Taforalt (Maroc oriental). Bull. Archeol. Marocaine 7, 11–56.

Roche, J., 1963. L'Epipaléolithique Marocaine. Calouste Gulbenkian, Lisbon.

Roche, J., 1953. Note préliminaire sur les fouilles de la grotte de Taforalt (Maroc Oriental). Hespéris 40, 89-116. Hespéris 40, 89–116.

Rogers, K.L., Wang, Y., 2002. Stable Isotopes in Pocket Gopher Teeth as Evidence of a Late Matuyama Climate Shift in the Southern Rocky Mountains. Quat. Res. 57, 200–207. doi:10.1006/qres.2001.2309

Rohling, E.J., Abu-Zied, R., Casford, J., Hayes, A., Hoogakker, B., 2009. The marine environment: present and past, in: Woodward, J. (Ed.), The Physical Geography of the Mediterranean. Oxford University Press, Oxford, pp. 33–68.

Rohling, E.J., Hayes, A., De Rijk, S., Kroon, D., Zachariasse, W.J., Eisma, D., 1998. Abrupt cold spells in the northwest Mediterranean. Paleoceanography 13, 316–322. doi:10.1029/98PA00671

Roucoux, K.H., de Abreu, L., Shackleton, N.J., Tzedakis, P.C., 2005. The response of NW Iberian vegetation to North Atlantic climate oscillations during the last 65kyr. Quat. Sci. Rev. 24, 1637–1653. doi:10.1016/j.quascirev.2004.08.022

Royer, A., Lécuyer, C., Montuire, S., Amiot, R., Legendre, S., Cuenca-Bescós, G., Jeannet, M., Martineau, F., 2013a. What does the oxygen isotope composition of rodent teeth record? Earth Planet. Sci. Lett. 361, 258–271. doi:10.1016/j.epsl.2012.09.058

Royer, A., Lécuyer, C., Montuire, S., Escarguel, G., Fourel, F., Mann, A., Maureille, B., 2013b. Late Pleistocene (MIS 3–4) climate inferred from micromammal communities and $\delta^{18}O$ of rodents from Les Pradelles, France. Quat. Res. 80, 113–124. doi:10.1016/j.yqres.2013.03.007

Royer, A., Lécuyer, C., Montuire, S., Primault, J., Fourel, F., Jeannet, M., 2014. Summer air temperaturea, reconstructions from the last glacial stage based on rodents from the site Taillis-des-Coteaux (Vienne), Western France. Quat. Res. (United States) 82, 420–429. doi:10.1016/j.yqres.2014.06.006

Rozanski, K., Araguás-Araguás, L., Gonfiantini, R., 1993. Isotopic patterns in modern global precipitation, in: Swart, P.K., Lohmann, K.C., McKenzie, J., Savin, S. (Eds.), Climate Change in Continental Isotopic Records. AGU, Washington, pp. 1–36. doi:doi:10.1029/GM078p0001

Rubino, M., Etheridge, D.M., Trudinger, C.M., Allison, C.E., Battle, M.O., Langenfelds, R.L., Steele, L.P., Curran, M., Bender, M., White, J.W.C., Jenk, T.M., Blunier, T., Francey, R.J., 2013. A revised 1000 year atmospheric $\delta^{13}C$-CO_2 record from Law Dome and South Pole, Antarctica. J. Geophys. Res. Atmos. 118, 8482–8499. doi:10.1002/jgrd.50668

Ruhlmann, A., 1951. La Grotte préhistorique de Dar es-Soltan. Collection Hésperis (Vol. 11, pp. 1–210). Institut des Hautes Études Marocaines, Paris.

Sage, R., Monson, R., 1998. C_4 Plant Biology. Academic Press, Cambridge.

Sage, R.F., Wedin, D.A., Li, M., 1999. The biogeogrpahy of C_4 photosynthesis: patterns and controlling factors, in: Sage, R.F., Monson, R.K. (Eds.), C_4 Plant Biology. Academic Press, London, pp. 313–373.

Sánchez Goñi, M., Eynaud, F., Turon, J.L., Shackleton, N., 1999. High resolution palynological record off the Iberian margin: direct land-sea correlation for the Last Interglacial complex. Earth Planet. Sci. Lett. 171, 123–137. doi:http://dx.doi.org/10.1016/S0012-821X(99)00141-7

Sánchez Goñi, M., Caco, I., Turon, J-L., Guiot, J., Sierro. F. J., Peypouquet, J-P., Grimalt, J.O., Shackleton, N.J., 2002. Synchroneity between marine and terrestrial responses to millennial scale climatic variability during the last glacial period in the Mediterranean region. Clim. Dyn. 19, 95–105. doi:10.1007/s00382-001-0212-x

Sauvage, C., 1963. Etages bioclimatiques. Atlas du Maroc. Comité National de Géographie du Maroc, Rabat.

Scerri, E.M.L., 2013. The Aterian and its place in the North African Middle Stone Age. Quat. Int. 300, 111–130. doi:10.1016/j.quaint.2012.09.008

Scerri, E.M.L., Drake, N.A., Jennings, R., Groucutt, H.S., 2014. Earliest evidence for the structure of Homo sapiens populations in Africa. Quat. Sci. Rev. 101, 207–216. doi:10.1016/j.quascirev.2014.07.019

Schaefer, H., Lourantou, A., Chappellaz, J., Luethi, D., Bereiter, B., Barnola, J.-M., 2011. On the suitability of partially clathrated ice for analysis of concentration and $\delta^{13}C$ of paleo-atmospheric CO_2. Earth Planet. Sci. Lett. 307, 334–340. doi:10.1016/j.epsl.2011.05.007

Schneider, R., Schmitt, J., Köhler, P., Joos, F., Fischer, H., 2013. A reconstruction of atmospheric carbon dioxide and its stable carbon isotopic composition from the penultimate glacial maximum to the last glacial inception. Clim. Past 9, 2507–2523. doi:10.5194/cp-9-2507-2013

Schoeninger, M.J., DeNiro, M.J., 1984. Nitrogen and carbon isotopic composition of bone collagen from marine and terrestrial animals. Geochim. Cosmochim. Acta 48, 625–639. doi:10.1016/0016-7037(84)90091-7

Schour, I., Massler, M., 1963. The teeth, in: Farris, E.J., Griffith, J.Q. (Eds.), The Rat in Laboratory Investigations. Hafner Publishing Co, New York, pp. 104–165.

Schrag, D.P., Adkins, J.F., McIntyre, K., Alexander, J.L., Hodell, D. a., Charles, C.D., McManus, J.F., 2002. The oxygen isotopic composition of seawater during the Last Glacial Maximum. Quat. Sci. Rev. 21, 331–342. doi:10.1016/S0277-3791(01)00110-X

Schwenninger, J., Collcutt, S., Barton, R.N., Bouzouggar, A., Clarck-Balzan, J., El Hajraoui, M.A., Nespoulet, R., Debénath, A., 2010. A new luminescence chronology for Aterian cave sites on the Atlantic coast of Morocco, in: Garcea, E.A.. (Ed.), South-Eastern Mediterranean Peoples. Between 130,000 and 10,000 Years Ago. Oxbow Books, Oxford, pp. 18–36.

Sealy, J.C., van der Merwe, N.J. Van Der, Lee-thorp, J.A., Lanham, J.L., 1987. Nitrogen isotopic ecology in southern Africa: implications for environmental and dietary tracing. Geochim. Cosmochim. Acta 51, 2707–2717.

Sharp, Z., 2007. Principles of Stable Isotope Geochemistry. Pearson Education, Upper Saddle River.

Sierro, F.J., Hodell, D.A., Curtis, J.H., Flores, J.A., Reguera, I., Colmenero-Hidalgo, E., Bárcena, M.A., Grimalt, J.O., Cacho, I., Frigola, J., Canals, M., 2005. Impact of iceberg melting on Mediterranean thermohaline circulation during Heinrich events. Paleoceanography 20, PA2019. doi:10.1029/2004PA001051

Smiley, T.M., Cotton, J.M., Badgley, C., Cerling, T.E., 2015.Small-mammal isotope ecology tracks climate and vegetation gradients across western North America. Oikos, doi:10.111/oik.02722

Smith, B.N., Epstein, S., 1971. Two categories of $^{13}C/^{12}C$ ratios for higher plants. Plant Physiol. 47, 380–4

Smith, H.J., Fischer, H., Wahlen, M., Mastroianni, D., Deck, B., 1999. Dual

modes fo the carbon cycle since the last glacial maximum. Nature 400, 248–250.

Smith, J.J., Millar, J.S., Longstaffe, F.J., Boonstra, R., 2010. The effect of metabolic rate on stable carbon and nitrogen isotope compositions in deer mice, *Peromyscus maniculatus*. Can. J. Zool. 88, 36–42. doi:10.1139/Z09-116

Smith, J.R., 2012. The Aterian of the oases of the Western Desert of Egypt: adpation to changing climatic conditions?, in: Modern Origins: A North African Perspective. Springer, New York, pp. 157–175. doi:10.1007/978-94-007-2929-2

Smith, T.M., Tafforeau, P., Reid, D.J., Grün, R., Eggins, S., Boutakiout, M., Hublin, J.-J., 2007. Earliest evidence of modern human life history in North African early *Homo sapiens*. Proc. Natl. Acad. Sci. 104, 6128–33. doi:10.1073/pnas.0700747104

Spinapolice, E.E., Garcea, E., 2014. Aterian lithic technology and settlement system in the Jebel Gharbi, North-Western Libya. Quat. Int. 350, 241–253. doi:10.1016/j.quaint.2014.07.062

Sponheimer, M., 1999. Isotopic Ecology of the Makapansgat Limeworks Fauna. Rutgers University.

Sponheimer, M., Lee-Thorp, J. A., 2001. The oxygen isotope composition of mammalian enamel carbonate from Morea Estate, South Africa. Oecologia 126, 153–157. doi:10.1007/s004420000498

Sponheimer, M., Robinson, T., Ayliffe, L., Roeder, B., Hammer, J., Passey, B., West, A., Cerling, T., Dearing, D., Ehleringer, J., 2003. Nitrogen isotopes in mammalian herbivores: hair $\delta^{15}N$ values from a controlled feeding study. Int. J. Osteoarchaeol. 13, 80–87. doi:10.1002/oa.655

Stevens, R.E., Jacobi, R., Street, M., Germonpré, M., Conard, N.J., Münzel, S.C., Hedges, R.E.M., 2008. Nitrogen isotope analyses of reindeer (*Rangifer tarandus*), 45,000 BP to 9,000 BP: Palaeoenvironmental reconstructions. Palaeogeogr. Palaeoclimatol. Palaeoecol. 262, 32–45. doi:10.1016/j.palaeo.2008.01.019

Stevens, R.E., Lister, A.M., Hedges, R.E.M., 2006. Predicting diet, trophic level and palaeoecology from bone stable isotope analysis: a comparative study of five red deer populations. Oecologia 149, 12–21. doi:10.1007/s00442-006-0416-1

Stewart, G.R., Turnbull, M.H., Schmidt, S., Erskine, P.D., 1995. $\delta^{13}C$ natural

abundance in plant communities along a rainfall gradient: a biological integrator of water availability. Aust. J. Plant Physiol. 22, 51 – 55.

Still, C.J., Berry, J. a., Collatz, G.J., DeFries, R.S., 2003. Global distribution of C_3 and C_4 vegetation: Carbon cycle implications. Global Biogeochem. Cycles 17, 1–14. doi:10.1029/2001GB001807

Stoetzel, E., 2009. Les microvertébrés du site d'occupation humaine d'El Harhoura 2 (Pléistocène supérieur-Holocène, Maroc): systématique, évolution, taphonomie et paléoécologie. Muséum national d'Histoire naturelle, Paris. PhD Thesis.

Stoetzel, E., Bailon, S., Nespoulet, R., El Hajraoui, M.A., Denys, C., 2010. Pleistocene and Holocene small vertebrates of El Harhoura 2 cave (Rabat–Témara, Morocco): an annotated preliminary taxonomic list. Hist. Biol. 22, 303–319. doi:10.1080/08912960903461288

Stoetzel, E., Campmas, E., Michel, P., Bougariane, B., Ouchaou, B., Amani, F., El Hajraoui, M.A., Nespoulet, R., 2014. Context of modern human occupations in North Africa: Contribution of the Témara caves data. Quat. Int. 320, 413-161. doi:10.1016/j.quaint.2013.05.017

Stoetzel, E., Denys, C., Bailon, S., El Hajraoui, M. A., Nespoulet, R., 2012. Taphonomic analysis of amphibian and squamate remains from El Harhoura 2 (Rabat-Temara, Morocco): contributions to palaeoecological and archaeological Interpretations. Int. J. Osteoarchaeol. 22, 616–635. doi:10.1002/oa.1275

Stoetzel, E., Denys, C., Michaux, J., Renaud, S., 2013. *Mus* in Morocco: a Quaternary sequence of intraspecific evolution. Linn. Soc. Biol. J. 109, 599–621. doi:10.1111/bij.12065

Stoetzel, E., Marion, L., Nespoulet, R., El Hajraoui, M.A., Denys, C., 2011. Taphonomy and palaeoecology of the late Pleistocene to middle Holocene small mammal succession of El Harhoura 2 cave (Rabat-Témara, Morocco). J. Hum. Evol. 60, 1–33. doi:10.1016/j.jhevol.2010.07.016

Street, A.F., Grove, A.T., 1979. Global maps of lake-level fluctuations since 30,000 yr B.P. Quat. Res. 12, 83–118.

Street-Perrott, F.A., Marchand, D.S., Roberts, N., Harrison, S.P., 1989. Global lake-level variations from 18,000 to 0 years ago: a paleoclimatic analysis, in: Department of Energy Technical Report 46, 20545.

Styring, A., Ater, M., Hmimsa, Y., Fraser, R., Miller, H., Neef, R., Pearson, J.A., Bogaard, A ., 2016. Disentangling the effect of farming practice from aridity

on crop stable isotope values: A present-day model from Morocco and its application to early farming sites in the eastern Mediterranean. Anthr. Rev. 3, 2–22.

Sullivan, C.H., Krueger, H.W., 1981. Carbon isotope analysis of separate chemical phases in modern and fossil bone. Nature 292, 333-335. doi:10.1038/292333a0

Swap, R.J., Aranibar, J.N., Dowty, P.R., Gilhooly, W.P., Macko, S.A., 2004. Natural abundance of 13 C and 15 N in C3 and C4 vegetation of southern Africa: patterns and implications. Glob. Chang. Biol. 10, 350–358. doi:10.1046/j.1529-8817.2003.00702.x

Symes, C.T., Wilson, J.W., Woodborne, S.M., Shaikh, Z.S., Scantlebury, M., 2013. Resource partitioning of sympatric small mammals in an African forest-grassland vegetation mosaic. Austral Ecol. 38, 721–729. doi:10.1111/aec.12020

Szpak, P., 2014. Complexities of nitrogen isotope biogeochemistry in plant-soil systems: implications for the study of ancient agricultural and animal management practices. Front. Plant Sci. 5, 288. doi:10.3389/fpls.2014.00288

Szpak, P., White, C.D., Longstaffe, F.J., Millaire, J.-F., Vásquez Sánchez, V.F., 2013. Carbon and nitrogen isotopic survey of northern peruvian plants: baselines for paleodietary and paleoecological studies. PLoS One 8, e53763. doi:10.1371/journal.pone.0053763

Taylor, V.K., Barton, R.N.E., Bell, M., Bouzouggar, A., Collcutt, S., Black, S., Hogue, J.T., 2011. The Epipalaeolithic (Iberomaurusian) at Grotte des Pigeons (Taforalt), Morocco: A preliminary study of the land Mollusca. Quat. Int. 244, 5–14. doi:10.1016/j.quaint.2011.04.041

Teeri, J., Stowe, L., 1976. Climatic patterns and the distribution of C_4 grasses in North America. Oecologia 23, 1–12. doi:10.1007/bf00351210

Tierney, J.E., Lewis, S.C., Cook, B.I., LeGrande, A.N., Schmidt, G. A., 2011. Model, proxy and isotopic perspectives on the East African Humid Period. Earth Planet. Sci. Lett. 307, 103–112. doi:10.1016/j.epsl.2011.04.038

Tieszen, L.L., 1991. Natural varitations in the carbon isotope values of plants: implications for archaeology, ecology and paleoecology. J. Archaeol. Sci. 18, 227–248.

Tieszen, L.L., Fagre, T., 1993. Effect of diet quality and composition in the isotopic composition of respiratory CO_2, bone collagen, bioapatitie, and soft

tissues, in: Lambert, J.B., Grupe, G. (Eds.), Prehistoric Human Bone: Archaeology at the Molecular Level. Springer-Verlag, Heidelberg, pp. 121–155.

Tillet, T., 1995. Recherches sur l'Atérien du Sahara Méridional (Bassins Tchadien et de Taoudenni): Position chrono-stratigraphique, définition, et étude comparative, in: Chenorkian, R. (Ed.), L'Homme Méditerranéen. Publications de L'Université de Provence, Aix-en-Provence, pp. 29–56.

Tixier, J., 1967. Procédés d'analyse et questions de terminologie concernant l'étude des ensembles industriels du Paléolithique récent et de l'Epipaléolithique dans l'Afrique du nord-ouest, in: Bishop, W.W., Clark, J.D. (Eds.), Background to Evolution in Africa. University of Chicago Press, Chicago, pp. 771–820.

Tjallingii, R., Claussen, M., Stuut, J.-B.W., Fohlmeister, J., Jahn, A., Bickert, T., Lamy, F., Röhl, U., 2008. Coherent high- and low-latitude control of the northwest African hydrological balance. Nat. Geosci. 1, 670–675. doi:10.1038/ngeo289

Tütken, T., Vennemann, T.W., Janz, H., Heizmann, E.P.J., 2006. Palaeoenvironment and palaeoclimate of the Middle Miocene lake in the Steinheim basin, SW Germany: A reconstruction from C, O, and Sr isotopes of fossil remains. Palaeogeogr. Palaeoclimatol. Palaeoecol. 241, 457–491. doi:10.1016/j.palaeo.2006.04.007

Tzedakis, P.C., Lawson, I.T., Frogley, M.R., Hewitt, G.M., Preece, R.C., 2002. Buffered tree population changes in a quaternary refugium: evolutionary implications. Science 297, 2044–7. doi:10.1126/science.1073083

Ulbrich, U., Lionello, P., Belusic, D., Jacobeit, J., Knippertz, P., Kuglitsch, F.G., Leckebusch, G.C., Luterbacher, J., Maugeri, M., Maheras, P., Nissen, K.M., Pavan, V., Pinto, J.G., Saaroni, H., Seubert, S., Toretri, A., Xoplaki, E., Ziv, B., 2012. Climate of the Mediterranean: synoptic patterns, temperature, precipitation, winds, and their extremes, in: Lionello, P. (Ed.), The Climate of the Mediterranean Region. Elsevier, London, pp. 301–346.

Valentini, R., Scarascia Mugnozza, G.E., Ehleringer, J.R., 1992. Hydrogen and carbon isotope rations of selected sspecies of a mediterranean macchia ecosystem. Funct. Ecol. 6, 627–631.

Valero-Garcés, B., Zeroual, E., Kelts, K., 1998. Arid phases in the Western Mediterranean region during the Last Glacial cycle reconstructed from lacustrine records, in: Benito, G., Baker, V.R., Gregory, K.J. (Eds.), Palaeohydrology and Environmental Change. Wiley, Chichester, pp. 67–80.

van der Merwe, N.J. Van Der, Medina, E., 1991. The canopy effect, carbon isotope ratios and foodwebs in Amazonia. J. Archaeol. Sci. 18, 249–259.

Van Peer, P., 1998. The Nile Corridor and the Out-of-Africa Model An Examination of the Archaeological Record. Curr. Anthropol. 39, 115–140. doi:10.1086/204692

Vogel, J., Fuls, A., Danin, A., 1986. Geographical and environmental distribution of C_3 and C_4 grasses in the Sinai, Negev, and Judean deserts. Oecologia 70, 258–265. doi:10.1007/BF00379249

Vogel, J.C., 1978. Recycling of CO_2 in a forest environment. Oecologia Plant. 13, 89–94.

Vogel, J.C., van der Merwe, N.J. Van Der, 1977. Isotopic evdience for early maize cultivation in New York State. Am. Antiq. 42, 238–242.

Waelbroeck, C., Labeyrie, L., Michel, E., Duplessy, J.C., McManus, J.F., Lambeck, K., Balbon, E., Labracherie, M., 2002. Sea-level and deep water temperature changes derived from benthic foraminifera isotopic records. Quat. Sci. Rev. 21, 295–305. doi:http://dx.doi.org/10.1016/S0277-3791(01)00101-9

Wang, Y., Kromhout, E., Zhang, C., Xu, Y., Parker, W., Deng, T., Qiu, Z., 2008. Stable isotopic variations in modern herbivore tooth enamel, plants and water on the Tibetan Plateau: Implications for paleoclimate and paleoelevation reconstructions. Palaeogeogr. Palaeoclimatol. Palaeoecol. 260, 359–374. doi:10.1016/j.palaeo.2007.11.012

Ward, S., 2007. Reconstructing Late Pleistocene vegetation dynamics from archaeological cave sites in the Western Mediterranean: links with climate and cultural changes. University of Oxford PhD Thesis.

Weiguo, L., Xiahong, F., Youfeng, N., Qingle, Z., Yunning, C., Zhisheng, a N., 2005. $\delta^{15}N$ variation of C_3 and C_4 plants across an Asian monsoon rainfall gradient in arid northwestern China. Glob. Chang. Biol. 11, 1094–1100. doi:10.1111/j.1365-2486.2005.00969.x

Wengler, L., 2006. Innovations et normes techniques dans le Paléolithique moyen et supérieur du Maghreb: Une alternative aux migrations? XXVIè rencontres internationales d'archéologie et d'histoire d'Antibes (Astruc, Bon, Léa, Milcent et Philibert dir.) (pp. 93–105). Editions APDCA, Antibes.

Wengler, L., 1993. Formations quaternaires et cultures préhistoriques au Maroc oriental. l'Université Bordeaux I PhD Thesis.

West, J.B., Sobek, A., Ehleringer, J.R., 2008. A simplified GIS approach to modeling global leaf water isoscapes. PLoS One 3, e2447. doi:10.1371/journal.pone.0002447

White, F., 1983. The Vegetation of Africa: A Descriptive Memoir to Accompany the UNESCO/AETFAT/UNSO Vegetation Map of Africa. UNESCO, Paris.

Williams, J., White, C., Longstaffe, F., 2005. Trophic level and macronutrient shift effects associated with the weaning process in the Postclassic Maya. Am. J. Phys. Anthropol. 128, 781–790.

Winkelmann, J.R., Getz, L.L., 1962. Water Balance in the Mongolian Gerbil. J. Mammal. 43, 150–154.

Winter, K., Troughton, J.H., 1978. Photosynthetic pathways in plants of coastal and inland habitats of Israel and the Sinai. Flora 1–34.

Wright, L.E., Schwarcz, H.P., 1998. Stable carbon and oxygen isotopes in human tooth enamel: identifying breastfeeding and weaning in prehistory. Am. J. Phys. Anthropol. 106, 1018.

Wrinn, P.J., Rink, W.J., 2003. ESR Dating of Tooth Enamel From Aterian Levels at Mugharet el ‘Aliya (Tangier, Morocco). J. Archaeol. Sci. 30, 123–133. doi:10.1006/jasc.2002.0813

Yakir, D., 1998. Oxygen-18 in leaf water: a crossroad for plant- associated isotopic signals, in: Griffiths, H. (Ed.), Stable Isotopes: The Integration of Biological, Ecological and Geochemical Processes. Bios Scientific, Oxford, pp. 147–168.

Yakir, D., 1992. Variations in the natural abundance of oxygen-18 and deuterium in plant carbohydrates. Plant, Cell Environ. 15, 1005–1020. doi:10.1111/j.1365-3040.1992.tb01652.x

Yakir, D., DeNiro, M.J., Ephrath, J.E., 1990. Effects of water stress on oxygen, hydrogen and carbon ratios in two species of cotton plants. Plant, Cell Environ. 13, 949–955.

Yeakel, J.D., Bennett, N.C., Koch, P.L., Dominy, N.J., 2007. The isotopic ecology of African mole rats informs hypotheses on the evolution of human diet. Proc. Biol. Sci. 274, 1723–30. doi:10.1098/rspb.2007.0330

Yi, X.F., Yang, Y.Q., 2006. Enrichment of stable carbon and nitrogen isotopes of plant populations and plateau pikas along altitudes. Jour. Anim. Feed. Sci. 15, 661–667.

Zaime, A., Gautier, J.Y., 1989. Comparaison des régimes alimentaires de trois espèces sympatriques de Gerbillidae en milieu saharien. Rev. d'Ecologie (La Terre la Vie) 44, 153–163.

Zaime, A., Gautier, J.Y., 1988. Analyse des fluctuations densitaires et de l'occupation de l'espace chez la Merione de Shaw (*Meriones shawii*) en milieu semi-aride au Maroc. Sci. Tech. Anim. Lab 13, 59–63.

Zaime, A., Laraki, M., Gautier, J.-Y., Garnier, D.H., 1992. Seasonal variations of androgens and of several sexual parameters in male *Meriones shawi* in Southern Morocco. Gen. Comp. Endocrinol. 86, 289–296.

10. Appendices

Appendix 1: Bayesian 'Sequence' model

```
Plot()
 {
  Outlier_Model("General",T(5),U(0,4),"t");
  Sequence("EH2")
  {
   Boundary("Start");
   OSL15= Age( N( 123700, 7400))
   {
    z=788.9;
    Outlier(0.05);
   };
   OSL14= Age( N(118300, 7100))
   {
    z=755.4;
    Outlier(0.05);
   };
   OSL13= Age( N(108100, 5900))
   {
    z=718.5;
    Outlier(0.05);
   };
   OSL12= Age( N(106700, 6600))
   {
    z=686.3;
    Outlier(0.05);
   };
   OSL11= Age( N(108100, 6300))
   {
    z=647.8;
    Outlier(0.05);
   };
   OSL10= Age( N(116400, 6600))
   {
    z=612.7;
    Outlier(0.05);
   };
   OSL9= Age( N(102600, 5700))
   {
    z=573.7;
    Outlier(0.05);
   };
   OSL8= Age( N( 99900, 5800))
   {
    z=532.4;
```

```
  Outlier(0.05);
 };
 Boundary("Boundary_level 6");
 OSL6= Age( N(73700, 4100))
 {
  z=475.3;
  Outlier(0.05);
 };
 Boundary("Boundary_phase 3");
 Phase("Level 3")
 {
  OSL4= Age( N( 57700, 4200))
  {
   z=422;
   Outlier(0.05);
  };
  OSL3= Age( N(61900, 4100))
  {
   z=405.5;
   Outlier(0.05);
  };
  OSL2= Age( N(51600, 3600))
  {
   z=401.8;
   Outlier(0.05);
  };
  OSL1= Age( N(61900, 3500))
  {
   z=400.2;
   Outlier(0.05);
  };
  OSL5= Age( N( 52600, 3300))
  {
   z=461.6;
   Outlier(0.05);
  };
  OSL7= Age( N( 57300, 4200))
  {
   z=502.5;
   Outlier(0.05);
  };
 };
 Boundary("end");
};
};
```

Appendix 1.2: Results of 'outlier analysis' run in Bayesian sequence model. Results show that none of the OSL dates are significant outliers.

Element	Ok	Outlier	Prior	Posterior	Model	Type
			5	5	General	t
			5	5	General	t
			5	5	General	t
			5	5	General	t
			5	5	General	t
			5	5	General	t
			5	5	General	t
			5	5	General	t
			5	5	General	t
			5	5	General	t
			5	5	General	t
			5	5	General	t
			5	5	General	t
			5	5	General	t
			5	5	General	t
			5	5	General	t

Appendix 2: The $\delta^{15}N$ and $\delta^{13}C$ composition of the gerbil bone collagen from 79 individuals (26 *Meriones* and 53 *Gerbillus*) and the $\delta^{18}O$ and $\delta^{13}C$ value for each gerbil molar tooth from the eight sites across NW Africa (M1= 1st molar, M2= 2nd molar, I=incisor). In the smaller *Gerbillus* species 2 x M1 or M1 + M2 were used to get enough sample powder for analyses. If no molar teeth were present in the gerbil mandible or maxilla incisor teeth were used to increase sample numbers.

Site	Sample No.	Genus	Species	Tooth/teeth sample	$\delta^{13}C_{(VPDB)}$ ‰	$\delta^{18}O_{(VPDB)}$ ‰	Bone sample	Repeat 1 $\delta^{13}C_{(VPDB)}$ ‰	Repeat 1 $\delta^{15}N_{(AIR)}$‰	Repeat 1 C:N Ratio	Repeat 2 $\delta^{13}C_{(VPDB)}$ ‰	Repeat 2 $\delta^{15}N_{(AIR)}$‰	Repeat 2 C:N Ratio	Average $\delta^{13}C_{(VPDB)}$ ‰	Average $\delta^{15}N_{(AIR)}$‰
Oued Nififikh	NA01 6	*Gerbillus*	*campestris*	2 x M1	**-13.4**	**-3.7**	Whole skull	-21.0	8.4	3.2	-20.8	8.1	3.3	**-20.9**	**8.2**
Oued Nififikh	NA01 12	*Gerbillus*	*campestris*	M1, M2	**-12.9**	**-3.8**	Mandible	-20.8	7.1	3.4	-20.8	7.1	3.4	**-20.8**	**7.1**
Oued Nififikh	NA01 13	*Gerbillus*	*campestris*	M1, M2	**-7.6**	**-5.1**	Mandible	-18.1	8.3	3.3	-18.0	8.4	3.3	**-18.1**	**8.3**
Oued Nififikh	NA01 14	*Gerbillus*	*campestris*	M1, M2	**-15.2**	**-4.0**	Mandible	-22.9	8.4	3.4	-22.6	8.4	3.3	**-22.7**	**8.4**
Oued Nififikh	NA01 15	*Gerbillus*	*campestris*	1 x Lower incisor	**-14.7**	**-3.2**	Mandible	-18.1	8.1	3.3	-18.0	8.0	3.3	**-18.1**	**8.0**
Oued Nififikh	NA01 16	*Gerbillus*	*campestris*	M1, M2	**-13.7**	**-2.6**									
Beni Abbes	BA 1	*Meriones*	cf. *crassus*	M1	**-13.7**	**3.3**	Whole skull	-20.0	6.3	3.2	-20.0	6.2	3.2	**-20.0**	**6.3**
Beni Abbes	BA 2	*Meriones*	cf. *crassus*	M1	**-12.8**	**2.1**	Skull fragments	-19.1	5.7	3.2	-19.1	5.7	3.2	**-19.1**	**5.7**
Beni Abbes	BA 3	*Gerbillus*	cf. *tarabuli*	2 x M1	**-13.1**	**3.7**	Skull fragments and mandible	-18.0	10.2	3.4	-18.1	10.4	3.4	**-18.0**	**10.3**
Beni Abbes	BA 4	*Gerbillus*	*nanus/ henleyi*	M1	**-13.3**	**-0.4**	2 x Mandibles	-18.2	3.9	3.4	-18.3	3.9	3.3	**-18.3**	**3.9**
Beni Abbes	BA 5	*Meriones*	cf. *libycus*	M1	**-16.3**	**0.2**	2 x Mandibles	-22.2	3.1	3.3	-22.3	2.9	3.3	**-22.2**	**3.0**
Beni Abbes	BA 6a	*Gerbillus*	*nanus/ henleyi*	2 x Lower incisors	**-13.2**	**2.8**	2 x Mandibles	-18.6	7.9	3.3	-18.7	7.3	3.4	**-18.7**	**7.6**
Beni Abbes	BA 6b	*Gerbillus*	cf. *tarabuli*	M1	**-12.1**	**3.8**	Mandible	-19.7	2.8	3.4	-19.7	2.9	3.4	**-19.7**	**2.9**
Beni Abbes	BA 7	*Gerbillus*	cf. *tarabuli*	M1	**-11.8**	**3.5**	Skull fragments	-18.6	7.1	3.3	-18.6	7.3	3.3	**-18.6**	**7.2**
Beni Abbes	BA 8	*Meriones*	cf. *crassus*	M1, M2	**-12.6**	**-0.6**	Mandibles	-21.1	3.8	3.4	-21.5	4.0	3.5	**-21.3**	**3.9**
Beni Abbes	BA 9	*Gerbillus*	cf. *tarabuli*	M1	**-14.9**	**-0.3**	Mandible and skull fragments	-20.8	5.5	3.3	-20.7	5.6	3.3	**-20.8**	**5.5**
Sidi Chicker	SC 1	*Meriones*	*shawii/ grandis*	M1	**-13.4**	**-1.0**	Skull fragment	-19.5	3.9	3.3	-19.5	3.8	3.3	**-19.5**	**3.9**

Sidi Chicker	SC 2	*Meriones*	*shawii/ grandis*	M1	**-11.9**	**-2.9**	Skull fragment	-19.4	4.8	3.2	-19.4	4.8	3.2	**-19.4**	**4.8**
Sidi Chicker	SC 3	*Meriones*	*shawii/ grandis*	M1	**-13.9**	**0.6**	Skull fragment	-20.7	4.3	3.2	-20.7	4.4	3.2	**-20.7**	**4.4**
Sidi Chicker	SC4	*Meriones*	*shawii/ grandis*	M1	**-13.0**	**-1.9**	Skull fragment	-19.1	3.9	3.3	-19.0	3.7	3.3	**-19.0**	**3.8**
Sidi Chicker	SC 5a	*Meriones*	*shawii/ grandis*				Mandible	-18.5	6.3	3.3	-18.5	5.9	3.3	**-18.5**	**6.1**
Sidi Chicker	SC 5b	*Meriones*	*shawii/ grandis*	M1	**-12.5**	**-2.1**	Mandible	-19.0	6.8	3.3	-19.2	6.6	3.4	**-19.1**	**6.7**
Sidi Chicker	SC 5c	*Meriones*	*shawii/ grandis*	M1	**-12.0**	**-3.0**	Mandible	-19.5	4.7	3.3	-19.5	4.9	3.3	**-19.5**	**4.8**
Sidi Chicker	SC 5d	*Meriones*	*shawii/ grandis*	M1	**-14.1**	**0.6**	Mandible	-21.0	4.9	3.3	-21.0	4.3	3.3	**-21.0**	**4.6**
Sidi Chicker	SC 5e	*Meriones*	*shawii/ grandis*										3.3		
Sidi Chicker	SC 6	*Gerbillus*	*campestris*	M1	**-15.5**	**-2.0**	Mandible	-21.4	5.3	3.3	-21.4	5.4	3.3	**-21.4**	**5.4**
Sidi Chicker	SC 7	*Gerbillus*	*campestris*	M1, M2	**-13.3**	**-2.3**	Skull fragment	-20.0	5.8	3.3	-20.1	5.7	3.2	**-20.0**	**5.8**
Sidi Chicker	SC 8	*Gerbillus*	*campestris*	M1, M2	**-11.9**	**-1.3**	Skull fragment	-18.8	5.4	3.2	-18.8	5.4	3.3	**-18.8**	**5.4**
Sidi Chicker	SC 9	*Gerbillus*	*campestris*	2 x M1	**-11.7**	**-2.5**	Skull fragment	-18.1	6.7	3.3	-18.2	6.7	3.2	**-18.1**	**6.7**
Sidi Chicker	SC 10	*Gerbillus*	*campestris*	M1, M2	**-13.2**	**-0.5**	Whole skull	-18.9	6.4	3.2	-18.8	6.4	3.3	**-18.8**	**6.4**
Sidi Chicker	SC 11	*Gerbillus*	*campestris*	M1	**-12.8**	**-2.8**	Whole skull	-19.1	4.7	3.2	-19.1	4.4	3.3	**-19.1**	**4.6**
Sidi Chicker	SC 12a	*Gerbillus*	*campestris*				Mandible	-19.0	9.0	3.2	-18.8	8.7	3.4	**-18.9**	**8.9**
Sidi Chicker	SC 12b	*Gerbillus*	*campestris*				Mandible	-19.3	5.6	3.4	-19.2	5.6	3.3	**-19.3**	**5.6**
Sidi Chicker	SC 12c	*Gerbillus*	*campestris*				Mandible	-19.8	4.3	3.3	-19.8	4.3	3.3	**-19.8**	**4.3**
Sidi Chicker	SC 12d	*Gerbillus*	*campestris*				Mandible	-19.6	10.8	3.4	-19.5	10.6	3.3	**-19.5**	**10.7**
Sidi Chicker	SC 12e	*Gerbillus*	*campestris*	M1, M2	**-12.7**	**-1.9**	Mandible	-19.0	5.0	3.4				**-19.0**	**5.0**
Sidi Chicker	SC 12f	*Gerbillus*	*campestris*	M1, M2	**-12.5**	**-0.5**	Mandible	-19.1	5.5	3.3	-19.0	5.2	3.3	**-19.1**	**5.4**
Sidi Chicker	SC 13	*Gerbillus*	*campestris*				Whole skull	-20.1	4.6	3.3	-20.1	4.6	3.3	**-20.1**	**4.6**
Sidi Chicker	SC 14	*Gerbillus*	*campestris*	M1	**-13.8**	**-2.4**	Whole skull	-20.0	5.1	3.2	-19.9	5.0	3.3	**-19.9**	**5.1**
Sidi Chicker	SC 15	*Gerbillus*	*campestris*	2 x M1	**-12.7**	**-2.8**	Whole skull	-19.8	5.7	3.3	-20.4	5.4	3.4	**-20.1**	**5.6**
Sidi Chicker	SC 16	*Gerbillus*	*campestris*	M1	**-12.5**	**-2.9**	Whole skull	-18.7	8.5	3.5	-18.8	8.5	3.3	**-18.7**	**8.5**
Sidi Chicker	SC 17	*Gerbillus*	*nanus/ henleyi*	M1, M2	**-12.5**	**-1.3**	Mandible	-19.5	5.5	3.3	-19.3	5.5	3.4	**-19.4**	**5.5**
Sidi Chicker	SC 18	*Gerbillus*	*campestris*				Whole skull	-18.4	7.7	3.3	-18.2	7.7	3.3	**-18.3**	**7.7**
Sidi Chicker	SC19	*Gerbillus*	*campestris*	2 x M1	**-12.9**	**-2.6**	Whole skull	-18.8	5.6	3.3	-18.6	5.7	3.2	**-18.7**	**5.7**
Sidi Chicker	SC 20	*Meriones*	*shawii/ grandis*	M1	**-12.9**	**-2.3**	Mandible	-20.7	6.3	3.3	-21.0	6.3	3.4	**-20.8**	**6.3**

Sidi Chicker	SC 21	*Meriones*	*shawii/ grandis*	M1	**-12.7**	**-2.4**	Mandible	-20.6	4.2	3.3	-20.6	4.4	3.3	**-20.6**	**4.3**
Sidi Chicker	SC 22	*Meriones*	*shawii/ grandis*	M1	**-13.1**	**-2.1**	Mandible (frags)	-21.0	6.7	3.4	-20.5	6.7	3.3	**-20.7**	**6.7**
Sidi Chicker	SC 23	*Meriones*	*shawii/ grandis*	M1	**-11.1**	**-1.5**	Mandible	-19.2	4.9	3.3	-19.2	4.8	3.3	**-19.2**	**4.8**
Sidi Chicker	SC 24	*Meriones*	*shawii/ grandis*	M1	**-13.8**	**-0.5**	Mandible	-20.2	5.1	3.3	-20.1	5.2	3.3	**-20.1**	**5.1**
Tata	Ta1a	*Gerbillus*	*gerbillus*	2 x M1	**-6.2**	**-0.2**	Skull fragments and mandibles	-11.2	9.8	3.2	-11.1	9.9	3.3	**-11.2**	**9.8**
Tata	Ta1b	*Gerbillus*	*gerbillus*				Skull fragments	-12.2	8.6	3.3	-12.2	8.5	3.3	**-12.2**	**8.6**
Tata	Ta2	*Gerbillus*	sp.	M1, M2	**-7.6**	**-0.9**		-9.8	8.8	3.3	-10.0	8.7	3.3	**-9.9**	**8.7**
Tata	Ta4	*Gerbillus*	*gerbillus*	2 x M1	**-5.0**	**-0.7**	Skull fragments and mandibles	-10.8	9.3	3.3	-10.8	9.4	3.4	**-10.8**	**9.3**
Tata	Ta13	*Gerbillus*	sp.	2 x Incisor	**-4.6**	**-2.1**	Skull fragments	-10.1	11.2	3.3	-10.1	11.1	3.3	**-10.1**	**11.2**
Tata	Ta16	*Gerbillus*	*gerbillus*	2 x M1	**-12.4**	**-1.4**	Skull fragments and mandibles	-17.0	10.9	3.3	-16.9	10.9	3.3	**-16.9**	**10.9**
Tata	Ta17	*Gerbillus*	*gerbillus*	2 x M1	**-9.4**	**-0.4**	Skull fragments and mandibles	-11.8	9.8	3.3	-11.5	9.8	3.3	**-11.7**	**9.8**
Tata	Ta22	*Gerbillus*	*gerbillus*	2 x Upper incisors	**-5.7**	**-1.1**	Skull fragments and mandible	-10.4	10.6	3.5	-9.4	10.5	3.4	**-9.9**	**10.5**
Tata	Ta24	*Gerbillus*	sp.	2 x Upper incisors	**-13.4**	**-0.5**	Skull fragments and mandibles	-18.9	8.6	3.3	-18.8	8.9	3.3	**-18.9**	**8.8**
Tata	Ta28	*Gerbillus*	sp.				Skull fragments	-10.1	8.3	3.3	-10.1	8.3	3.3	**-10.1**	**8.3**
Guenfonda	GU 1	*Meriones*	*shawii*	M1	**-14.8**	**-2.5**	Mandible	-22.6	6.1	3.3	-22.7	6.1	3.2	**-22.7**	**6.1**
Guenfonda	GU 3	*Meriones*	*shawii*	M1	**-15.5**	**-1.8**	Mandible	-23.3	5.2	3.3	-23.1	5.1	3.3	**-23.2**	**5.1**
Guenfonda	GU 8	*Meriones*	*shawii*	M1	**-16.2**	**-1.6**	Mandible	-21.9	5.3	3.3	-22.0	5.3	3.3	**-22.0**	**5.3**
Guenfonda	GU 21a	*Gerbillus*	*campestris*	M1	**-14.8**	**-4.4**	Mandible and long bone	-22.4	6.7	3.3	-22.6	6.9	3.3	**-22.5**	**6.8**
Guenfonda	GU21b	*Meriones*	cf. *shawii*	M1	**-13.0**	**-3.3**	Mandible	-20.6	8.9	3.3	-20.6	8.9	3.3	**-20.6**	**8.9**

Ouled Boughadi	OB 1	*Gerbillus*	*campestris*	M1	**-14.9**	**-2.6**	Mandible and long bone	-21.0	7.8	3.3	-21.0	7.7	3.3	**-21.0**	**7.8**
Ouled Boughadi	OB 2	*Gerbillus*	*campestris*	M1, M2	**-15.2**	**-2.1**	Mandible	-21.1	7.5	3.4	-21.1	7.6	3.3	**-21.1**	**7.6**
Ouled Boughadi	OB 4	*Gerbillus*	*campestris*	M1, M2	**-14.7**	**-3.4**	Mandible	-21.4	8.1	3.3	-21.4	8.0	3.3	**-21.4**	**8.1**
Ouled Boughadi	OB 5	*Meriones*	*shawii*				Femur	-23.3	5.6	3.3	-23.3	5.6	3.3	**-23.3**	**5.6**
Ouled Boughadi	OB 6	*Meriones*	*shawii*	M1	**-15.0**	**-4.4**	Mandible	-22.8	3.1	3.3	-22.8	3.1	3.3	**-22.8**	**3.1**
Ouled Boughadi	OB 7	*Meriones*	*shawii*	M1	**-14.2**	**-4.4**	Mandible	-22.7	4.5	3.3	-22.7	4.5	3.3	**-22.7**	**4.5**
Ouled Boughadi	OB 8	*Meriones*	*shawii*	M1	**-15.6**	**-3.5**	Mandible	-23.4	5.1	3.2	-23.3	5.1	3.3	**-23.3**	**5.1**
Ouled Boughadi	OB 9	*Gerbillus*	*campestris*	M1	**-14.8**	**-3.5**	Mandible	-20.9	7.9	3.3	-20.9	7.8	3.3	**-20.9**	**7.8**
Ouled Boughadi	OB 10	*Meriones*	*shawii*	M1	**-14.5**	**-3.9**	Mandible	-22.5	4.0	3.3	-22.5	3.9	3.3	**-22.5**	**3.9**
Merga Zerga	MZ 1	*Gerbillus*	*campestris*	M1	**-15.2**	**-4.5**	Mandible and long bone	-20.8	4.2	3.3	-20.8	4.3	3.3	**-20.8**	**4.2**
Merga Zerga	MZ 2	*Gerbillus*	*campestris*	M1, M2	**-15.3**	**-3.5**	Mandible	-22.8	4.7	3.5	-22.5	4.6	3.3	**-22.7**	**4.6**
Merga Zerga	MZ 3	*Gerbillus*	*campestris*	M1	**-14.6**	**-4.9**	Mandible	-18.8	8.4	3.3	-18.8	8.4	3.4	**-18.8**	**8.4**
Merga Zerga	MZ 4	*Gerbillus*	*campestris*	M1	**-12.8**	**-4.9**	Mandible	-18.4	4.8	3.4	-18.3	4.7	3.3	**-18.3**	**4.8**
Merga Zerga	MZ 5	*Gerbillus*	*campestris*	M1, M2	**-14.1**	**-5.2**	Mandible (frag)	-22.0	4.4	3.5				**-22.0**	**4.4**
Merga Zerga	MZ 6	*Gerbillus*	*campestris*	M1, M2	**-12.2**	**-4.3**	Mandible (frag)	-17.2	5.6	3.4	-17.1	5.8	3.4	**-17.1**	**5.7**
Berrachid	BE4	*Gerbillus*	cf. *maghrebi*	M1, M2	**-14.5**	**-3.2**	Mandible	-20.6	7.5	3.4	-20.7	7.3	3.4	**-20.7**	**7.4**
Berrachid	BE5	*Gerbillus*	cf. *maghrebi*	M1, M2	**-15.1**	**-4.2**	Mandible	-21.9	9.0	3.3	-21.9	9.0	3.3	**-21.9**	**9.0**

Appendix 3.1: Post Hoc Tukey tests showing differences in $\delta^{18}O_{mt}$ between 7 modern sites (Berrechid removed from analysis). Significant values are shown in bold.

Site	*P* value
Guenfonda-Beni Abbes	**0.0000000**
Merga Zerga-Beni Abbes	**0.0000000**
Oued Nififikh-Beni Abbes	**0.0000000**
Ouled Boughadi-Beni Abbes	**0.0000000**
Sidi Chicker-Beni Abbes	**0.0000000**
Tata-Beni Abbes	**0.0000604**
Merga Zerga-Guenfonda	0.1091154
Oued Nififikh-Guenfonda	0.7247949
Ouled Boughadi-Guenfonda	0.8863878
Sidi Chicker-Guenfonda	0.6180876
Tata-Guenfonda	**0.0875091**
Oued Nififikh-Merga Zerga	0.8702752
Ouled Boughadi-Merga Zerga	0.5689662
Sidi Chicker-Merga Zerga	**0.0000183**
Tata-Merga Zerga	**0.0000021**
Ouled Boughadi-Oued Nififikh	0.9994287
Sidi Chicker-Oued Nififikh	**0.0046932**
Tata-Oued Nififikh	**0.0003000**
Sidi Chicker-Ouled Boughadi	**0.0067971**
Tata-Ouled Boughadi	**0.0004193**
Tata-Sidi Chicker	**0.4827537**

Appendix 3.2: Post Hoc Tukey tests showing differences in $\delta^{13}C_{mt}$ between 7 modern sites (Berrechid removed from analysis). Significant values are shown in bold.

Site	*P* value
Guenfonda-Beni Abbes	0.6753830
Merga Zerga-Beni Abbes	0.9873203
Oued Nififikh-Beni Abbes	0.9986605
Ouled Boughadi-Beni Abbes	0.5045253
Sidi Chicker-Beni Abbes	0.9871040
Tata-Beni Abbes	**0.0000001**
Merga Zerga-Guenfonda	0.9836371
Oued Nififikh-Guenfonda	**0.4942488**
Ouled Boughadi-Guenfonda	1.0000000

Sidi Chicker-Guenfonda	**0.2210400**
Tata-Guenfonda	**0.0000000**
Oued Nifififkh-Merga Zerga	0.9133353
Ouled Boughadi-Merga Zerga	0.9689125
Sidi Chicker-Merga Zerga	0.7421832
Tata-Merga Zerga	**0.0000002**
Ouled Boughadi-Oued Nifififkh	**0.3477958**
Sidi Chicker-Oued Nifififkh	1.0000000
Tata-Oued Nifififkh	**0.0000196**
Sidi Chicker-Ouled Boughadi	**0.0730348**
Tata-Ouled Boughadi	**0.0000000**
Tata-Sidi Chicker	**0.0000000**

Appendix 3.3: Post Hoc Tukey tests showing differences in $\delta^{15}N_{col}$ between 7 modern sites (Berrechid removed from analysis). Significant values are shown in bold.

Site	***P* value**
Guenfonda-Beni Abbes	0.9685891
Merga Zerga-Beni Abbes	0.9998759
Oued Nifififkh-Beni Abbes	**0.1177625**
Ouled Boughadi-Beni Abbes	0.9995209
Sidi Chicker-Beni Abbes	0.9999983
Tata-Beni Abbes	**0.0000122**
Merga Zerga-Guenfonda	0.9209695
Oued Nifififkh-Guenfonda	0.7260484
Ouled Boughadi-Guenfonda	0.9978919
Sidi Chicker-Guenfonda	0.967747
Tata-Guenfonda	**0.0111702**
Oued Nifififkh-Merga Zerga	**0.1098423**
Ouled Boughadi-Merga Zerga	0.9922124
Sidi Chicker-Merga Zerga	0.9984305
Tata-Merga Zerga	**0.000057**
Ouled Boughadi-Oued Nifififkh	**0.2655207**
Sidi Chicker-Oued Nifififkh	**0.064785**
Tata-Oued Nifififkh	0.5522199
Sidi Chicker-Ouled Boughadi	0.9998132
Tata-Ouled Boughadi	**0.0001089**
Tata-Sidi Chicker	**0.0000001**

Appendix 3.4: Post Hoc Tukey tests showing differences in $\delta^{13}C_{col}$ between 7 modern sites (Berrechid removed from analysis). Significant values are shown in bold.

Site	*P* value
Guenfonda-Beni Abbes	**0.0754125**
Merga Zerga-Beni Abbes	0.9998739
Oued Nifififkh-Beni Abbes	0.9986202
Ouled Boughadi-Beni Abbes	**0.0240962**
Sidi Chicker-Beni Abbes	0.9999858
Tata-Beni Abbes	**0**
Merga Zerga-Guenfonda	**0.2534933**
Oued Nifififkh-Guenfonda	**0.3962345**
Ouled Boughadi-Guenfonda	0.9999999
Sidi Chicker-Guenfonda	**0.0159446**
Tata-Guenfonda	**0**
Oued Nifififkh-Merga Zerga	0.9999974
Ouled Boughadi-Merga Zerga	**0.1577223**
Sidi Chicker-Merga Zerga	0.9971678
Tata-Merga Zerga	**0**
Ouled Boughadi-Oued Nifififkh	**0.2982356**
Sidi Chicker-Oued Nifififkh	0.9881358
Tata-Oued Nifififkh	**0**
Sidi Chicker-Ouled Boughadi	**0.0012286**
Tata-Ouled Boughadi	**0**
Tata-Sidi Chicker	**0**

Appendix 4.1: The $\delta^{18}O$ and $\delta^{13}C$ composition of the left-right Gerbillinae molar and incisor teeth.

			$\delta^{18}O$ composition of teeth (‰)		$\delta^{13}C$ composition of teeth (‰)	
Molar pairs	**Genus**	**Upper/Lower**	**Left**	**Right**	**Left**	**Right**
1	*Meriones*	Upper	-1.0	-0.8	-13.4	-13.5
2	*Meriones*	Upper	-2.9	-2.8	-11.7	-12.0
3	*Meriones*	Upper	0.6	0.6	-13.9	-14.1
4	*Meriones*	Upper	-1.4	-1.9	-12.9	-13.0
5	*Meriones*	Lower	-2.1	-0.7	-12.5	-12.4
Incisor pairs						
1	*Gerbillus*	Upper	-1.7	-0.7	-13.5	-14.3
2	*Gerbillus*	Upper	-1.7	-2.0	-14.6	-14.5
3	*Meriones*	Upper	-0.2	0.6	-15.5	-15.8
4	*Meriones*	Upper	-1.8	-1.0	-13.9	-13.4
5	*Gerbillus*	Upper	-1.2	-1.1	-13.7	-14.3

Appendix 4.2: $\delta^{18}O$ and $\delta^{13}C$ values for gerbil inter-tooth analysis. * denotes where 2 M1's were combined and ^ demotes where M1 + M2 were combined.

		Incisor		1st Molar		2nd Molar	
Meriones	**Upper/Lower**	**$\delta^{18}O$**	**$\delta^{13}C$**	**$\delta^{18}O$**	**$\delta^{13}C$**	**$\delta^{18}O$**	**$\delta^{13}C$**
1	Upper	-0.2	-15.5	-0.62	-13.9	0.7	-14.0
2	Lower	0.8	-14.5	-1.5	-11.1	-1.7	-11.2
3	Lower	-4.3	-17.7	-2.5	-14.8	-2.6	-14.8
4	Lower	-1.1	-15.8	-1.8	-15.5	-1.8	-15.3
5	Lower	-0.8	-14.5	-1.6	-16.1	-1.6	-15.6
6	Lower	-5.1	-14.9	-4.3	-14.1	-4.5	-14.0
7	Lower	-4.9	-16.4	-3.5	-15.6	-3.4	-15.4
8	Lower	-4.3	-14.8	-3.9	-14.5	-4.0	-14.5
9	Upper	-1.1	-14.5	-1.0	-13.4	-0.4	-13.3
10	Upper	-2.7	-16.1	-2.9	-11.9	-2.8	-11.8
11	Upper	-1.8	-13.9	-1.9	-13.0	-1.5	-12.9
Gerbillus	**Upper/Lower**	**$\delta^{18}O$**	**$\delta^{13}C$**	**$\delta^{18}O$**	**$\delta^{13}C$**	**$\delta^{18}O$**	**$\delta^{13}C$**
1	Lower	5.22	-12.7	*3.7	*-13.1		
2	Upper	-1.2	-12.1	-0.4	-13.2		
3	Upper	-1.7	-13.5	3.8	-12.1		
4	Upper	0.9	-13.7	3.5	-11.6		
5	Upper	-1.7	-14.6	^-0.3	^-14.9		
6	Upper	-1.2	-13.7	*-2.8	*-12.7		
7	Lower	-4.5	-13.7	^-2.6	^-14.9		

Appendix 5: The δ18O and δ13C values of molars and incisors from El Harhoura 2 (molars n= 109, incisors n= 55).

Site	Level	Square	Sample No.	Species	Tooth	$\delta^{13}C_{(VPDB)}$‰	$\delta^{18}O_{(VPDB)}$‰
El Harhoura 2	2	N14	NNGOV	*Meriones shawii/grandis*	molar	-8.6	-2.2
El Harhoura 2	2	N14	FMLTJ	*Meriones shawii/grandis*	molar	-8.9	-1.8
El Harhoura 2	2	N14	FMLTJ	*Meriones shawii/grandis*	molar	-10.8	-2.2
El Harhoura 2	2	N14	QHUYV	*Meriones shawii/grandis*	molar	-8.5	-1.4
El Harhoura 2	2	N14	BOMWH	*Meriones shawii/grandis*	molar	-8.6	-3.3
El Harhoura 2	2	N14	DGWDJ	*Meriones shawii/grandis*	molar	-9.3	-2.8
El Harhoura 2	2	N14	DGWDJ	*Meriones shawii/grandis*	molar	-8.8	-1.6
El Harhoura 2	2	N14	TACMV	*Meriones shawii/grandis*	molar	-8.2	-2.9
El Harhoura 2	2	N14	TACMV	*Meriones shawii/grandis*	molar	-8.0	-2.5
El Harhoura 2	2	N14	TACMV	*Meriones shawii/grandis*	molar	-8.7	-3.0
El Harhoura 2	2	N14	BOMWH	*Meriones shawii/grandis*	incisor	-9.3	-4.1
El Harhoura 2	2	N14	BQSHE	*Meriones shawii/grandis*	incisor	-9.3	-2.9
El Harhoura 2	2	N14	QHUYN	*Meriones shawii/grandis*	incisor	-8.4	-2.9
El Harhoura 2	2	N14	EBRTQ	*Meriones shawii/grandis*	incisor	-8.7	-2.4
El Harhoura 2	2	N14	PKHLH	*Meriones shawii/grandis*	incisor	-8.4	-3.6
El Harhoura 2	3	Q11	ORXVB	*Meriones shawii/grandis*	molar	-8.5	-2.3
El Harhoura 2	3	Q12	ORXVB	*Meriones shawii/grandis*	molar	-9.5	-4.2
El Harhoura 2	3	O13	BOPGZ	*Meriones shawii/grandis*	molar	-8.4	-3.2
El Harhoura 2	3	O13	BOPGZ	*Meriones shawii/grandis*	molar	-9.1	-2.5
El Harhoura 2	3	O13	BOPGZ	*Meriones shawii/grandis*	molar	-9.0	-4.1
El Harhoura 2	3	O13	BOPGZ	*Meriones shawii/grandis*	molar	-8.6	-4.1
El Harhoura 2	3	O13	BOPGZ	*Meriones shawii/grandis*	molar	-8.9	-3.8
El Harhoura 2	3	O13	VFXPQ	*Meriones shawii/grandis*	molar	-9.1	-3.7

El Harhoura 2	3	O13	VFXPQ	*Meriones shawii/grandis*	molar	-8.9	-3.7
El Harhoura 2	3	O13	VFXPQ	*Meriones shawii/grandis*	molar	-9.0	-3.2
El Harhoura 2	3	Q12	HQQHH	*Meriones shawii/grandis*	incisor	-9.3	-4.0
El Harhoura 2	3	P13	SFVIM	*Meriones shawii/grandis*	incisor	-9.4	-4.9
El Harhoura 2	3	P13	SFVIM	*Meriones shawii/grandis*	incisor	-7.9	-2.3
El Harhoura 2	3	D13	BOPGZ	*Meriones shawii/grandis*	incisor	-8.8	-4.8
El Harhoura 2	3	D13	BOPGZ	*Meriones shawii/grandis*	incisor	-8.5	-3.9
El Harhoura 2	4a	Q11	GJKNH	*Meriones shawii/grandis*	molar	-9.4	-2.8
El Harhoura 2	4a	Q11	GJKNH	*Meriones shawii/grandis*	molar	-9.6	-3.5
El Harhoura 2	4a	Q12	WPJKW	*Meriones shawii/grandis*	molar	-9.3	-2.2
El Harhoura 2	4a	Q12	WPJKW	*Meriones shawii/grandis*	molar	-8.7	-3.6
El Harhoura 2	4a	Q12	WPJKW	*Meriones shawii/grandis*	molar	-9.3	-3.8
El Harhoura 2	4a	Q11	BUMFP	*Meriones shawii/grandis*	molar	-9.2	-4.1
El Harhoura 2	4a	Q11	BUMFP	*Meriones shawii/grandis*	molar	-8.7	-4.4
El Harhoura 2	4a	Q11	BUMFP	*Meriones shawii/grandis*	molar	-8.3	-3.6
El Harhoura 2	4a	Q11	BUMFP	*Meriones shawii/grandis*	molar	-8.9	-4.5
El Harhoura 2	4a	Q11	BUMFP	*Meriones shawii/grandis*	molar	-8.7	-3.5
El Harhoura 2	4a	Q11	TATIS	*Meriones shawii/grandis*	incisor	-8.8	-4.5
El Harhoura 2	4a	Q11	BUMFP	*Meriones shawii/grandis*	incisor	-9.4	-4.6
El Harhoura 2	4a	Q12	HJLYD	*Meriones shawii/grandis*	incisor	-8.3	-4.0
El Harhoura 2	4a			*Meriones shawii/grandis*	incisor	-9.2	-4.2
El Harhoura 2	4a			*Meriones shawii/grandis*	incisor	-9.0	-4.9
El Harhoura 2	4b	O11	VCUTE	*Meriones shawii/grandis*	molar	-8.8	-4.3
El Harhoura 2	4b	O11	VCUTE	*Meriones shawii/grandis*	molar	-8.7	-3.1
El Harhoura 2	4b	O11	VCUTE	*Meriones shawii/grandis*	molar	-8.7	-2.7
El Harhoura 2	4b	O11	VCUTE	*Meriones shawii/grandis*	molar	-9.6	-3.4

El Harhoura 2	4b	O11	VCUTE	*Meriones shawii/grandis*	molar	-9.1	-4.0
El Harhoura 2	4b	O11	VCUTE	*Meriones shawii/grandis*	molar	-9.1	-3.9
El Harhoura 2	4b	O11	VCUTE	*Meriones shawii/grandis*	molar	-9.7	-4.2
El Harhoura 2	4b	O11	VCUTE	*Meriones shawii/grandis*	molar	-9.5	-5.1
El Harhoura 2	4b	O11	VCUTE	*Meriones shawii/grandis*	molar	-10.0	-4.3
El Harhoura 2	4b	O11	JQDGU	*Meriones shawii/grandis*	incisor	-9.0	-4.4
El Harhoura 2	4b	O11	VCUTE	*Meriones shawii/grandis*	incisor	-9.5	-3.6
El Harhoura 2	4b	O11	WS6UB	*Meriones shawii/grandis*	incisor	-9.3	-4.7
El Harhoura 2	4b	O11	WS6UB	*Meriones shawii/grandis*	incisor	-9.0	-4.2
El Harhoura 2	4b	O11	WS6UB	*Meriones shawii/grandis*	incisor	-9.7	-4.5
El Harhoura 2	5	O12	JBMFW	*Meriones shawii/grandis*	molar	-9.5	-4.3
El Harhoura 2	5	O12	JBMFW	*Meriones shawii/grandis*	molar	-10.3	-5.3
El Harhoura 2	5	O12	JBMFW	*Meriones shawii/grandis*	molar	-9.8	-4.1
El Harhoura 2	5	O12	JBMFW	*Meriones shawii/grandis*	molar	-9.3	-5.0
El Harhoura 2	5	O12	JBMFW	*Meriones shawii/grandis*	molar	-9.6	-3.7
El Harhoura 2	5	O12	JBMFW	*Meriones shawii/grandis*	molar	-9.7	-5.5
El Harhoura 2	5	O12	JBMFW	*Meriones shawii/grandis*	molar	-9.5	-4.6
El Harhoura 2	5	P12	CFRNF	*Meriones shawii/grandis*	molar	-10.1	-3.8
El Harhoura 2	5	P12	CFRNF	*Meriones shawii/grandis*	molar	-8.3	-3.1
El Harhoura 2	5	P12	CFRNF	*Meriones shawii/grandis*	molar	-8.1	-2.9
El Harhoura 2	5	O12	JBMFW	*Meriones shawii/grandis*	incisor	-8.6	-4.2
El Harhoura 2	5	O12	JBMFW	*Meriones shawii/grandis*	incisor	-9.3	-4.1
El Harhoura 2	5	P12	CFRNF	*Meriones shawii/grandis*	incisor	-9.2	-4.3
El Harhoura 2	5	P12	CFRNF	*Meriones shawii/grandis*	incisor	-10.1	-4.9
El Harhoura 2	5	P12	CFRNF	*Meriones shawii/grandis*	incisor	-9.3	-4.8
El Harhoura 2	6	P12	HKOIH	*Meriones shawii/grandis*	molar	-9.0	-4.2

El Harhoura 2	6	P12	HKOIH	*Meriones shawii/grandis*	molar	-9.3	-3.0
El Harhoura 2	6	P12	HKOIH	*Meriones shawii/grandis*	molar	-9.1	-4.1
El Harhoura 2	6	P12	HKOIH	*Meriones shawii/grandis*	molar	-8.1	-3.6
El Harhoura 2	6	P12	HKOIH	*Meriones shawii/grandis*	molar	-9.1	-2.5
El Harhoura 2	6	P12	HKOIH	*Meriones shawii/grandis*	molar	-8.3	-3.2
El Harhoura 2	6	P12	HKOIH	*Meriones shawii/grandis*	molar	-9.5	-3.2
El Harhoura 2	6	O12	PECJF	*Meriones shawii/grandis*	molar	-9.2	-3.8
El Harhoura 2	6	O12	PECJF	*Meriones shawii/grandis*	molar	-9.4	-4.8
El Harhoura 2	6	O12	PECJF	*Meriones shawii/grandis*	molar	-8.9	-4.6
El Harhoura 2	6	O12	PECJF	*Meriones shawii/grandis*	incisor	-8.6	-3.7
El Harhoura 2	6	O12	PECJF	*Meriones shawii/grandis*	incisor	-9.4	-4.1
El Harhoura 2	6	P12	HKOIH	*Meriones shawii/grandis*	incisor	-8.8	-4.3
El Harhoura 2	6	P12	HKOIH	*Meriones shawii/grandis*	incisor	-9.3	-3.8
El Harhoura 2	6	P12	HKOIH	*Meriones shawii/grandis*	incisor	-8.2	-3.0
El Harhoura 2	7	P11	XDRIQ	*Meriones shawii/grandis*	molar	-10.1	-7.0
El Harhoura 2	7	P11	XDRIQ	*Meriones shawii/grandis*	molar	-6.4	-11.0
El Harhoura 2	7	P11	XDRIQ	*Meriones shawii/grandis*	molar	-10.5	-6.5
El Harhoura 2	7	P11	XDRIQ	*Meriones shawii/grandis*	molar	-10.1	-5.3
El Harhoura 2	7	P11	XDRIQ	*Meriones shawii/grandis*	molar	-9.4	-5.3
El Harhoura 2	7	P11	XDRIQ	*Meriones shawii/grandis*	molar	-9.8	-6.3
El Harhoura 2	7	P11	XDRIQ	*Meriones shawii/grandis*	molar	-9.7	-6.6
El Harhoura 2	7	P11	XDRIQ	*Meriones shawii/grandis*	molar	-10.7	-5.2
El Harhoura 2	7	P11	XDRIQ	*Meriones shawii/grandis*	molar	-9.4	-5.9
El Harhoura 2	7	P11	XDRIQ	*Meriones shawii/grandis*	molar	-10.1	-5.4
El Harhoura 2	7	P11	XDRIQ	*Meriones shawii/grandis*	incisor	-8.6	-5.1
El Harhoura 2	7	P11	XDRIQ	*Meriones shawii/grandis*	incisor	-8.9	-4.4
El Harhoura 2	7	O12	SVURX	*Meriones shawii/grandis*	incisor	-9.0	-4.2

El Harhoura 2	7	O12	SVURX	*Meriones shawii/grandis*	incisor	-8.5	-5.0
El Harhoura 2	7	O12	SVURX	*Meriones shawii/grandis*	incisor	-7.9	-4.7
El Harhoura 2	8	P12	UIVMV	*Meriones shawii/grandis*	molar	-8.4	-4.3
El Harhoura 2	8	P12	UIVMV	*Meriones shawii/grandis*	molar	-9.6	-6.2
El Harhoura 2	8	P12	UIVMV	*Meriones shawii/grandis*	molar	-10.6	-6.6
El Harhoura 2	8	P12	UIVMV	*Meriones shawii/grandis*	molar	-9.4	-4.9
El Harhoura 2	8	P12	UIVMV	*Meriones shawii/grandis*	molar	-9.2	-4.2
El Harhoura 2	8	P12	UIVMV	*Meriones shawii/grandis*	molar	-9.9	-9.4
El Harhoura 2	8	P12	UIVMV	*Meriones shawii/grandis*	molar	-10.2	-5.1
El Harhoura 2	8	P12	UIVMV	*Meriones shawii/grandis*	molar	-9.4	-4.9
El Harhoura 2	8	P12	UIVMV	*Meriones shawii/grandis*	molar	-10.5	-5.3
El Harhoura 2	8	P12	UIVMV	*Meriones shawii/grandis*	molar	-10.1	-6.8
El Harhoura 2	8	P12	APCTR	*Meriones shawii/grandis*	incisor	-8.9	-5.2
El Harhoura 2	8	P12	APCTR	*Meriones shawii/grandis*	incisor	-9.3	-5.0
El Harhoura 2	8	O12	KHIIK	*Meriones shawii/grandis*	incisor	-9.0	-5.4
El Harhoura 2	8	O12	KHIIK	*Meriones shawii/grandis*	incisor	-9.2	-5.3
El Harhoura 2	8	O12	KHIIK	*Meriones shawii/grandis*	incisor	-8.7	-4.4
El Harhoura 2	9	P12	SMKAF	*Meriones shawii/grandis*	molar	-11.0	-5.1
El Harhoura 2	9	P12	SMKAF	*Meriones shawii/grandis*	molar	-9.3	-5.2
El Harhoura 2	9	P12	SMKAF	*Meriones shawii/grandis*	molar	-10.6	-5.2
El Harhoura 2	9	P12	SMKAF	*Meriones shawii/grandis*	molar	-8.7	-5.3
El Harhoura 2	9	P12	SMKAF	*Meriones shawii/grandis*	molar	-10.2	-4.7
El Harhoura 2	9	O12	XSJVC	*Meriones shawii/grandis*	molar	-10.1	-6.6
El Harhoura 2	9	O12	XSJVC	*Meriones shawii/grandis*	molar	-9.9	-4.9
El Harhoura 2	9	O12	XSJVC	*Meriones shawii/grandis*	molar	-8.9	-4.6
El Harhoura 2	9	O12	XSJVC	*Meriones shawii/grandis*	molar	-10.0	-5.3

El Harhoura 2	9	O12	XSJVC	*Meriones shawii/grandis*	molar	-9.8	-5.6
El Harhoura 2	9	O12	XSJVC	*Meriones shawii/grandis*	incisor	-8.5	-4.7
El Harhoura 2	9	O12	XSJVC	*Meriones shawii/grandis*	incisor	-8.8	-4.8
El Harhoura 2	9	O12	XSJVC	*Meriones shawii/grandis*	incisor	-8.8	-4.8
El Harhoura 2	9	O12	XSJVC	*Meriones shawii/grandis*	incisor	-8.6	-5.0
El Harhoura 2	9	O12		*Meriones shawii/grandis*	incisor	-8.6	-5.1
El Harhoura 2	10	P12	GOAIH	*Meriones shawii/grandis*	molar	-10.7	-5.8
El Harhoura 2	10	P12	GOAIH	*Meriones shawii/grandis*	molar	-9.3	-4.6
El Harhoura 2	10	P12	GOAIH	*Meriones shawii/grandis*	molar	-8.9	-4.0
El Harhoura 2	10	P12	GOAIH	*Meriones shawii/grandis*	molar	-9.9	-5.1
El Harhoura 2	10	P12	GOAIH	*Meriones shawii/grandis*	molar	-10.1	-4.7
El Harhoura 2	10	P12	GOAIH	*Meriones shawii/grandis*	molar	-10.1	-5.3
El Harhoura 2	10	P12	GOAIH	*Meriones shawii/grandis*	molar	-9.5	-5.8
El Harhoura 2	10	P12	GOAIH	*Meriones shawii/grandis*	molar	-10.2	-5.2
El Harhoura 2	10	P12	GOAIH	*Meriones shawii/grandis*	molar	-9.3	-4.9
El Harhoura 2	10	P12	GOAIH	*Meriones shawii/grandis*	molar	-9.5	-4.4
El Harhoura 2	10	O12	FMEIW	*Meriones shawii/grandis*	incisor	-9.0	-5.0
El Harhoura 2	10	O12	FMEIW	*Meriones shawii/grandis*	incisor	-8.3	-5.0
El Harhoura 2	10	O12	FMEIW	*Meriones shawii/grandis*	incisor	-8.6	-5.9
El Harhoura 2	10	O12	FMEIW	*Meriones shawii/grandis*	incisor	-8.3	-6.6
El Harhoura 2	10	O12	FMEIW	*Meriones shawii/grandis*	incisor	-8.4	-6.2
El Harhoura 2	11	O12	TIGNT	*Meriones shawii/grandis*	molar	-9.5	-4.9
El Harhoura 2	11	O12	TIGNT	*Meriones shawii/grandis*	molar	-9.2	-5.9
El Harhoura 2	11	O12	TIGNT	*Meriones shawii/grandis*	molar	-9.3	-6.1
El Harhoura 2	11	O12	TIGNT	*Meriones shawii/grandis*	molar	-9.5	-5.3
El Harhoura 2	11	O12	TIGNT	*Meriones shawii/grandis*	molar	-9.8	-5.9

El Harhoura 2	11	O12	TIGNT	*Meriones shawii/grandis*	molar	-9.3	-5.6
El Harhoura 2	11	O12	TIGNT	*Meriones shawii/grandis*	molar	-9.6	-5.1
El Harhoura 2	11	O12	TIGNT	*Meriones shawii/grandis*	molar	-9.4	-6.1
El Harhoura 2	11	O12	TIGNT	*Meriones shawii/grandis*	molar	-9.8	-6.4
El Harhoura 2	11	O12	TIGNT	*Meriones shawii/grandis*	molar	-10.3	-5.4
El Harhoura 2	11	O12	TIGNT	*Meriones shawii/grandis*	incisor	-8.4	-4.8
El Harhoura 2	11	O12	TIGNT	*Meriones shawii/grandis*	incisor	-9.0	-5.6
El Harhoura 2	11	O12	TIGNT	*Meriones shawii/grandis*	incisor	-8.7	-5.6
El Harhoura 2	11	O12	TIGNT	*Meriones shawii/grandis*	incisor	-8.4	-4.4
El Harhoura 2	11	O12	TIGNT	*Meriones shawii/grandis*	incisor	-8.8	-5.3

Appendix 6.1: Post Hoc Tukey tests showing differences in $\delta^{18}O_{teeth}$ between 11 Levels at El Harhoura 2. Significant values are shown in bold.

Level	*P* value
11-10	0.9959843
2-10	**0**
3-10	**0.0000002**
4a-10	**0.0000125**
4b-10	**0.00027**
5-10	**0.0140844**
6-10	**0.0000009**
7-10	0.9913151
8-10	1
9-10	0.9963127
2-11	**0**
3-11	**0**
4a-11	**0.0000001**
4b-11	**0.0000034**
5-11	**0.0003447**
6-11	**0**
7-11	1
8-11	0.9795801
9-11	0.6753368
3-2	**0.0039958**
4a-2	**0.0001327**
4b-2	**0.0000132**
5-2	**0**
6-2	**0.0012873**
7-2	**0**
8-2	**0**
9-2	**0**
4a-3	0.9988329
4b-3	0.9376096
5-3	**0.2641954**
6-3	0.9999999
7-3	**0**
8-3	**0.0000006**
9-3	**0.0000223**
4b-4a	0.9999493
5-4a	0.8135027
6-4a	0.9999766
7-4a	**0.0000001**

8-4a	**0.0000361**
9-4a	**0.0008591**
5-4b	0.989885
6-4b	0.9873902
7-4b	**0.0000021**
8-4b	**0.00069**
9-4b	**0.0105596**
6-5	**0.4466499**
7-5	**0.000226**
8-5	**0.029574**
9-5	**0.2096468**
7-6	**0**
8-6	**0.0000027**
9-6	**0.000085**
8-7	0.9642831
9-7	0.6056537
9-8	0.9996372

Appendix 6.2: Post Hoc Tukey tests showing differences in $\delta^{18}O_{teeth}$ between 9 Levels at Taforalt (Level 16 removed from analysis). Significant values are shown in bold.

Level	***P* value**
23D/F-14	0.5787724
23G-14	**0.0272778**
23H-14	**0.0159046**
23I/K-14	**0.0055367**
Y1-14	**0.0070355**
Y2-14	**0.00405**
Y4-14	**0.0052997**
Y6-14	**0.0136759**
23G-23D/F	0.839672
23H-23D/F	0.8706603
23I/K-23D/F	0.7266759
Y1-23D/F	0.7978136
Y2-23D/F	0.7696953
Y4-23D/F	0.7185452
Y6-23D/F	0.710313
23H-23G	0.9999996
23I/K-23G	1
Y1-23G	1
Y2-23G	0.9999999

Y4-23G	1
Y6-23G	0.9999998
23I/K-23H	0.9999994
Y1-23H	1
Y2-23H	1
Y4-23H	0.999999
Y6-23H	0.9999093
Y1-23I/K	1
Y2-23I/K	0.9999998
Y4-23I/K	1
Y6-23I/K	0.999999
Y2-Y1	1
Y4-Y1	0.9999999
Y6-Y1	0.9999659
Y4-Y2	0.9999997
Y6-Y2	0.9999323
Y6-Y4	0.9999993

Appendix 6.3: Post Hoc Tukey tests showing differences in $\delta^{13}C_{teeth}$ between 9 Levels at Taforalt (Level 16 removed from analysis). Significant values are shown in bold.

Level	***P* value**
23D/F-14	0.9995083
23G-14	0.8057815
23H-14	**0.2712679**
23I/K-14	**0.0075083**
Y1-14	0.9999999
Y2-14	0.8906469
Y4-14	**0.0310373**
Y6-14	**0.2388609**
23G-23D/F	0.9863458
23H-23D/F	0.7249134
23I/K-23D/F	**0.0737637**
Y1-23D/F	0.9999322
Y2-23D/F	0.9991696
Y4-23D/F	**0.2077773**
Y6-23D/F	0.6252963
23H-23G	0.9995575
23I/K-23G	0.6648961
Y1-23G	0.8400808
Y2-23G	0.9998527

Y4-23G	0.8969893
Y6-23G	0.9939198
23I/K-23H	0.8959663
Y1-23H	**0.261846**
Y2-23H	0.9066823
Y4-23H	0.9925128
Y6-23H	0.9999901
Y1-23I/K	**0.0044829**
Y2-23I/K	**0.0904817**
Y4-23I/K	0.9998563
Y6-23I/K	0.9949647
Y2-Y1	0.9157155
Y4-Y1	**0.0223557**
Y6-Y1	**0.2401932**
Y4-Y2	**0.2934875**
Y6-Y2	0.8228471
Y6-Y4	0.9999755

Appendix 7: The $\delta^{18}O$ and $\delta^{13}C$ values of incisors and molars from Taforalt (molars n= 50, incisors n= 24).

Site	Sample No.	Sector	Level	Spit	Square	Sample No.	Species	Tooth	$\delta^{13}C_{(VPDB)}‰$	$\delta^{18}O_{(VPDB)}‰$
Taforalt	58	8	Y1		B-C22	719	*Meriones* sp.	incisor	-8.7	-3.9
Taforalt	22.1	8	Y1	397cm	B-C22 Quad C	887	*Meriones* sp.	molar	-9.1	-5.1
Taforalt	22.2	8	Y1	397cm	B-C22 Quad C	887	*Meriones* sp.	molar	-5.4	-4.8
Taforalt	22.3	8	Y1	397cm	B-C22 Quad C	887	*Meriones* sp.	molar	-9.0	-4.1
Taforalt	41	8	Y1	397cm	B-C22 Quad C	887	*Meriones* sp.	incisor	-7.9	-4.9
Taforalt	42	8	Y1	397cm	B-C22 Quad C	887	*Meriones* sp.	incisor	-7.3	-5.4
Taforalt	21.1	8	Y1	398cm	B-C22 Quad B	888	*Meriones* sp.	molar	-8.1	-3.9
Taforalt	21.2	8	Y1	398cm	B-C22 Quad B	888	*Meriones* sp.	molar	-6.9	-4.0
Taforalt	49	8	Y1	398cm	B-C22 Quad B	888	*Meriones* sp.	incisor	-7.1	-4.9
Taforalt	50	8	Y1	398cm	B-C22 Quad B	888	*Meriones* sp.	incisor	-7.0	-5.6
Taforalt	4	8	Y2	414cm	B24	10849	*Meriones* sp.	incisor	-7.7	-5.4
Taforalt	4.1	8	Y2	414cm	B24	10849	*Meriones* sp.	molar	-9.8	-3.7
Taforalt	4.2	8	Y2	414cm	B24	10849	*Meriones* sp.	molar	-6.2	-6.6
Taforalt	4.3	8	Y2	414cm	B24	10849	*Meriones* sp.	molar	-9.7	-4.3
Taforalt	19	8	Y2	426cm	B-C22 Quad B	1175	*Meriones* sp.	incisor	-6.9	-6.8
Taforalt	19.1	8	Y2	426cm	B-C22 Quad B	1175	*Meriones* sp.	molar	-9.1	-4.1
Taforalt	19.2	8	Y2	426cm	B-C22 Quad B	1175	*Meriones* sp.	molar	-8.5	-3.9
Taforalt	19.3	8	Y2	426cm	B-C22 Quad B	1175	*Meriones* sp.	molar	-8.9	-3.0
Taforalt	19.4	8	Y2	426cm	B-C22 Quad B	1175	*Meriones* sp.	molar	-8.8	-4.2
Taforalt	19.5	8	Y2	426cm	B-C22 Quad B	1175	*Meriones* sp.	molar	-8.5	-3.3
Taforalt	56	8	Y2	426cm	B-C22 Quad B	1175	*Meriones* sp.	incisor	-8.0	-5.1
Taforalt	57	8	Y2	426cm	B-C22 Quad B	1175	*Meriones* sp.	incisor	-8.2	-4.8
Taforalt	61	8	Y2	426cm	B-C22 Quad B	1175	*Meriones* sp.	incisor	-7.0	-5.1

Taforalt	16	8	Y4	spit 1	B-C 22 Quad C	1901	*Meriones* sp.	molar	-11.1	-4.1
Taforalt	17.1	8	Y4	spit 2	C21	2140	*Meriones* sp.	molar	-9.1	-4.3
Taforalt	17.2	8	Y4	spit 2	C21	2140	*Meriones* sp.	molar	-9.0	-3.9
Taforalt	20	8	Y4	spit 3	C22	2105	*Meriones* sp.	incisor	-8.6	-6.7
Taforalt	20.1	8	Y4	spit 3	C22	2105	*Meriones* sp.	molar	-9.2	-2.8
Taforalt	20.2	8	Y4	spit 3	C22	2105	*Meriones* sp.	molar	-9.6	-5.3
Taforalt	20.3	8	Y4	spit 3	C22	2105	*Meriones* sp.	molar	-9.0	-4.6
Taforalt	18.1	8	Y4	spit 4	C22	2170	*Meriones* sp.	molar	-9.1	-5.9
Taforalt	18.2	8	Y4	spit 4	C22	2170	*Meriones* sp.	molar	-9.7	-5.0
Taforalt	1.1	8	Y6	spit 1	D22	3303	*Meriones* sp.	molar	-9.5	-4.8
Taforalt	1.2	8	Y6	spit 1	D23	3303	*Meriones* sp.	incisor	-8.1	-5.1
Taforalt	2	8	Y6	spit 3	D22	3514	*Meriones* sp.	molar	-8.9	-3.1
Taforalt	3	8	Y6	spit 5	D22	3581	*Meriones* sp.	molar	-10.0	-5.4
Taforalt	59	8	Y6			3487	*Meriones* sp.	incisor	-9.3	-6.1
Taforalt	36.1a	2	R14		M14	1684	*Meriones* sp.	molar	-8.1	-2.6
Taforalt	36.1b	2	R14		M14	1684	*Meriones* sp.	incisor	-7.5	-2.9
Taforalt	36.2	2	R14		M14	1684	*Meriones* sp.	molar	-8.7	-2.7
Taforalt	54	2	R14		M14	1684	*Meriones* sp.	incisor	-7.1	-3.4
Taforalt	55	2	R14		M14	1684	*Meriones* sp.	incisor	-6.1	-3.0
Taforalt	62	2	R14		N13	10727	*Meriones* sp.	incisor	-7.5	-2.2
Taforalt	64	2	R14		N13	10727	*Meriones* sp.	incisor	-7.8	-2.9
Taforalt	12	2	R16		N14	9078	*Meriones* sp.	molar	-9.7	-2.2
Taforalt	15	2	R16		L13	1868	*Meriones* sp.	molar	-7.5	-2.0

Taforalt	10	2	23D		O13 Quad D	9041	*Meriones* sp.	incisor	-5.1	-3.0
Taforalt	10.1	2	23D		O13 Quad D	9041	*Meriones* sp.	molar	-10.4	-4.9
Taforalt	10.2	2	23D		O13 Quad D	9041	*Meriones* sp.	molar	-9.3	-4.0
Taforalt	6	2	23F		O13 Quad A	8706	*Meriones* sp.	molar	-8.3	-3.7
Taforalt	60	2	23F		O13 Quad A	8706	*Meriones* sp.	incisor	-8.4	-5.2
Taforalt	44	2	23F		N14/15	10330	*Meriones* sp.	incisor	-5.9	-2.3
Taforalt	5.1	2	23G		O13 Quad A	8899	*Meriones* sp.	incisor	-9.3	-6.1
Taforalt	5.2	2	23G		O13 Quad A	8899	*Meriones* sp.	molar	-8.4	-3.7
Taforalt	11.1	2	23G		P13 Quad A	9042	*Meriones* sp.	molar	-9.1	-5.2
Taforalt	11.2	2	23G		P13 Quad A	9042	*Meriones* sp.	molar	-6.4	-3.7
Taforalt	11.3	2	23G		P13 Quad A	9042	*Meriones* sp.	molar	-9.5	-5.1
Taforalt	7	2	23H		O13 Quad A	8908	*Meriones* sp.	incisor	-8.0	-5.1
Taforalt	7.1	2	23H		O13 Quad A	8908	*Meriones* sp.	molar	-10.7	-6.2
Taforalt	8.1	2	23H		O13 Quad A	8975	*Meriones* sp.	molar	-9.8	-3.8
Taforalt	8.2	2	23H		O13 Quad A	8975	*Meriones* sp.	incisor	-8.1	-5.6
Taforalt	9.2	2	23H		P13 Quad A	9007	*Meriones* sp.	molar	-9.2	-4.4
Taforalt	13.1	2	23H		P13 Quad A	9093	*Meriones* sp.	molar	-8.7	-4.2
Taforalt	13.2	2	23H		P13 Quad A	9093	*Meriones* sp.	molar	-9.0	-4.6
Taforalt	14	2	23H		O13 Quad D	9082	*Meriones* sp.	molar	-7.7	-3.0
Taforalt	34	2	23I		O14	10973	*Meriones* sp.	molar	-10.1	-5.4
Taforalt	35	2	23I		O14	10973	*Meriones* sp.	molar	-8.9	-4.6
Taforalt	28a	2	23K		O14	11270	*Meriones* sp.	molar	-9.3	-3.2
Taforalt	28b	2	23K		O14	11270	*Meriones* sp.	molar	-10.0	-3.9

Taforalt	29	2	23k		O14	11270	*Meriones* sp.	molar	-9.4	-5.3
Taforalt	30	2	23K		O14	11270	*Meriones* sp.	molar	-10.2	-5.1
Taforalt	31	2	23k		O14	11270	*Meriones* sp.	molar	-9.3	-5.0
Taforalt	32	2	23K		O14	11270	*Meriones* sp.	molar	-10.7	-5.4
Taforalt	33	2	23k		O14	11270	*Meriones* sp.	molar	-9.0	-4.8

Appendix 8: The $\delta^{13}C$ values of end member C_3 and C_4 Meriones diet calculated using an approach adapted from Passey et al. (2002), which accounts for Late Pleistocene variation in $\delta^{13}CO2$ on the $\delta^{13}C$ values of vegetation by correcting to past records of $\delta^{13}CO_2$ from the Antarctic ice core records. Ice core data from Lourantou et al.2010a (a), Lourantou et al.2010b (b), Smith et al. 1999 (c), Leuenberger et al. 1992 (e), Elsig et al. 2009 (f), Keeling et al. 2005 (h), Schaefer et al. 2011 (i), Schneider et al. 2013 (j).

Late Pleistocene $\delta^{13}CO_2$				Calculated $\delta^{13}C$ values of vegetation corrected for changes in $\delta^{13}CO_2$						Calculated $\delta^{13}C$ value of *Meriones* diet					
Publication	**Age (BP)**	**$\delta^{13}C$ $_{PCO2}$‰**	**±1σ**	**$\delta^{13}C$ min C_3**	**$\delta^{13}C$ max C_3**	**$\delta^{13}C$ average C_3**	**$\delta^{13}C$ min C_4**	**$\delta^{13}C$ max C_4**	**$\delta^{13}C$ average C_4**	**$\delta^{13}C$ min C_3 diet**	**$\delta^{13}C$ max C_3 diet**	**$\delta^{13}C$ average C_3 diet**	**$\delta^{13}C$ min C_4 diet**	**$\delta^{13}C$ max C_4 diet**	**$\delta^{13}C$ average C_4 diet**
(h)	-65.00 (Modern)	-8.2	0.0	-30.5	-21.8	-26.6	-13.4	-15.0	-11.0	-19.7	-10.9	-15.8	-2.5	-4.0	0.0
j)	154543	-6.7	0.1	-29.1	-20.4	-25.2	-12.0	-13.5	-9.5	-18.3	-9.5	-14.3	-1.0	-2.6	1.5
j)	154115	-6.8	0.1	-29.1	-20.4	-25.2	-12.0	-13.6	-9.6	-18.3	-9.5	-14.4	-1.0	-2.6	1.4
j)	153346	-6.9	0.1	-29.2	-20.5	-25.3	-12.1	-13.7	-9.6	-18.4	-9.6	-14.4	-1.1	-2.7	1.4
j)	152324	-6.8	0.0	-29.1	-20.4	-25.2	-12.0	-13.6	-9.6	-18.3	-9.5	-14.4	-1.0	-2.6	1.5
(a)	151703	-6.9	0.1	-29.2	-20.5	-25.3	-12.1	-13.7	-9.7	-18.4	-9.6	-14.5	-1.1	-2.7	1.4
(a)	151179	-7.2	0.1	-29.5	-20.8	-25.6	-12.4	-14.0	-10.0	-18.7	-9.9	-14.8	-1.4	-3.0	1.0
(a)	150636	-7.1	0.2	-29.4	-20.7	-25.5	-12.3	-13.9	-9.9	-18.6	-9.8	-14.7	-1.4	-2.9	1.1
j)	150490	-6.9	0.1	-29.2	-20.5	-25.3	-12.1	-13.7	-9.6	-18.4	-9.6	-14.5	-1.1	-2.7	1.4
j)	150137	-6.9	0.2	-29.2	-20.5	-25.3	-12.1	-13.7	-9.6	-18.4	-9.6	-14.5	-1.1	-2.7	1.4
j)	149174	-6.9	0.1	-29.2	-20.5	-25.3	-12.1	-13.7	-9.7	-18.4	-9.6	-14.5	-1.1	-2.7	1.4
j)	148790	-6.8	0.0	-29.1	-20.4	-25.2	-12.0	-13.6	-9.6	-18.3	-9.5	-14.4	-1.0	-2.6	1.5
j)	148111	-6.8	0.1	-29.1	-20.4	-25.2	-12.1	-13.6	-9.6	-18.4	-9.5	-14.4	-1.1	-2.7	1.4
j)	146954	-6.6	0.0	-29.0	-20.3	-25.1	-11.9	-13.4	-9.4	-18.2	-9.4	-14.2	-0.9	-2.5	1.6
j)	144907	-6.8	0.1	-29.1	-20.4	-25.2	-12.0	-13.6	-9.5	-18.3	-9.5	-14.3	-1.0	-2.6	1.5
j)	143818	-6.9	0.1	-29.2	-20.5	-25.3	-12.1	-13.7	-9.6	-18.4	-9.6	-14.5	-1.1	-2.7	1.4
j)	143165	-6.7	0.1	-29.1	-20.3	-25.2	-12.0	-13.5	-9.5	-18.3	-9.5	-14.3	-1.0	-2.6	1.5
j)	142758	-6.9	0.1	-29.3	-20.6	-25.4	-12.2	-13.7	-9.7	-18.5	-9.7	-14.5	-1.2	-2.8	1.3

(a)	141740	-6.8	0.1	-29.1	-20.4	-25.2	-12.0	-13.6	-9.5	-18.3	-9.5	-14.4	-1.0	-2.6	1.5
j)	141658	-6.8	0.1	-29.1	-20.4	-25.2	-12.1	-13.6	-9.6	-18.4	-9.5	-14.4	-1.1	-2.7	1.4
j)	140762	-6.8	0.0	-29.1	-20.4	-25.2	-12.0	-13.6	-9.5	-18.3	-9.5	-14.3	-1.0	-2.6	1.5
(a)	140514	-6.7	0.1	-29.1	-20.4	-25.2	-12.0	-13.6	-9.5	-18.3	-9.5	-14.3	-1.0	-2.6	1.5
(a)	139966	-6.7	0.1	-29.1	-20.4	-25.2	-12.0	-13.5	-9.5	-18.3	-9.5	-14.3	-1.0	-2.6	1.5
j)	139426	-6.8	0.2	-29.1	-20.4	-25.2	-12.1	-13.6	-9.6	-18.4	-9.5	-14.4	-1.1	-2.7	1.4
(a)	138872	-6.7	0.1	-29.1	-20.4	-25.2	-12.0	-13.5	-9.5	-18.3	-9.5	-14.3	-1.0	-2.6	1.5
j)	138462	-6.8	0.1	-29.2	-20.4	-25.3	-12.1	-13.6	-9.6	-18.4	-9.6	-14.4	-1.1	-2.7	1.4
(a)	137817	-6.8	0.2	-29.1	-20.4	-25.2	-12.0	-13.6	-9.6	-18.3	-9.5	-14.4	-1.1	-2.6	1.4
j)	137498	-7.0	0.1	-29.3	-20.6	-25.4	-12.3	-13.8	-9.8	-18.5	-9.7	-14.6	-1.3	-2.9	1.2
(a)	136803	-6.9	0.1	-29.2	-20.5	-25.3	-12.1	-13.7	-9.7	-18.4	-9.6	-14.5	-1.1	-2.7	1.3
(a)	135791	-6.9	0.1	-29.3	-20.5	-25.3	-12.2	-13.7	-9.7	-18.5	-9.6	-14.5	-1.2	-2.8	1.3
(a)	135295	-6.6	0.0	-29.0	-20.3	-25.1	-11.9	-13.5	-9.4	-18.2	-9.4	-14.2	-0.9	-2.5	1.6
(a)	134805	-6.6	0.1	-28.9	-20.2	-25.0	-11.8	-13.4	-9.4	-18.1	-9.3	-14.2	-0.9	-2.4	1.6
j)	134390	-6.9	0.1	-29.2	-20.5	-25.3	-12.1	-13.7	-9.7	-18.4	-9.6	-14.5	-1.1	-2.7	1.4
j)	134137	-6.8	0.1	-29.1	-20.4	-25.2	-12.0	-13.6	-9.5	-18.3	-9.5	-14.4	-1.0	-2.6	1.5
(a)	133981	-6.9	0.1	-29.3	-20.6	-25.4	-12.2	-13.8	-9.7	-18.5	-9.7	-14.5	-1.2	-2.8	1.3
j)	133661	-6.8	0.1	-29.1	-20.4	-25.2	-12.0	-13.6	-9.6	-18.3	-9.5	-14.4	-1.1	-2.6	1.4
(a)	133238	-7.1	0.1	-29.4	-20.7	-25.5	-12.3	-13.9	-9.9	-18.6	-9.8	-14.7	-1.3	-2.9	1.1
(a)	132954	-7.1	0.1	-29.4	-20.7	-25.5	-12.4	-13.9	-9.9	-18.7	-9.8	-14.7	-1.4	-3.0	1.1
j)	132813	-7.0	0.1	-29.3	-20.6	-25.4	-12.2	-13.8	-9.7	-18.5	-9.7	-14.5	-1.2	-2.8	1.3
j)	132633	-6.9	0.0	-29.3	-20.5	-25.4	-12.2	-13.7	-9.7	-18.5	-9.7	-14.5	-1.2	-2.8	1.3
j)	132598	-7.0	0.1	-29.3	-20.6	-25.4	-12.2	-13.8	-9.7	-18.5	-9.7	-14.5	-1.2	-2.8	1.3
(a)	132267	-6.9	0.1	-29.3	-20.5	-25.3	-12.2	-13.7	-9.7	-18.5	-9.6	-14.5	-1.2	-2.8	1.3
j)	131851	-6.8	0.1	-29.2	-20.5	-25.3	-12.1	-13.6	-9.6	-18.4	-9.6	-14.4	-1.1	-2.7	1.4
(a)	131621	-7.0	0.2	-29.3	-20.6	-25.4	-12.2	-13.8	-9.7	-18.5	-9.7	-14.5	-1.2	-2.8	1.3
j)	131309	-7.0	0.1	-29.4	-20.6	-25.4	-12.3	-13.8	-9.8	-18.6	-9.8	-14.6	-1.3	-2.9	1.2
(a)	131153	-6.8	0.1	-29.1	-20.4	-25.2	-12.0	-13.6	-9.6	-18.3	-9.5	-14.4	-1.0	-2.6	1.5

j)	130829	-7.0	0.1	-29.4	-20.6	-25.4	-12.3	-13.8	-9.8	-18.6	-9.8	-14.6	-1.3	-2.9	1.2
(a)	130678	-7.0	0.1	-29.3	-20.6	-25.4	-12.2	-13.8	-9.7	-18.5	-9.7	-14.5	-1.2	-2.8	1.3
j)	130369	-6.8	0.1	-29.1	-20.4	-25.2	-12.0	-13.6	-9.6	-18.3	-9.5	-14.4	-1.0	-2.6	1.5
(a)	130236	-7.2	0.1	-29.5	-20.8	-25.6	-12.4	-14.0	-10.0	-18.7	-9.9	-14.8	-1.4	-3.0	1.1
(a)	130008	-7.2	0.0	-29.5	-20.8	-25.6	-12.4	-14.0	-10.0	-18.7	-9.9	-14.8	-1.5	-3.0	1.0
j)	129696	-7.0	0.0	-29.3	-20.6	-25.4	-12.2	-13.8	-9.7	-18.5	-9.7	-14.6	-1.2	-2.8	1.3
(a)	129628	-6.7	0.1	-29.1	-20.3	-25.2	-12.0	-13.5	-9.5	-18.3	-9.4	-14.3	-1.0	-2.6	1.5
j)	129624	-6.7	0.1	-29.1	-20.3	-25.2	-12.0	-13.5	-9.5	-18.3	-9.5	-14.3	-1.0	-2.6	1.5
(a)	129446	-7.0	0.0	-29.4	-20.6	-25.4	-12.3	-13.8	-9.8	-18.6	-9.7	-14.6	-1.3	-2.9	1.2
(a)	129273	-6.6	0.1	-28.9	-20.2	-25.0	-11.8	-13.4	-9.4	-18.1	-9.3	-14.2	-0.8	-2.4	1.6
j)	129095	-6.7	0.0	-29.0	-20.3	-25.1	-11.9	-13.5	-9.5	-18.2	-9.4	-14.3	-0.9	-2.5	1.5
(a)	128920	-6.9	0.0	-29.2	-20.5	-25.3	-12.1	-13.7	-9.6	-18.4	-9.6	-14.5	-1.1	-2.7	1.4
j)	128919	-6.8	0.1	-29.2	-20.4	-25.3	-12.1	-13.6	-9.6	-18.4	-9.6	-14.4	-1.1	-2.7	1.4
j)	128916	-6.8	0.1	-29.1	-20.4	-25.2	-12.0	-13.6	-9.6	-18.3	-9.5	-14.4	-1.0	-2.6	1.4
(a)	128585	-7.2	0.1	-29.6	-20.9	-25.7	-12.5	-14.0	-10.0	-18.8	-10.0	-14.8	-1.5	-3.1	1.0
j)	128553	-6.7	0.1	-29.0	-20.3	-25.1	-11.9	-13.5	-9.4	-18.2	-9.4	-14.3	-0.9	-2.5	1.6
j)	128316	-6.7	0.1	-29.0	-20.3	-25.1	-11.9	-13.5	-9.4	-18.2	-9.4	-14.2	-0.9	-2.5	1.6
j)	128268	-6.6	0.1	-29.0	-20.2	-25.1	-11.9	-13.4	-9.4	-18.2	-9.4	-14.2	-0.9	-2.5	1.6
j)	128107	-6.7	0.0	-29.0	-20.3	-25.1	-11.9	-13.5	-9.5	-18.2	-9.4	-14.3	-1.0	-2.5	1.5
(a)	127934	-7.5	0.2	-29.9	-21.1	-25.9	-12.8	-14.3	-10.3	-19.1	-10.3	-15.1	-1.8	-3.4	0.7
(a)	127773	-6.8	0.1	-29.1	-20.4	-25.2	-12.0	-13.6	-9.6	-18.3	-9.5	-14.4	-1.0	-2.6	1.5
j)	127595	-6.7	0.1	-29.1	-20.4	-25.2	-12.0	-13.5	-9.5	-18.3	-9.5	-14.3	-1.0	-2.6	1.5
(a)	127595	-6.6	0.1	-28.9	-20.2	-25.0	-11.8	-13.4	-9.4	-18.1	-9.3	-14.2	-0.8	-2.4	1.6
j)	127510	-6.8	0.1	-29.1	-20.4	-25.2	-12.0	-13.6	-9.5	-18.3	-9.5	-14.3	-1.0	-2.6	1.5
j)	127429	-6.7	0.1	-29.0	-20.3	-25.1	-11.9	-13.5	-9.4	-18.2	-9.4	-14.2	-0.9	-2.5	1.6
(a)	127225	-6.7	0.0	-29.0	-20.3	-25.1	-11.9	-13.5	-9.5	-18.2	-9.4	-14.3	-1.0	-2.5	1.5
j)	127119	-6.7	0.1	-29.0	-20.3	-25.1	-11.9	-13.5	-9.4	-18.2	-9.4	-14.2	-0.9	-2.5	1.6
(a)	126856	-6.7	0.1	-29.0	-20.3	-25.1	-11.9	-13.5	-9.4	-18.2	-9.4	-14.3	-0.9	-2.5	1.6

j)	126823	-6.6	0.1	-28.9	-20.2	-25.0	-11.8	-13.4	-9.4	-18.1	-9.3	-14.2	-0.8	-2.4	1.7
j)	126772	-6.9	0.1	-29.2	-20.5	-25.3	-12.1	-13.7	-9.7	-18.4	-9.6	-14.5	-1.1	-2.7	1.4
(a)	126484	-7.0	0.1	-29.3	-20.6	-25.4	-12.2	-13.8	-9.8	-18.5	-9.7	-14.6	-1.2	-2.8	1.2
j)	126231	-6.7	0.1	-29.1	-20.4	-25.2	-12.0	-13.5	-9.5	-18.3	-9.5	-14.3	-1.0	-2.6	1.5
(a)	126058	-7.0	0.2	-29.3	-20.6	-25.4	-12.2	-13.8	-9.8	-18.5	-9.7	-14.6	-1.2	-2.8	1.2
j)	126001	-6.8	0.1	-29.1	-20.4	-25.2	-12.0	-13.6	-9.5	-18.3	-9.5	-14.4	-1.0	-2.6	1.5
(a)	125859	-6.6	0.0	-29.0	-20.2	-25.0	-11.9	-13.4	-9.4	-18.2	-9.3	-14.2	-0.9	-2.5	1.6
(a)	125633	-6.9	0.1	-29.2	-20.5	-25.3	-12.1	-13.7	-9.6	-18.4	-9.6	-14.4	-1.1	-2.7	1.4
(a)	125633	-6.6	0.2	-28.9	-20.2	-25.0	-11.8	-13.4	-9.4	-18.1	-9.3	-14.2	-0.8	-2.4	1.6
j)	125598	-6.7	0.1	-29.0	-20.3	-25.1	-11.9	-13.5	-9.5	-18.2	-9.4	-14.3	-0.9	-2.5	1.6
(a)	125223	-6.6	0.2	-28.9	-20.2	-25.0	-11.8	-13.4	-9.4	-18.1	-9.3	-14.2	-0.8	-2.4	1.6
j)	125187	-6.7	0.1	-29.1	-20.3	-25.2	-12.0	-13.5	-9.5	-18.3	-9.5	-14.3	-1.0	-2.6	1.5
j)	124785	-6.7	0.1	-29.1	-20.4	-25.2	-12.0	-13.5	-9.5	-18.3	-9.5	-14.3	-1.0	-2.6	1.5
j)	124346	-6.7	0.1	-29.0	-20.3	-25.1	-11.9	-13.5	-9.5	-18.2	-9.4	-14.3	-0.9	-2.5	1.5
j)	123965	-6.6	0.2	-28.9	-20.2	-25.0	-11.8	-13.4	-9.4	-18.1	-9.3	-14.2	-0.9	-2.4	1.6
j)	123385	-6.6	0.1	-28.9	-20.2	-25.0	-11.8	-13.4	-9.4	-18.1	-9.3	-14.2	-0.8	-2.4	1.7
j)	122725	-6.8	0.1	-29.1	-20.4	-25.2	-12.0	-13.6	-9.6	-18.3	-9.5	-14.4	-1.0	-2.6	1.5
j)	122548	-6.7	0.1	-29.0	-20.3	-25.1	-11.9	-13.5	-9.5	-18.2	-9.4	-14.3	-0.9	-2.5	1.6
j)	122320	-6.6	0.1	-29.0	-20.2	-25.0	-11.9	-13.4	-9.4	-18.2	-9.3	-14.2	-0.9	-2.5	1.6
j)	121910	-6.5	0.1	-28.9	-20.2	-25.0	-11.8	-13.3	-9.3	-18.1	-9.3	-14.1	-0.8	-2.4	1.7
j)	121082	-6.5	0.1	-28.8	-20.1	-24.9	-11.7	-13.3	-9.3	-18.0	-9.2	-14.1	-0.8	-2.3	1.7
j)	120674	-6.5	0.1	-28.8	-20.1	-24.9	-11.7	-13.3	-9.3	-18.0	-9.2	-14.1	-0.8	-2.3	1.7
j)	120238	-6.5	0.1	-28.9	-20.1	-25.0	-11.8	-13.3	-9.3	-18.1	-9.3	-14.1	-0.8	-2.4	1.7
j)	119798	-6.5	0.1	-28.8	-20.1	-24.9	-11.7	-13.3	-9.3	-18.0	-9.2	-14.1	-0.7	-2.3	1.7
j)	118263	-6.5	0.1	-28.9	-20.1	-24.9	-11.8	-13.3	-9.3	-18.1	-9.2	-14.1	-0.8	-2.4	1.7
j)	117814	-6.6	0.1	-28.9	-20.2	-25.0	-11.8	-13.4	-9.3	-18.1	-9.3	-14.1	-0.8	-2.4	1.7
j)	117043	-6.7	0.1	-29.0	-20.3	-25.1	-11.9	-13.5	-9.5	-18.2	-9.4	-14.3	-0.9	-2.5	1.6
j)	116552	-6.8	0.1	-29.1	-20.4	-25.2	-12.0	-13.6	-9.6	-18.3	-9.5	-14.4	-1.0	-2.6	1.5

j)	116087	-6.6	0.1	-28.9	-20.2	-25.0	-11.8	-13.4	-9.4	-18.1	-9.3	-14.2	-0.8	-2.4	1.7
j)	115491	-6.8	0.1	-29.1	-20.4	-25.2	-12.0	-13.6	-9.6	-18.3	-9.5	-14.4	-1.0	-2.6	1.5
j)	114955	-6.8	0.1	-29.1	-20.4	-25.2	-12.0	-13.6	-9.6	-18.3	-9.5	-14.4	-1.0	-2.6	1.4
j)	114404	-6.7	0.1	-29.0	-20.3	-25.1	-11.9	-13.5	-9.4	-18.2	-9.4	-14.2	-0.9	-2.5	1.6
j)	113835	-6.7	0.1	-29.0	-20.3	-25.1	-11.9	-13.5	-9.4	-18.2	-9.4	-14.3	-0.9	-2.5	1.6
j)	113644	-6.9	0.1	-29.2	-20.5	-25.3	-12.1	-13.7	-9.7	-18.4	-9.6	-14.5	-1.2	-2.7	1.3
j)	113323	-6.8	0.1	-29.1	-20.4	-25.2	-12.0	-13.6	-9.5	-18.3	-9.5	-14.3	-1.0	-2.6	1.5
j)	112678	-6.7	0.1	-29.0	-20.3	-25.1	-11.9	-13.5	-9.4	-18.2	-9.4	-14.3	-0.9	-2.5	1.6
j)	111366	-6.7	0.1	-29.0	-20.3	-25.1	-11.9	-13.5	-9.5	-18.2	-9.4	-14.3	-0.9	-2.5	1.6
j)	110672	-6.6	0.1	-28.9	-20.2	-25.0	-11.8	-13.4	-9.3	-18.1	-9.3	-14.1	-0.8	-2.4	1.7
j)	110033	-6.6	0.1	-29.0	-20.2	-25.1	-11.9	-13.4	-9.4	-18.2	-9.4	-14.2	-0.9	-2.5	1.6
j)	109315	-6.6	0.1	-28.9	-20.2	-25.0	-11.8	-13.4	-9.4	-18.1	-9.3	-14.2	-0.8	-2.4	1.6
j)	107820	-6.5	0.1	-28.8	-20.1	-24.9	-11.7	-13.3	-9.3	-18.0	-9.2	-14.1	-0.7	-2.3	1.7
j)	107181	-6.6	0.1	-29.0	-20.2	-25.0	-11.9	-13.4	-9.4	-18.2	-9.3	-14.2	-0.9	-2.5	1.6
j)	107069	-6.5	0.1	-28.8	-20.1	-24.9	-11.7	-13.3	-9.3	-18.0	-9.2	-14.1	-0.7	-2.3	1.7
j)	106565	-6.8	0.1	-29.1	-20.4	-25.2	-12.0	-13.6	-9.5	-18.3	-9.5	-14.4	-1.0	-2.6	1.5
j)	106005	-6.7	0.1	-29.0	-20.3	-25.1	-11.9	-13.5	-9.5	-18.2	-9.4	-14.3	-1.0	-2.5	1.5
j)	105368	-6.7	0.1	-29.0	-20.3	-25.1	-11.9	-13.5	-9.4	-18.2	-9.4	-14.2	-0.9	-2.5	1.6
j)	104735	-6.6	0.1	-28.9	-20.2	-25.0	-11.8	-13.4	-9.4	-18.1	-9.3	-14.2	-0.8	-2.4	1.7
i)	49116	-6.4	0.1	-28.8	-20.1	-24.9	-11.7	-13.2	-9.2	-18.0	-9.2	-14.0	-0.7	-2.3	1.8
i)	48743	-6.5	0.1	-28.8	-20.1	-24.9	-11.7	-13.3	-9.2	-18.0	-9.2	-14.0	-0.7	-2.3	1.8
i)	48274	-6.4	0.2	-28.7	-20.0	-24.8	-11.6	-13.2	-9.2	-17.9	-9.1	-14.0	-0.6	-2.2	1.9
i)	47925	-6.5	0.2	-28.8	-20.1	-24.9	-11.7	-13.3	-9.3	-18.0	-9.2	-14.1	-0.8	-2.3	1.7
i)	47421	-6.7	0.1	-29.1	-20.3	-25.1	-12.0	-13.5	-9.5	-18.3	-9.4	-14.3	-1.0	-2.6	1.5
i)	47355	-6.5	0.1	-28.8	-20.1	-24.9	-11.7	-13.3	-9.3	-18.0	-9.2	-14.1	-0.7	-2.3	1.8
i)	47180	-6.7	0.1	-29.0	-20.3	-25.1	-11.9	-13.5	-9.4	-18.2	-9.4	-14.2	-0.9	-2.5	1.6
i)	47006	-6.6	0.0	-28.9	-20.2	-25.0	-11.8	-13.4	-9.3	-18.1	-9.3	-14.1	-0.8	-2.4	1.7
i)	46957	-6.8	0.2	-29.1	-20.4	-25.2	-12.1	-13.6	-9.6	-18.4	-9.5	-14.4	-1.1	-2.7	1.4

i)	46510	-6.4	0.2	-28.8	-20.1	-24.9	-11.7	-13.2	-9.2	-18.0	-9.2	-14.0	-0.7	-2.3	1.8
i)	46236	-6.5	0.1	-28.9	-20.1	-24.9	-11.8	-13.3	-9.3	-18.1	-9.2	-14.1	-0.8	-2.4	1.7
i)	46173	-6.7	0.2	-29.0	-20.3	-25.1	-11.9	-13.5	-9.4	-18.2	-9.4	-14.3	-0.9	-2.5	1.6
i)	45959	-6.6	0.1	-28.9	-20.2	-25.0	-11.8	-13.4	-9.4	-18.1	-9.3	-14.2	-0.8	-2.4	1.7
i)	45648	-6.7	0.2	-29.1	-20.4	-25.2	-12.0	-13.5	-9.5	-18.3	-9.5	-14.3	-1.0	-2.6	1.5
i)	45410	-6.4	0.2	-28.7	-20.0	-24.8	-11.6	-13.2	-9.2	-17.9	-9.1	-14.0	-0.6	-2.2	1.9
i)	45190	-6.8	0.2	-29.1	-20.4	-25.2	-12.1	-13.6	-9.6	-18.4	-9.5	-14.4	-1.1	-2.7	1.4
i)	44629	-6.5	0.2	-28.8	-20.1	-24.9	-11.7	-13.3	-9.3	-18.0	-9.2	-14.1	-0.8	-2.3	1.7
i)	44476	-6.5	0.1	-28.8	-20.1	-24.9	-11.7	-13.3	-9.2	-18.0	-9.2	-14.0	-0.7	-2.3	1.8
i)	44113	-6.7	0.1	-29.0	-20.3	-25.1	-11.9	-13.5	-9.5	-18.2	-9.4	-14.3	-1.0	-2.5	1.5
i)	43821	-6.5	0.0	-28.8	-20.1	-24.9	-11.7	-13.3	-9.3	-18.0	-9.2	-14.1	-0.7	-2.3	1.7
i)	43579	-6.7	0.2	-29.1	-20.4	-25.2	-12.0	-13.5	-9.5	-18.3	-9.5	-14.3	-1.0	-2.6	1.5
i)	43084	-6.5	0.1	-28.9	-20.1	-25.0	-11.8	-13.3	-9.3	-18.1	-9.3	-14.1	-0.8	-2.4	1.7
i)	42937	-6.5	0.1	-28.9	-20.1	-24.9	-11.8	-13.3	-9.3	-18.1	-9.2	-14.1	-0.8	-2.4	1.7
(e)	42890	-7.0	0.1	-29.3	-20.6	-25.4	-12.2	-13.8	-9.7	-18.5	-9.7	-14.5	-1.2	-2.8	1.3
(e)	42590	-6.8	0.1	-29.2	-20.4	-25.3	-12.1	-13.6	-9.6	-18.4	-9.6	-14.4	-1.1	-2.7	1.4
i)	42583	-6.5	0.1	-28.8	-20.1	-24.9	-11.7	-13.3	-9.2	-18.0	-9.2	-14.1	-0.7	-2.3	1.8
i)	41513	-6.5	0.1	-28.8	-20.1	-24.9	-11.7	-13.3	-9.3	-18.0	-9.2	-14.1	-0.7	-2.3	1.7
i)	40622	-6.5	0.1	-28.8	-20.1	-24.9	-11.7	-13.3	-9.3	-18.0	-9.2	-14.1	-0.7	-2.3	1.7
(e)	36880	-6.8	0.1	-29.2	-20.4	-25.3	-12.1	-13.6	-9.6	-18.4	-9.6	-14.4	-1.1	-2.7	1.4
(e)	36180	-7.1	0.1	-29.4	-20.7	-25.5	-12.3	-13.9	-9.9	-18.6	-9.8	-14.7	-1.3	-2.9	1.1
(e)	34570	-6.9	0.1	-29.2	-20.5	-25.3	-12.2	-13.7	-9.7	-18.5	-9.6	-14.5	-1.2	-2.8	1.3
(e)	33730	-7.1	0.1	-29.4	-20.7	-25.5	-12.3	-13.9	-9.8	-18.6	-9.8	-14.6	-1.3	-2.9	1.2
(e)	32420	-6.8	0.1	-29.1	-20.4	-25.2	-12.1	-13.6	-9.6	-18.4	-9.5	-14.4	-1.1	-2.7	1.4
(e)	30090	-6.4	0.1	-28.8	-20.1	-24.9	-11.7	-13.2	-9.2	-18.0	-9.2	-14.0	-0.7	-2.3	1.8
(e)	27920	-6.9	0.1	-29.3	-20.5	-25.4	-12.2	-13.7	-9.7	-18.5	-9.7	-14.5	-1.2	-2.8	1.3
(c)	25011	-6.6	0.1	-28.9	-20.2	-25.0	-11.8	-13.4	-9.3	-18.1	-9.3	-14.1	-0.8	-2.4	1.7
(c)	24948	-6.4	0.1	-28.8	-20.1	-24.9	-11.7	-13.2	-9.2	-18.0	-9.2	-14.0	-0.7	-2.3	1.8

(c)	24948	-6.7	0.1	-29.1	-20.3	-25.1	-12.0	-13.5	-9.5	-18.3	-9.4	-14.3	-1.0	-2.6	1.5
(e)	24790	-6.5	0.1	-28.8	-20.1	-24.9	-11.7	-13.3	-9.3	-18.0	-9.2	-14.1	-0.7	-2.3	1.8
(c)	24273	-6.5	0.1	-28.8	-20.1	-24.9	-11.7	-13.3	-9.3	-18.0	-9.2	-14.1	-0.7	-2.3	1.7
(c)	23830	-6.8	0.1	-29.2	-20.4	-25.3	-12.1	-13.6	-9.6	-18.4	-9.6	-14.4	-1.1	-2.7	1.4
(c)	23518	-6.7	0.1	-29.0	-20.3	-25.1	-11.9	-13.5	-9.5	-18.2	-9.4	-14.3	-0.9	-2.5	1.6
(c)	22863	-6.7	0.1	-29.0	-20.3	-25.1	-11.9	-13.5	-9.5	-18.2	-9.4	-14.3	-0.9	-2.5	1.6
(e)	22640	-7.0	0.1	-29.3	-20.6	-25.4	-12.3	-13.8	-9.8	-18.5	-9.7	-14.6	-1.3	-2.9	1.2
(b)	22009	-6.6	0.1	-28.9	-20.2	-25.0	-11.8	-13.4	-9.4	-18.1	-9.3	-14.2	-0.8	-2.4	1.6
(e)	21800	-6.7	0.1	-29.0	-20.3	-25.1	-11.9	-13.5	-9.4	-18.2	-9.4	-14.3	-0.9	-2.5	1.6
(b)	19950	-6.8	0.0	-29.1	-20.4	-25.2	-12.0	-13.6	-9.6	-18.3	-9.5	-14.4	-1.0	-2.6	1.4
(b)	19703	-6.5	0.2	-28.8	-20.1	-24.9	-11.7	-13.3	-9.3	-18.0	-9.2	-14.1	-0.7	-2.3	1.7
(b)	19300	-6.7	0.0	-29.0	-20.3	-25.1	-11.9	-13.5	-9.4	-18.2	-9.4	-14.3	-0.9	-2.5	1.6
(b)	18824	-6.4	0.1	-28.7	-20.0	-24.8	-11.6	-13.2	-9.1	-17.9	-9.1	-14.0	-0.6	-2.2	1.9
(b)	18502	-6.4	0.1	-28.8	-20.1	-24.9	-11.7	-13.3	-9.2	-18.0	-9.2	-14.0	-0.7	-2.3	1.8
(b)	18239	-6.6	0.0	-29.0	-20.2	-25.1	-11.9	-13.4	-9.4	-18.2	-9.4	-14.2	-0.9	-2.5	1.6
(b)	17906	-6.4	0.1	-28.8	-20.0	-24.8	-11.7	-13.2	-9.2	-18.0	-9.1	-14.0	-0.7	-2.3	1.8
(b)	17766	-6.5	0.1	-28.8	-20.1	-24.9	-11.7	-13.3	-9.3	-18.0	-9.2	-14.1	-0.7	-2.3	1.8
(c)	17450	-6.5	0.1	-28.9	-20.1	-24.9	-11.8	-13.3	-9.3	-18.1	-9.2	-14.1	-0.8	-2.4	1.7
(b)	17335	-6.5	0.0	-28.8	-20.1	-24.9	-11.7	-13.3	-9.3	-18.0	-9.2	-14.1	-0.8	-2.3	1.7
(b)	16834	-6.6	0.1	-28.9	-20.2	-25.0	-11.8	-13.4	-9.3	-18.1	-9.3	-14.1	-0.8	-2.4	1.7
(b)	16611	-6.6	0.1	-28.9	-20.2	-25.0	-11.8	-13.4	-9.4	-18.1	-9.3	-14.2	-0.8	-2.4	1.7
(c)	16433	-6.8	0.1	-29.1	-20.4	-25.2	-12.1	-13.6	-9.6	-18.4	-9.5	-14.4	-1.1	-2.7	1.4
(b)	16413	-6.8	0.3	-29.1	-20.4	-25.2	-12.0	-13.6	-9.6	-18.3	-9.5	-14.4	-1.0	-2.6	1.5
(c)	15969	-7.0	0.1	-29.4	-20.6	-25.4	-12.3	-13.8	-9.8	-18.6	-9.8	-14.6	-1.3	-2.9	1.2
(c)	15903	-6.9	0.1	-29.3	-20.6	-25.4	-12.2	-13.7	-9.7	-18.5	-9.7	-14.5	-1.2	-2.8	1.3
(b)	15718	-6.8	0.1	-29.1	-20.4	-25.2	-12.0	-13.6	-9.5	-18.3	-9.5	-14.4	-1.0	-2.6	1.5
(b)	15541	-6.7	0.2	-29.0	-20.3	-25.1	-11.9	-13.5	-9.4	-18.2	-9.4	-14.3	-0.9	-2.5	1.6
(b)	15369	-6.9	0.1	-29.3	-20.5	-25.4	-12.2	-13.7	-9.7	-18.5	-9.7	-14.5	-1.2	-2.8	1.3

(b)	14978	-7.0	0.1	-29.3	-20.6	-25.4	-12.2	-13.8	-9.8	-18.5	-9.7	-14.6	-1.3	-2.8	1.2
(b)	14756	-6.7	0.1	-29.0	-20.3	-25.1	-11.9	-13.5	-9.5	-18.2	-9.4	-14.3	-0.9	-2.5	1.6
(c)	14740	-6.7	0.1	-29.0	-20.3	-25.1	-11.9	-13.5	-9.4	-18.2	-9.4	-14.3	-0.9	-2.5	1.6
(b)	14697	-6.8	0.1	-29.2	-20.5	-25.3	-12.1	-13.6	-9.6	-18.4	-9.6	-14.4	-1.1	-2.7	1.4
(e)	14670	-7.0	0.1	-29.4	-20.7	-25.5	-12.3	-13.8	-9.8	-18.6	-9.8	-14.6	-1.3	-2.9	1.2
(e)	14610	-7.1	0.1	-29.4	-20.7	-25.5	-12.3	-13.9	-9.8	-18.6	-9.8	-14.6	-1.3	-2.9	1.2
(b)	14473	-6.7	0.0	-29.1	-20.4	-25.2	-12.0	-13.6	-9.5	-18.3	-9.5	-14.3	-1.0	-2.6	1.5
(c)	14359	-6.7	0.1	-29.0	-20.3	-25.1	-11.9	-13.5	-9.4	-18.2	-9.4	-14.2	-0.9	-2.5	1.6
(b)	14357	-6.8	0.0	-29.1	-20.4	-25.2	-12.0	-13.6	-9.6	-18.3	-9.5	-14.4	-1.0	-2.6	1.5
(b)	14176	-6.8	0.2	-29.1	-20.4	-25.2	-12.0	-13.6	-9.6	-18.3	-9.5	-14.4	-1.0	-2.6	1.5
(c)	14109	-6.7	0.1	-29.1	-20.3	-25.2	-12.0	-13.5	-9.5	-18.3	-9.5	-14.3	-1.0	-2.6	1.5
(b)	14066	-7.0	0.1	-29.3	-20.6	-25.4	-12.2	-13.8	-9.8	-18.5	-9.7	-14.6	-1.2	-2.8	1.2
(b)	14066	-6.8	0.1	-29.1	-20.4	-25.2	-12.0	-13.6	-9.6	-18.3	-9.5	-14.4	-1.0	-2.6	1.5
(b)	13945	-6.9	0.1	-29.2	-20.5	-25.3	-12.1	-13.7	-9.6	-18.4	-9.6	-14.4	-1.1	-2.7	1.4
(b)	13780	-6.7	0.2	-29.0	-20.3	-25.1	-11.9	-13.5	-9.5	-18.2	-9.4	-14.3	-1.0	-2.5	1.5
(b)	13511	-6.5	0.2	-28.9	-20.2	-25.0	-11.8	-13.3	-9.3	-18.1	-9.3	-14.1	-0.8	-2.4	1.7
(c)	13379	-6.9	0.1	-29.2	-20.5	-25.3	-12.1	-13.7	-9.6	-18.4	-9.6	-14.5	-1.1	-2.7	1.4
(b)	13235	-6.6	0.1	-28.9	-20.2	-25.0	-11.8	-13.4	-9.4	-18.1	-9.3	-14.2	-0.8	-2.4	1.6
(b)	13174	-6.6	0.0	-29.0	-20.3	-25.1	-11.9	-13.4	-9.4	-18.2	-9.4	-14.2	-0.9	-2.5	1.6
(b)	13174	-6.6	0.1	-28.9	-20.2	-25.0	-11.8	-13.4	-9.4	-18.1	-9.3	-14.2	-0.8	-2.4	1.7
(c)	13045	-6.8	0.1	-29.2	-20.5	-25.3	-12.1	-13.6	-9.6	-18.4	-9.6	-14.4	-1.1	-2.7	1.4
(b)	13000	-6.8	0.1	-29.1	-20.4	-25.2	-12.0	-13.6	-9.6	-18.3	-9.5	-14.4	-1.0	-2.6	1.5
(b)	12918	-6.8	0.1	-29.1	-20.4	-25.2	-12.0	-13.6	-9.6	-18.3	-9.5	-14.4	-1.0	-2.6	1.5
(b)	12889	-6.8	0.1	-29.1	-20.4	-25.2	-12.0	-13.6	-9.6	-18.3	-9.5	-14.4	-1.1	-2.6	1.4
(b)	12734	-6.9	0.1	-29.2	-20.5	-25.3	-12.2	-13.7	-9.7	-18.4	-9.6	-14.5	-1.2	-2.8	1.3
(b)	12734	-6.6	0.1	-28.9	-20.2	-25.0	-11.8	-13.4	-9.3	-18.1	-9.3	-14.1	-0.8	-2.4	1.7
(b)	12585	-6.6	0.1	-29.0	-20.3	-25.1	-11.9	-13.5	-9.4	-18.2	-9.4	-14.2	-0.9	-2.5	1.6
(b)	12585	-6.8	0.2	-29.2	-20.5	-25.3	-12.1	-13.6	-9.6	-18.4	-9.6	-14.4	-1.1	-2.7	1.4

(b)	12346	-6.8	0.0	-29.1	-20.4	-25.2	-12.0	-13.6	-9.5	-18.3	-9.5	-14.4	-1.0	-2.6	1.5
(c)	12241	-6.9	0.1	-29.2	-20.5	-25.3	-12.1	-13.7	-9.6	-18.4	-9.6	-14.4	-1.1	-2.7	1.4
(c)	12117	-6.9	0.1	-29.2	-20.5	-25.3	-12.1	-13.7	-9.6	-18.4	-9.6	-14.4	-1.1	-2.7	1.4
(e)	12080	-6.7	0.1	-29.1	-20.3	-25.2	-12.0	-13.5	-9.5	-18.3	-9.5	-14.3	-1.0	-2.6	1.5
(b)	12029	-6.9	0.2	-29.3	-20.5	-25.4	-12.2	-13.7	-9.7	-18.5	-9.7	-14.5	-1.2	-2.8	1.3
(b)	12029	-7.0	0.1	-29.3	-20.6	-25.4	-12.2	-13.8	-9.8	-18.5	-9.7	-14.6	-1.3	-2.8	1.2
(c)	11860	-6.7	0.1	-29.0	-20.3	-25.1	-11.9	-13.5	-9.5	-18.2	-9.4	-14.3	-0.9	-2.5	1.6
(b)	11796	-6.9	0.2	-29.2	-20.5	-25.3	-12.2	-13.7	-9.7	-18.5	-9.6	-14.5	-1.2	-2.8	1.3
(b)	11796	-7.0	0.0	-29.3	-20.6	-25.4	-12.2	-13.8	-9.7	-18.5	-9.7	-14.5	-1.2	-2.8	1.3
(c)	11675	-6.8	0.1	-29.2	-20.4	-25.3	-12.1	-13.6	-9.6	-18.4	-9.6	-14.4	-1.1	-2.7	1.4
(b)	11612	-7.1	0.2	-29.4	-20.7	-25.5	-12.3	-13.9	-9.9	-18.6	-9.8	-14.7	-1.3	-2.9	1.2
(b)	11612	-7.0	0.0	-29.3	-20.6	-25.4	-12.2	-13.8	-9.8	-18.5	-9.7	-14.6	-1.2	-2.8	1.2
(c)	11555	-6.7	0.1	-29.0	-20.3	-25.1	-11.9	-13.5	-9.5	-18.2	-9.4	-14.3	-0.9	-2.5	1.6
(c)	11434	-6.7	0.1	-29.0	-20.3	-25.1	-11.9	-13.5	-9.5	-18.2	-9.4	-14.3	-1.0	-2.5	1.5
(b)	11324	-6.7	0.0	-29.1	-20.4	-25.2	-12.0	-13.6	-9.5	-18.3	-9.5	-14.3	-1.0	-2.6	1.5
(b)	11324	-6.8	0.1	-29.2	-20.4	-25.2	-12.1	-13.6	-9.6	-18.4	-9.5	-14.4	-1.1	-2.7	1.4
(b)	11124	-6.8	0.0	-29.2	-20.4	-25.2	-12.1	-13.6	-9.6	-18.4	-9.5	-14.4	-1.1	-2.7	1.4
(b)	11064	-6.8	0.1	-29.1	-20.4	-25.2	-12.0	-13.6	-9.6	-18.3	-9.5	-14.4	-1.0	-2.6	1.4
(f)	10919	-6.7	0.1	-29.1	-20.3	-25.1	-12.0	-13.5	-9.5	-18.3	-9.4	-14.3	-1.0	-2.6	1.5
(c)	10880	-6.6	0.1	-28.9	-20.2	-25.0	-11.8	-13.4	-9.4	-18.1	-9.3	-14.2	-0.8	-2.4	1.7
(f)	10874	-6.6	0.0	-28.9	-20.2	-25.0	-11.8	-13.4	-9.4	-18.1	-9.3	-14.2	-0.8	-2.4	1.7
(f)	10787	-6.5	0.0	-28.8	-20.1	-24.9	-11.7	-13.3	-9.3	-18.0	-9.2	-14.1	-0.7	-2.3	1.7
(f)	10721	-6.5	0.1	-28.8	-20.1	-24.9	-11.7	-13.3	-9.3	-18.0	-9.2	-14.1	-0.7	-2.3	1.7
(e)	10650	-6.8	0.1	-29.1	-20.4	-25.2	-12.0	-13.6	-9.6	-18.3	-9.5	-14.4	-1.0	-2.6	1.5
(e)	10620	-6.8	0.1	-29.1	-20.4	-25.2	-12.0	-13.6	-9.5	-18.3	-9.5	-14.3	-1.0	-2.6	1.5
(e)	10610	-6.8	0.1	-29.1	-20.4	-25.2	-12.0	-13.6	-9.5	-18.3	-9.5	-14.4	-1.0	-2.6	1.5
(b)	10604	-6.8	0.0	-29.2	-20.4	-25.2	-12.1	-13.6	-9.6	-18.4	-9.5	-14.4	-1.1	-2.7	1.4
(e)	10530	-6.8	0.1	-29.1	-20.4	-25.2	-12.0	-13.6	-9.6	-18.3	-9.5	-14.4	-1.1	-2.6	1.4

(f)	10507	-6.6	0.1	-29.0	-20.2	-25.1	-11.9	-13.4	-9.4	-18.2	-9.4	-14.2	-0.9	-2.5	1.6
(b)	10401	-6.7	0.1	-29.1	-20.4	-25.2	-12.0	-13.5	-9.5	-18.3	-9.5	-14.3	-1.0	-2.6	1.5
(c)	10394	-6.4	0.1	-28.7	-20.0	-24.8	-11.6	-13.2	-9.1	-17.9	-9.1	-13.9	-0.6	-2.2	1.9
(f)	10282	-6.5	0.0	-28.8	-20.1	-24.9	-11.7	-13.3	-9.3	-18.0	-9.2	-14.1	-0.7	-2.3	1.8
(b)	10278	-6.7	0.1	-29.1	-20.4	-25.2	-12.0	-13.5	-9.5	-18.3	-9.5	-14.3	-1.0	-2.6	1.5
(f)	10086	-6.6	0.0	-29.0	-20.3	-25.1	-11.9	-13.4	-9.4	-18.2	-9.4	-14.2	-0.9	-2.5	1.6